Nano/Micro Scale Macromolecular Materials: Design, Synthesis, Self-Assembly, Lighting and Photonic Applications

A Thesis Submitted for the Degree

DOCTOR OF PHILOSOPHY

BY

Y S L V NARAYANA

School of Chemistry
University of Hyderabad
Hyderabad-500 046
INDIA

November-2015

Dedicated to All My Best Wishers

CONTENTS

DECLARATION

I, Y S L V Narayana declare that the work presented in this thesis is the result of research carried out by me in the School of Chemistry, University of Hyderabad, Hyderabad, under the supervision of Assoc. Prof. Rajadurai Chandrasekar. This work is also free from plagiarism. I hereby agree that my thesis can be submitted in Shodhganga/INFLIBNET.

In keeping with the general practice of reporting scientific observations, due acknowledgements have been made wherever the work described is based on the findings of other investigators. Any omission or error that might have crept in is regretted.

[**Y S L V Narayana**]

University of Hyderabad

Central University (P.O), Hyderabad-500046, India.

Certificate

This is to certify that the work described in this thesis entitled **"Nano/Micro Scale Macromolecular Materials: Design, Synthesis, Self-Assembly, Lighting and Photonic Applications"** has been carried out by Mr. Y S L V Narayana (Reg.No.09CHPH54) under my supervision and the same has not been submitted elsewhere for any degree.

Assoc. Prof. R. Chandrasekar
[Thesis Supervisor]
School of Chemistry
University of Hyderabad
Hyderabad-500046, INDIA.

Forwarded by:

Prof. M. Durga Prasad
Dean
School of Chemistry
University of Hyderabad
Hyderabad-500046, INDIA.

ACKNOWLEDGEMENTS

I would like to take this opportunity to acknowledge many individuals whom I am very thankful to complete this journey. First of all the most important person I am thankful to is my research supervisor Assoc. Prof. Dr. Rajadurai Chandrasekar, for being the most wonderful supervisor ever. I really appreciate his patience and his obligation towards me to achieve academic excellence and put me at ease to achieve my goals. Without his constant guidance, demands, advice and persistent help this dissertation would not have been possible. I am very much grateful to him for giving me so many valuable lectures during my Ph.D time not only about science but also social activities in the society. I have learned so many things from him. He was always there whenever I needed anything at all and for that, I am still indebted to him. I am also thankful to him for he treated me as a family member. My journey with him is a great achievement for me and most cherished and unforgettable one in my life.

I would like to thank the present and former Deans, School of Chemistry, for their support and help on various occasions. I am extremely thankful individually to all the faculty members of the school for their kind help and cooperation at various stages of my stay in the campus. Especially my doctoral committee members Prof. Tushar Jana and Prof. K. Muralidharan for their constant support throughout my research career. I am very much grateful to Prof. K. C. Kumar Swamy and Prof. Samar Kumar Das, for initially they gave me wonderful opportunity for entering the School of Chemistry and continuing their support till date. I thank all non-teaching staff, School of Chemistry for their cooperation.

I am very much thankful to Prof. Dr. Klaus Müllen, Prof. Dr. Martin Baumgarten (Max-Planck-Institut für Polymerforschung), for their support throughout my research work. I also sincerely acknowledge Dr. Ahamad Mohiddon for his valuable and timely assistance during various microscope/Raman imaging measurements.

I would also like to express my sincere gratitude to central instrumental laboratory (CIL), UoH especially Mr. Pavan for his help with SEM experiments, Ms. Nalini for her help with laser confocal fluorescence measurements. I also sincerely acknowledge Center for Nanotechnology

for providing TEM, SNOM, and CLSM facilities and especially thank Mr. Durga Prasad (Centre for Nanotechnology, UOH) for his help with TEM and FE-SEM experiments.

It is great pleasure to thank my lovable labmates like Dr. NC, Dr. Supratim, Dr. Pramiti, Dr. Ajay, Mr. Krishna Rao, Mr. Ramudu, Ms. Radhika, Ms. Anjana and Dr. M. Annadhasan (Kothari Post-Doc Fellow) in my Ph.D life. I specially thank my M.Sc classmate, my Ph.D labmate and also one of my loving friends Dr. Naisa Chandrasekhar (NC) for his association and support during hard time in research life. I acknowledge my junior brothers and sisters Mr. D.V. Krishnarao, Mr. U. Ramudu, Ms. Radhika and Ms. Anjana for maintaining the friendly atmosphere in the lab. My special thanks to project students Mr. Vinod, Mr. Suresh, Mrs. Nitheen Kaperi, Ms. Sowmya, Mr. Veeraprasad Ms. Madhuri dey, Mr. Arani Biswas, Mr. M. Hamanth, and Mr. Ajay for exploring new insights in materials science along with them. I also thank visiting research scholars to our lab Dr. Thameem Ansari, M. Annadhasan, Siva, Uday, Stanley, Muthuraja, Ramu (ILS), Selvam, Bala chandar, Balaji, who always providing a chance to explore new research topics during their stay in the lab. I would also like thank Dr. B. Satya Narayana (Kotari Post-doctoral fellow) for his valuable suggestions.

I would also like to express my sincere thanks to all my beloved past seniors in school of chemistry with whom I have wonderful memories in this campus life. The some of my seniors who still matter are Dr. N.N. Bhuvan Kumar, Dr. Phani Pavan, Dr. Venu srinivas, Dr. O. Anjaneyulu, Dr. GDP, Dr. Rambabu, Dr. Srinivas, Dr. Bharath, Dr. Kishore, Dr. Santhosh, Dr. Anand, Dr. DK, Dr. Krishna Chaitanya, Dr. Ramesh, Dr. Rajesh, Dr. Ravi, Dr. Gupta, Dr. Hari, Dr. Venu, Dr. Seshadri, Dr. Mallesh, Dr. Bhanu, and Dr. Laxman, with whom I have shared many unforgettable moments in this campus and who were never really like a seniors to me.

I am really lucky for my close association with some of my friends in HCU which include Dr. Srinu (Allu), Dr. Nagarjuna (VB lab), Sunny, Dr. Gangadhar, Dr. Ramu Yadav, Dr. Nagarjuna (AKS lab), Ramakrishna (PRS lab), Sudheer, Ganesh (RB lab), Krishnamachari, Naveen, Yasin, Sashi, Pavan, Rajagopal Reddy, Nanda, Obaiah, Sateesh, Vikranth, Veera Raghavaiah, Obul Reddy, Raju (SKD), Ramakrishna (SKD), Krishna (SKD), Chandrasekhar Reddy, Lings Varma, Saiyanna, Prasad, Vignesh, Srinivas (RB lab), Sridevi Akka, Geeta,

LIST OF ACRONYMS

^1H	proton
$CDCl_3$	deuterated chloroform
CH_2Cl_2	dichloromethane
CH_3CN	acetonitrile
$CHCl_3$	chloroform
DCM	dichloromethane
DMSO	dimethyl sulfoxide
EtOH	ethanol
MeOH	methanol
H_2O	water
THF	tetrahydrofuran
cm	centimeter
μm	micrometer
nm	nanometer
ns	nanosecond
CT	charge transfer
CuI	copper iodide
CW	continuous wave
D	deuterium
EDTA	ethylenediaminetetraacetic acid
EDXS	energy dispersive x-ray spectroscopy
$Eu(tta)_3$	tris[4,4,4-trifluoro-1-(2-thienyl)-1,3-butanediono]europium
$Tb(acac)_3$	terbium acetylacetonate
FRET	Förster resonance energy transfer
Hz	Hertz
hυ	light energy
IR	infrared
K_2CO_3	potassium carbonate
kDa	kilo Dalton
KOH	potassium hydroxide
KF	potassium fluoride
LED	light emitting diode
$lm\ W^{-1}$	lumens per watt
M.P	melting point
MHz	megaHertz
M	molecular weight
$\overline{X_n}$	number-average degree of polymerization
$\overline{M_w}$	weight average molecular weight
$\overline{M_n}$	number average molecular weight
PDI	polydispersity
MSP	metallo-supramolecular polymers
CP	conjugated polymers

MCCP	metal containing conjugated polymers
NMR	nuclear magnetic resonance spectroscopy
Pd(PPh$_3$)$_4$	tetrakis(triphenylphosphine)palladium (0)
PL	photoluminescence
PS	polystyrene
RPM	revolutions per minute
RT	room temperature
SEM	scanning electron microscope
FESEM	field emission scanning electron microscope
AFM	atomic force microscopy
TEM	transmission electron microscopy
SAED	selected area electron diffraction
T	temperature
bpp	bis(pyrazolyl)pyridine
terpy	terpyridine
TGA	thermogravimetric analysis
DSC	differential scanning calorimetry
UV	ultraviolet
OLED	organic light-emitting diode
WLEPM	white light emitting polymer materials
WGMs	whispering gallery modes
FSR	free spectral range
Q-factor	quality factor
Δ	heat energy
δ	nmr chemical shift reported in ppm
$\Delta\lambda$	change in wavelength of emission or absorption
λ	wavelength
λmax	wavelength of emission or absorption maximum
π-π	pi-pi
FL	fluorescence
NIR	near infrared ray
Vis	Visible

1.1 History of 2,6-Bis(pyrazolyl)pyridine:

Tridentate pyridine-centered heteroaromatic ligands are important coordination frameworks that are used in various fields of research, such as in supramolecular self-assembly, coordination chemistry, optoelectronics, photochemical applications, and in the developments of catalysts and magnetic materials. Numerous tridentate coordinating motifs have been reported in the literature to date;[1] including (but not limited to) derivatives of dipicolinic acid (dpa), 2,6-bis(oxazoline)-pyridine (pybox), 2,6-bis(tetrazol-4-yl)pyridines (pytz), bis(1,2,4-triazolyl)pyridines (btp), 2,2';6',2"-terpyridine (terpy) and very recently 2,6-bis(pyrazolyl)pyridine (bpp). In this thesis work, bpp units are employed to create macromolecules for light emitting materials applications, hence further discussion will be limited to only bpp and its derivatives.
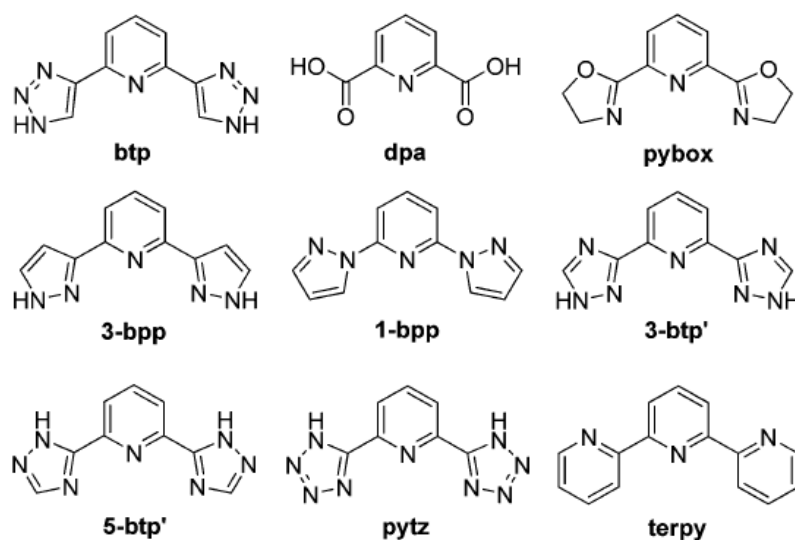
Figure 1.1 Nitrogen containing tridentate ligands.

In 1990 Goldsby et al [2] have synthesized bpp ligand for the first time and since then it gained great attention among the inorganic chemists due to its structural resemblance to the well-known tridentate ligands like terpy and btp. After eleven years, Halcrow et al.[3] have reported for the first time, bpp coordinating ability as a tridentate ligand with Ni(II), Co(II) and Cu(II) metal ions. Later, Brunet and his co-workers[4] have prepared water soluble macrocyclic chelates by attaching diethylenetriaminepentaacetic acid to bpp. The chelates showed high luminescence properties upon binding with Eu(III) and Tb(III) metal ions. They also proposed the energy

transfer from bpp to lanthanide metal centre. Along with bpp, its derivative 2,6-bis(3,5-dimethylpyrazol-1-yl)pyridine (Me$_4$bpp) also forms coordination complexes with Ru(II) and Ni(II) ions.[5] Baumgarten et al.[6] have functionalized bpp in the 4- and 4"-pyrazole carbons by direct H(4)-pyrazole halogen exchange. The un-symmetrically and symmetrically substituted dihalo and monohalo derivatives provide simple access to other functionalities through Grignard exchange and Sonogashira coupling reactions.
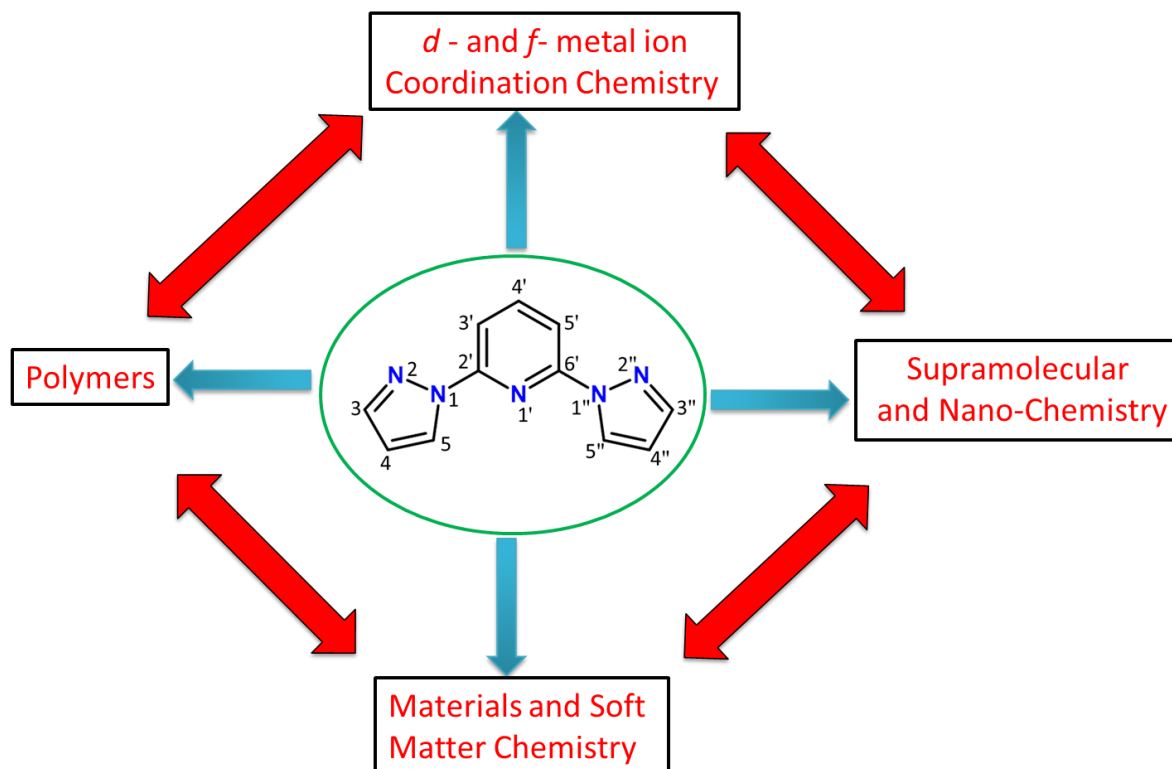
Figure 1.2 Graphical representation of diverse applications of bpp.

In 2006, Ruben and his co-workers[7] have synthesized a 1-D metallo-supramolecular complex [Fe^{II}(L)$_2$H](ClO$_4$)$_3$·MeOH [where, L = 4′-(4‴-pyridyl)-1,2′:6′1″-bis(pyrazolyl)pyridine] using head-to-tail N$^+$-H···N-type hydrogen-bonding. In the same year, Halcrow and his coworkers [8] functionalized the 4-pyridyl carbon of bpp with nucleobase substituents. For the first time, the same group has synthesized back-to-back coupled bpp separated by a CH$_2$-CH$_2$ spacer. In 2007, Ruben et al.[9] have reported a back-to-back coupled bpp ligand bridged by a phenyl spacer and its 1-D metallo-supramolecular polymer with Fe(II) ions. Oshio et al.[10] have developed Fe(II) complexes of bpp ligand carrying doublet state nitronylnitroxide radicals. Latter

coordination complexes of bpp with rare earth metals like Eu(III), Tb(III), Yb(III) opened window for so many applications in various fields such as near-infrared (NIR) emission, two-photon absorption spectroscopy and the formation of radiant gels.
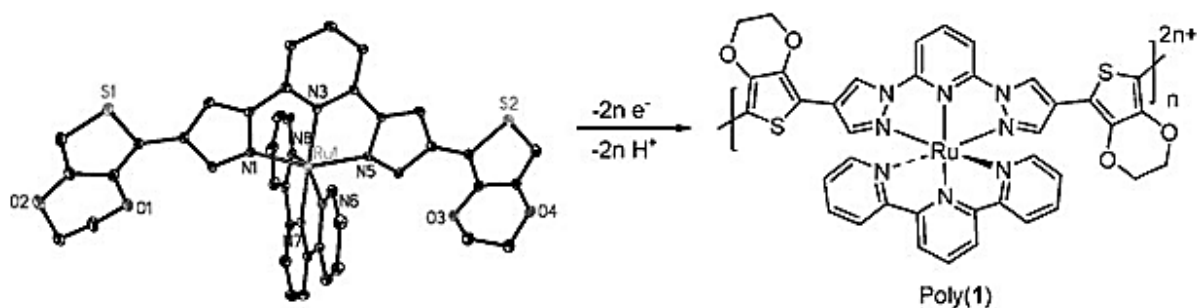
Figure 1.3 Electropolymerization of bpp-thiophene derivative by Holliday. [Adopted from Ref. 11].

Holliday and his group[11] have first carried out the electropolymerization of bpp unit to synthesize a high molecular weight bpp based conjugated copolymer for lighting applications. They have developed a conductive metallopolymer from thiophene appended bpp derivative coordinated to Ru(II) ion by electropolymerization method (Fig. 1.3). His group further reported on the synthesis of a red luminescent nine-coordinated Eu(III) complex of bpp and its photo-physical properties. The structure of the complex had been determined by single-crystal X-ray
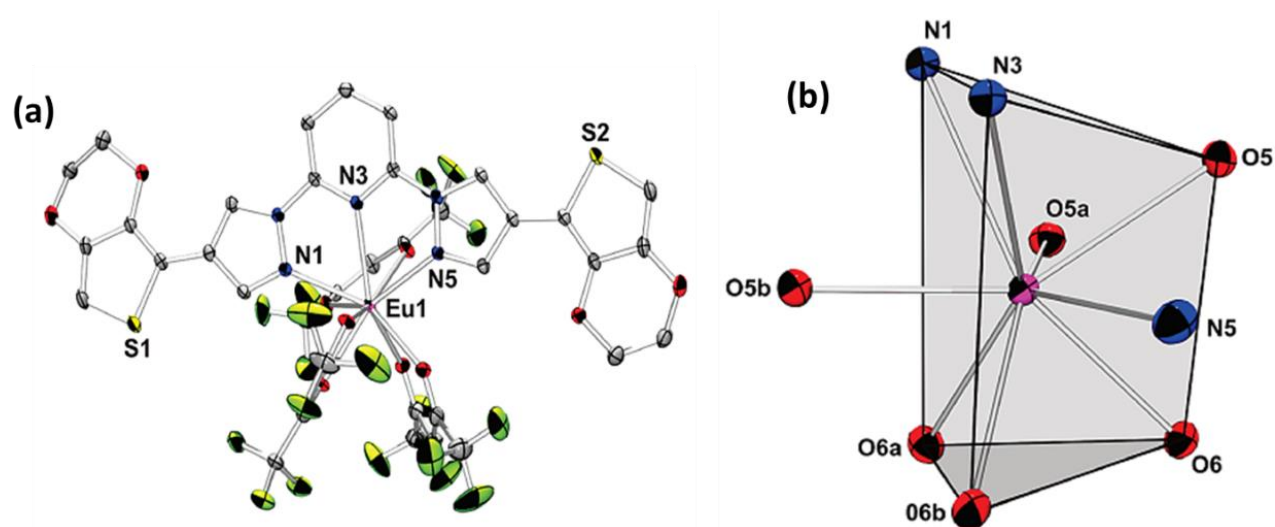
Figure 1.4 a) Crystal structure of nine coordinated complex of BPP with Eu(III) ion. b) Tricapped trigonal prism geometry around Eu(III) ion. [Adopted from Ref. 12].

crystallography and the geometry of the local coordination environment around the Eu(III) ion has been shown to be a slightly distorted tricapped trigonal prism[12] (Fig 1.4 a and b). Ye and coworkers have developed a dual-bpp chelating ligand which showed weak luminescence upon coordination with Tb(III) ion. The same ligand coordinated with Zn(II) ions showed improved selectivity and increased intensity of luminescence. The Tb(III) chelate-based luminescent chemosensor is highly selective and very sensitive to recognize Zn(II) ions in living cells.[13] In 2011, Nishihara and co-workers[14] have designed and synthesized bpp decorated with stilbene and its Fe(II) complex exhibiting a visible light photoisomerization from *Z*-2 to *E*-2, in both solution and solid states. Ziessel and coworkers[15] have prepared lanthanide complexes of ligands constructed from a bpp core bearing various chelating arms of mixed carboxylate/phosphonate substituents. These ligands formed stable complexes with Tb(III) and Eu(III) which display outstanding spectroscopic properties suitable for applications in bio-labeling.
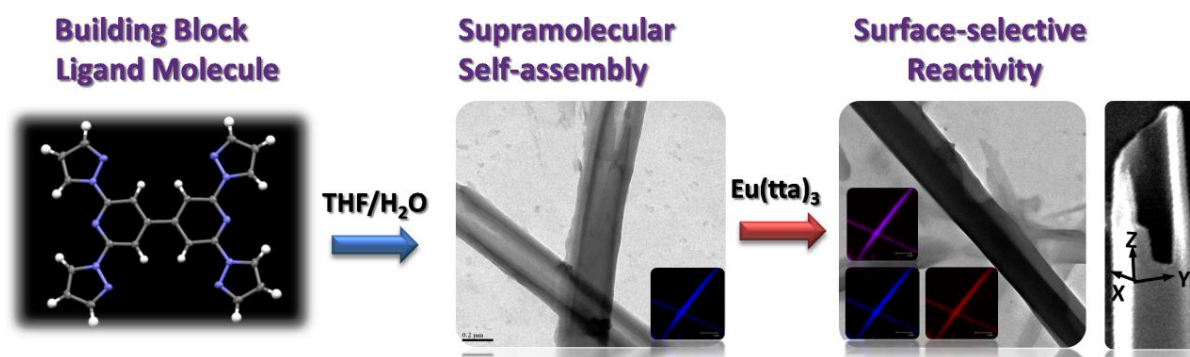
Figure 1.5 Self-assembly of a back-to-back coupled **bpp** unit into parallepipedic tubes and subsequent surface selective coordination of Eu(tta)$_3$ on the tubes to generate dual emitting nano structures. [Adopted from Ref. 17].

In 2010, Chandrasekar et al.[16] has self-assembled a back-to-back coupled bpp for the first time to produce fluorescent nanotapes and submicrotubes via solvent-assisted supramolecular bottom-up self-assembly methodology. Moreover, the same group has made first attempts to use self-assembled ligand nano structures as a template for "surface coordination chemistry".[17] For example, they have fabricated fluorescent parallepipedic tubes with rectangular cavities from a directly back-to-back homo coupled bpp via self-assembly approach and subsequently Eu(tta)$_3$ had been coordinated selectively to ligand molecules available on the surface of the parallepipedic tubes. The resultant tube showed dual emission down to single particle level in the blue and red regions (Fig. 1.5). In 2013, taking advantage of 4 and 4' halo substituted bpp,

Chandrasekar et al.[18] have reported the preparation of bpp and fluorene based light emitting conjugated copolymers ($\overline{M}_n$ ~ 10 KDa) using Sonogashira cross coupling reaction. The resultant polymers upon aggregation showed cyan colour emissions (blue and green). This copolymer was further coordinated with red emitting Eu(III) ions to get white emitting metal containing conjugated polymers in the solid state with a CIE values of x=0.31and y=0.35, which are very close to white light.

1.2 Metallo-Supramolecular Polymers (MSPs) and Metal–Containing Conjugated Polymers (MCCPs)

1.2.1   Introduction About MSPs

Supramolecular chemistry[19] has become one of the most active and emerging research fields of chemistry after the award of 1987-Chemistry Nobel Prize to J.-M. Lehn, C. J. Pederson and D. J. Cram. Self-assembly and self-recognition are the basic elements of supramolecular chemistry and the interactions are predominantly non-covalent (*e.g.* van der Waals,[19] π-π interactions,[20] ionic,[21] hydrogen bonding,[22] or coordinative interactions[23]). These interactions are very weak and generally reversible compared to covalent bonds. Because of weak interactions, supramolecular polymers differ from conventional polymers as the non-covalent interactions are reversible in nature which has led to their use as smart polymeric materials. The growth of supramolecular chemistry introduced a new perspective to modern chemistry and material science by applying non-covalent interactions in a directed way to organize functional molecular building blocks forming robust supramolecular architectures.

Polymers formed by coordination of metals to bi- or multifunctional ligands are called MSPs. Coordination polymers often blend together the properties of both their organic and inorganic counterparts, e.g. the flexibility of organic polymers combined with the increased thermal stability associated with inorganic species. Some of the coordination polymers are stable even up to 500 °C and can provide sufficient flexibility so as to enable them to be studied by gel permeation chromatography, viscosity, and solid-state NMR.[24] MSPs find diverse of applications in catalysis, sensing and media storage.[25] Some of the back-to-back coupled ligands developed by several research groups[17, 26] to achieve metallo supramolecular structures in various dimensions are given in Fig. 1.6.
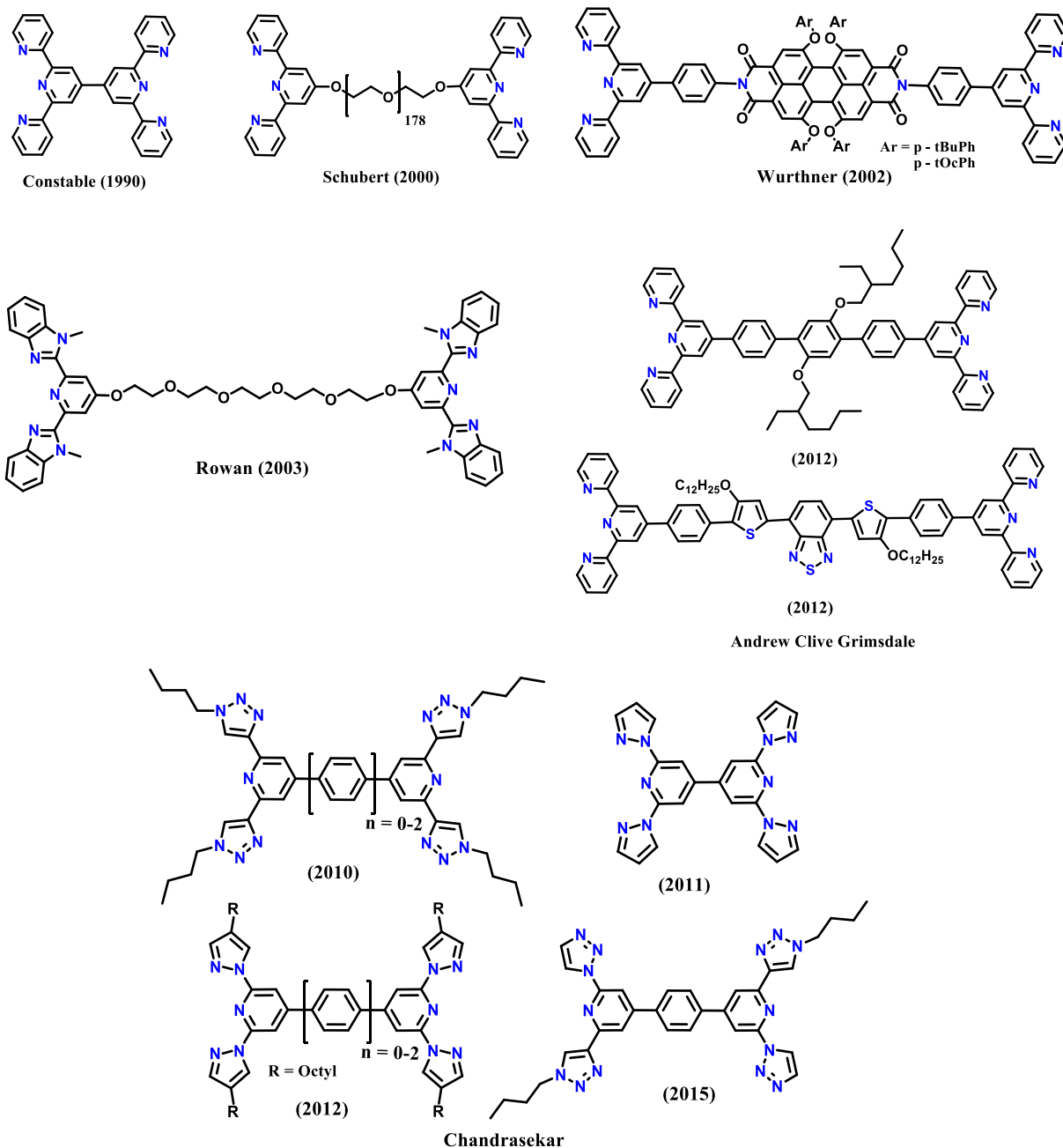
Figure 1.6 Chemical structure of supramolecular tridentate ligand building blocks for MSPs.

MSPs have been prepared using the interactions between metal ions and ditopic ligand molecules. Depending upon the direction of interactions between metal ion and ligand molecules MSP can be mainly classified into (i) main-chain MSPs (where interactions between metal ion and ligand is linear), and (ii) star-shaped macromolecules.
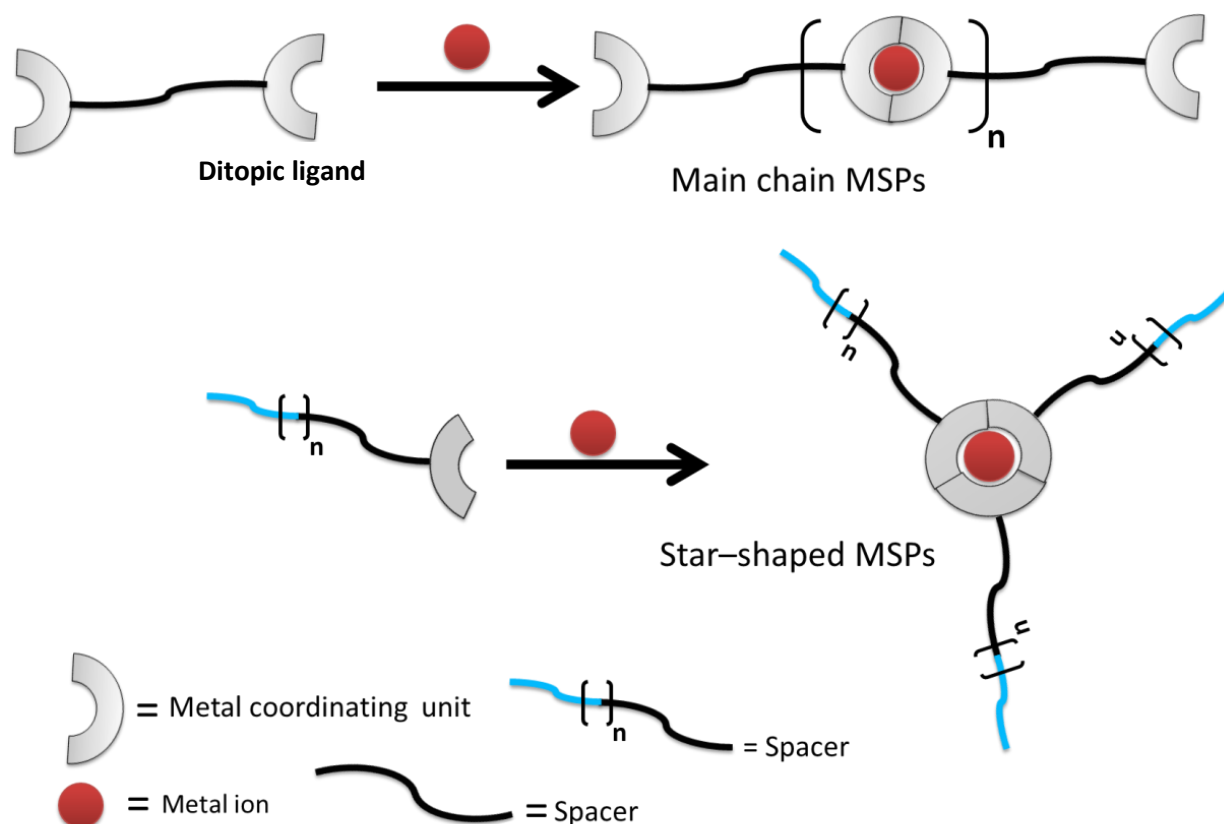
Figure 1.7 Schematic representation of main chain and star shaped MSPs.

1.2.1.1 Main Chain MSPs

Main chain MSPs contain directly incorporated metal-ligand in the polymer main chain. This type of polymers can be attained only by addition of the appropriate metal-ions to a ditopic ligand molecule end-capped monomer in a 1:1 ratio resulting in a MSP with many metal-ligand complexes along the polymer main chain. Rehahn and coworkers [27] have prepared for the first time, well defined transition metal containing main-chain MSP by reacting Cu(I) or Ag(I) ions to a solution of ditopic phenanthroline ligand derivatives (Fig 1.8).The macromolecular nature of the MSP was [average chain length P≥20] had been determined using ^{1}H NMR spectroscopy technique. These polymers form cyclic ring structures in coordinating solvents and retain their polymeric nature in non-coordinating solvents.
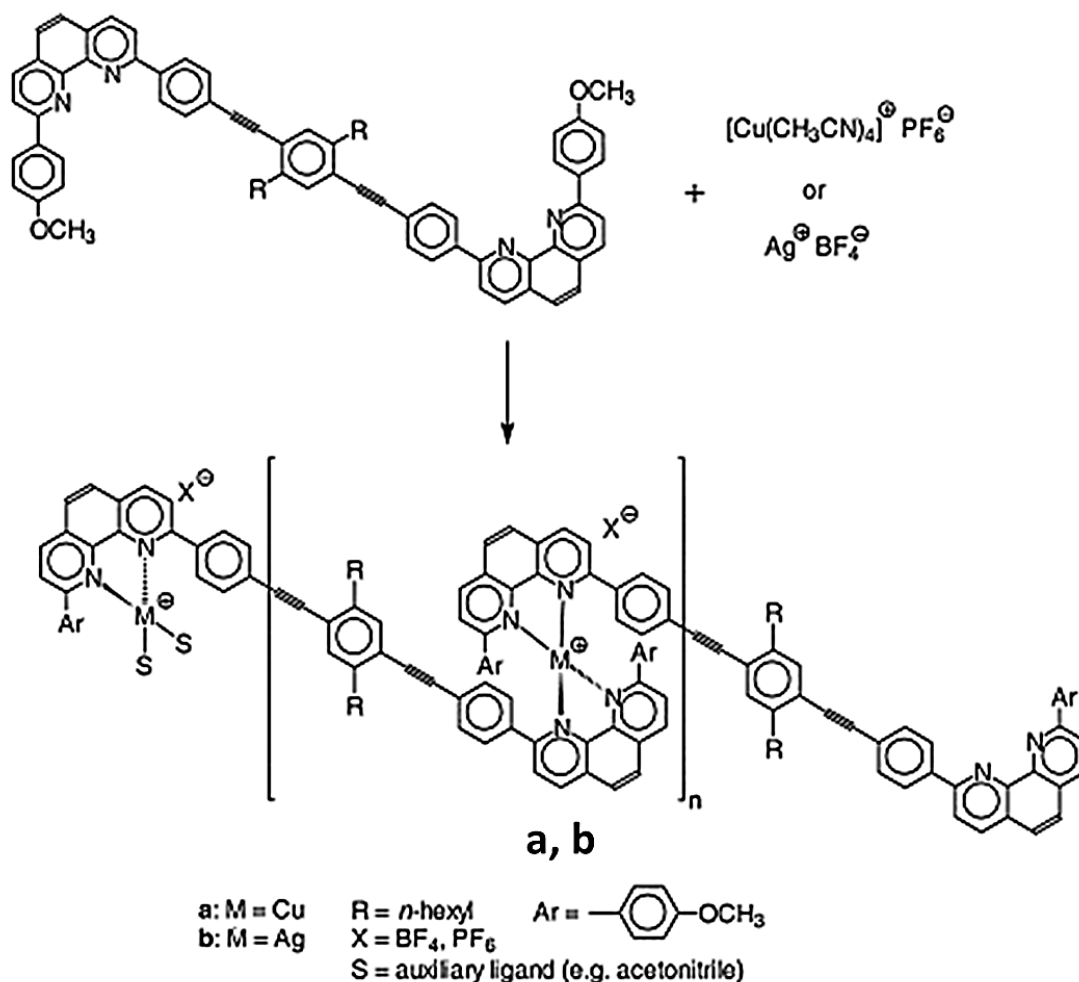
Figure 1.8 Main chain MSP synthesized by Rehahn et al. [Adopted from Ref. 27].

A series of water soluble main-chain MSPs have been synthesized by Schubert and coworkers [28] by combining a ditopic terpyridine end-capped poly(ethylene glycol) with a wide variety of transition metal-ions to achieve high molecular weight polymers (Fig. 1.9a). The linear MSPs formation had been confirmed by using viscosity and observing the film forming properties. The terpyridine/Fe(II) containing MSP was thermally stable up to 210 $^{\circ}$C. The absorption spectra of terpydine monomer and corresponding MSP with Fe(II) are shown in Fig 1.9b.[28a] The appearance of 559 nm metal-ligand charge transfer band in absorption spectrum of MSP clearly indicated the complex formation. Further, they authors have also studied morphological changes associated with complex formation using atomic force microscopy. The morphology of the MSP revealed a double-lamella structure (Fig 1.9d). For thermally annealed monomer compound, double-lamella morphology had not been obtained. Unusual folds result in

double-lamella morphology and the folding is believed to result from hydrogen bonding of the free hydroxyl groups in MSP.
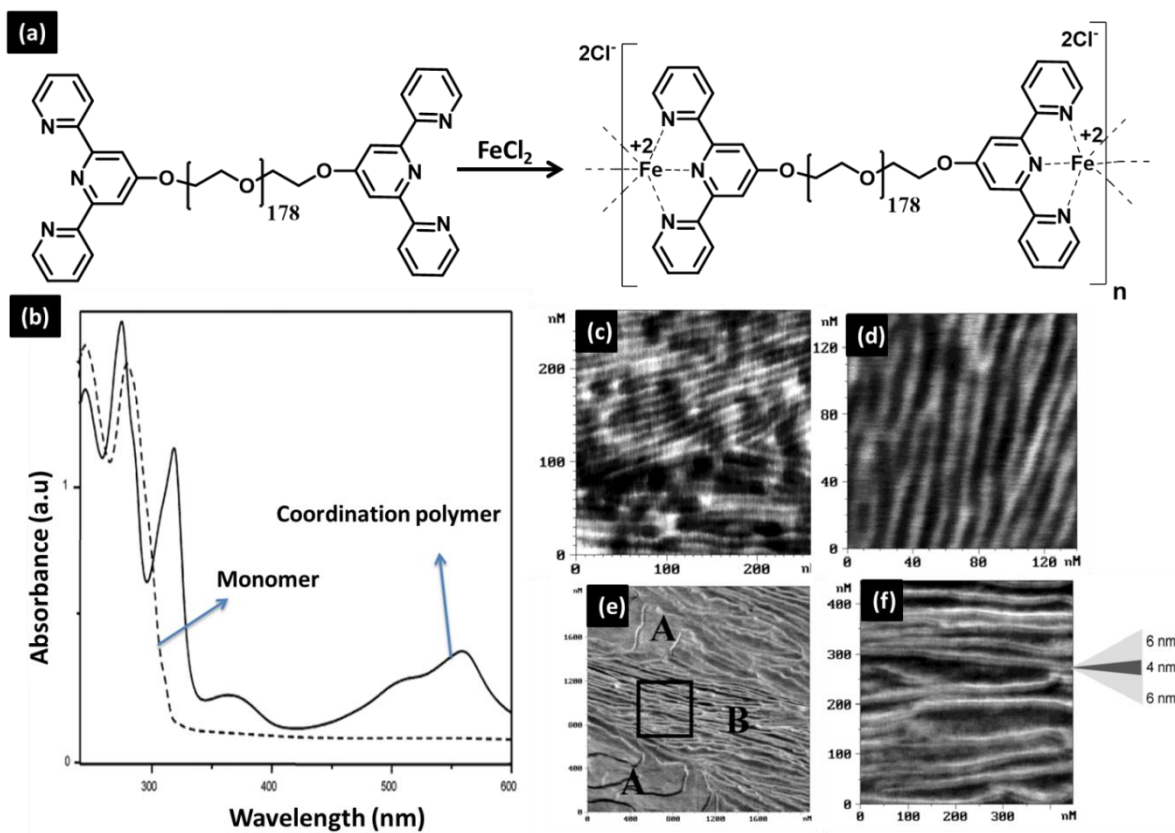
Figure 1.9 a) Ditopic terpyridine based main chain MSPs prepared by Schubert et al. b) The UV-Visible spectra of monomer (dotted lines) and iron(II) containing MSP (solid line). c) and d) AFM images of monomer and MSP showing lamellar structures. e) AFM phase image of annealed MSP (70 °C, 30 min) lamella are seen face on (A) and edge on (B) f) Single lamella with a double line feature consist of two phase domains of about 6 nm separated by 4 nm domain of opposite phase. [Adopted from Ref. 28a].

Terech and coworkers[29] have prepared a small molecular weight gelator comprised of two different types of metal-ion receptor sites; terpyridine end-groups with a cyclam core (Fig 1.10a). The gel formed by complexation of Co(II) or Ni(II) showed stimuli-responsive property including mechanically-induced gel-sol transitions (thixotropic) and response to electrical stimulus. The effect of metal ions in MSP on gel formation is shown in Fig 1.10b.
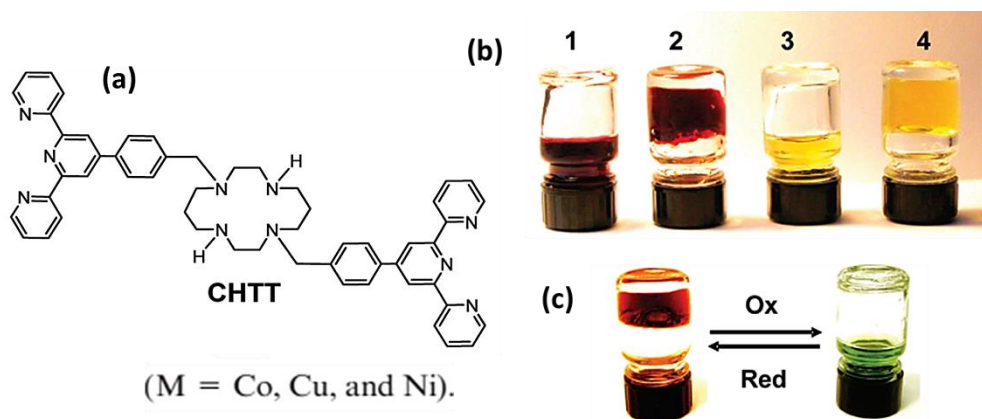
Figure 1.10 a) Terpyridine end-groups with a cyclam core (CHTT). b) Formation of gels in CH_3CN as function of counter anions (1) $CoCl_2$, (2) $Co(NO_3)_2$, (3) $NiCl_2$, and (4) $Ni(NO_3)_2$ (M_2^{II} CHTT- 2.15 mM) c) Redox controlled gel to liquid (reversible) of Co_2^{II} CHTT in DMF solvent. [Adopted from Ref. 29].

Rowan and coworkers developed benzimidazol based multi-responsive MSP gel[30] exhibiting diverse properties such as coupling[31] and decoupling[32] of optical properties, thermo-, chemo-responsive shape-memory functions[33], in situ formation of metal nanoparticle in polymer films[34] and optically healability[35]. They have prepared Zn containing MSP for gel formation and
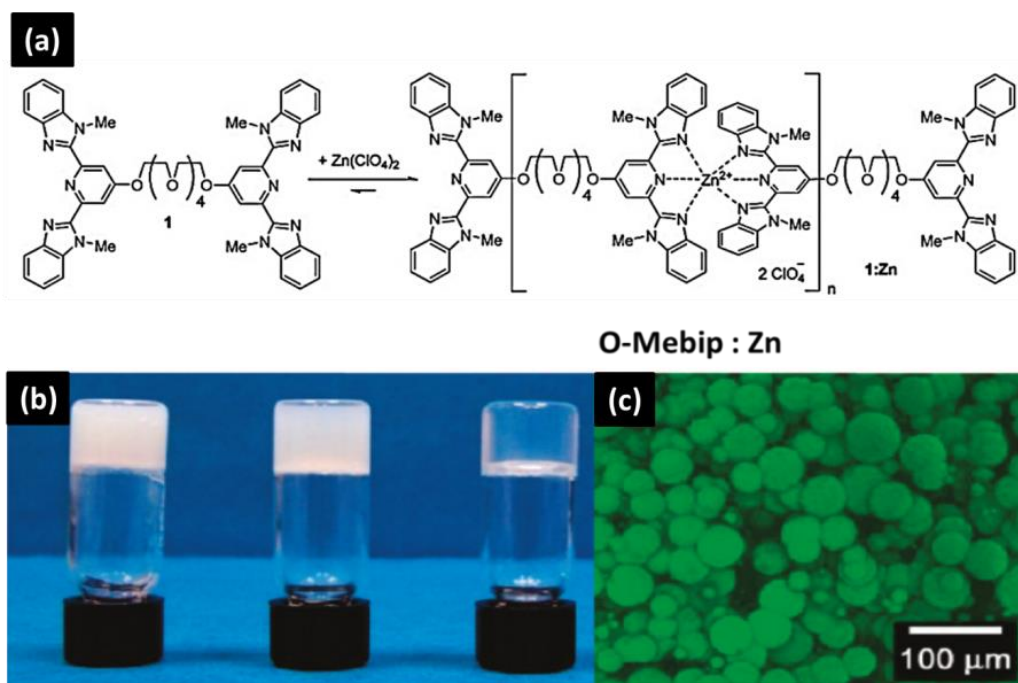
Figure 1.11 a) MSP prepared by Rowan et al. b) Gels formation of MSP in mixed solvents DMSO/water (left to right ratio of DMSO/water is 60/40, 70/30, and 80/20 (v/v) c) Laser scanning confocal microscopy (LSCM) z-projection image of the MSP gel formed in 60/40 (v/v) DMSO/water. [Adopted from Ref. 30a].

stimuli responsive properties. The gel formation property had been checked in a mixture of polar/non-polar (DMSO/H$_2$O) solvents. The appropriate ratio for gel formation of MSP had been found to be 60/40 (v/v).[30a] The globular particles formed with average diameter around 50 μm at 60/40 ratio of DMSO/H$_2$O. The particle size had gradually decreased upon variation of the ratio of DMSO/H$_2$O from 60/40 to 80/20 (v/v). This trend coincided with a decrease in the opacity of the gel samples.

1.2.1.2 Star-Shaped MSPs

Demas, Fraser and their co-workers[36] have developed a ruthenium based star-shaped metallo-supramolecular polymer for application in oxygen sensing. In this context, ruthenium tris(bipyridine)-centered polystyrene materials ([Ru(bpy(PS)$_2$)$_3$](PF$_6$)$_2$) had been prepared by
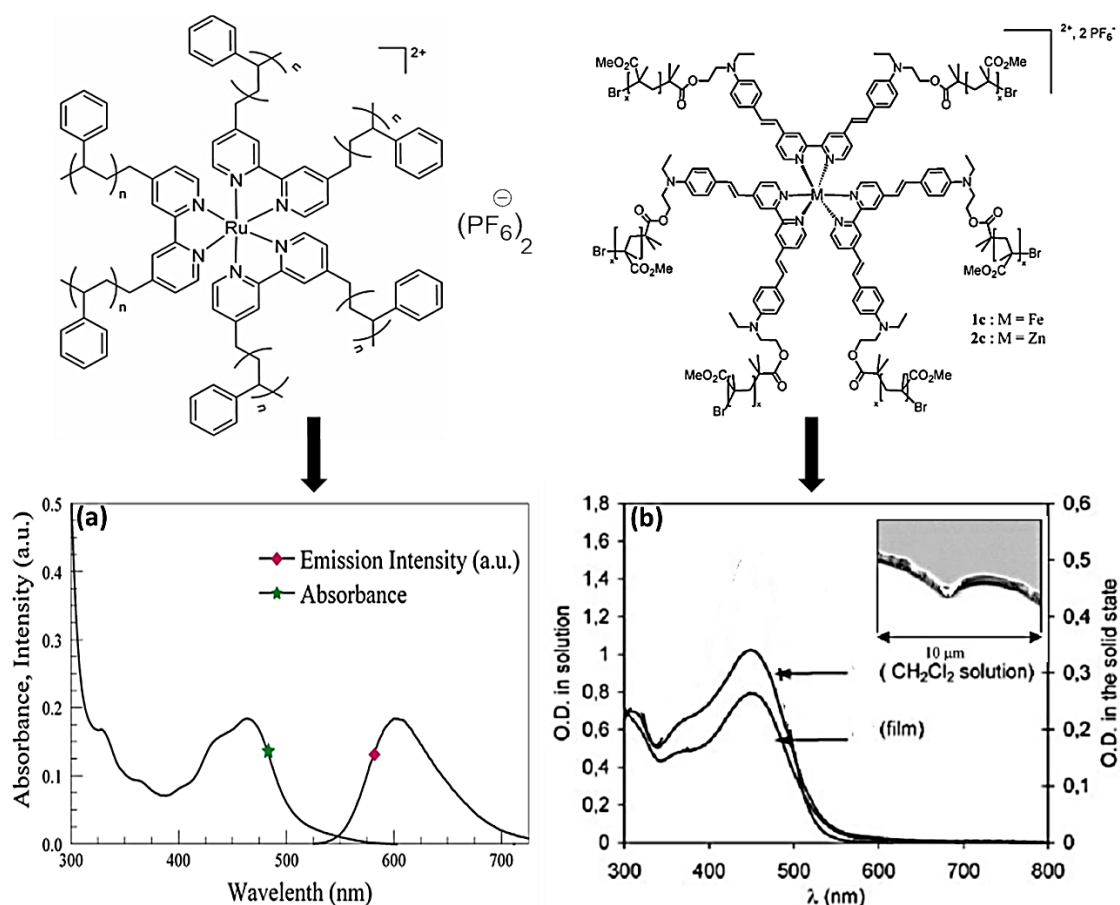
Figure 1.12 Star shaped ruthenium and iron, zinc based MSPs. a) Absorption and emission spectra of ([Ru(bpy(PS)$_2$)$_3$](PF$_6$)$_2$) in DCM. b) Emission spectra of zinc based star shaped MSP (inset- SEM image of zinc-star shaped MSP thin film). [Adopted from Ref. 36 and Ref. 37].

atom transfer radical polymerization (ATRP) of styrene from a hexafunctional Ru complex initiator, $[Ru\{bpy(CH_2Cl)_2\}_3](PF_6)_2$. In 2003, H.L Bozec and his coworkers[37] also have developed a Fe(II) and Zn(II) based star shaped MSPs for nonlinear optical (NLO) applications. The absorption and emission spectra of ruthenium and zinc star shaped MSP are presented in Fig 1.12. The solid absorption clearly proved that the metallic tris(terpyridine) remain intact within thin film state. Further SEM images revealed the formation of very uniform thin films with a varied thinckness of 1 μm-2 μm without any chromophore aggregation.

1.2.2 *Introduction about MCCPs*

In MCCPs the metal complexes are formed on covalently connected conjugated polymers containing ligand groups, hence the polymer back bone is stable and irreversible. Metal containing synthetic polymers are emerging as an interesting and broad class of easily processable materials with properties and functions that complement those of state-of-the-art organic macromolecular materials. Incorporation of metal atoms into synthetic polymer chains may also lead to appropriate properties and thereby generate a new and flexible class of functional materials. Further a diverse range of different metal centers ranging from main-group and transition metals to even lanthanide ions can be used to tune the optical/magnetic properties. The strong interaction between organic and inorganic components also creates unique photophysical, electrochemical and photochemical properties. These hybrid conjugated polymer materials have found potential applications in sensors, solar energy conversion, electroluminescence, nonlinear optics, and photo refraction.[38] Polymers that contain bidentate or tridentate ligands on the main chain were mostly used for metal incorporation. Conjugated polymers are characterized by the presence of a metal directly coupled to the polymer backbone or coupled to the backbone by a conjugated linker group. As a result the polymer and the metal group can affect each other's properties directly. Based on the position of metal complexes in the polymer backbone, MCCPs are mainly divided into two types:

 1.2.2.1 Main-chain MCCPs
 1.2.2.2 Side chain MCCPs

1.2.2.1 Main-Chain MCCPs

Main chain MCCPs can be synthesized by direct incorporation of metal-ligand moiety into the conjugated polymer main chain (Fig. 1.13). Until now, a number of novel conjugated polymers containing transition-metal complexes have been explored, and significant advances in their optical and electronic applications had been achieved. Unlike pure organic or inorganic polymers, the metal containing conjugated polymers have properties of both of them.
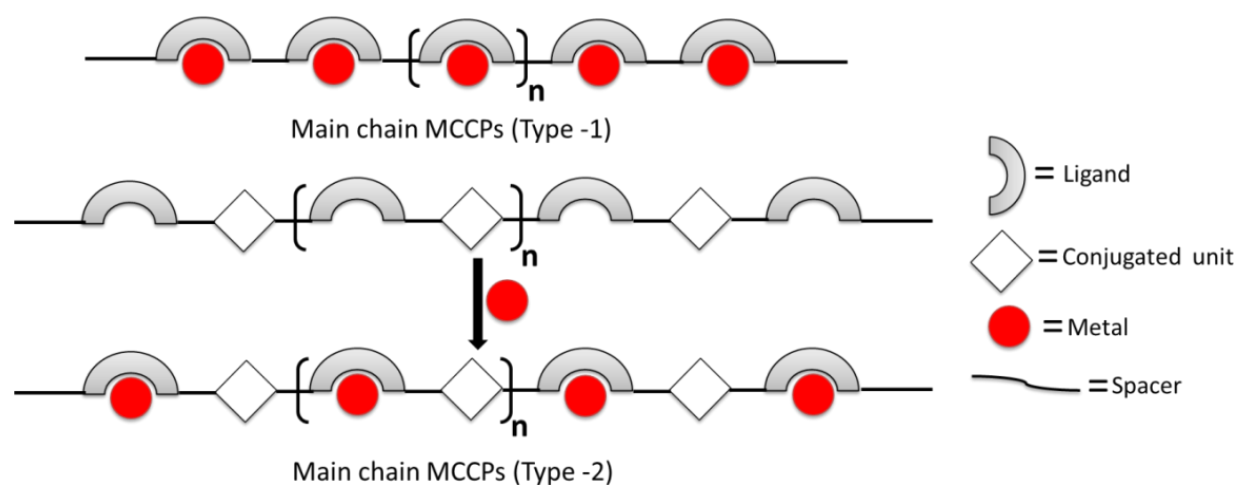
Figure 1.13 Schematic representation of main chain MCCPs

This imparts unique properties to the molecular systems so formed, making them very useful materials in the form of synthetic metallic conductors, ferroelectrics, molecular ferromagnets, one-dimensional conductors and NLO materials.[39] Transition-metal complexes containing conjugated polymers exhibit excellent electronic and optical properties.[40] Hence, study of this class of polymers has attracted great interest in recent years.

Bipy, terpy, and phenanthroline ligands are important building blocks for metal containing conjugated polymers because of their strong binding affinity towards metals such as transition metals and *f*-block elements. Several research groups have been working on the generation of various luminescent conjugated copolymer structures containing transition metals in the polymer main chain.[41-45] Yamamoto and his co-workers[41] have prepared ligands containing polymers such as poly(pyridine-2,5-diyl) (PPy), poly(2,2'-bipyridine-5,5'-diyl) (PBpy), 3-,4-, and 6-methylated poly(pyridine-2,5-diyl)s (PMePy's), poly(6-hexylpyridine-2,5-

diyl) (P6HexPy), poly(3,3'-dimethyl-2,2'bipyridine-5,5'-diyl (P3MeBpy) and poly(6,6'-dihexyl-2,2'-bipyridine-5,5'-diyl) (P6HexBpy) from their corresponding monomer dihalo compounds by dehalogenation polycondensation and further investigated their transition metal complex formation, catalytic reactions, n-type electrically conducting properties, optical properties, and alignment on various substrates.
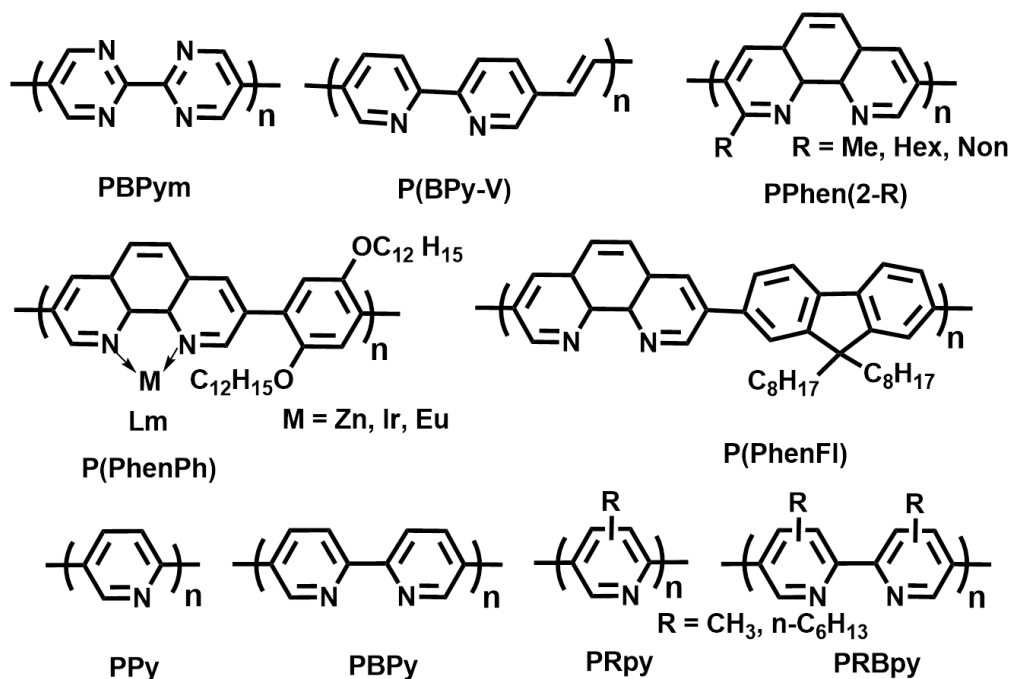
Figure 1.14 Main chain ligand containing conjugated polymers prepared by Yamamoto and his coworkers.

1,10-phenanthroline containing polymers are very important for metal coordination. Yamamoto et al.[41a] have tuned the emission color of polymer P(PhenPh) by changing the metal ion (Fig 1.15b, c). They have also studied acid effect on the optical properties of polymers. The changes in absorption and emission spectra of P(PhenPh) are shown in Fig 1.15a,b. The absorption spectra clearly indicated the red shift of absorption from 385 nm to 440 nm. The PL of polymer had quenched drastically due to the protonation on nitrogen of imine. The same phenomenon had been observed for other polymers as well. The P(PhenFl) polymer had shown excellent response to a wide variety of metal ions including alkali and alkali earth metal ions.[41b] The emission color of polymer P(PhenFl) had been tuned wide range of colors by changing the metal ions Mg^{2+}, Zn^{2+}, Al^{3+} and Ni^{2+} (Fig 1.15c).
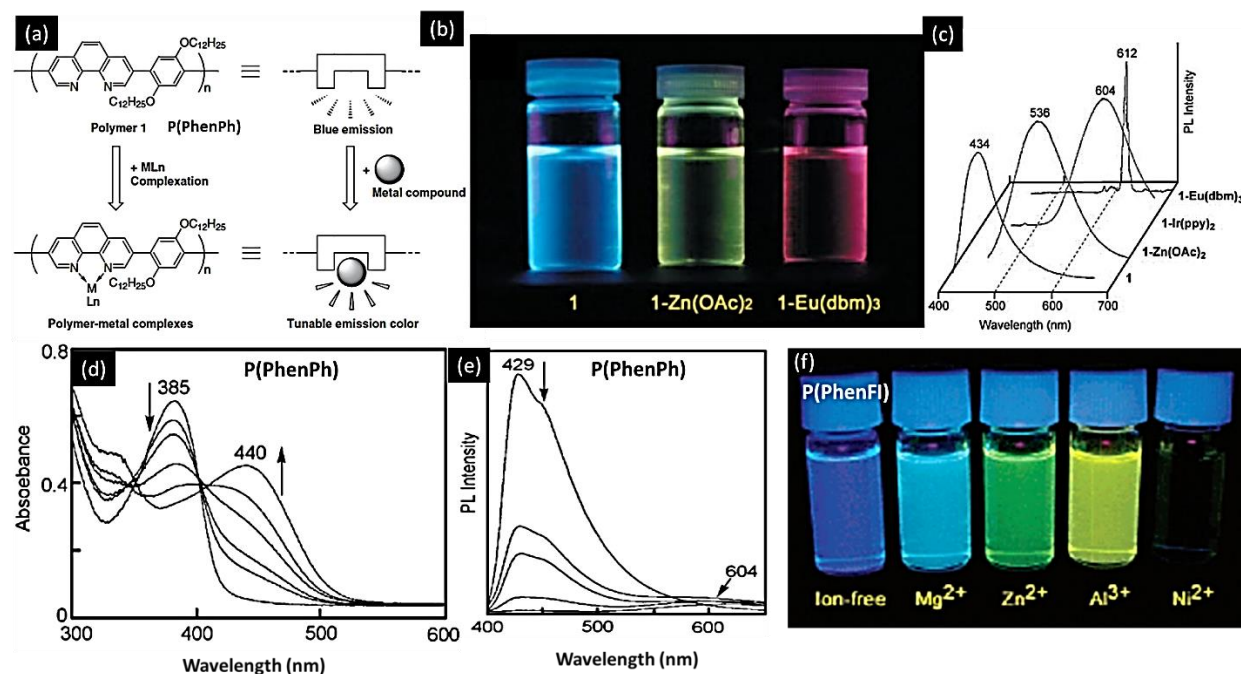
Figure 1.15. a) Chemical structure of P(PhenPh) polymer and its metal-complex. b) and c) Emission colors of P(PhenPh) and its metal complexes under UV-irradiation and their PL spectra. d) and e) Changes in absorption and emission spectra of P(PhenPh) in $CHCl_3$ (2.0 × 10^{-5} M - repeating unit) at various concentrations of trifluoroacetic acid. f) Emission colors of P(PhenFl) without and with metal ions in mixture of THF-methanol (The photographs has taken under excitation with UV-light (365 nm). [Adopted from Ref. 41a, b].

Cyclic Phen-BT-bPy
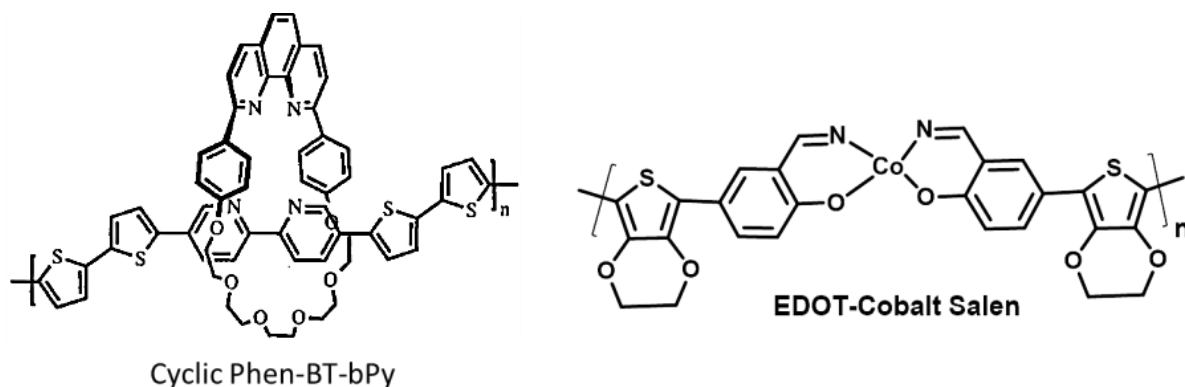
Figure 1.16 Main chain ligand containing conjugated polymers prepared by Swager and his coworkers.

Swager et al.[42] have prepared the first conducting conjugated polymer-based metallorotaxanes by electrochemical polymerization (cyclic Phen-BT.bpy); that are capable of responding to transition metal ions like Cu^{2+} or Zn^{2+}. They have also demonstrated the use of an Co(II) based electropolymerizable metallo polymers based on EDOT as a sensor for nitric oxide (NO) (Fig. 1.16). Card and Neckers have[43] developed one of the earliest methods of using a

grafting approach to attach bipyridine to an existing polystyrene polymer strand is a ligand. Peng et al.[44] had reported the direct copolymerization of charged Ru(II) bipyridine complexes using the Heck coupling reaction which is the one of the first examples of this category. They have measured UV-Visible spectra for monomer and polymers (Fig. 1.17). The absorption spectra of polymers had shown interesting properties.
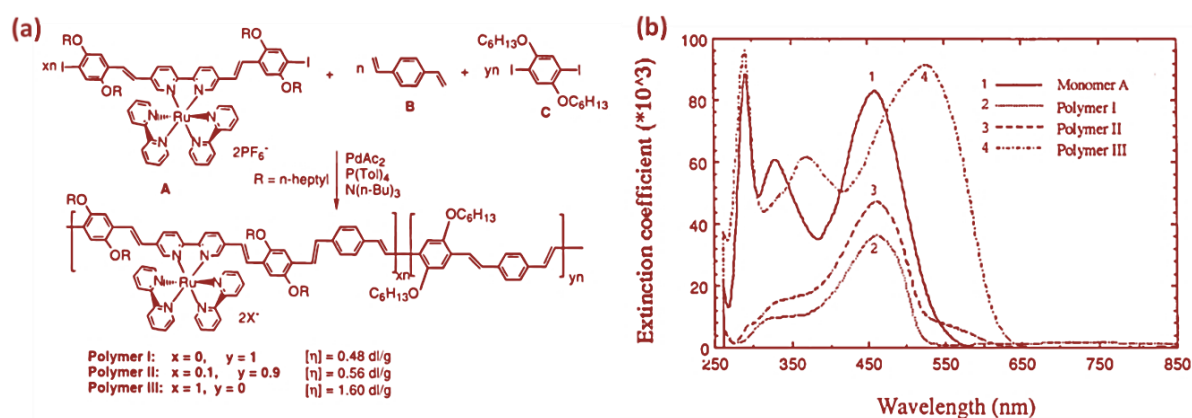
Figure 1.17 a) Main chain ligand containing conjugated polymers prepared by Peng et. al and b) absorption spectra of monomer and polymers I-III.[Adopted from Ref. 44].

The ligand-centered transition due to bipyridine still exists at around 285 nm even after polymerization (Fig. 1.17). The absorption band shifted towards longer wavelengths for metal centered transition (around 326 to 370 nm). In polymer, the metal to ligand transition (MLCT) has also shifted towards longer wavelengths compared to monomer. By controlling the ratio of monomers, the longer wavelength absorption band of polymer has been adjusted (Fig 1.17). Wang et al.[45] have explored conjugated polymeric systems with a bipyridyl-phenylene vinylene backbone (Fig. 1.18) for Pb^{2+}, Fe^{2+}, Fe^{3+}, Cu^+, Sb^{3+}, and lanthanides metal ions sensing.
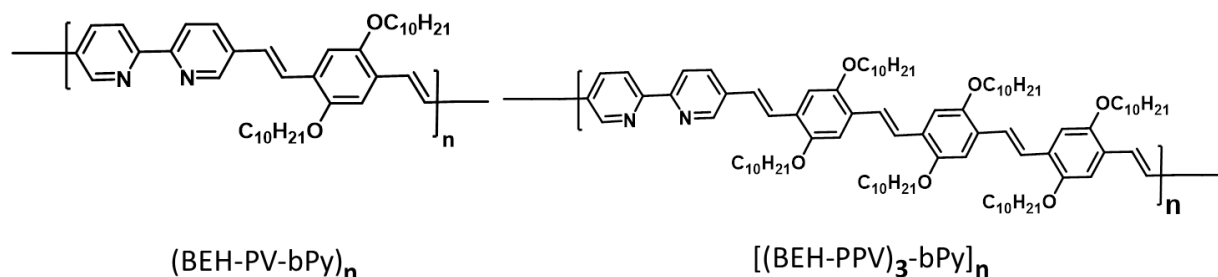
Figure 1.18 Main chain ligand containing conjugated polymers have prepared by Wang et al.[45]

1.2.2.2 Side-Chain MCCPs
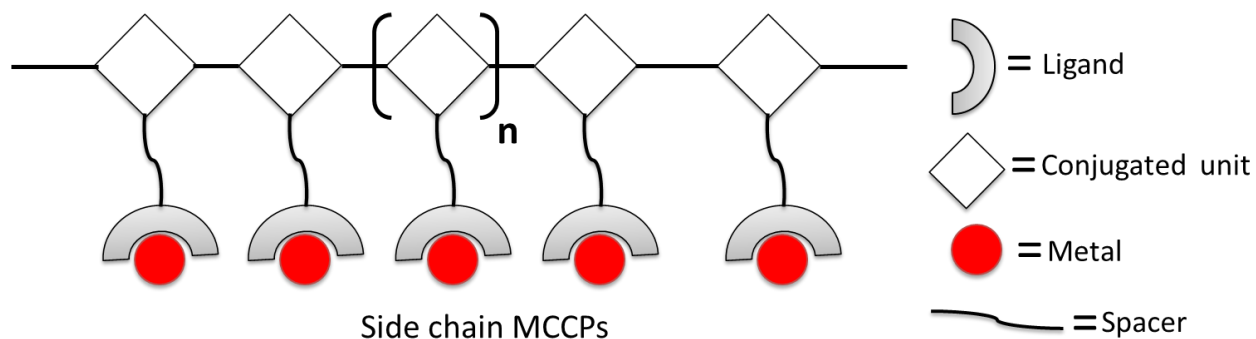
Figure 1.19. Schematic representation of side chain MCCPs

Side-chain metal containing conjugated polymers is a selected sub-field of polymer science, which mainly deals with the building of novel electro-optical and catalytic materials. A variety of hybrid materials displaying metal-specific properties such as luminescence, magnetism and conductivity had been achieved keeping the advantage of processability and solubility inherent to the polymer backbone. In this regard, the metal ions from the lanthanide series are particularly interesting because of their characteristic intense emissions with distinctive colors depending on the choice of metal.

In 1998, Kimara et al.[46] have developed poly(p-phenylenevinylene) (PPV) based side chain metal containing conjugated polymer for fluorescence chemosensing of metal ions. They have synthesized PPV containing terpyridyl fragments in the side chain using Witting reaction. The fluorescence of polymer had quenched or shifted by the addition of different metal ions. In 1999, Chan and his workers[47] have prepared light emitting conjugated polymers side chain bearing terpyridine. They have prepared a series of yellow light emitting PPVs which contain pendant bis(2,2′:6′,2′′-terpyridyl) ruthenium(II) $[Ru(tpy)_2]^{2+}$ and bipyridine type complexes. The absorption spectra of polymers (1b, 2b) showed an approximately 440 nm band correspond to the π-π^* electronic transitions of polymer main chain (Fig 1.20). Another intense peak had been observed at around 290 nm, due to pyridine ligand π-π^* electronic transitions. Moreover, a shoulder has been found at around 500 nm, which had originated from MLCT.
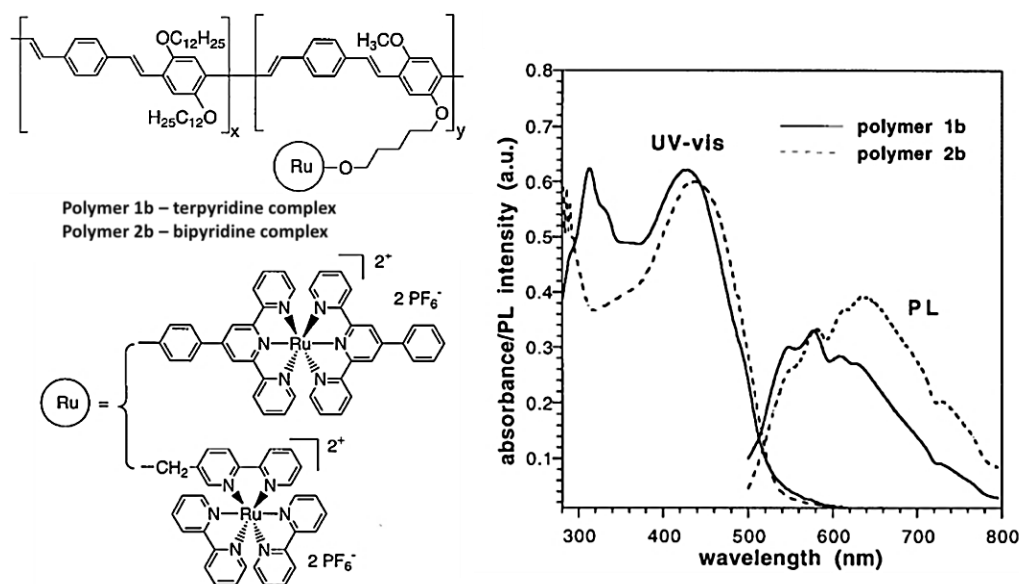
Figure 1.20 Poly(p-phenylenevinylene) based side chain metal containing conjugated polymer and absorption and emission spectra polymer 1b and 2b. [Adopted from Ref. 46].

1.2.3 *Side Chain Metal Containing Polymers*

Shunmugam et al.[48] have investigated the optical properties of poly(methylmethacrylates) (PMMA) functionalized with terpyridine groups on the side-chains coordinated with Eu(III) and Tb(III) ions (Fig. 1.21). The polymer films upon coordination with Eu(III) displayed a characteristic metal-based red emission while those prepared with Tb(III) showed green
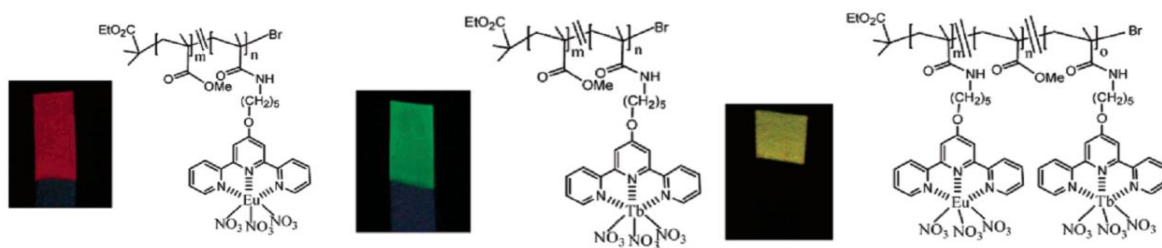
Figure 1.21 The optical properties of poly(methylmethacrylates) (PMMA) functionalized on the side-chains with terpyridine groups coordinated with Eu(III) and/or Tb(III). [Adopted from Ref. 48].

emission. A unique yellow luminescence was generated when these two different metal ions were together incorporated (1:1 ratio) into the polymer backbone. The same group has also reported a novel white-light emitting terpyridine based MSPs,[49] comprising of two-emitter system, a blue-emitting dysprosium-chelated polymer and a red-emitting ruthenium complex.

Fustin et al.[50] have reported the synthesis of a water soluble side-chain terpyridine-functionalized copolymer and its assembly into metallo-supramolecular gels. First, they have synthesized copolymer via controlled radical polymerization using 2-(dimethylamino)ethyl methacrylate and terpyridine-functionalized methacrylate monomers. From the ^{1}H-NMR analysis, the composition of the copolymer was found to be P(DMAMEA$_{200}$-co-TpyMA$_{4.5}$) which was further confirmed by size exclusion chromatography. The P(DMAMEA$_{200}$-co-TpyMA$_{4.5}$) copolymer has been used as a precursor for the formation of metallo-supramolecular hydrogels. A concentrated aqueous solution of the copolymer was prepared by dissolution in water. Upon the addition of cobalt (II) ions to the free-flowing concentrated polymer solution, it turned into supramolecular gel. Also, the color change (orange-brown color) (Fig. 1.22) arising from the addition of cobalt (II) ions as their chloride salt strongly supported the formation of metal-terpyridine bis-complexes between polymer chains.
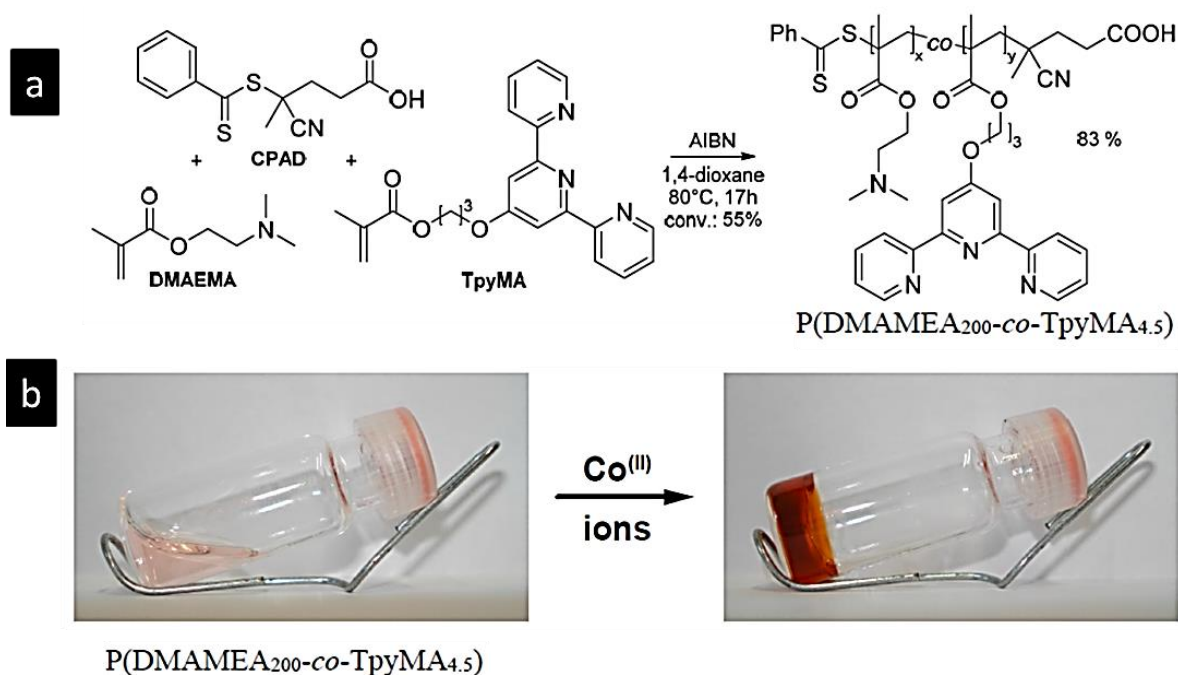
Figure 1.22 (a) Synthesis of side-chain terpyridine-functionalized poly(2-(dimethylamino)ethyl methacrylate). b) Photographs of metallo-supramolecular hydrogels obtained from a P(DMAMEA$_{200}$-co-TpyMA$_{4.5}$) copolymer solution upon the addition of cobalt(II) ions. [Adopted from Ref. 50].

1.3 White Light Emitting Polymer Materials (WLEPM)

1.3.1 *Introduction about WLEPM*

White light-emitting devices based on small organic molecules (WOLEDs), oligomers or polymers (WPLEDs) have attracted much attention among scientific and industrial communities due to their potential applications in areas such as full-colour flat-panel electroluminescent (EL) displays, back-lighting sources for liquid-crystal displays and next-generation solid-state lighting sources.[51] WOLEDs with various configurations can be obtained by doping one or more emission layers with fluorescent or phosphorescent materials. Another alternative approach to so called fluorescent/phosphorescent (*F/P)* WOLED is by replacing two of the three primary color emitting dopants with fluorophors, while still retaining its ability to achieve 100% internal quantum efficiency (IQE).

Recently, the WOLEDs have gained distinct interests because they have advantages over fluorescent lamps which contain significant amounts of toxic mercury in the tube and incandescent lighting bulb which converts 90% of consumed power into heat. Indeed, several laboratories have achieved power efficiency of WPLEDs exceeding 20 lm W^{-1} which beats incandescent light bulbs in efficiency,[52] suggesting WPLEDs can find practical applications as large area lighting sources in the near future. In 1931, Commission Internationale d'Eclairage (CIE) setup a set of standard colorimetric system, referred to as CIE1931, which is most widely used colorimetric system until now. CIE 1931 standardizes the color coordinates of equal energy point of white light as *x*=0.33, *y*=0.33 (Fig. 1.23). According to optical principles, all the colors can be achieved by mixing the three primary colors (red, green,

Figure 1.23 The CIE 1931 color space chromaticity diagram.

and blue), including white light. Different approaches for generating white light emission from polymers are discussed here.

1.3.2 Approaches for WLEPMs

1.3.2.1 Small-Molecule-Doped Polymer Type

1.3.2.2 Polymer Blend Type

1.3.2.3 Polymer Doped Small Molecule Type

1.3.2.4 Molecule-Dispersed Polymer Type

1.3.2.5 Excimer White EL Polymer Type

1.3.2.6 Preparing PWLED Through The Multilayer Device

1.3.2.1. Small-Molecule-Doped Polymer Type

This is a simple method for generating white light emission. In this method, a small amount of narrow band gap light-emitting molecules are doped into the host polymers. The partial energy transfer between doped small molecule and host polymer can be used to realize white light emission (See for example Fig.1.24 lower right corner). The host polymer is typically blue light-emitting materials and one, two, or different kinds of guest materials can be mixed.
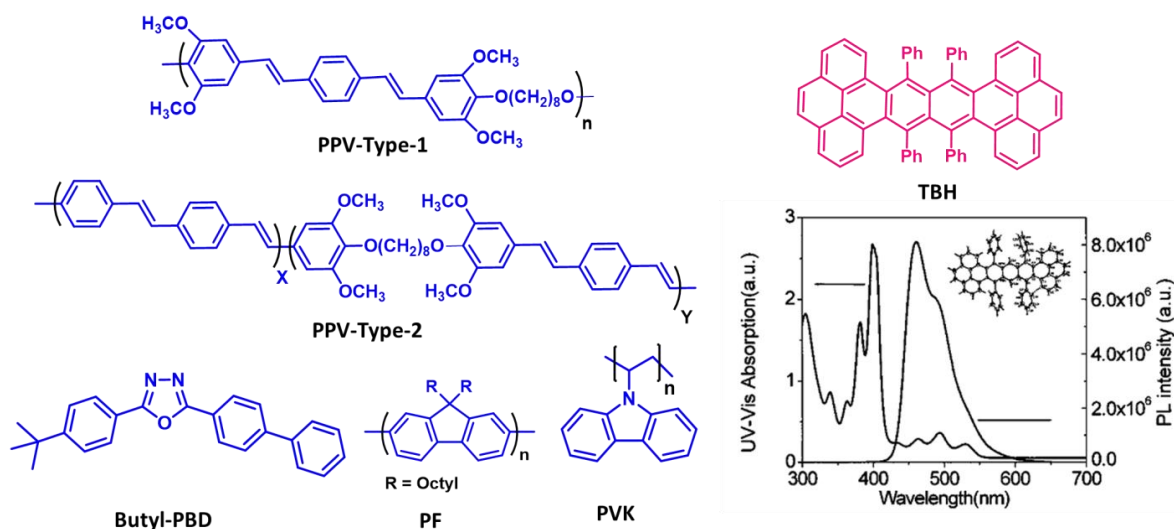
Figure 1.24 Chemical structures of PPV, PVK, PF polymer and fluorescent dye molecules, Butyl-PBD, TBH. The absorption of TBH solution and PL spectra of PF thin film is given in the right side. Note-The overlap of the two spectra infers energy transfer in this system (inset- the structure of TBH compound). [Inset – The absorption and emission spectra adopted from Ref. 53].

Normally the dopant content is in between 1000 to 1%. The basic necessity for the mixture of host and guest is that the mixture should be homogenous and stable without any phase separation. These criteria will increase the efficiency of the device and color stability as well. Regardless of thermodynamic compatibility, doping guest molecules are generally divided into fluorescence and phosphorescence dye molecules.

Hu and their coworkers [53] have reported doping of a light-emitting polymer (PPV-type 1, PPV-type 2) and small fluorescent molecule 2-(4-biphenylyl)-5-(4-tert-butylphenyl)-1, 3, 4-oxadiazole (butyl-PBD) into poly(N-vinyl carbazole) (PVK) host material, and then systematically studied the blue, green, red, and white device with PVK as the host material. The emission color of the device can be controlled by choosing reasonable chromophores and their concentrations (Fig. 1.24). Optimized white device external quantum efficiency has reached at 2.6% with color coordinates x=0.36, y=0.35.
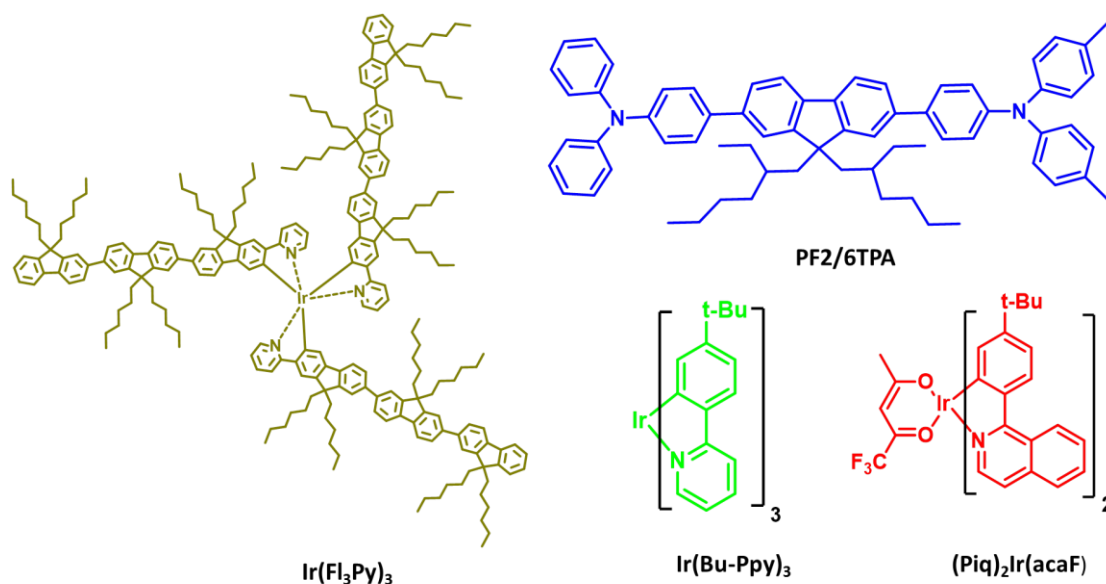
Figure 1.25 Chemical structures of polymers and phosphorescence dye molecules.

Yang's et al.[54] have reported a single orange dye (a twist acene, 6,8,15,17-tetraphenyl-1.18,4.5,9.10,13.14-tetrabenzoheptacene) (TBH) doped into blue emitting polyfluorene (PF). By this approach, a stable single layer white device was achieved (Fig. 1.24). Efficient white light can be possibly obtained by properly regulating excitons of singlet and triplets in device. Attar et al.[55] have obtained PWLED through doping of yellow-green phosphorescence iridium complexes: iridium [tri-fluorenyl] pyridine Ir(Fl$_3$Py) (Fl= fluorenyl) into blue emitting

triphenylamine end-capped polyfluorene (PF$_2$/6TPA) (Fig. 1.25). The device color coordinates were *x*=0.34, *y*=0.36 where the doping amount of phosphorescent chromophore was 2%–3%. Xu and coworkers have obtained white color emission by adjusting ratios of doped green phosphorescent *fac-tris* [2-(4′-*ter*-butyl)phenylpyridine]iridium(III) (Ir(Bu-PPy)$_3$) and red phosphorescent *bis*-(1-phenylisoquinolyl) iridium(III) (1-trifluoro)acetylacetonate (Piq)$_2$Ir(acaF), into blue emitting polyfluorene host material.

1.3.2.2 Polymer Blend Type

A polymer blend is a member of a class of materials equivalent to metal alloys. The basic principle of generating white emission device through polymer blend method is same as that of small-molecule-doped white emission polymer. Compared with small-molecules doped polymer, this technique is typically considered to possess the benefit that phase separation between materials decreases and thereby improves the device stability. Granstrom and Inganas[56]
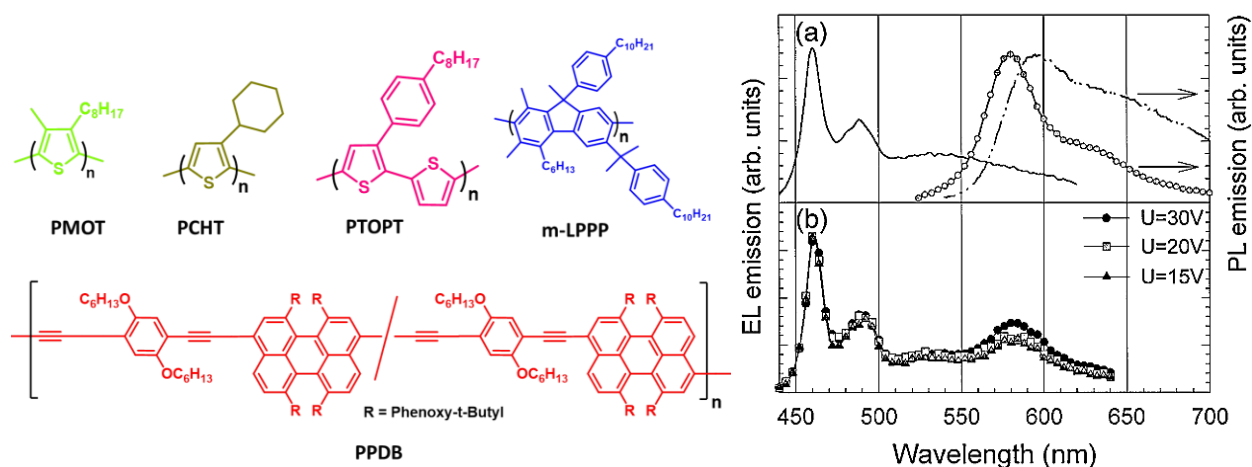
Figure 1.26 Left: Chemical structures of different light emitting polymers. Right: a) EL spectra of m-LLP (solid line), PL spectra of PPDB in solution and solid states (filled circles line – solution, dashed line – solid state). b) White PLED EL spectra from ITO/m-LPPP: PPBD/Al (thickness of polymer layer is 80 nm) as function of applied voltage. [The emission spectra adopted from Ref. 56].

have reported white emitting polymer blend of the bilayer device (Fig. 1.26). In this aspect, several polythiophene derivatives, poly (3-methyl-4-octylthiophene) (PMOT) poly (3-cyclohexylthiophene) (PCHT) and poly[3-(4-octylphenyl)-2, 2′-bithiophene] (PTOPT), have been combined to produce the white light emission. But unfortunately, the device performance was not good. Müllen and co-workers[57] have obtained a white emitting device with external quantum efficiency of 1.2% and the CIE coordinates of *x*=0.31 and *y*=0.33, by using methyl-

substituted ladder-type poly(paraphenylene) (m-LPPP) as the blue emitter and a newly synthesized perylene alkyne polymer poly(perylene co-diethynylbenzene) (PPDB) as the red-orange emitter.

Shih et al. [58] have prepared a blue emitting polyfluorene with bipolar transporting capacity poly{[9,9-bis(4-(5-(4-tert-butylphenyl)-[1,3,4]-oxadiazol-2-yl)phenyl)-9′,9′-di-n-octyl-[2,2′] bifluoren-7,7-diyl]-*stat*-[9,9-bis(4-(N,N-di(4-n-butylphenyl)amino)phenyl)-9,9-din-octyl-[2,2]-bifluoren-7,7-diyl]} (PFTO) and blended it with bipolar orange doping guest PFTO-BSeD5. Molecule PFTO-BSeD5 was made by incorporation of benzoselenadiazole (BSeD) (5 mol %) into PFTO. Highly efficient PWLED has been achieved by controlling the blending ratio of PFTO and PFTO-BSeD5. For this system, CIE coordinates obtained were x=0.32 and y=0.33; a maximum external quantum efficiency of 1.64% (4.8 cd A^{-1}) and a maximum brightness of 7328 cd m^{-2} had been achieved (Fig. 1.27).
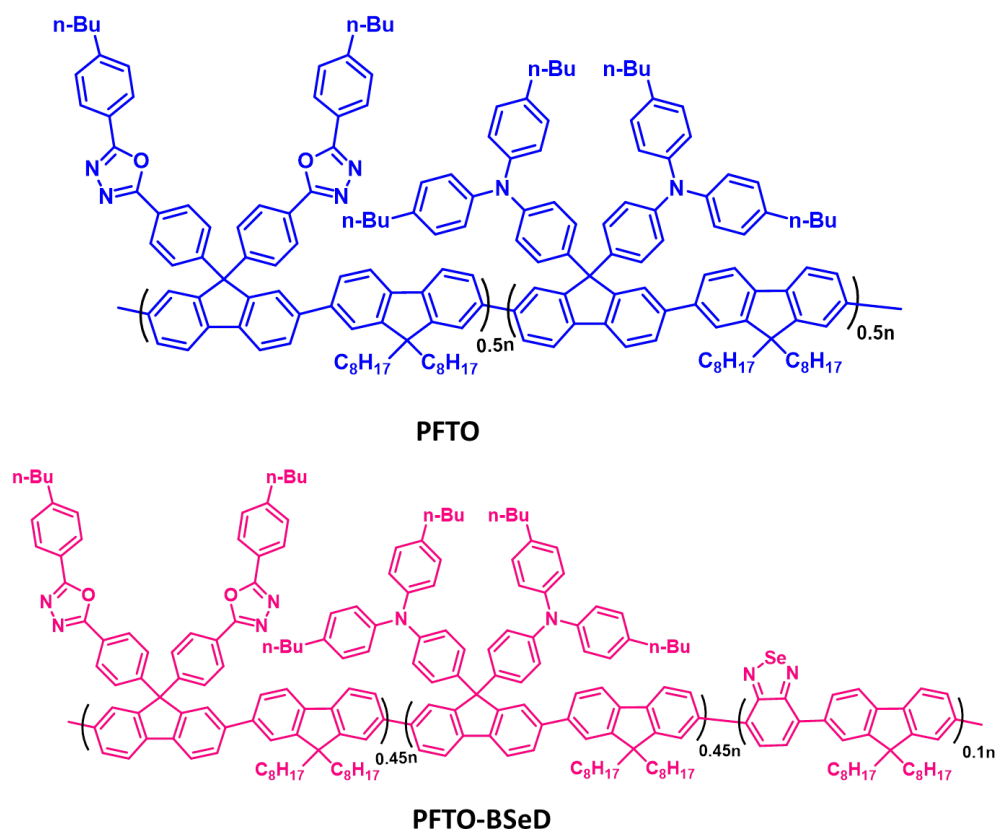
Figure 1.27 Chemical structures of different light emitting polymers.

1.3.2.3 Polymer Doped Small Molecule Type

This method is similar to small molecule doped polymer type. Here, the light emitting small molecule acts as host and light emitting polymer acts as doping guest. Wei et al.[59] have used blue emitting 9-(4-(2-ethylhexyloxyphenyl))-2, 9-dipyrenylfluorene (2PPPF) as host molecule and (2-methoxy-5 (2'-ethyl-hexyloxy)-1,4-phenylene vinylene) (MEH-PPV) as doping guest. In order to get single layer white light emitting electroluminescent device, 0.25 % of MEH-PPV was doped into 2PPPF and thereby achieved the maximum brightness of 5710 cd m^{-2}, the peak efficiency of 1.84 cd A^{-1} and the CIE coordinates of x=0.29 and y=0.38 correspond to white color (Fig. 1.28).
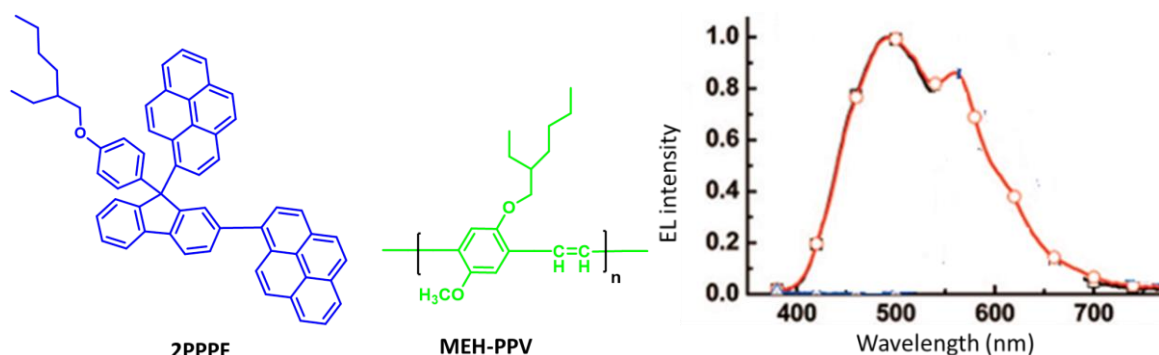
Figure 1.28 Chemical structures of MEH-PPV and 2PPPF and white electroluminescence from device of MEH-PPV and 2PPPF blend. [The emission spectrum adopted from Ref. 59].

1.3.2.4 Molecule-Dispersed Polymer Type

Fabrication of PWLED by doping and polymer blend methods have serious problem with phase separation, which leads to poor reproducibility and device performance. One solution is chemically embedding the low-band-gap dye in the conjugated polymer main chain. White emission can be achieved by adjusting the ratio of different chromospheres in polymer main chain and controlling the energy transfer between them. Wang and their coworkers have for the first time reported a single polymer chain for white light emission, which belongs to the category of molecule dispersed polymer type.[60] They have prepared blue emitting poly(fluorene) main chain based polymer (Fig. 1.29), by incorporating red chromophore into the polymer's main chain, and hanging the green chromophore in the polymer side chain. Hence red, green and blue chromophores were connected in a single polymer chain (PF-G-R). They were able to achieve highly efficient PWLED with a
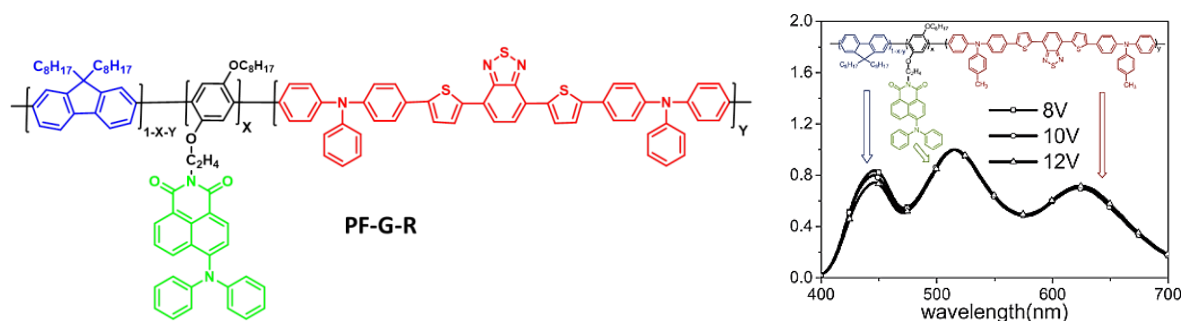
Figure 1.29 Chemical structures of fluorescent molecule dispersed type white light polymer and EL spectra of PF-G-R as a function of applied voltage. [The emission spectra adopted from Ref. 60].

maximum brightness of 3786 cd m^{-2} with good color coordinates x=0.31, y=0.34, and device efficiency of 1.59 cd A^{-1}.

Liu et al.[61] have by précising the total possible design ideas of molecule-dispersed white light-emitting polymer type, and reported two types of single white light-emitting EL polymers: (1) within a polyfluorene (blue chromophores) main chain, green and red chromophore molecules has been grafted on the side chains of polymer WRGB-P1; (2) within polyfluorene main chain, small amount of red chromophore has been embedded, while hanging green chromophore on the side chain WRGB-P2 (Fig. 1.30). Because of its high efficiency, phosphorescent dye molecule
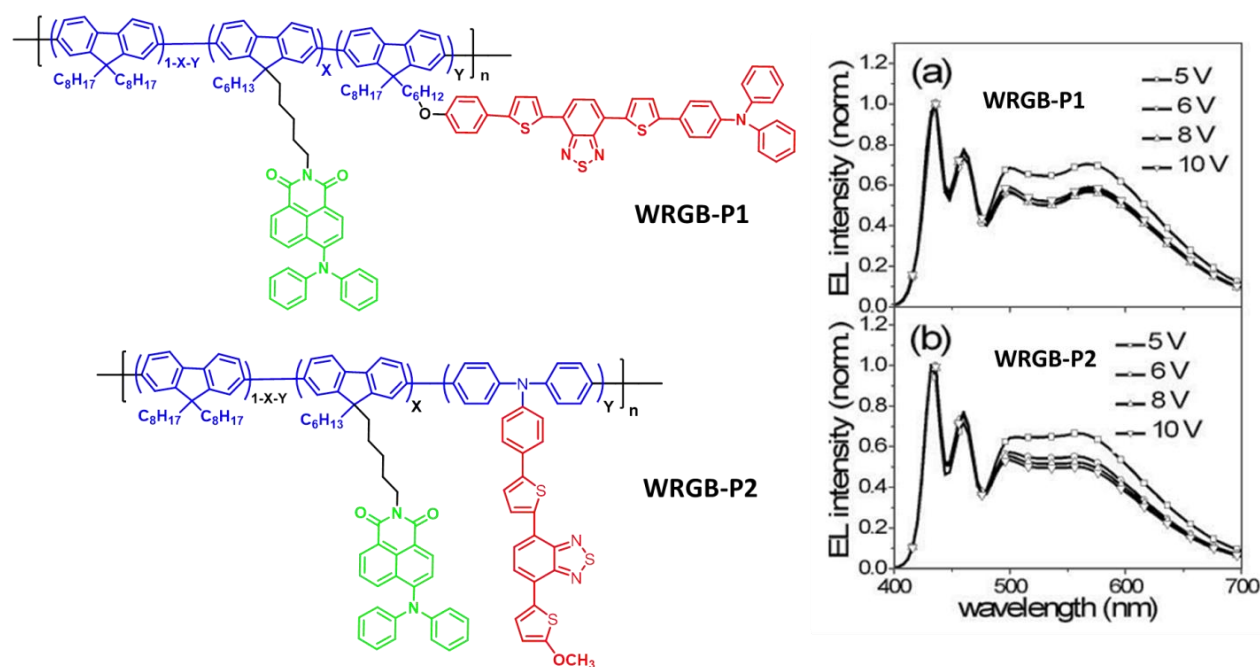
Figure 1.30 Chemical structures of single molecule white light polymer and the EL spectra of WRGB-P1, WRGB-P2 as a function of applied voltages. [The emission spectra a and b adopted from Ref. 61].

has also been dispersed into the polymer. Unprecedentedly, Cao and coworkers[62] have first introduced the triplet phosphorescent material into the molecule-distributed white EL material and thereby developed a single molecule white EL material (Fig.1.31). A blue emitting polyfluorene host polymer had been taken, with a little yellow green benzothiazole chromophores doped on the main chain. The side chain had been grafted with the red triplet iridium complexes PFBT-Phq (Fig 1.31). Adjusting the ratio of copolymerizing chromophores yielded a pure white EL. The optimized color coordinates (x=0.32, y=0.33) approached white colour. A highest luminous efficiency (6.1 cd A^{-1}) has been achieved for single-layer devices made by the series of materials, but the spectra stability has been not as good as a fluorescent molecule-dispersed polymer.
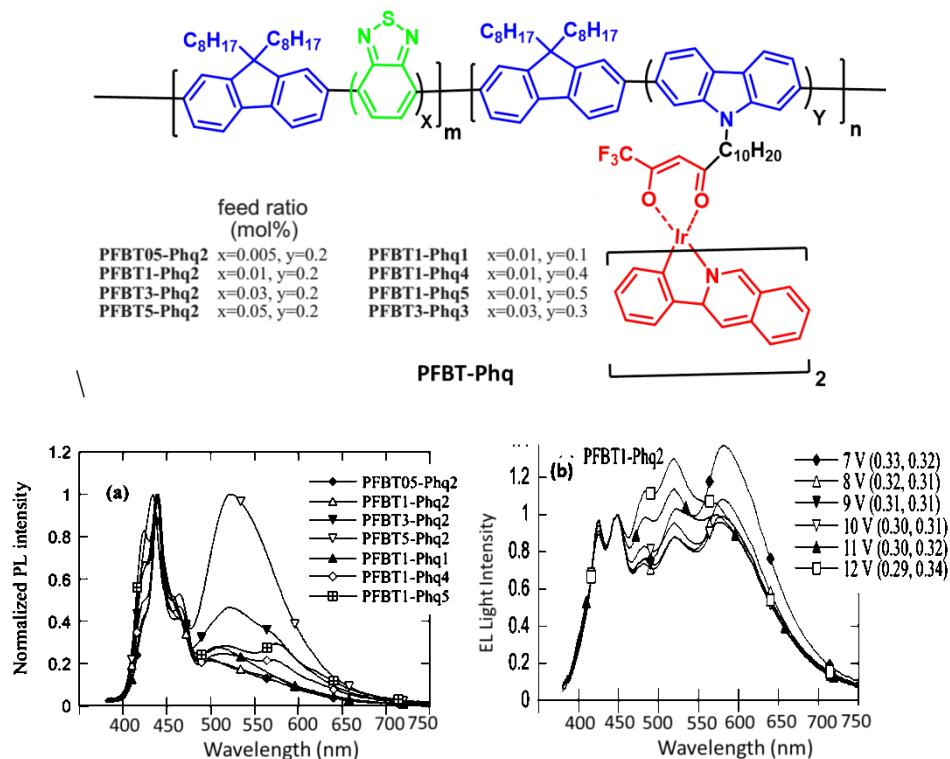
Figure 1.31 Chemical structures of phosphorescent molecule dispersed polymer and a) PL spectra of copolymer (PFBT-Phq) films. b) EL spectra of devices from copolymer PFBT1-Phq2. [PL and EL spectra of polymers adopted from Ref. 62].

In another report, corresponding to the triplet state material grafted onto the side chain, they have reported a molecule dispersed white EL polymer (**PFIrR1G04**), where the main chain contained a triplet state chromophore.[63] Here within a blue polyfluorene host material, a little

yellow-green benzothiadiazole chromophore had been doped and the iridium compound had been introduced into the polymer main chain (Fig 1.32). Further, adjusting the ratio of chromophore yielded white EL.
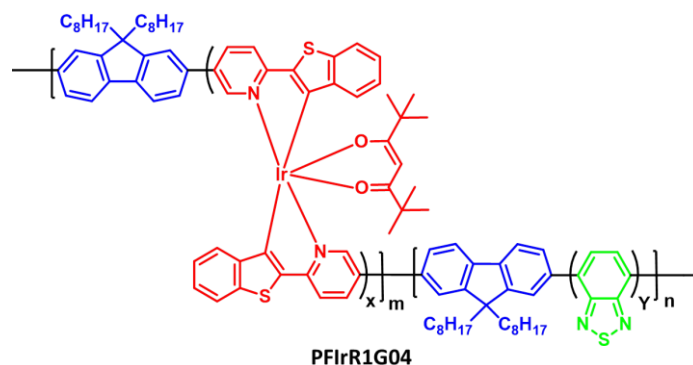
Figure 1.32 Chemical structures of phosphorescent molecule dispersed polymer.

The luminous efficiency of 3.9 cd A^{-1}, with color coordinates of x=0.31 and y=0.32. Shim and co-workers[64] have reported a single white EL copolymer poly{9,9-bis(4-octyloxyphenyl)fluorene-2,7-diyl-co-(N-hexylcarbazole-3,6-diyl)-co-[bis(2-benzothiazol-2-yl-ethylcarbazole)iridium-1,3-bis(p-bromophenyl)-propanedione-1,3-diyl]}**(PFCzIrbecs)**, in which blue fluorene-carbazole had been used as the host, and the BOPF doped with a red light-emitting $(bec)_2$IrdbmBr group, had been used as guest. When the ratio of blue light-emitting segment and red light-emitting unit was 0.98:0.02, the EL device based on polymer $PFCzIr(bec)_2$ showed white color coordinates (x= 0.31, y= 0.32).
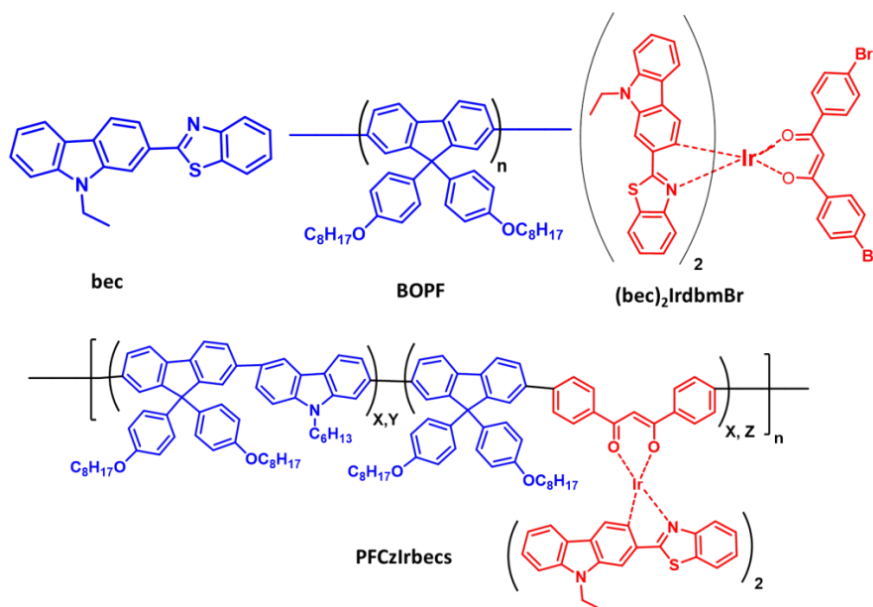
Figure 1.33 Chemical structures of phosphorescent molecule dispersed polymer.

1.3.2.5 Excimer White EL Polymer Type

Tsai et al.[65] have prepared a white light-emitting polymer by hanging the blue light emitting chromophore anthraquinone on the side chain. It showed a blue-green light in the dichloromethane solution (Fig 1.34). In the low-energy part (550 and 600 nm), the film emission spectrum displayed two small peaks, due to excimer of anthracene chromophore between side chains. When the red emission was combined with the blue emission of anthracene, a complementary white EL was achieved. The device showed color coordinates (x=0.30, y=0.34) at 12 V, but the overall performance was poor.
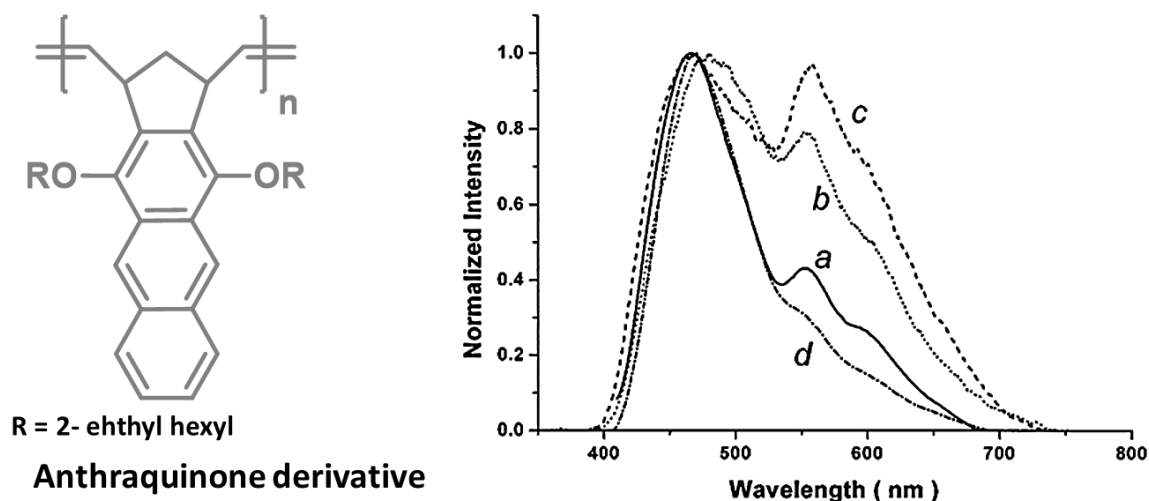
Figure 1.34 Chemical structures of white light polymer. a) PL spectrum of solid thin film. b) and c) EL spectra of single layer device at 8V and 12V. d) The emission from double layer device at 12V. [The emission spectra adopted from Ref. 65].

Kawamoto and coworkers [66] have synthesized a light-emitting polymer PACF containing 2-[4-(11-methacryloyloxy-1-undecyloxy)biphenyl-4-yl]-5-(4-trifluoromethylphenyl)-1,3,4-oxadiazole (M11OXDCF) and poly(2-[4-(6-methacryloyloxy-1-hexyloxy)biphenyl-4-yl]-5-(4-N,N-diphenylaminophenyl)-1,3,4-oxadiazole) (PM6OXDPA), with liquid crystal properties. The polymer had a certain bipolar properties because of the presence of both triphenylamine and oxadiazole units in the side chain of the polymer (Fig.1.35). The emission spectrum of PACF film has showed only one emission peak at 448 nm. Its device exhibited a new broad emission band at 550 nm along with 448 nm emission peak which was attributed to excimer formation. The device has showed maximum luminous efficiency of only 0.1 cd A^{-1} and color coordinates (x=0.29, y=0.32) at 20 V.
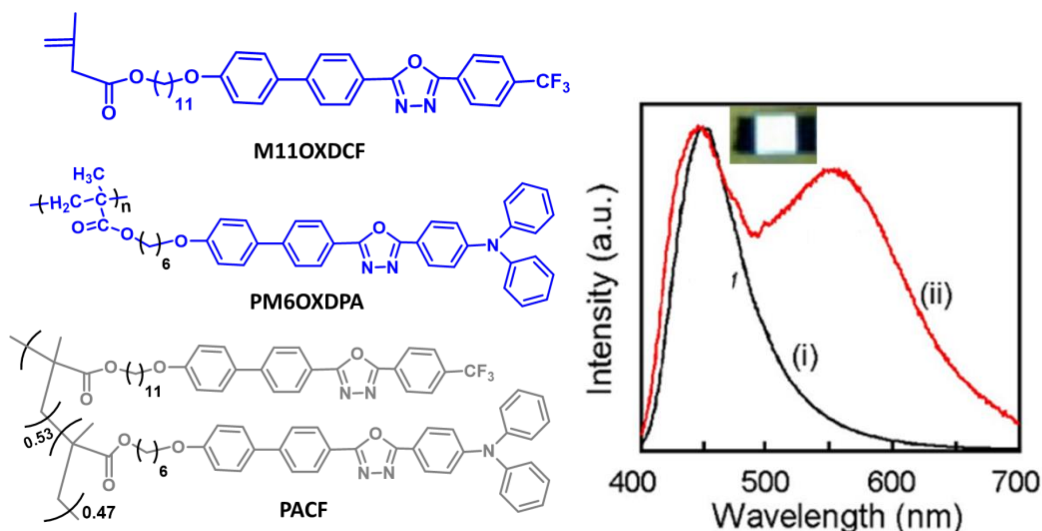
Figure 1.35 Chemical structures of white light polymer (PACF) and it's PL, EL spectra (inset - photograph of EL emission from PACF) (i) PL (ii) ITO/PACF/MgAg. [The emission spectra adopted from Ref. 66].

1.3.2.6. Preparation of PWLED Multilayer Devices

In this method, different colors are used as emitting layer to get white emission. Xu et al.[67] have reported a double-layer type PWLED (Fig. 1.36); they have used poly(N-vinyl-carbazole) (PVK) as the first blend layer and certain amount of red emitting copolymer of 9,9-dioctyl fluorene, and 4,7-di(3-hexyl-thien-2-yl)-2,1,3-benzothiadiazole (PFO–DHDBT) doped into PVK layer. The polyhedral oligomeric silsesquioxane-terminated poly(9,9-dioctylfluorene) and phenyl-substituted PPV derivative (PFO-poss:P-PPV) blend was spin-coated on top of the first layer after thermal treatment for 1 h at 60 °C. The white emitting device had been achieved by adjusting the blend ratio of each layer (PVK: PFO-DHDBT = 100:3, and PFO:P-PPV = 100:1). The device showed near white color coordinates (*x*=0.33, *y*=0.32), with maximum brightness (6300 cd m^{-2}) and luminous efficiency 4.4 cd A^{-1}(Fig. 1.37).
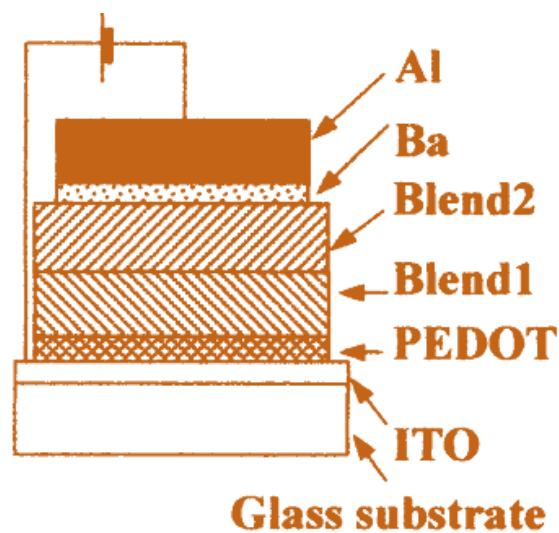
Figure 1.36 Basic diagram of a double layer PWLED device. [Adopted from Ref. 67].
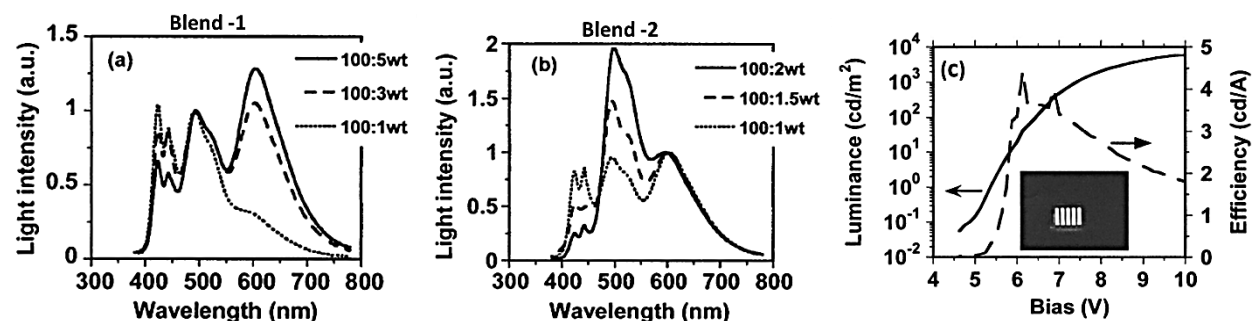
Figure 1.37 EL spectra of devices (thickness 40 nm) for blend 1 and blend 2 at a applied current density of 2 mA. a) PVK to PFO-DHDBT blend weight ratio (at weight ratio of PFO-poss:P-PPV (100:1)). b) PFO-poss to P-PPV blend weight ratio (PVK to PFO-DHDBT weight ratio is (100:3)). c) Luminous and efficiency for the device (40 nm thickness for blend 1 and blend 2, blend weight ratios of 100:1 for PFO-poss:P-PPV, 100:3 for PVK to PFO-DHDBT). Inset shows the picture of white EL emitting device. [Adopted from Ref. 68].

Sun et al.[68] have reported exciplex type PWLED composed of a polymer interfaced double layer structure (Fig. 1.38). The first layer of the device made of blend materials of (1:1 ratio) poly-TPD:PVK to enhance the hole transport and block the electrons, and the second layer used blue light-emitting poly(9,9-dihexylfluorene-alt-co-2,5-dioctyloxy-*para*-phenylene) (PDHFDOOP) and green emitting poly[6,6′-bi-(9,9 ′-dihexylfluorene)-co-(9,9 ′-dihexylfluorene-3-thiophene-5′-yl)] (PFT) blend system. The white light emitted by the device showed near white color coordinates (*x*=0.31, *y*=0.32) with a luminous efficiency of 3 cd/A^{-1} and brightness of 4800 cd/m^2.

PDHFDOOP

PFT
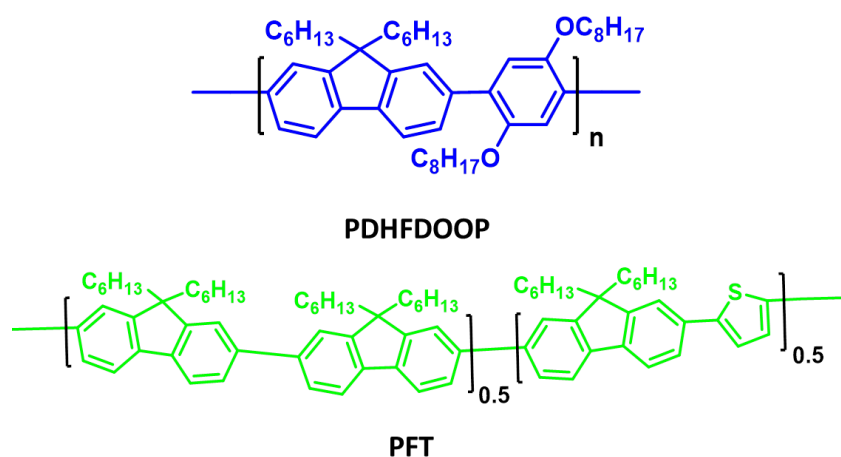
Figure 1.38 Chemical structures of different light polymers.

In 2014, Chandrasekar and coworkers[69] have a developed hierarchical reactive contact printing mediated coordination chemistry technique and created multicolor (including white color) pixels lower than 3 μm resolution (Fig. 1.39). For that, they have homopolymerised bpp unit for the first time to get a blue emitting polymer of M_n~7-8 KDa. They have fabricated polymer thin film on the glass slide which acts as template for coordination chemistry of metal ions through contact printing technique. On top of this bpp polymer film (poly), a layer of high resolution cross stripes had been printed using red (Eu(III)), and green (Tb(III)) luminescent metal ions inks over a large surface area of around 100×100 μm^2. This method finally produced a flexible film composed of multi colors pixels including white high resolution pixels of area (0.64 μm^2) in the nano/micro space.
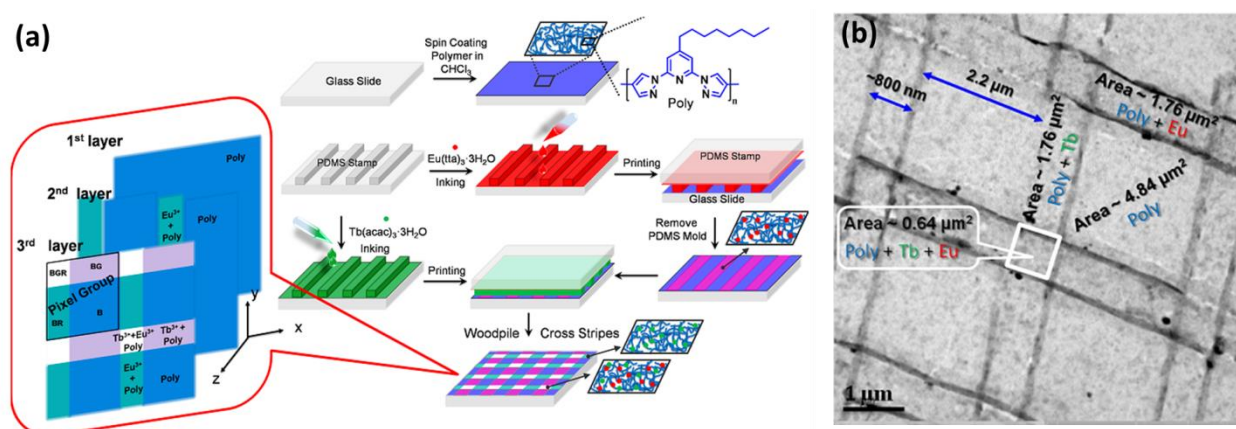
Figure 1.39 a) Graphical representation of a hierarchical reactive contact printing process leading to multicolor matrix pixels. b) TEM image of Eu(tta)$_3$ and Tb(acac)$_3$ cross stripes formed on polymer surface. [Adopted from Ref. 69].

1.4 Self-Assembly of Conjugated Polymers

Self-assembly is a process in which a disordered system of pre-existing elements forms an organized structure or pattern due to interactions among the constituents themselves, lacking external direction. When the constitutive elements are molecules, the process is called molecular self-assembly.

Molecular Self-Assembly

It is a self-governing organization of components into arrays or structures without human involvement. Macromolecular self-assembly involves spontaneous formation of supramolecular aggregates and structures in various states. Self-assembly involves the spontaneous association

of organic, inorganic or hybrid building blocks, mediated by non-covalent interactions (e.g. electrostatic,[70] van der Waals[19] and hydrophobic forces,[71] π–π stacking,[20] hydrogen bonding [22]), into stable, well-defined aggregates that exhibit structural and morphological organization across multiple length scale.

Self-assembly of macromolecules is a powerful tool for producing functional materials that combine several properties like optical, electrical, and mechanical and may respond to external conditions. For example, self-assembly provides unique potential to obtain concurrent control over the aggregation and optoelectronic properties of conjugated polymers due to their immense structural versatility, further it improves the processability of nano/micro structured materials. Self-assembled polymers materials are used in photovoltaics,[72] polymeric light-emitting devices,[73] nonlinear optics,[74] photonic bandgap materials (or dielectric mirrors),[75] optical storage[76] and recently as photonic resonators[77] (which will be discussed in detail in Chapter 5).

In principle, nanoparticles of conjugated polymers are accessible either by post polymerization dispersion of separately prepared polymers or directly by polymerization in dispersed heterophase systems. Both approaches have their advantages and limitations. The polymer chains possess a collapsed conformation in these particles, which accounts for the spherical particle shapes representing the thermodynamically favorable lowest surface per volume despite the rigidity of the polymer chain. The studies on self-assembly of synthetic macromolecules started in 1980s.[78] Self-assembly approaches have increasingly emerged as an elegant bottom-up approach for the design and fabrication of reproducible micro and nanoscale structures both in
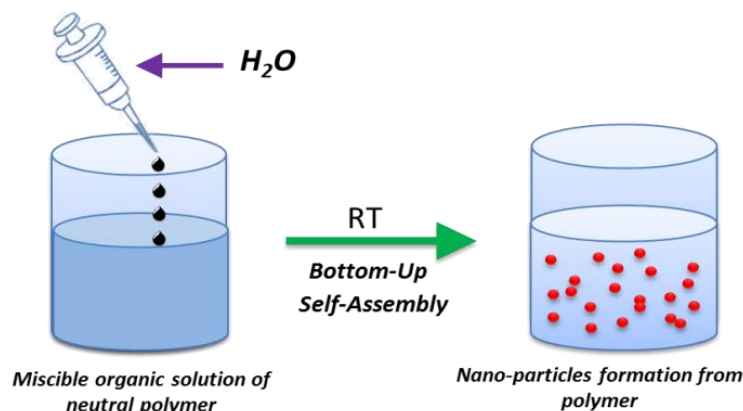
Figure 1.40 Graphical representation of formation of colloidal nanoparticles from neutral polymer in polar/non-polar solvent mixture.

solution and the solid state. Polymer scientists have begun to use self-assembly as a powerful fabrication tool. In general, macromolecular self-assembly refers to the assembly of synthetic polymers, supramolecular polymers and bio-macromolecules. Swift addition of a miscible organic solution of a neutral conjugated polymer into an excess of water results in the self-assembly of neutral conjugated polymers into isolated nanoparticles, supported by the driving force for aggregation utilized by the hydrophobic backbone (Fig. 1.40). Chen et al. [79] have prepared conjugated polymers which can form vesicles through self-assembly. They self-assembled a stiff oligomer, like polyether imide (PEI) with amino groups on its both ends and stearic acid (SA) in cyclohexane/chloroform to grow large vesicles.

1.5 Organic–Inorganic Hybrid Conjugated Polymers Materials

Figure 1.41 Pictorial representation of organic –inorganic polymer hybrid materials.

Organic–inorganic hybrids have the benefits of both soft organic frame and hard inorganic building blocks in a particular material. The unique characteristics of hybrids originate from individual characteristics of both the organic and inorganic constituents along with the interfacial contributions. The incorporation of conjugated polymers into an inorganic medium leads abundant possibilities to achieve superior and multiple materials properties. For example, hybrid materials have the conductivity property of conjugated polymers and magnetic and

optical, the redox properties of metal complexes.[80] A number of different methods have been reported to make organic-inorganic hybrid nanoballs. Figure 1.42 illustrates[81] the different possible approaches already available for preparing organic/inorganic hybrid materials.
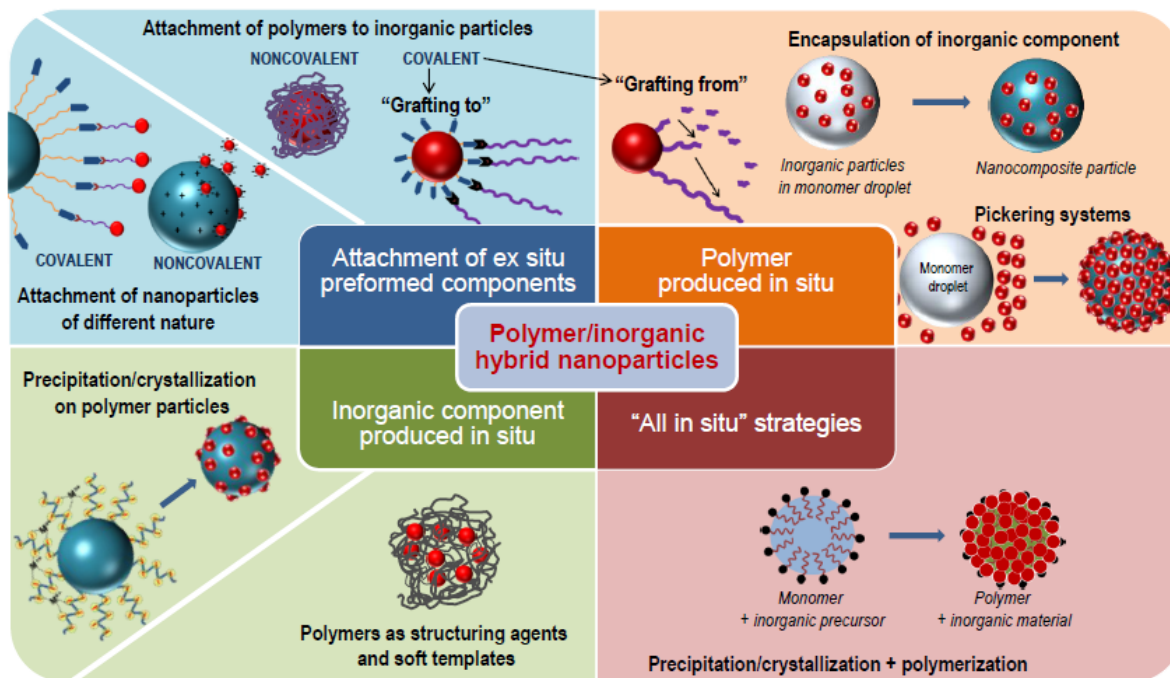
Figure 1.42 Approaches for the preparation of polymer/inorganic hybrid nanoparticles. [Adopted from Ref. 81].

Polymer/inorganic hybrid nanoparticles have several applications in various areas, including biomedicine,[82] optoelectronics,[83] coatings,[84] and catalysis[85]. In general terms, the polymer part typically has structural functions like solubility and processability and may alter the optical and electronic properties of the final materials, whereas the inorganic constituent can provide functionalities such as thermal properties, luminescence, magnetism, catalytic activity, etc.[86] The ultimate properties of the organic/inorganic hybrid nanoparticles are very often not a simple combination of the properties of the individual component, but a unique result from combined effects from organic/inorganic parts. The development of hybrid materials is so important because of they have found potential applications in various fields. Most of the polymer/inorganic materials prepared from polymer composite and sol-gel methods.[84] In 2011, Chandrasekar and his coworkers[17] have reported for the first time organic-inorganic hybrid materials by performing coordination chemistry on the surface of the self-assembled ligand structures (see Fig. 1.5 for general discussion and also Chapter 4).

1.6   Conjugated Polymer Spheres as Photonic Micro-Resonators

1.6.1 *Whispering Gallery Modes (WGMs)*

WGMs are waves that can travel around a concave surface. In 1878, Lord Rayleigh first discovered and explained the whispering-gallery effect of sound waves observed in St. Paul's Cathedral[88] (Fig. 1.43). For instance, light waves having WGMs have important applications in nondestructive testing,[89] cooling, [90] sensing, [91] lasing, [92] and in astronomy.[93] WGMs are electromagnetic resonances that are found in circularly symmetric dielectrics, which trap light in a circling orbit by total internal reflection. However, they can also exist for other waves such as light, microwaves,[94] in the form of matter waves for neutrons,[95] and electrons.[96] Optical WGMs occur in small dielectric circular shapes like spheres,[77] hemisphere,[97] rings,[98] spheroidal,[99] toroidal [100] and cylinders,[101] with diameters of a few micrometers. In an on resonance situation, when mλ = Ln$_{eff}$ (where *m* stands for the angular mode number, λ is the wavelength of the light, *L* is the circumference of the microcavity and n_{eff} is the effective refractive index) the circulating light returns to the same point in phase giving standing waves for certain resonance frequencies (modes).
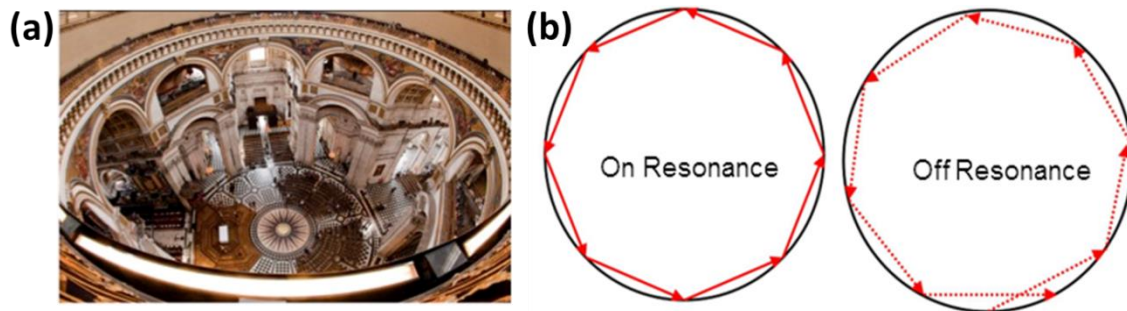
Figure 1.43 a) St. Paul's Cathedral exhibiting WGM effect of sound waves. b) Schematic representation of a spherical WGM resonator with ON/OFF resonance.

WGM resonators can have an exceptionally high-quality factor *Q* (is discussed in section 1.6.2) that makes them promising devices for applications in optoelectronics and fundamental physics.[102] Optical micro resonators have been recently anticipated as an effective method to achieve label-free detection of target material for chemical and bio-sensing applications.[103] Specifically, WGM sensors exploit sharp photonic resonances arising from light orbiting repeatedly by quasitotal internal reflection. Small changes of the refractive index in the region surrounding the microresonator, for example due to the attachment of target biomolecules at its

surface, can be probed with high sensitivity via the corresponding frequency shift in the WGM resonances.

1.6.2 *Quality Factor of Resonators*

One of the most significant quantities that define the performance of any resonator (on resonance) is the quality factor or Q-factor. It can be defined as:[104]

$$Q = \omega_0 \frac{\text{Stored energy}}{\text{Power loss}} = \omega_0 \tau = \frac{\omega_0}{\Delta\omega_{\text{FWHM}}}$$

Here $\omega_0 = 2\pi\upsilon_0$ is the angular frequency and υ_0 is the frequency of the resonance, τ is the cavity ring down lifetime i.e. the time required for the field intensity to decay by a factor of e and $\Delta\omega_{\text{FWHM}} = \tau^{-1}$ is the line width of the resonance peak at full-width-at-half-maximum or FWHM depicted in angular frequency. In general, high Q–resonators possess Q-factors of ~ 10^3 to 10^6 and those with Q–factors above 10^7 are called ultra-high Q–resonators. In this thesis work we have made some attempts to create high Q–resonators composed of self-assembled polymer blends (discussed in Chapter 5).

The above equations for the quality factor can be explained in two different ways. The Q-factor measures the time for the exponential decay of the photon energy stored or trapped inside the resonator taking into consideration the number of full field oscillations (times 2π). Therefore a resonator with higher Q-factor can store or trap energy inside for more time. Q-factor can be construed as the total energy of the circulating modes inside the resonator at equilibrium divided by the amount of energy that has to be pumped (through laser) to the resonator in the time of one full field oscillation (times 2π) so as to sustain the equilibrium. This means that for a higher Q-factor, the total energy stored inside the resonator of the circulating modes is proportionally higher at the same pumping power. Ultra-high Q-factors resonators can accordingly allow the circulating intensities to attain very high values. Normally Q-factor is measured from the frequency of the resonant peak in terms of the number of FWHM line widths of that resonance peak.

1.6.3 *Free Spectral Range (FSR)*

The FSR is the frequency interval between the intensity maximum of two resonant peaks. The FSR of the any resonator is the reciprocal relationship with the photon round trip time in the

cavity. In order to achieve wide spectral range between the peaks, we have to choose small diameter having ring. The FSR of the ring is inversely proportional to the circumferences of the ring. The FSR or $\Delta\lambda_m$ of the cavity is presented by

$$\Delta\lambda_m = \frac{\lambda^2}{2n_g l}$$

Where l is length the of the cavity, λ is the wavelength of light, n_g is the group refractive index of medium.

1.6.4 *Spherical WGM μ-Resonators*

`In 1939, Richtmyer et al.[105] have reported an innovative approach to investigate the resonances in a spherical microparticle made of a dielectric material exhibiting high-resonance modes. In 1961, first time Garrett et al.[106] have reported that spherical resonators of optical waves could be used as laser resonators; they have observed pulse laser oscillation in highly polished Sm^{+3}-doped CaF_2 spheres with a diameters in the range of one and two millimeters. A vital condition for the microsphere to trap light is the refractive index of microsphere should be higher than that of the medium. Light can be trapped in a sphere due to continual total reflection to realize lasing action. It has been proven in dye solution droplets. Recently, dye-doped conjugated polymer particles are found to be superior to such dye solution droplets for practical uses. Gonokami et al.[107] have studied it using organic dye-doped polystyrene particles with diameters in the range of 2-20 μm. They have observed lasing action in spherical cavity modes with very high Q-factors and effective optical nonlinearity suitable for optical data processing systems. Until now, WGM photoemission and lasing have been reported on inorganic microdisks and spheres. Moreover, numerous organic microstructures exhibit WGM emission such as polymeric thin films,[108] polymer disks,[109] polymer blends,[110] rings,[111] spheres and fibers, [112] liquid crystals and liquid droplets [113] most of which consists of a dielectric medium doped with a fluorescent dye. But only two recent reports are available for WGMs observed from self-assembled conjugated PL polymers microspheres.

In November 2014, Tabata et al. [77a] have reported WGM photoemission from self-assembled conjugated polymer microspheres. They have synthesized alternating copolymers based on two arylene groups as the repeating units (one of the polymers having fluorene and

thiophene as repeating units), made microspheres through simple bottom–up self-assembly technique and observed WGM photoemission from microspheres of conjugated polymers upon laser pumping at room temperature. Moreover, they have also investigated WGM photoemission from a single microsphere and different sized μ-spheres by irradiating laser illumination at different position of the μ-sphere (Fig 1.44).
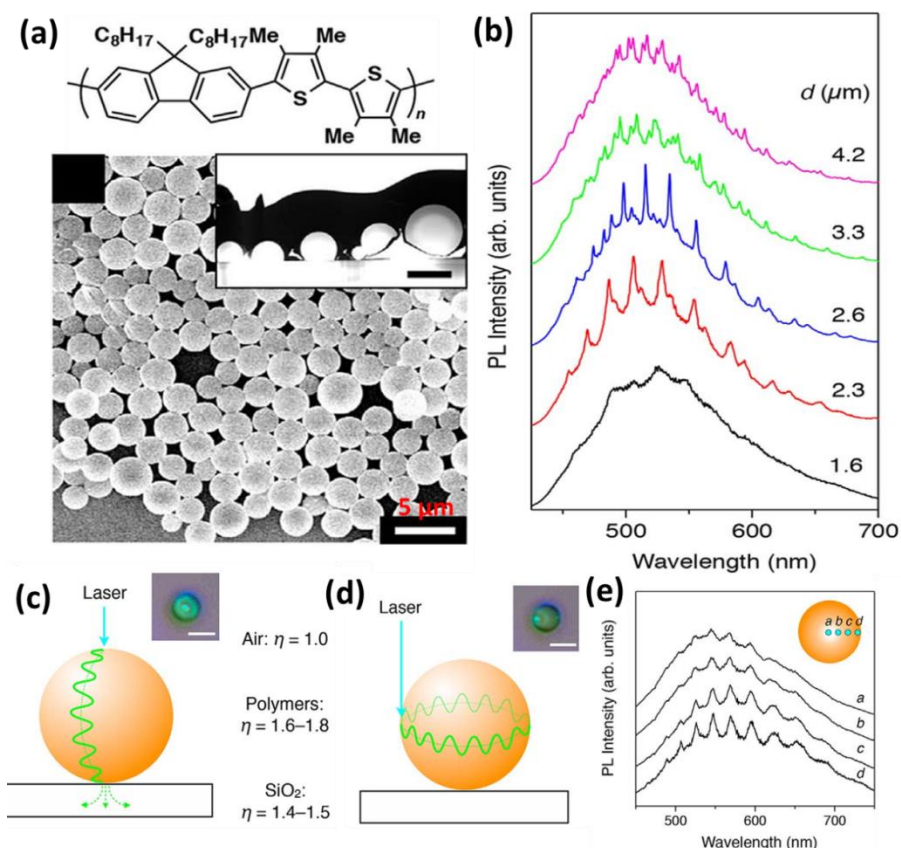
Figure 1.44 a) Chemical structure of polymer and SEM images of polymer μ-spheres. b) PL spetcra of single μ-sphere with different sizes. c, d) Graphical representation of the laser excitation at the center c) edge d) of a microsphere e) PL spectra of a microsphere (d ~ 3.5 μm) consisting of polymer 1 with different position of the laser excitation spots. Inset shows a schematic representation of the top view of a single sphere, showing the excitation spots a (center) to d (edge). [Adopted from Ref. 77a].

In 2015, Chandrasekar and his coworkers[114] have reported for the first time WGM resonances from μ-hemisphere self-assembled from a well-known, 1,4-bis(α-cyano-4-diphenylaminostyryl)-2,5-diphenylbenzene dye molecules (DCM dye). They have prepared μ-hemisphere of diameters from 1.0 μm to 15.0 μm range and studied WGMs optical resonances from a single DCM dye μ-hemisphere at ambient conditions by micro-PL (μ-PL) measurements using 488 nm lasers. Further, they have also studied WGM optical resonances from μ-

hemisphere of different sizes. Due to photon trapping action of the resonators an eight fold increase of the PL intensity had been observed compared to DCM thin film (Fig. 1.45b). The Q-factor value increased
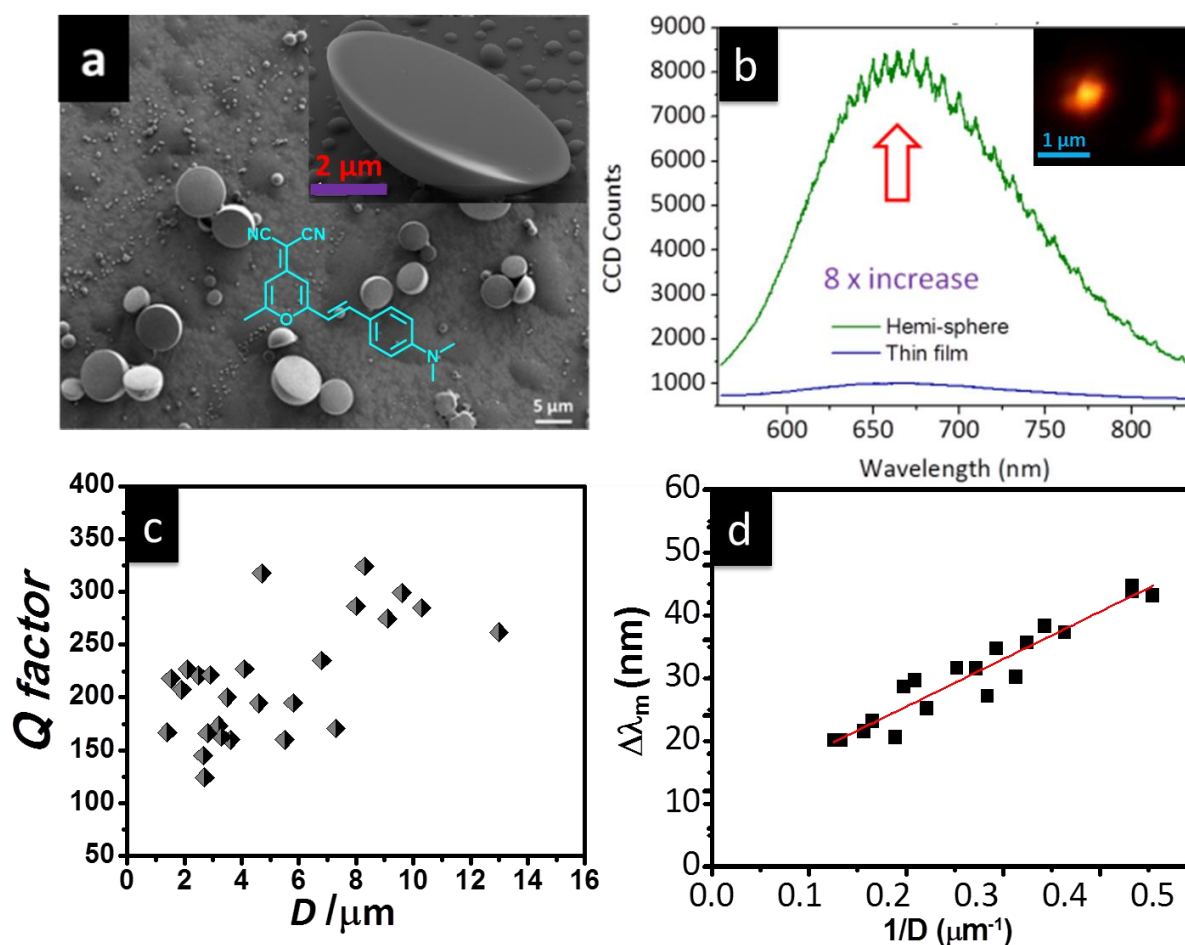
Figure 1.45 a) FESEM image of hemi-spheres on glass substrate (Inset- chemical structure of DCM dye molecule). b) 8 fold-increases in PL intensity of hemi µ-sphere compared to thin film PL (Insert – laser (Wavelength- 488 nm) illuminated hemi µ-sphere). c) The plot of Q factor as a function of µ-hemisphere diameter. d) FSR vs 1/D plot with a linear fit. [Adopted from Ref. 114].

linearly with increasing cavity size up to 3.5×10^2 (Fig. 1.45c). The µ-hemisphere showed increase of the $\Delta\lambda_m$ or FSR values upon decreasing the cavity diameter as per FSR vs 1/D relationship (Fig. 1.45d).

In the same year (September-2015), Yamamoto and coworkers[77b] have reported WGM photoemission from isolated microspheres self-assembled from conjugated polymers. They have prepared several π-conjugated alternating copolymers that form well-defined microspheres

quantitatively via bottom up self-assembly method. The slow diffusion of a polar non-solvent vapor into a solution of polymer formed spheres with diameters in the range of submicrometer to various micrometers. Upon laser excitation of a single microsphere, WGMs were observed in the photoemission. Moreover, they have also investigated size effect on the WGM photoemission resonances of conjugated polymer microspheres (Fig 1.46c).
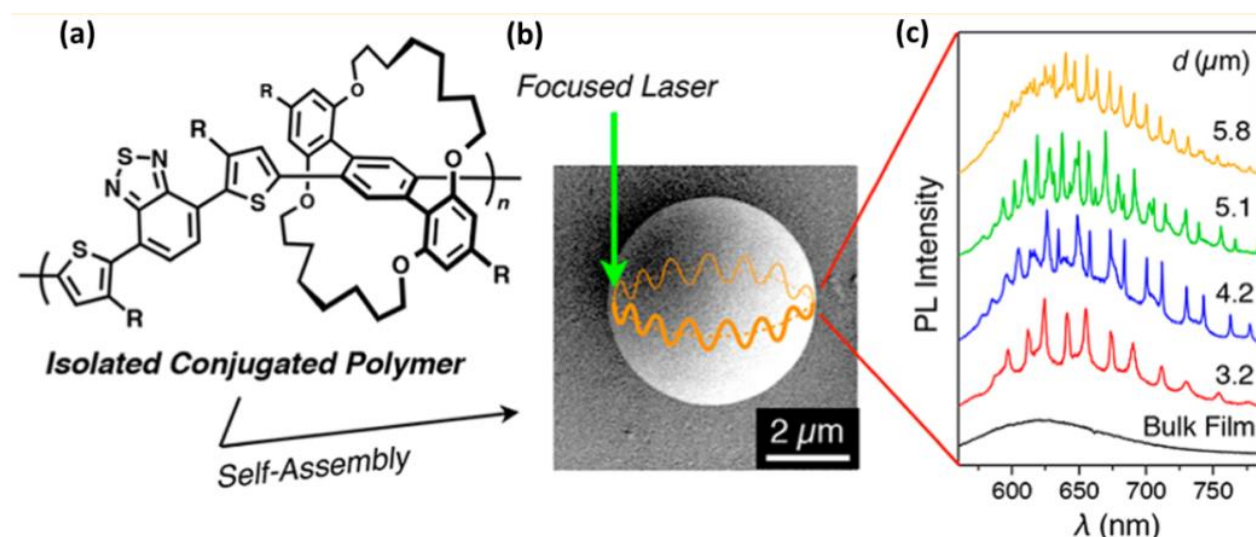
Figure 1.46 a) Structure of the 3-n-dodecylthiophene−benzothiadiazole−3'-n-dodecylthiophene conjugated polymer. b) Laser illumination on self-assembled single polymer microsphere. c) PL spectra of polymer bulk film and microspheres with different diameters exhibiting diameter dependent FSR values. [Adopted from Ref. 77b].

1.7 Aims of the Thesis Work

Macromolecules and metallo-macromolecules emitting fluorescent (FL) radiation have potential applications in various fields such as light emitting diodes (LEDs), back light of liquid crystal displays, full color displays, light emitting electrochemical cells (LECs), solar cells, photonic crystals, photonic devices and organic field effect transistors. FL macromolecules have been known since 19th century and have realistic applications in various fields such as optoelectronics and photovolatics. The synthesis and study of metallo-supramolecular polymers are well known but conjugated polymers with ligand as repeating units and metal containing (in the main chain) conjugated polymers (MCCPs) are not well explored because of solubility issues and difficulties in finding suitable ligand for polymerization. Self-assembly of macromolecules is one of emerging areas in nano materials science and is an important tool for improving the

properties of macromolecules. To the best of my knowledge only a few groups made attempts to self-assemble macromolecules for lighting and photonic applications.

Therefore this thesis focus is directed towards the synthesis of ligand containing FL macromolecules for metal coordination to achieve tunable light emissions (visible-near infrared) and their self-assembly into organic and/or organic/inorganic hybrid nano particles. Attempts also have been made to investigate usefulness of self-assembled structures for nano-photonic applications such as lighting, energy storage, sensors and nano-lasers. Various chapters of this thesis present, synthesis of different metal containing macromolecules, their structural characterization using general techniques such as NMR, FT-IR, GPC, TGA, UV-Visible, Fluorescence/Raman spectroscopy and finally their self-assembly studies. Throughout the thesis for the nano-characterizations tools such as electron microscopy (FESEM, SEM and TEM), energy dispersive x-ray analysis (EDS), confocal laser micro Raman microscopy/spectroscopy and laser confocal fluorescence microscopy were used.

The production of white light in solid state is very important for solid state light and light emitting displays. Until 2011, no attempts have been made to use self-assembled ligand nano/micro structures as a template for surface coordination chemistry. In 2011, for the first time, Chandrasekar et al have prepared nanostructure templates self-assembled from ligand molecules and subsequently demonstrated their use by performing "coordination chemistry on the surface of the organic ligand templates" to generate multi-luminescent organic/inorganic hybrid (Core-Shell type) nanostructures.[17] By following similar protocol, in this thesis a design strategy was developed to create white light emission from polymer/inorganic nanostructures. In this context, a ligand containing conjugated polymer namely, 2,6-bis(pyrazolyl)pyridine-*co*-octylated phenylethynyl, was prepared. Here the 2,6-bis(pyrazolyl)pyridine is known to coordinate with *f*–block elements. Further the polymer was self-assembled into microspheres for the nano-surface coordination chemistry with (Eu(tta)$_3$) to achieve white light emission. Same methodology was further extended to generate multicolor emitting microspheres from alternated copolymers of thiophene oligomers and 2,6-bis(pyrazolyl)pyridine (see Chapter 3). In this chapter, the optical emission range of the copolymers were fine-tuned from blue to red and white by changing the conjugation length of thiophene oligomers and coordinating of metals like Eu^{+3} and Tb^{+3} both in the solution, solid state and solid state assemblies.

The fabrication of shape-defined luminescent nano/micro scale objects from small molecules has attracted increasing attention among scientist owing to their unique optical and electronic properties. The generation of multicolor emissions from single organic and organic/inorganic hybrid nano-object in a single wavelength excitation is of great interest due to their potential use in solid state lighting and color barcode applications. In order to attain this goal, post-metal functionalization has to be performed on the surface of the self-assembled organic architecture. Although several self-assembled organic particles are reported in the literature, none of them are based on ligand molecules, and hence no further metal functionalization can be performed. Till 2011, no attempts have been made to prepare dual emission molecules through breaking the conjugation between two chromophore molecules containing ligand units. This approach requires a step-by-step careful design and synthesis. A dual emitting (blue and green) amphiphilic ligand molecule was synthesized by connecting two units of blue emitting 4-triazolyl-2,6-bis(pyrazolyl)pyridine derivative with a green emitting 4,7-triazolyl-benzo-1,2,5-thiadiazole derivative using two octyl chain linkers via Click chemistry see (Chapter 4). Triple color emitting organic/inorganic hybrid spheres were produced by performing coordination chemistry using red-emitting Eu(III) ions on the surface of the dual emitting spheres in the same pot. WGM microcavities are very important for essential studies of light-mater interaction and applications such as optical mode filters, micro lasers, optical switches and biosensors. Finally light confinement of FL light inside the organic microsphere was carried out by performing light-matter interaction studies down to single-particle level.

One of the great challenges in polymer photonic device structure is improving the emission intensity. To date, WGM photoemission has been observed mostly in the visible electromagnetic region from microstructures of varying shapes (such as hemispheres, rings, spheres, fibers and disks), which are built from inorganics, organics, dye doped polymers, and recently from conjugated polymer. Till now, to our knowledge no reports are available in the literature on WGM photonic microcavities made from MCCP based active luminescent material. Further, the preparation of MCCPs involves major challenges such as, synthesizing novel ligand containing polymers for metal coordination, achieving good solution processability, blending compatibility, wide tunable emission properties, and to bring about new nanoscale photonic particles with smooth surfaces. Considering this in mind, in Chapter 5, a simple and inexpensive self-assembly route was followed to create polymer particles from a judicial blend of polystyrene

and novel yellow emitting MCCP. Extensive single particle μ-FL investigation unraveled the WGM resonating capacity of self-assembled polymer particles in the Vis-NIR range with a high Q factor of up to 7×10^2.

References

1. J. P. Byrne, J. A. Kitchenb, T. Gunnlaugsson, *Chem. Soc. Rev*. **2014**, *43*, 5302-5325.

2. D. L. Jameson, K. A. Goldsby*, J. Org. Chem.* **1990**, *55*, 4992–4994.

3. a) N. K. Solanki, M. A. Leech, E. J. L. Mcinnes, J. P. Zhao, F. E. Mabbs, N. Feeder, J. A. K. Howard, J. E. Davies, J. M. Rawsona, M. A. Halcrow, *J. Chem. Soc. Dalton Trans.* **2001**, 2083-2088; b) J. M. Holland, C. A. Kilner, M. Thornton-Pett, M. A. Halcrow, *Polyhedron* **2001**, *20,* 2829-2840.

4. E. Brunet, O. Juanes, R. Sedano, J. C. Rodríguez-Ubis, *Org. Lett.* **2002**, *4*, 213-216.

5. a) R. Kurtarana, C. Arıcı, K. C. Emregül, D. Ülküb, O. Atakol, M. Z. Taştekin, *Anorg. Allg. Chem.* **2003**, *629*, 1617-1621; b) K. Chryssou, T. Stergiopoulos, P. Falaras, *Polyhedron* **2002**, *21,* 2773-2781.

6. G. Zoppellaro, M. Baumgarten, *Eur. J. Org. Chem.* **2005**, 2888–2892.

7. R. Chandrasekar, F. Schramm, S. Brink, O. Fuhr, M. Ghafari, R. Kruk, M. Ruben, *Inorg. Chem.* **2006**, *45,* 10019–10021.

8. J. Elhaïk, C. M. Pask, C. A. Kilner, M. A. Halcrow, *Tetrahedron* **2007**, *67*, 291-298.

9. R. Chandrasekar, Z. Qu, O. Fuhr, B. Gopalan, R. Kruk, M. Ghafari, M. Ruben, *Dalton Trans.* **2007**, 3531-3537.

10. M. Nihei, T. Maeshima, Y. Kose, H. Oshio, *Polyhedron* **2007**, *26*, 1993-1996.

11. X. J. Zhu, B. J. Holliday, *Macromol. Rapid Commun.* **2010**, *31*, 904-909.

12. J. M. Stanley, X. Zhu, X. Yang, B. J. Holliday, *Inorg.Chem.* **2010**, *49*, 2035-2037.

13. Z. Ye, G. Wang, J. Chen, X. Fu, W. Zhang, J. Yuan, *Biosensors and Bioelectronics* **2010**, *26*, 1043-1048.

14. Y. Hasegawa, K. Takahashi, S. Kume, H. Nishihara, *Chem. Commun.* **2011**, *47*, 6846-6848.

15. a) M. Starck, R. Ziessel, *Dalton Trans*. **2012**, *41*, 13298-13307; b) R. Ziessel, A. Sutter, M. Starck, *Tet. Lett.* **2012**, *53*, 3714-3717.

16. N. Chandrasekhar, R. Chandrasekar, *Chem. Commun.* **2010**, *46*, 2915-2917.

17.   S. Basak, R. Chandrasekar, *Adv. Funct. Mater.* **2011**, *21*, 667–673.

18.   S. Basak, Y. S. L. V. Narayana, M. Baumgarten, K. Mullen, R. Chandrasekar *Macromolecules* **2013**, *46*, 362−369.

19.   J. –M. Lehn, Supramolecular Chemistry, Concepts and Perpectives, VCH, Weinheim, Germany, **1995**.

20.   S. Burattini, H. M. Colquhoun, J. D. Fox, D. Friedmann, B. W. Greenland, P. J. F. Harris, W. Hayes, M. E. Mackay, S. J. Rowan, *Chem. Commun.* **2009**, 6717-6719.

21.   a) J. N. Hunt, K.E. Feldman, N. A. Lynd, J. Deek, L. M. Campos, J. M. Spruell, B.M. Hernandez, E. J. Kramer, C. J. Hawker, *Adv. Mater.* **2011**, *23*, 2327–2331; b) Y. Hisamatsu, S. Banerjee, M. B. Avinash, T. Govindaraju, C. A. Schmuck, *Angew. Chem. Int. Ed.* **2013**, *52*, 12550-12554.

22.   a) G. Armstrong, M. Buggy, *J. Mater. Sci.* **2005**, *40*, 547-559; b) T. Aida, E. W. Meijer, S. I. Stupp, *Science* **2012**, *335*, 813-817.

23.   a) G. R. Whittell, M. D. Hager, U. S. Schubert, I. Manners, *Nat. Mater.* **2011**, *10*, 176-188; b) B. M. McKenzie, S. J. Rowan, *Molecular Recognition and Polymers*, ed. V. M. Rotello, S. Thayumanavan, John Wiley and Sons, Hoboken, NJ, **2008**, Ch. 7, 157; c) G. R. Whittell, I. Manners, *Adv. Mater.* **2007**, *19*, 3439-3468.

24.   C.E. Carraher, Jr., *J. Macromol. Sci. Chem.* **1982**, Al7, 1293.

25.   a) A.S Abd-El-Aziz, I. Manners, Frontiers in Transition-Metal-Containing Polymers. Hoboken, NJ: John Wiley & Sons Inc.; **2007**, 704; b) I. Manners, Synthetic Metal-Containing Polymers. Weinheim: Wiley-VCH; **2004**, 275; c) U.S. Schubert, G.R. Newkome, I. Manners, editors. Metal-Containing and Metallosupramolecular Polymers and Materials. ACS Symposium Ser 928. Washington, DC: Am Chem Soc; **2006**, 575; d) J. E. Sheats, J. C .E Carraher, J. C. P Pittman, M, Zeldin, B, Currell ,editors. Inorganic and Metal-Containing Polymeric Materials. New York: Plenum Press; **1985**, 406; e) F. Jäkle, *Chem. Rev.* **2010**, *110*, 3985–4022; f) A. S. Abd-El-Aziz, *Macromol. Rapid Commun.* **2002** *23*, 995–1031; g) J. B. Beck, J. M, Ineman, S. J. Rowan, *Macromolecules* **2005**, *38*, 5060–5068; h) B. D. Korth, P. Keng, I. Shim, S. E. Bowles, C. Tang, T. Kowalewski, K. W. Nebesny, J. Pyun, *J. Am. Chem. Soc.* **2006**, *128*, 6562–6565; i) S. K. Yang, A. V. Ambade, M. Weck, *Chem. Soc. Rev.* **2011**, *40*, 129–137; j) X. Wang, R. M. Hale, *Macromol. Rapid Commun.* **2010**, *31*, 331–350; k) P.Y. Keng, B.Y. Kim, I. B. Shim, R, Sahoo, P. E.

Veneman, N. R. Armstrong, H. Yoo J. E. Pemberton, M. M. Bull, J. J. Griebel, E. L. Ratcliff, K. G. Nebesny, J. Pyun. *ACS Nano* **2009**, *3*, 3143–3157; l) K. J. Calzia, G. N. Tew, *Macromolecules* **2002**, *35*, 6090–6093; m) X. Wang, K. Cao, Y. Liu, B. Tsang, S. Liew, *J. Am. Chem. Soc.* **2013**, *135*, 3399–3402.

26.   a) E. C. Constable, M. D. Ward, *J. Chem. Soc. Dalton Trans.* **1990**, 1405-1409; b) S. Schmatloch, A. M. J. van den Berg, A. S. Alexeev, H. Hofmeier, U. S. Schubert, *Macromolecules* **2003**, *36*, 9943; c) J. B. Beck, S. J. Rowan, *J. Am. Chem. Soc.* **2003**, *125*, 13922-13923; d) R. Dobrawa, F. Würthner, *Chem. Commun.* **2002**, 1878–1879; e) D. Rajwar, X. Liu, Z. B. Lim, S. J. Cho, S. Chen, J. M. H. Thomas, A. Trewin, Y. M. Lam, T. C. Sum, A. C. Grimsdale *RSC Adv.* **2014**, *4*, 17680–17693; f) N. Chandrasekhar, R. Chandrasekar *J. Org. Chem.* **2010**, *75*, 4852–4855; g) S. Basak, P. Hui, B. Sathyanarayana, R. Chandrasekar *J. Org. Chem.* **2012**, *77*, 3620−3626; i) U. Venkataramudu, N. Chandrasekhar, S. Basak, M. D. Prasad, R. Chandrasekar *Macromol. Rapid Commun.* **2015**, *36*, 647−653.

27.   B. Lahn, M. Rehahn, *Macromol. Symp.* **2001**, *163*, 157-176.

28.   a) S. Schmatloch, A. M. J. van den Berg, A. S. Alexeev, H. Hofmeier, U. S. Schubert *Macromolecules* **2003**, *36,* 9943-9949; b) S. Schmatloch, M.F. Gonzalez, U.S. Schubert, *Macromol. Rapid Commun.* **2002**, *23*, 957-961; c) U.S. Schubert, O. Hien, C. Eschbaumer, *Macromol. Rapid Commun.* **2000**, *21*, 1156-1161; d) H. Hofmeier, S. Schmatloch, D. Wouters, U.S. Schubert, *Macromol. Chem. Phys.* **2003**, *204*, 2197-2203; e) S. Schmatloch, U. S. Schubert, *Macromol. Symp.* **2003**, *199*, 483-497.

29.   A. Gasnier, G. Royal, P. Terech, *Langmuir* **2009**, *25*, 8751-8762.

30.   a) W. Weng, Z. Li, A. M. Jamieson, S. J. Rowan, *Macromolecules* **2009**, *42*, 236-246. b) J. B. Beck, S. J. Rowan, *J. Am. Chem. Soc.* **2003**, *125*, 13922-13923; c) W. Weng, J. B. Beck, A. M. Jamieson, S. J. Rowan, *J. Am. Chem. Soc.* **2006**, *128*, 11663-11672.

31.   a) K. I. Parameswar, J. B. Beck, C. Weder, S. J. Rowan, *Chem. Commun.* **2005**, 319-321; b) D. Knapton, S. J. Rowan, C. Weder, *Macromolecules* **2006**, *39*, 651-657.

32.   a) M. Burnworth, J. D. Mendez, M. Schroeter, S. J. Rowan, C. Weder, *Macromolecules* **2008**, *41*, 2157-2561.

33. a) S. Sivakova, D. A. Bohnsack, M. E. Mackay, P. Suwanmala, S. J. Rowan, *J. Am. Chem. Soc.* **2005**, *127*, 18202-18211; b) J. D. Fox, S. J. Rowan, *Macromolecules* **2009**, *42*, 6823-6835; c) J. R. Kumpfer, S. J. Rowan, *J. Am. Chem. Soc.* **2011**, *133*, 12866-12874.

34. S. W. Lee, J. R. Kumpfer, P. A. Lin, G. Li, X. P. A. Gao, S. J. Rowan, R. M. Sankaran, *Macromolecules* **2012**, *45*, 8201-8210.

35. a) G. L. Fiore, S. J. Rowan, C. Weder, *Chem. Soc. Rev.* **2013**, *42*, 7278-7288; b) M. Burnworth, L. Tang, J. R. Kumpfer, A. J. Duncan, F. L. Beyer, G. L. Fiore, S. J. Rowan, C. Weder, *Nature* **2011**, *472*, 334-337.

36. S. J. Payne, G. L. Fiore, C. L. Fraser, J. N. Demas, *Anal. Chem.* **2010**, *82,* 917–921.

37. L. Viau, M. Even, O. Maury, D. M. Haddleton, H. L. Bozec, *Macromol. Rapid Commun.* **2003**, *24*, 630–635.

38. a) T. J. Meyer, *Acc. Chem. Res.* **1989**, *22*, 163-170; b) S. C. Yu, S. J. Hou, W. K. Chan, *Macromolecules* **2000**, *33*, 3259-3273; c) R. Grigg, J. M. Holmes, S. K. Jones, W. Norbert, *J. Chem. Soc., Chem. Commun.* **1994**, 185-187; d) J. K. Lee, D. Yoo, M. F. Rubner, *Chem. Mater.* **1997**, *9*, 1710-1712; e) Organic Light Emitting Devices: Synthesis, Properties and Applications; K. Müllen, U. Scherf, Eds.; Wiley VCH: Weinheim, Germany, **2006**. f) B. J. Holliday, T. M. Swager, *Chem. Comm.* **2005**, 23–36; g) C. Li, M. Liu, N. G. Pschirer, M. Baumgarten, K. Müllen, *Chem. Rev.* **2010**, *110*, 6817−6855; h) X. Guo, S. R. Puniredd, M. Baumgarten, W. Pisula, K. Müllen, *J. Am. Chem. Soc.* **2012**, *134*, 8404-8407; i) V. Kamm, G. Battagliarin, I. A. Howard, W. Pisula, A. Mavrinskiy, C. Li, K. Müllen, F. Laquai. *Adv. Energy Mater.* **2011**, *1*, 297-302.

39. a) Inorganic and Metal-Containing Polymeric Materials; J. E. Sheats, C. E. Carraher, C. U. Pittman, Jr., M. Zeldin, B. Currell, Eds.; Plenum Press: New York, **1990**; b) G. R. Newkome, E. He, C. N. Moorefield, *Chem. Rev.* **1999**, *99*, 1689-1746; c) M. J. MacLachlan, M. Ginzburg, N. Coombs, T. W. Coyle, N. P. Raju, J. E. Greedan, G. A. Ozin, I. Manners, *Science* **2000**, *287*, 1460-1463.

40. a) I. Manners, *Adv. Mater.* **1994**, *6*, 68-71; b) M. Rosenblum, *Adv. Mater.* **1994**, *6*, 159-162; c) J. E. Sheats, C. E. Carraher, C. U. Pittman, *Metal Containing Polymer Systems*; Plenum: New York, **1985**; d) P. F. Brandt, T. B. Rauchfuss, *J. Am. Chem. Soc.* **1992**, *114*, 1926-1927; e) M. E. Wright, M. S. Sigman, *Macromolecules* **1992**, *25*, 6055-6058; f) G. Hochwimmer, O. Nuyken, U. S. Schubert, *Macromol. Rapid Commun.* **1998**, *19,* 309-331.

41. a) T. Yasuda, I. Yamaguchi, T. Yamamoto, *Adv. Mater.* **2003**, *15*, 293-296; b) T. Yasuda, T. Yamamoto, *Macromolecules* **2003**, *36*, 7513-7519; c) T. Yamamoto, T. Maruyama, Z. Zhou, T. Ito, T. Fukuda, Y. Yoneda, F. Begum, T. Ikeda, S. Sasaki, H. Takezoe, A. Fukuda, K. Kubotall, *J. Am. Chem. Soc.* **1994**, *116*, 4832−4845; d) T. Yamamoto, K. Anzai, T. Iijima, H. Fukumoto, *Macromolecules* **2004**, *37*, 3064-3067.

42. a) S. S. Zhu, P. J. Carroll, T. M. Swager, *J. Am. Chem. Soc.* **1996**, *118*, 8713−8714; b) S. S. Zhu, T. M. Swager, *J. Am. Chem. Soc.* **1997**, *119*, 12568−12577; c) S. S. Zhu, T. M. Swager, *Adv. Mater.* 1996, *8*, 497−500; d) R. P. Kingsborough, T. M. Swager, *Adv. Mater.* **1998**, *10*, 1100-1104.

43. R. J. Card, D. C. Neckers, *Inorg. Chem.* **1978**, *17*, 2345−2349.

44. Z. Peng, L. Yu, *J. Am. Chem. Soc.* **1996**, *118,* 3777-3778.

45. B. Wang, M. R. Wasielewski, *J. Am. Chem. Soc.* **1997**, *119*, 12-21.

46. M. Kimura, T. Horai, K. Hanabusa, H. Shirai, *Adv. Mater.* **1998**, *10*, 459-462.

47. C. T. Wong, W. K. Chan, *Adv. Mater.* **1999**, *11*, 455-458.

48. a) R. Shunmugam, G. N. Tew, *J. Am. Chem. Soc.* **2005**, *127*, 13567-13572; b) R. Shunmugam, G.N. Tew, *Macromol. Rapid Commun.* **2008**, *29*, 1355-1362.

49. R. Shunmugam, G. N. Tew, *Polym. Adv. Technol .***2008**, *19*, 596-601.

50. a) J. Brassinne, F. D. Jochum, C. A. Fustin, J. F. Gohy, *Int. J. Mol. Sci.* **2015**, *16*, 990-1007.

51. a) B. W. D'Andrade, S. R. Forrest, *Adv. Mater.* **2004**, *16*, 1585-1595; b) Y. Liu, M. Nishiura, Y. Wang, Z. Hou, *J. Am. Chem. Soc.***2006**, *128*, 5592-5593.

52. F. Huang, P.-I. Shih, C.-F. Shu, Y. Chi, A. K.-Y. Jen, *Adv. Mater.* **2009**, *21*, 361-365.

53. B. Hu, F. E. Karasz, *J. Appl. Phys.* **2003**, *93*, 1995-2001.

54. Q. Xu, H. M. Duong, F. Wudl, Y. Yang, *Appl. Phys. Lett.* **2004**, 85, 3357-3358.

55. H. A. Al Attar, A. P. Monkman, M. Tavasli, S. Bettington, M. R. Bryce, *Appl. Phys. Lett.* **2005**, *86*, 121101.

56. M. Granstrom, O. Inganas, *Appl. Phys. Lett.* **1996**, *68*, 147-149.

57. S. Tasch, E. J. W. List, O. Ekstrom, W. Graupner, G. Leising, P. Schlichting, U. Rohr, Y. Geerts, U. Scherf, K. Mullen, *Appl. Phys. Lett.* **1997**, *71*, 2883-2885.

58. P. I. Shih, Y. H. Tseng, F. I. Wu, A. K. Dixit, C. F. Shu, *Adv. Funct. Mater.* **2006**, *16*, 1582-1589.

59. F. Liu, C. Tang, Q. Q. Chen, F. F. Shi, H. B. Wu, L. H. Xie, B. Peng, W. Wei, Y. Cao, W. Huang, *J. Phys. Chem. C* **2009**, *113*, 4641-4647.

60. J. Liu, Q. G. Zhou, Y. X. Cheng, Y. H. Geng, L. X. Wang, D. G. Ma, X. B. Jing, F. S. Wang, *Adv. Mater.* **2005**, *17*, 2974-2978.

61. J. Liu, Z. Y. Xie, Y. X. Cheng, Y. H. Geng, L. X. Wang, X. B. Jing, F. S. Wang, *Adv. Mater.* **2007**, *19*, 531-535.

62. J. X. Jiang, Y. H. Xu, W. Yang, R. Guan, Z. Q. Liu, H. Y. Zhen, Y. Cao, *Adv. Mater.* **2006**, *18*, 1769-1773.

63. H. Y. Zhen, W. Xu, W. King, Q. L. Chen, Y. H. Xu, J. X. Jiang, J. B. Peng, Y. Cao *Macromol. Rapid Comm.* **2006**, *27*, 2095-2100.

64. M. J. Park, J. Kwak, J. Lee, I. H. Jung, H. Kong, C. Lee, D. H. Hwang, H. K. Shim, *Macromolecules* **2010**, *43*, 1379-1386.

65. M. L. Tsai, C. Y. Liu, M. A. Hsu, T. J. Chow, *Appl. Phys. Lett.* **2003**, *82*, 550-552.

66. M. Kawamoto, T. Tsukamoto, M. Kinoshita, T. Ikeda, *Appl. Phys. Lett.* **2006**, *89*, 121920.

67. Y. H. Xu, J. B. Peng, Y. Q. Mo, Q. Hou, Y. Cao, *Appl. Phys. Lett.* **2005**, *86*, 163502.

68. Q. J. Sun, B. H. Fan, Z. A. Tan, C. H. Yang, Y. F. Li, Y. Yang, *Appl. Phys. Lett.* **2006**, *88*, 163510-163512.

69. S. Basak, M. A. Mohiddon, M. Baumgarten, K. Mullen, R. Chandrasekar, *Sci. Rep*, **2015**, *5*, 8406.

70. a) A. M. Christofi, P. J. Garratt, G. Hogarth, A. J. Ibbett, Y. F. Ng, J. W. Steed, *Tetrahydron* **2002**, *58*, 4543-4549; b) R. Hilgenfeld, W. Saenger, *Angew. Chem. Int. Ed.* **1981**, *20*, 1045-1046. c) M. Makinen, M. Nissinen, K. Rissanen, P. Vainiotalo, *J. Am. Soc. Mass Spec.* **2003**, *14*, 143-151.

71. J. W. Steed, J. L. Atwood, Supramolecular Chemistry, 19-30, Wiley, (**2000**).

72. a) U. Stalmach, B. de Boer, C. Videlot, P. F. van Hutten, G. Hadziioannou, *J. Am. Chem. Soc*. **2000**, *122*, 5464–5472; b) B. de Boer, U. Stalmach, P. F. van Hutten, C. Melzer, V. V. Krasnikov, G. Hadziioannou, *Polymer* **2001**, *42*, 9097–9109; c) S.-S. Sun, *Solar Energy Mater. Solar Cells* **2003**, *79*, 257–264; d) K. Sivula, Z. T. Ball, N. Watanabe, J. M. J. Fréchet, *Adv. Mater.* **2006**, *18*, 206–210; e) Z. T. Ball, K. Sivula, J. M. J. Fréchet, *Macromolecules* **2006**, *39*, 70–72; f) S. Sun, Z. Fan, Y. Wang, J. Haliburton, *J. Mater. Sci.* **2005**, *40*, 1429–1443.

73.   a) A. Kraft, A. C. Grimsdale, A. B. Holmes, *Angew. Chem., Int. Ed. Engl.* **1998**, *37*, 402-428; b) R. M. Tarkka, X. Zhang, S. A. Jenekhe, *J. Am. Chem. Soc.* **1996**, *118*, 9438-9439; c) X. Zhang, A. S. Shetty, S. A. Jenekhe, *Macromolecules* **1999**, *32*, 7422-7429; d) X. Zhang, A. S. Shetty, S. A. Jenekhe, *Acta. Polym.* **1998**, *49*, 52-55.

74.   a) A. Molinos-Gómes, M. Maymó, X. Vidal, D. Velasco, J. Martorell, F. López-Calahorra, *Adv. Mater.* **2007**, *19*, 3814-3818; b) C. J. Yang, S. A. Jenekhe, J. S. Meth, H. Vanherzeele, *Ind. Eng. Chem. Res.* **1999**, *38*, 1759-1774.

75.   a) M. Deutsch, Y. A. Vlasov, D. J. Norris, *Adv. Mater.* **2000**, *12*, 1176–1180; b) S. A. Jenekhe, X. L. Chen, *Science* **1998**, *279*, 1903-1907; c) S. A. Jenekhe, X. L. Chen, *Science* **1999**, *283*, 372-375; d) X. L. Chen, S. A. Jenekhe, *Langmuir* **1999**, *15*, 8007-8017; d) S. Gottardo, R. Sapienza, P. D. García, A. Blanco, D.S. Wiersma, C. López, *Nat. Photon.* **2008**, 2, 429-432; e) T. Kanai, T. Sawada, A. Toyotama, K. Kitamura, *Adv. Fun. Mater.* **2005**, *15*, 25-29.

76.   B. J. Siwick, O. Kalinina, E. Kumacheva, R. J. D. Miller, J. Noolandi, *J. Appl. Phys.*, **2001**, *90*, 5328-5334.

77.   a) K. Tabata, D. Braam, S. Kushida, L.Tong, J. Kuwabara, T. Kanbara, A. Beckel, A. Lorke, Y. Yamamoto, *Sci. Rep* **2014**, *4*, 5902. b) S. Kushida, D. Braam, C. Pan, T. D. Dao, K. Tabata, K. Sugiyasu, M. Takeuchi, S. Ishii, T. Nagao, A. Lorke, Y. Yamamoto, *Macromolecules* **2015**, *48*, 3928−3933.

78.   a) J. Edwards, R. Fisher, B. Vincent, *Makromol. Chem., Rapid Commun.* **1983**, *4*, 393-397; b) R. B. Bjorklund, B. Liedberg, *J. Chem. Soc., Chem. Commun.* **1986**, 1293-1295; c) S. P. Armes, M. Aldissi, *J. Chem. Soc., Chem. Commun.* **1989**, 88-89.

79.   M. Mu, F. Ning, M. Jiang, D. Chen, *Langmuir* **2003**, *19*, 9994- 9996.

80.   a) *Functional Hybrid Materials*; P. Gomez-Romero, C. Sanchez, Eds.; Wiley-VVerlag GmbH & Co. KGaA: Weinheim, Germany, **2004**; b) U. Schubert, *Macromol. Symp.* **2008**, *267*, 1–8; c) P. Gomez-Romero, *Adv. Mater.* **2001**, *13*, 163–174; d) P. Judeinstein, C. Sanchez, *J. Mater. Chem.* **1996**, *6*, 511–525; e) P. Gó mez-Romero, C. Sanchez, Hybrid materials, functional applications. An introduction. In *Functional Hybrid Materials*; Eds.; Wiley-VCH Verlag GmbH & Co. KGaA: Weinheim, Germany, **2004**; 1–14.

81.   M. A. Hood, M. Mari, R. M. Espí, *Materials* **2014**, *7*, 4057-4087.

82. a) N. T. K. Thanh, L. A. W. Green, *Nano Today* **2010**, *5*, 213–230; b) K.G. Neoh, E.T. Kang, *Polym. Chem.* **2011**, *2*, 747–759; c) M. J. Sailor, J.-H. Park, *Adv. Mater.* **2012**, *24*, 3779–3802.

83. a) M. Law, D. J. Sirbuly, J. C. Johnson, J. Goldberger, R. J. Saykally, P. Yang, *Science* **2004**, *305*, 1269-1273 b) J. C. Johnson, H. –J. Choi, K. P. Knutsen, R. D. Schaller, P. Yang, R. J. Saykally, *Nat. Mater.* **2002**, *1*, 106-110.

84. a) S. Amberg-Schwab, E. Arpac, W. Glaubitt, K. Rose, G. Schottner, U. Schubert, Materials Science Monographs - High Performance Ceramic Films and Coatings, vol. 67, ed. P. Vincenci, Elsevier, Amsterdam, **1991**, 203; b) G. Schottner, *Chem. Mater.* **2001**, *13*, 3422-3435; c) K. Gigant, U. Posset, G. Schottner, L. Baia, W. Kiefer, J. Popp, *J. Sol–Gel Sci. Technol.* **2003**, 26, 369-373; d) K. H. Haas, S. Amberg-Schwab, K. Rose, G. Schottner, *Surf. Coat. Technol.* **1999**, *111*, 72-79.

85. a) U. Schubert, *New J. Chem.* **1994**, *18*, 1049–1058; b) E. Karakhanov, A. Maximov, S. Kardashev, Y. Kardasheva, A. Zolotukhina, E. Rosenberg, J. Allen, *Macromol. Symp.* **2011**, *304*, 55–64; c) A. P. Wight, M. E. Davis, *Design Chem. Rev.* **2002**, *102*, 3589–3613; d) A. Zamboulis, N. Moitra, J. J. E. Moreau, X. Cattoen, C. M. M. Wong, *J. Mater. Chem.* **2010**, *20*, 9322–9338.

86. a) J.W. Gilman, *Appl. Clay Sci.* **1999**, *15*, 31–49; b) J. W. Gilman, C. L. Jackson, A. B. Morgan, Jr. R. Harris, E. Manias, E. P. Giannelis, M. Wuthenow, D. Hilton, S. H. Phillips, *Chem. Mater.* **2000**, *12*, 1866–1873; c) D. Y. Godovski, *Adv. Polym. Sci.* **1995**, *119*, 79–122.

87. a) A. D. Pomogailo, Hybrid polymer–inorganic nanocomposites. *Russ. Chem. Rev.* **2000**, *69*, 53–80; b) U. Schubert, N. Husing, A. Lorenz, *Chem. Mater.* **1995**, *7*, 2010–2027; c) C. J. Brinker, G. W. Scherer, *Sol–gel science*. San Diego: Academic Press; **1990**; d) Y. Chujo, T. Saegusa, *Adv. Polym. Sci.* **1992**, *100*, 11–29; e) Q. Deng, W. Jarrett, R. B. Moore K. A. Mauritz, *J. Sol–Gel Sci. Technol.* **1996**, *7*, 177–1790; f) H. Shen, A. Eisenberg, *Angew. Chem. Int. Ed.* **2000**, *39*, 3310–3312; g) E. B. Zhulina, O. V. Borisov, *Macromolecules* **2002**, *35*, 9191–9203; h) Y. -H. Han, A. Taylor, M. D. Mantle, K. M. Knowles, *J. Non-Cryst. Solids*, **2007**, *353*, 313–320.

88. Lord Rayleigh, Theory of Sound, vol. II, 1st edition, (London, MacMillan), **1878**.

89. L. Cartz, (**1995**). *Nondestructive Testing*. A S M International. ISBN 978-0-87170-517-4.

90. T. J. Kippenberg, K. J. Vahala, *Science* **2008**, *321*, 1172-1176.

91. S. Arnold, M. Khoshsima, I. Teraoka, S. Holler, F. Vollmer. *Opt. Lett*. **2003**, *28*, 272-   274

92. Y. P. Rakovich, J. F. Donegan, *Laser & Photon. Rev*. **2010**, *4*, 179-191.

93. M. M., L. E. García-Muñoz, H. G. L. Schwefel, F. Sedlmeir, M. Schneidereit, A. R, D. Segovia-Vargas, in *Proc. EOS 2014, Italy*, **2014**.

94. P. L. Stanwix, M. E. Tobar, P.Wolf, M. Susli, C. R. Locke, E. N. Ivanov, J. Winter flood, F. Kann, *Phys. Rev. Lett*. **2005**, *95*, 040404.

95. V. V. Nesvizhevsky, A. Y. Voronin, R. Cubitt, K. V. Protasov, *Nature Phys*. **2009**, *6*, 114-117.

96. G. Reecht, H. Bulou, F. Scheurer, V. Speisser, B. Carrière, F. Mathevet, G. Schull, *Phys Rev. Lett*. **2013**, *110*, 056802.

97. a) V. D. Ta , R. Chen , H. D. Sun , *Sci. Rep.* **2013**, *3*, 1362-1366; b) A. Espinha, M. C. Serrano, A. Blanco, C. López, *Adv. Opt. Mater.* **2015**, *3*, 1080-1087.

98. a) K. Takazawa, J.-I. Inoue, K. Mitsuishi, T. Takamasu, *Adv. Mater.* **2011**, *23*, 3659-3663.

99. a) F. Vollmer, S. Arnold, D. Keng, *Proc. Natl. Acad. Sci*. U.S.A. **2008**, *105*, 20701–20704; b) A. A. Savchenkov, A. B. Matsko, V. S. Ilchenko, L. Maleki, *Opt. Exp.* **2007**, *15*, 6768-6773; c) Y. Dumeige, S. Trebaol, L. Ghis, T. K. N. Nguyen, H. Tavernier, P. Feron, *J. Opt. Soc. Am. B* **2008**, 25, 2073-2080.

100. a) D. K. Armani, T. J. Kippenberg, S. M. Spillane, K. J. Vahala, *Nature* **2003**, 421, 925-928; b) D. K. Armani, B. K. Min, A. L. Martin, K. J. Vahala, *Appl. Phys. Lett.*, **2004**, *85*, 5439-5441; c) T. Kippenberg, S. Spillane, K. J. Vahala *Phys. Rev. Lett.*, **2004**, *93,* 083904; d) M. Hossein-Zadeh, K. J. Vahala, *Opt. Exp.* **2007**, *15*, 166-175.

101. T. A. Birks, J. C. Knight, T. E. Dimmick, *IEEE Phot. Techn. Lett.* **2000**, *12*, 182-183.

102. a) V. B. Braginsky, M. L. Gorodetsky, V. S. Ilchenko, *Phys. Lett. A* **1989**, *137*, 393-396; b) H. Mabuchi, H. J. Kimble, *Opt. Lett*. **1994**, *19*, 749-751; c) V. Sandoghdar, F. Treussart, J. Hare, V. Lefevre-Seguin, J. -M. Raimond, S. Haroche, *Phys. Rev. B* **1996**, *54*, R1777-R1780; d) V. V. Vasiliev, V. L. Velichansky, M. L. Gorodetsky, V. S. Ilchenko, L. Hollberg, A. V. Yarovitsky, *Quant. Electron.* **1996**, *26*, 657-665.

103. a) S. Arnold, S. Shopova, S. Holler, *Opt. Exp*. **2010**, *18,* 281-287; b) F. Vollmer, S. Arnold, D. T. I. Braun, A. Libchaber, *J. Biophys.* **2003**, 85, 1974-1979; c) H. Zhu, J. D.

Suter, I. M. White, X. Fan, *Sensors*, **2006**, 6, 785-795; d) F. Vollmer, D. Braun, A. Libchaber, M. Khoshsima, I. Teraoka S. Arnold, *Appl. Phys. Lett.* **2002**, *80*, 4057-4059.

104. L. Tobing, P. Dumon, *Photonic Microresonator Research and Applications* **2010**, *156*, 1-27

105. R. D. Richtmyer, *J. Appl. Phys.* **1939**, *10*, 391-398.

106. C. Garret, W. Kaiser, W. Bond, *Phys. Rev. Lett.* **1961**, *15*, 1807-1809.

107. a) M. K. Gonokami, K. Takeda, *Opt. Mater.* **1998**, *9*, 12-17; b) M. K. Gonokami, K. Ema, K. Takeda, 5th Int. Conf., Unconventional Photoactive Solids, *Symp. Molecular Systems*, Okazaki, **1991**.

108. a) N. Tessler, G. J. Denton, R. H. Friend, *Nature* **1996**, *382*, 695– 697; b) W. Holzer, A. Penzkofer, S. H. Gong, A. Bleyer, D. D. C. Bradley, *Adv. Mater.* **1996**, *8*, 975–978; c) S. V. Frolov, M. Ozaki, W. Gellermann, Z. V. Vardeny, K. Yoshino, *Jpn. J. Appl. Phys., Part 2* **1996**, *35*, L1371–L1373. d) H. J. Brouwer, V. V. Krasnikov, A. Hilberer, G. Hadziioannou, *Adv. Mater.* **1996**, *8*, 935–937.

109. S. L. MacCall, A. F. J. Levi, R. E. Slusher, S. J. Pearton, R. A. Logan, *Appl. Phys. Lett.* **1992**, *60*, 289-291.

110. F. Hide, M. A. Diaz-Garcia, B. J. Schwartz, M. R. Andersson, Q. Pei, A. J. Heeger, *Science* **1996**, *273*, 1833–1836.

111. S. V. Frolov, M. Shkunov, Z. V. Vardeny, K. Yoshino, *Phys. Rev. B* **1997**, *56*, R4363–R4366.

112. V. D. Ta, R. Chen, L. Ma, Y. J. Ying, H. D. Sun, *Laser Photon. Rev.* **2013**. *7*, 133–139.

113. a) S. K. Y. Tang, R. Derda, Q. Quan, M. Loncar, G. M. Whitesides, *Opt. Exp.* **2011**, *19*, 2204– 2215; b) M. Humar, M. Ravnik, S. Pajk, I. Musevic, *Nature Photon*. **2009**, *3*, 595–600.

114. D. V. Venkatakrishnarao, R. Chandrasekar, *Adv. Opt. Mater.* **2015**, DOI**:**10.1002/adom.20500362.

2

White-Emitting Polymer/Inorganic Hybrid Spheres: Phenylethynyl and 2,6-Bis(pyrazolyl)pyridine Copolymer Coordinated to Eu(tta)$_3$

2.1 Abstract

This chapter focuses on the syntheses of two cyan colour (blue and green emission) displaying high molecular weight 2,6-bis(pyrazolyl)pyridine-co-octylatedphenylethynyl conjugated polymers (CPs). The CPs was solution processed to prepare spin coated thin films and further self-assembled into nano/micro scale spheres exhibiting cyan colour under UV light exposure. Additionally, the metal coordinating ability of the 2,6-bis(pyrazolyl)pyridine (bpp) available on the surface of the CP films and spheres were exploited to prepare red emitting Eu(III) metal ion containing conjugated polymer (MCCP) layer. The resultant hybrid (CP/MCCP) films and spheres exhibit bright white-light under UV light exposure. The CIE coordinates were found to be x = 0.33; y = 0.37 for hybrid films and x = 0.30; y = 0.35 for spheres. These values are almost close to the designated CIE coordinates for ideal white-light colour (x = 0.33; y = 0.33). This easy and efficient fabrication technique to generate white colour displaying films and nano/micro spheres signify an important method in bottom-up nanotechnology of CPs based hybrid solid state assemblies.
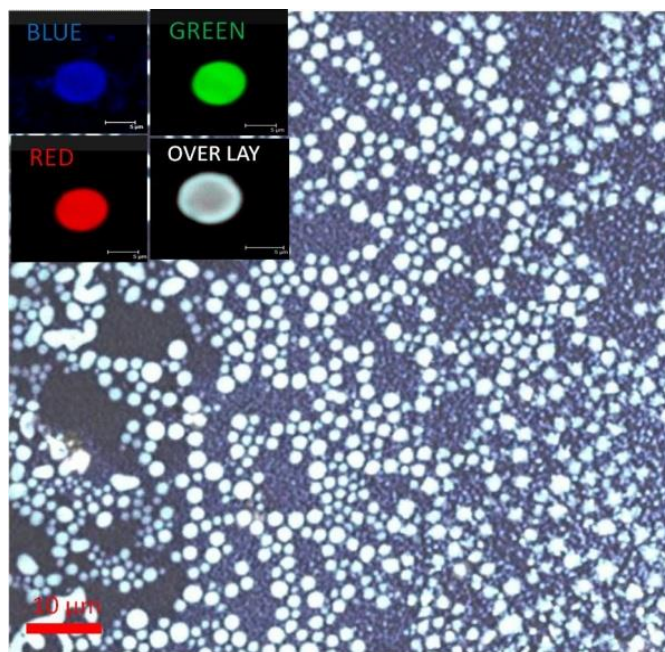
2.2 Introduction

π-Conjugated polymers[1-6] (CPs) play an important role in organic electronic devices[2a] such as polymer light emitting diodes (PLEDs),[2b] back light of liquid crystal displays, full color display applications, light emitting electrochemical cells (LECs),[2c] solar cells,[2d] photonic crystals,[2e] photonic devices[2f] and organic field effect transistors (OFET).[2g] Amongst CP, particularly the design and synthesis of white-light-emitting polymers have attracted much attention because of their direct applications in display and lighting devices.[2h] Additionally, CP based spherical beads, spheres and colloidal crystals are attractive in the area of photonic crystals and non-linear optical studies.[2i-k] An ideal white-light-emitting system requires to emit three primary BGR (blue, green, and red) or two BY (blue and yellow) colors so that the emission spectrum covers the whole visible range wavelength from 400 to 700 nm.[2l] A straightforward strategy to acquire solid state white emission is to integrate several light emitters with dissimilar but complementary emission wavelengths into a single polymer layer in order to realize synergistic color emission. However this method suffers from unwanted energy transfer from the high band gap chromophores to lower band gap moieties.[2m-o]

In this regard metal containing conjugated polymers (MCCP) [4-6] are of interest since they offer a wide option for color tunability by varying the choice of photoluminescent transition metal (Ru^{3+}, Ir^{3+})[4] and lanthanide (Ln^{3+})[5,6] ions. As discussed earlier, in the synthesis of MCCP three types of approaches have been followed: i) the metal can be tethered to the conjugated polymer back bone via alkyl linker chains carrying ligands;[7] ii) self-assembly of ditopic ligands[8a-g] with metal ions to form linear metallo-supramolecular polymers; and through iii) direct coordination of luminescent metal ions to the conjugated polymeric ligand back bone.[9] In this chapter a synthetically challenging last approach has been adopted, since this class of polymer offer the possibility to achieve a range of emission colors by the incorporating a variety of luminescent metal ions on the polymer film surface *via* spin- or dip-coating techniques.[5f,10] Additionally, by following our original approach[8g,h] "coordination chemistry on the surface of the self-assembly solids" (e.g. spheres, particles, tubes etc.) can also be performed, to fabricate MCCP containing soft microspheres emitting wide spectrum of colors.

This chapter presents a novel one-pot approach to accomplish white color emitting CP/MCCP hybrid films and nano/micro spheres (Scheme 2.1). At first, this chapter presents the syntheses of model compounds **EBOB**, (**m1-m2**), copolymers **P1** and **P2** (Scheme 2.2), and

fabrication of cyan emitting copolymer film and spheres composed of **P1**. Preparation method for white color emitting film and spheres via coordination with Eu(III) will also be discussed. Additionally, the chapter focuses also on the comparative photophysical and energy transfer properties of model complex (**M3**·Eu(tta)$_3$) with Eu(tta)$_3$ coordinated polymers of **P1**. Meticulous characterization of self-assembled white emitting spheres using electron microscopy (FESEM/SEM/TEM), atomic force microscopy (AFM), confocal μ-Raman spectroscopy (CRS) and confocal fluorescence microscopy (CFM) techniques has also been presented.
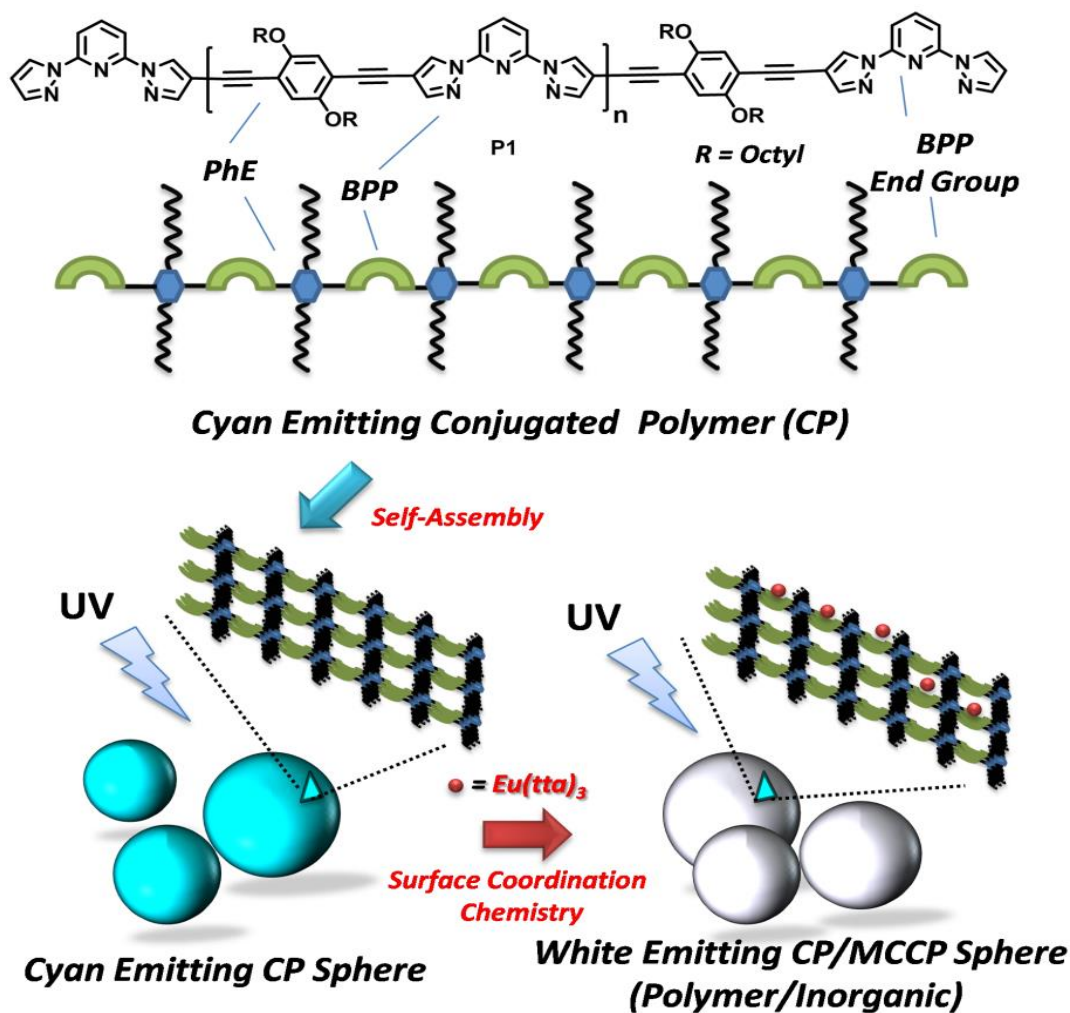
Scheme 2.1 Illustration of white emitting nano/micro spheres obtained from Eu(III) coordinated conjugated copolymer **P1** via self-assembly. BPP: 2, 6-bis(pyrazolyl)pyridine CP: Conjugated Copolymer, PhE: octylated phenyl thynyl, MCCP: Metal Containing Conjugated Copolymer.

2.3 Results and Discussion

2.3.1 *Syntheses of Monomers, Model Compounds, Copolymers and Metal - Complexes of Model Compounds.*
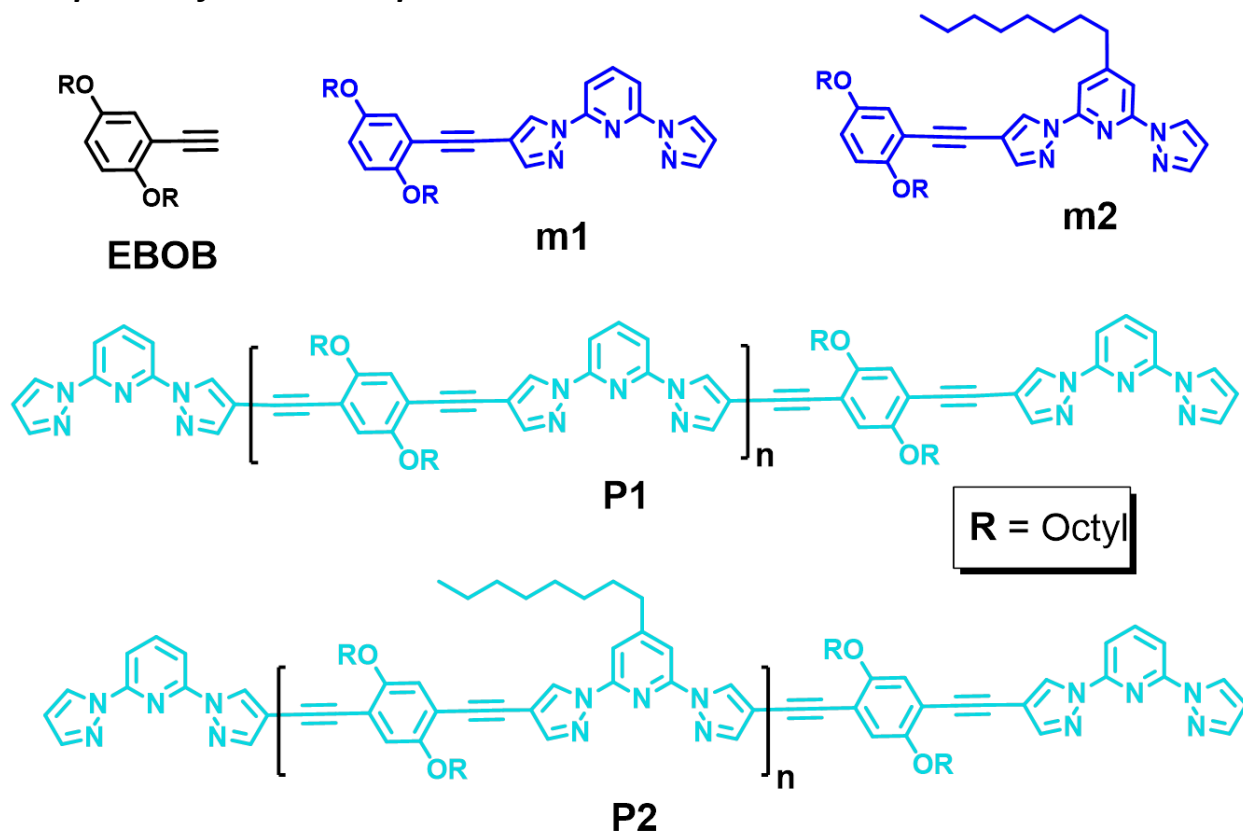
Chart 2.1 Chemical structures of model compounds **EBOB** and (**m1** and **m2**) and copolymers **P1** and **P2**.

2,6-bis(4-iodo-1H-pyrazol-1-yl)pyridine (**1**): This compound was prepared as per our reported procedure.[11c]

2,6-di(1*H*-pyrazol-1-yl)pyridine (1.0 g, 4.74 mmol) in a round-bottomed flask was treated under N_2 with acetic acid (20 mL) and H_2SO_4 (25% in water, 1.0 mL) and heated to 70 °C. A deep violet aqueous solution (H_2O, 10 mL) containing HIO_3 (0.837g, 4.74 mmol), I_2 (1.203 g, 9.48 mmol) and four drops of concentrated H_2SO_4 was added to the solution. This solution was then left under N_2 at 70 °C for a further 6 h. After the mixture was cooled to room temperature, $Na_2S_2O_3$ was added to quench the unreacted iodine. A $NaHCO_3$ solution was used to neutralize the acetic acid/H_2SO_4 mixture and the product 2,6-bis(4-iodo-1*H*-pyrazol-1-yl)pyridine was

extracted with $CHCl_3$ and the $CHCl_3$ solution was evaporated to get off white solid. The solid was washed with MeOH to remove colored impurity which yielded a white solid. Yield 1.75 g, (80%). ^{1}H-NMR (400 MHz, $CDCl_3$) δ/ppm: 8.58 (s, 2H), 7.95-7.90 (dd, $^3J_{H,H}$ = 6.95 Hz, 1H), 7.82-7.77 ($d_{asymmetric}$, $^3J_{H,H}$ = 7.27 Hz, 2H), 7.70 (s, 2H).

2,6-bis(4-iodo-1H-pyrazol-1-yl)-4-octylpyridine (2): This compound was prepared as per our reported procedure.[5f]

4-octyl-2,6-di(1*H*-pyrazol-1-yl)pyridine (0.37 g, 1.051 mmol) in a round-bottomed flask was treated under N_2 with acetic acid (6 mL) and H_2SO_4 (25% in water, 0.8 mL) and heated to 70 °C. A deep violet aqueous solution (H_2O, 5 mL) containing HIO_3 (0.15g, 0.75 mmol), I_2 (0.427 g, 1.7 mmol) and four drops of concentrated H_2SO_4 was added to the solution. This solution was then left under N_2 at 70 °C for a further 6 h. After the mixture was cooled to room temperature, $Na_2S_2O_3$ was added to quench the pale rose color. A $NaHCO_3$ solution was used to neutralize the acetic acid/H_2SO_4 mixture and the product 2,6-bis(4-iodo-1*H*-pyrazol-1-yl)-4-octylpyridine was extracted with $CHCl_3$ and the $CHCl_3$ solution was evaporated to get an shiny off white solid. The solid was washed with MeOH to remove colored impurity which yielded a white solid. Yield 0.75 g, (98%). ^{1}H NMR (400 MHz, $CDCl_3$) δ/ppm: 8.60 (s, 2H), 7.76 (s, 2H), 7.69 (s, 2H), 2.72-2.69 (t, J = 5.4 Hz, 2H, Py-CH_2), 1.74-1.69 (m, 2H), 1.35-1.33 (m, 10H), 0. 88 (t, J = 4.0 Hz, 3H, CH_3).

1,4-diethynyl-2,5-bis(octyloxy)benzene (3): This compound was prepared as per reported procedure.[11b]

A mixture of 1,4-Bis(trimethylsilylethynyl)-2,5-bis(octyloxy)benzene (1.0 g, 1.9 mmol) and KOH (0.140 g, 2.47 mmol) were added to a two-neck round-bottom flask, and was purged with nitrogen for 10 min. Then, CH_3OH (40 ml) and THF (20 ml) were added to the reaction mixture under nitrogen, and the mixture was stirred at room temperature for 2 h. The aqueous layer was separated, and the organic layer was extracted with $CHCl_3$. The organic layer was dried over anhydrous sodium sulfate and evaporated to give the desired product **3** (0.710 g, 97%). ^{1}H-NMR (400 MHz, $CDCl_3$) δ/ppm: 6.91 (s, 2H, Ph-H), 3.91 (t, J = 5.8 Hz, 4H, O-CH_2), 3.33 (s, 2H, ≡C-H), 1.78-1.75 (m, 4H), 1.54 -1.28 (m, 20H), 0.9 (t, J = 4.2 Hz, 6H, CH_3).

2-(4-iodo-1H-pyrazol-1-yl)-6-(1H-pyrazol-1-yl)pyridine (***4***)***:*** This compound was prepared as per our reported procedure.[5f]

2,6-di(1*H*-pyrazol-1-yl)pyridine (0.5 g, 2.37 mmol) was charged in a round-bottomed flask containing AcOH (5 mL) and aq H_2SO_4 (25%, 0.8 mL). A deep-violet aqueous solution (30 mL) containing HIO_3 (0.27 g, 1.75 mmol), I_2 (0.78 g, 3.1 mmol) and two drops of concentrated H_2SO_4. This solution was added drop wise to the above solution within 30 minutes and the reaction was monitored by TLC to increase the mono iodinated product. When the possible maximum amount of mono iodinated product was formed the reaction was quenched by adding aqueous $Na_2S_2O_3$ solution, followed by aq sat.$NaHCO_3$. The white precipitate that formed was extracted with $CHCl_3$ (2 × 50mL), dried over Na_2SO_4 and evaporated under reduced pressure. The crude solid mixture was further purified by column chromatographed on silica gel using 5% EtoAc/Hexane to get desired compound in 0.185 g yield, (23%). R_f ~ value 0.41. ^{1}H NMR (400 MHz, $CDCl_3$) δ/ppm: 8.60 (s, 1H), 8.53 (d, *J* = 6.0 Hz, 1H), 7.20-7.84 (m, 2H), 7.80-7.72 (m, 3H), 6.51 (t, *J* = 4.2 Hz, 1H, Pyrazole).

2-(4-iodo-1H-pyrazol-1-yl)4-octyl-6-(1H-pyrazol-1-yl)pyridine (***5***)***:*** This compound was prepared as per our reported procedure.[5f]

4-octyl-2,6-di(1*H*-pyrazol-1-yl)pyridine (0.98 g, 2.18 mmol) was charged in a round-bottomed flask containing AcOH (7 mL) and H_2SO_4 (25%, 1.3 mL). A violet aqueous solution (35 mL) containing HIO_3 (0.26 g, 1.47 mmol), I_2 (0.715 g, 2.81 mmol) and three drops of concentrated H_2SO_4. This solution was added drop-wise to the above solution and the reaction was monitored by TLC to increase the mono iodinated product. When the maximum amount of mono iodinated product was formed the reaction was stopped by adding aqueous $Na_2S_2O_3$ solution to quench any excess iodine. The mixture was quenched with aqueous sat. $NaHCO_3$ until the solution was reached neutral state. The white precipitate that formed was extracted with $CHCl_3$ (4 × 50mL), dried over Na_2SO_4 and evaporated under reduced pressure. The crude solid mixture was column chromatographed on silica gel using 4% EtoAc/Hexane to get 4-octyl-2,6-di(1*H*-pyrazol-1-yl)pyridine. Yield 325 mg, (22%). R_f value ~ 0.40. ^{1}H NMR (400 MHz, $CDCl_3$) δ/ppm: 8.81 (s, 1H), 8.62 (s, 1H), 8.1-7.9 (m, 3H), 7.67 (s, 1H), 6.52 (s, 1H, Pyrazole), 2.89 (t, *J* = 5.4 Hz, 2H, Py-CH$_2$), 1.78 (t, *J* = 3.6 Hz, 2H), 1.67-1.65 (m, 10H), 0.92 (t, *J* = 2.8 Hz, 3H, CH$_3$).

2-ethynyl-1,4-bis(octyloxy)benzene (**EBOB**)***:*** This compound was prepared as per reported procedure.[11b]

A mixture of 2-Trimethylsilylethynyl-1,4-bis(octyloxy)benzene (1.0 g, 2.32 mmol) and KOH (0.300 g, 5.34 mmol) were added to a two-neck round-bottom flask, and was purged with nitrogen for 10 min. Then, CH_3OH (40 ml) and THF (20 ml) were added to the reaction mixture under nitrogen, and the mixture was stirred at room temperature for 2 h. The aqueous layer was separated, and the organic layer was extracted with $CHCl_3$. The organic layer was dried over anhydrous sodium sulfate and evaporated to give the desired product **1** (0.800 g, 96%). ^{1}H-NMR (400 MHz, $CDCl_3$) δ/ppm: 7.10 (d, $J = 6.2$ Hz, 1H), 6.87 (q, $J = 5.8$ Hz, 2H), 3.95 (t, $J = 4.8$ Hz, 4H, O-CH_2), 3.32 (s, 1H, C≡C-H), 1.82-1.79 (m, 4H), 1.58 -1.55 (m, 20H), 0. 91 (t, $J = 3.2$ Hz, 6H, CH_3).
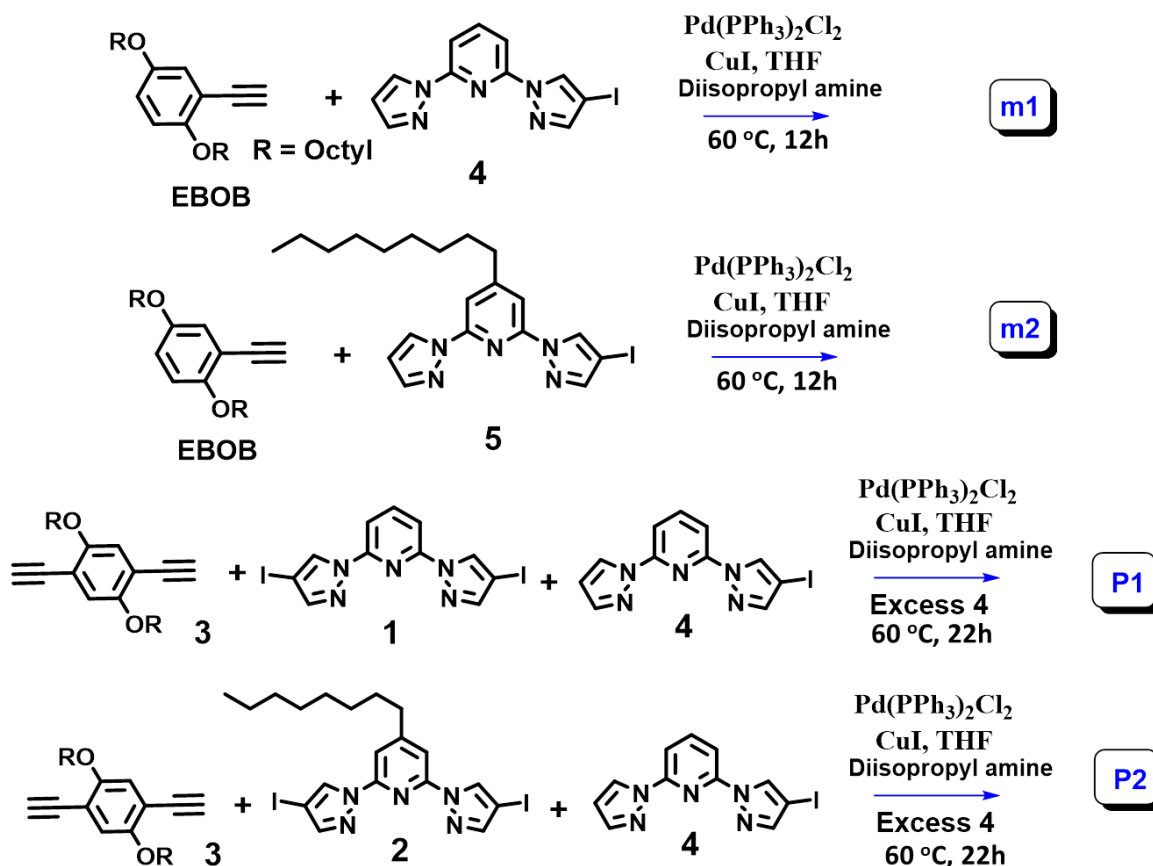
Scheme 2.2 Syntheses of model compounds (**m1** and **m2**) and copolymers **P1** and **P2**.

Synthesis of model compound (m1): 2-ethynyl-1,4-bis(octyloxy)benzene (106 mg, 0.296 mmol), 2-(4-iodo-1*H*-pyrazol-1-yl)-6-(1*H*-pyrazol-1-yl)pyridine (100 mg, 0.296 mmol), THF (10.0 mL), and diisopropylamine (20.0 mL) were added to a two-neck round-bottom flask, and the solution was purged with nitrogen for 10 min. Afterwards the reaction was degassed by a repeated sequence of freeze-pump-thaw cycles. $PdCl_2(PPh_3)_2$ (18 mg, 0.0256 mmol), and CuI (5 mg, 0.0262 mmol) were added to the reaction under nitrogen, and the mixture was stirred at 60 °C overnight. It was then cooled to room temperature; the solvent from the mixture was evaporated under vacuum to afford pale yellowish oil. The product was further purified on a silica column (SiO_2) chromatography with an EtoAc/hexane (1:10) eluent mixture. R_f value ~ 0.60. The compound was obtained as fine yellowish oil (100 mg, yield 60%). ^{1}H-NMR (400 MHz, $CDCl_3$, 298K) δ/ppm: 8.74 (s, 1H), 8.58 (s, 1H), 7.94 (t, *J* = 6.2 Hz, 1H), 7.89-7.86 (m, 2H), 7.79 (s, 1H), 7.0 (s, 1H, Ph-H), 6.85 (s, 2H, Ph-H), 6.58 (t, *J* = 5.8 Hz, 2H, Pyrazole), 3.94 (t, *J* = 4.8 Hz, 4H) 1.40-1.36 (m, 63H), 0.91-0.88 (m, 6H, CH_3). ^{13}C-NMR (100 MHz, $CDCl_3$, 298K) δ/ppm: 153.9, 152.8, 150.1, 144.5, 142.5, 141.5, 129.1, 128.8, 127.0, 118.2, 116.6, 114.1, 109.8, 109.4, 108.1, 106.2, 88.1, 83.5, 69.8, 63.1, 32.8, 31.0, 26.08, 26.05, 25.7, 22.7, 22.6, 14.0. FT-IR (KBr) ν in cm^{-1}**:** 2926, 2854, 1618 (C=C, aromatic), 1745, 1572, 1496, 1466, 1394, 1273, 1217, 1113, 1039, 968, 864, 792, 756. LCMS analysis: m/z calcd 567.76, found = 567.30 (negative mode). Anal. Calcd for $C_{35}H_{45}N_5O_2$: C, 74.04; H, 7.99; N, 12.33. Found: C, 74.12; H, 7.99; N, 12.25.

Synthesis of model compound (m2): 2-ethynyl-1,4-bis(octyloxy)benzene (100 mg, 0.279 mmol), 2-(4-iodo-1*H*-pyrazol-1-yl)-4-octyl-6-(1*H*-pyrazol-1-yl)pyridine (125 mg, 0.270 mmol), THF (10.0 mL), and diisopropylamine (20.0 mL) were added to a two-neck round-bottom flask, and the solution was purged with nitrogen for 10 min. Afterwards the reaction was degassed by a repeated sequence of freeze-pump-thaw cycles. $PdCl_2(PPh_3)_2$ (18 mg, 0.0256 mmol) and CuI (5 mg, 0.029 mmol) were added to the reaction under nitrogen, and the mixture was stirred at 60 °C overnight. It was then cooled to room temperature; the solvent from the mixture was evaporated under vacuum to afford pale yellowish oil. The product was further purified on a silica column (SiO_2) with an EtOAc / hexane (1:10) mixture. R_f value ~ 0.60. The compound was obtained as fine yellowish oil (120 mg, Yield 63%). ^{1}H-NMR (400 MHz, $CDCl_3$, 298K) δ/ppm: 8.74 (s, 1H), 8.57 (s, 1H), 7.89 (s, 1H), 7.75 (t, *J* = 6.0 Hz, 2H), 7.02 (d, *J* = 5.2 Hz, 1H, Ph-H), 6.86 (s, 2H, Ph-H), 6.51 (t, *J* = 6.2 Hz, 1H, Pyrazole), 4.02 (d, *J* = 4.8 Hz, 2H), 3.92 (d, *J* = 4.4 Hz, 2H), 2.7 (t, *J* = 3.2 Hz, 2H, Py-CH_2), 2.0 -1.96 (m, 4H), 1.53-1.14 (m, 33H), 0.91-0.87 (m, 9H, CH_3).

^{13}C-NMR (100 MHz, CDCl$_3$, 298K) δ/ppm: 173.3, 158.5, 154.0, 150.1, 147.0, , 142.2, 129.3, 127.1, 124.4, 123.9, 119.1, 118.3, 117.6, 116.5, 114.2, 109.8, 109.5, 107.9, 106.0, 88.0, 83.6, 69.9, 68.7, 62.1, 35.9, 31.8, 31.4, 30.2, 29.7, 29.6, 29.3, 27.2, 26.0, 25.9, 24.9, 24.8, 22.6, 14.0. FT-IR (KBr) ν in cm^{-1}: 2926, 2854, 1745, 1620 (C=C, aromatic), 1572, 1498, 1466, 1394, 1273, 1219, 1114, 1082, 1039, 968, 866, 792, 758, 723, 652, 611. LCMS analysis: m/z calcd 679.98, found = 678.60 (negative mode). Anal. Calcd for C$_{43}$H$_{61}$N$_5$O$_2$: C, 75.95; H, 9.04; N, 10.30. Found: C, 75.86; H, 9.12; N, 10.43.

Synthesis of polymer (**P1**)*:* 1,4-diethynyl-2,5-bis(octyloxy)benzene (200 mg, 0.522 mmol) 2,6-bis(4-iodo-1*H*-pyrazol-1-yl)pyridine (217 mg, 0.470 mmol), 2-(4-iodo-1*H*-pyrazol-1-yl)-6-(1*H*-pyrazol-1-yl)pyridine (35 mg, 0.10 mmol), THF (10.0 mL), and diisopropylamine (20.0 mL) were added to a two-neck round-bottom flask, and the solution was purged with nitrogen for 10 min. Afterwards the reaction was degassed by a repeated sequence of freeze-pump-thaw cycles. PdCl$_2$(PPh$_3$)$_2$ (36 mg, 0.052 mmol) and CuI (20.0 mg, 0.1 mmol) were added to the reaction under nitrogen, and the mixture was stirred at 60 °C overnight. After 18 h, a small excess of 2-(4-iodo-1*H*-pyrazol-1-yl)-6-(1*H*-pyrazol-1-yl) pyridine (35 mg, 0.10 mmol) was added, and the reaction mixture was stirred for another 4 h. The hot suspension was subsequently poured into a saturated aqueous EDTA solution (100 mL), and the mixture was stirred for 2 h. The organic layer was separated, and the aqueous layer was extracted with CHCl$_3$. The combined organic layer was washed with water, and the volume of the solvent was reduced under rotary evaporator. The concentrated organic layer was redissolved in CHCl$_3$ and MeOH was added drop wise to precipitate off the yellow color polymer. The precipitate was filtered and washed with boiling MeOH, EtOH, acetone followed by room temperature hexane and MeOH and cold CHCl$_3$. Subsequently it was dried in air at room temperature to get **P1** as yellow powder. Yield 270 mg. $\overline{X}_n$ = 12, $\overline{M}_n$ = 5500 by ^{1}H NMR. From GPC data $\overline{M}_n$ = 5600, $\overline{M}_w$ = 18654, PDI = 3.25. ^{1}H-NMR (400 MHz, CDCl$_3$, 298K) δ/ppm: 8.70 (d, *J* = 4.0 Hz, 13H), 8.6 (d, *J* = 3.6 Hz, 2H, end group), 8.5 (s, 4H, end group), 7.96-7.94 (m, 48H), 7.70-7.67 (m, 18H), 7.0 (s, 24H), 6.58 (t, *J* = 2.8 Hz, 2H, end group), 4.05 (t, *J* = 2.8 Hz, 48H), 1.87-1.82 (m, 45H), 1.53-1.48 (m, 282H), 0.86-0.82 (m, 101H). ^{13}C-NMR (100 MHz, CDCl$_3$, 298K) δ: 151.5, 151.3, 149.5, 144.7, 142.5, 134.4, 132.3, 132.2, 132.1, 132.0, 131.9, 131.5, 129.0, 128.4, 116.9, 110.0, 108.1, 106.2, 127.1, 88.1, 85.1, 69.7, 31.7, 29.7, 29.26, 29.36, 29.31, 29.2, 29.1, 26.0, 25.9, 22.63, 14.1, 14.0. FT-IR

(KBr) ν in cm^{-1}**:** 2922, 2851, 2216 (C≡C, str), 1604 (C=C, aromatic), 1581, 1496, 1469, 1433, 1390, 1269, 1188, 1143, 1116, 1006, 960, 947, 860, 798, 777, 719, 692, 653, 613, 540.

Synthesis of polymer **(P2)*:*** Similar procedure was followed as in **P1** synthesis. Here 2,6-bis(4-iodo-1*H*-pyrazol-1-yl)pyridine was replaced by 2,6-bis(4-iodo-1*H*-pyrazol-1-yl)-4-octyl pyridine (217 mg, 0.470 mmol). For purification the yellow color polymer precipitate was filtered and washed with boiling MeOH, EtOH, CH$_3$CN, and room temperature hexanes and MeOH followed by cold CHCl$_3$. Afterwards it was dried in air at room temperature to yield **P2** as yellow color powder. (270 mg): $\overline{X_n}$ = 20, $\overline{M_n}$ = 10600 by ^{1}H NMR. From GPC data: $\overline{M_n}$ = 8.1 KDa, $\overline{M_w}$ = 62.5 KDa, PDI = 7.68. ^{1}H-NMR (400 MHz, CDCl$_3$, 298 K) δ/ppm: 8.70 (d, *J* = 4.4 Hz, 16H), 8.6 (d, *J* = 3.0 Hz, 3H, end group), 8.57 (d, *J* = 3.2 Hz, 2H end group) 7.81 (s, 4H, end group), 7.96-7.92 (m, 72H), 7.70-7.67 (m, 18H), 6.58 (t, *J* = 3.0 Hz, 2H, end group), 4.05 (t, *J* = 2.8 Hz, 75H), 2.7 (t, *J* = 3.2 Hz, 28H) 1.93-1.88 (m, 80H), 1.53-1.48 (m, 528H), 0.86-0.82 (m, 176H). ^{13}C-NMR (100 MHz, CDCl$_3$, 298K) δ/ppm: 158.8, 155.0, 154.8, 153.5, 153.3, 149.5, 149.4, 149.2, 144.5, 144.4, 144.3, 142.3, 131.7, 129.4, 129.3, 129.2, 117.9, 117.7, 117.0, 116.8, 114.0, 110.0, 109.5, 107.9, 106.0, 105.9 88.0, 85.2, 79.3, 69.7, 59.9, 35.9, 31.8, 31.7, 30.1, 29.7, 29.3, 29.2, 29.3, 29.2, 29.1, 29.0, 26.0, 25.9, 22.6, 14.1, 14.0. FT-IR (KBr) ν in cm^{-1}**:** 2942, 2852, 2206 (C≡C, str), 1616 (C=C, aromatic), 1570, 1494, 1464, 1388, 1271, 1203, 1095, 1035, 966, 860, 792, 752, 692, 650, 617, 570, 526.

Preparation of m2.Eu(tta)₃ complex: Model compound **m2** (40 mg, 0.058 mmol) and Eu(tta)$_3$·(H$_2$O)$_3$ (0.051, 0.058 mmol) were dissolved in 20 mL toluene. The reaction mixture was stirred for 12 h at 110 °C. The solvent was removed under vacuum leaving a yellow greasy solid as a crude product, which was further purified by washing with hexane and methanol to remove unreacted metal ion. Yield 60 mg (69%). FT-IR (KBr) ν in cm^{-1}**:** 2964, 2915, 2860, 1616 (C=C, aromatic), 1742, 1567, 1501, 1463, 1265, 1095, 1030, 860, 800. MS analysis: m/z calcd 1495.0, found = 1495.0. Anal.Calcd for C$_{67}$H$_{73}$N$_5$O$_8$S$_3$F$_9$Eu: C, 53.76; H, 4.88; N, 4.68. Found: C, 53.61; H, 4.96; N, 4.58.

Preparation of P1.Eu(tta)₃ complex: Copolymer **P1** (60 mg, 0.006 mmol) and Eu(tta)$_3$·(H$_2$O)$_3$ (0.010, 0.006 mmol) were dissolved in 30 mL toluene. The reaction mixture was stirred for 12 h at 110 °C. The solvent was removed under vacuum to get a brown solid as the crude product. This was further purified by washing with solvents hexane and methanol to remove unreacted

metal complex. Yield 40 mg (64%). ^{1}H-NMR (400 MHz, CDCl$_3$, 298 K) δ/ppm: 8.80 (br), 8.6 (end group, br and small), 7.9 (br), 7.45 (br and small), 7.0 (br), 6.82 (br), H$_c$ (3) in tta), 6.50 (s, end group), 6.30 (br), H$_f$ (1)), 5.85 (br), H$_c$ (1)), 4.05 (br), 2.52 (br) 1.82 (br), 1.21 (br), 0.86 (br). FT-IR (KBr) ν in cm^{-1}: 2926, 2847 (sp^3- CH$_3$, CH$_2$ and CH, str), 1610 (C=C, aromatic), 1466, 1178, 1127, 951, 859, 766, 719, 679, 640, 578. UV-Vis: 331 nm, 363 nm and shoulder at 428 nm. Emission (λ$_{max}$): 444 nm (Blue region), 532 nm (Green region) and 612 nm (Red region).
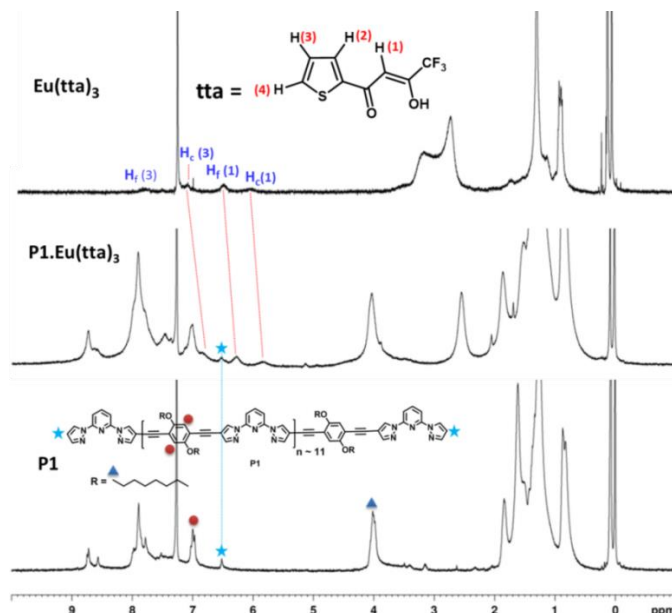
Figure 2.1 ^{1}H-NMR spectra of copolymer **P1**, Eu(tta)$_3$ and MCCP **P1**.Eu(tta)$_3$.

Model compound 2-ethynyl-1,4-bis(octyloxy)benzene (**EBOB**) was prepared as per the reported procedure.[11b] Further **m1** and **m2** were synthesized via Sonogashira cross-coupling conditions by reacting **EBOB** with 2-(4-iodo-1H-pyrazol-1-yl)-6-(1H-pyrazol-1-yl)pyridine (**4**) and 2-(4-iodo-1H-pyrazol-1-yl)-4-octyl-6-(1H-pyrazol-1-yl)pyridine (**5**), respectively in ca. 60% yields. For the synthesis of cyan emitting copolymer **P1**, 1,4-diethynyl-2,5-bis(octyloxy)benzene was prepared from hydroquinone.[11b] 2,6-bis(4-iodo-1H-pyrazol-1-yl)pyridine (bpp) was synthesized from 2,6-dibromopyridine in >80% yield.[11c] Preparation of copolymer **P1** end capped with bpp was effected under Sonogashira cross-coupling reaction conditions in presence of diisopropyl amine/THF to synthesize a cyan emitting copolymer. For the purification, the concentrated organic layer was redissolved in CHCl$_3$ and MeOH was added drop-wise to form an off brown colored precipitate. The precipitate was filtered and washed with boiling MeOH, acetone followed by room temperature hexane and MeOH, and cold CHCl$_3$ to isolate yellow polymer

powder. For the synthesis of **P2**, the same procedure as for **P1** was followed to get a yellow polymer powder. To improve the solubility of **P2**, 2,6-bis(4-iodo-1*H*-pyrazol-1-yl)-4-octylpyridine (**5**) and (**3**) were copolymerized using Sonogashira cross-coupling reaction with **4** as an end capping agent to obtain good soluble polymer **P2**. To determine the molecular weight ($\overline{M_n}$) of **P1** from the ^{1}H-NMR spectrum (see Fig. 2.2), the pyrazole proton (a) chemical shift ($\delta \sim$ 6.6 – 6.4 ppm) of the end-capping unit (**4**) was used. The ratio of the protons on phenyl ring (marked by "d") to bpp (marked as "a") was 24:2, but for a corresponding monomer (i.e. having one phenyl unit) the ratio is 1:1. This ratio showed that there are 12 repeating phenyl units in the polymer; from this result the calculated $\overline{M_n}$ value was in the range of 5.5 KDa. Similarly for **P2** the ratio of protons on phenyl ring (marked as "d") to bpp (marked as "a") was 40:2, but for a corresponding monomer the ratio is 1:1. From this the calculated $\overline{M_n}$ value becomes $\sim$ 11 KDa (Fig. 2.2). Additionally the obtained polymers were subjected to Soxhlet extraction to remove low molecular weight polymer chains and to isolate thin film forming higher molecular weight fractions. The GPC analysis showed improved ($\overline{M_n}$) in the range of 5.6 KDa and 8.1 KDa, for **P1** and **P2**, respectively (Table 2.1). A model Ln containing metallo-copolymer i.e., **P1**.Eu(tta)$_3$ was prepared by heating the toluene solutions of **P1** and Eu(tta)$_3$ to reflux for 12 h to get brown color solid. The unreacted Eu(tta)$_3$ was removed by washing with hexane and MeOH. The comparative ^{1}H-NMR spectra of **P1**, Eu(tta)$_3$ **P1**.Eu(tta)$_3$ complex are presented in Figure 2.1. In Eu(tta)$_3$, protons corresponding to H$_{c, f}$ (1) and H$_c$ (3) are 6.05, 7.05 and 6.50 ppm, where H$_c$ and H$_f$ stand for complex and free ligand protons.[11d] The chemical shift 5.85, 6.82 and 6.30 ppm of these protons are shifted slightly up field in **P1**.Eu(tta)$_3$ complex indicating coordination of Eu(tta)$_3$ with main chain bpp units of **P1**.

Table 2.1. $\overline{M_n}$, $\overline{M_w}$ and T$_D$ of Copolymers (**P1** and **P2**).

Polymer	$\overline{M_n}$ (by ^{1}H NMR)	$\overline{M_n}$ by GPC (after Soxhlet extraction)	$\overline{M_w}$ by GPC	PDI	T$_D$ (°C) (by TGA)
P1	5500	5600	18654	3.25	270
P2	10000	8100	62500	7.68	314

T$_D$ = Decomposition temperature
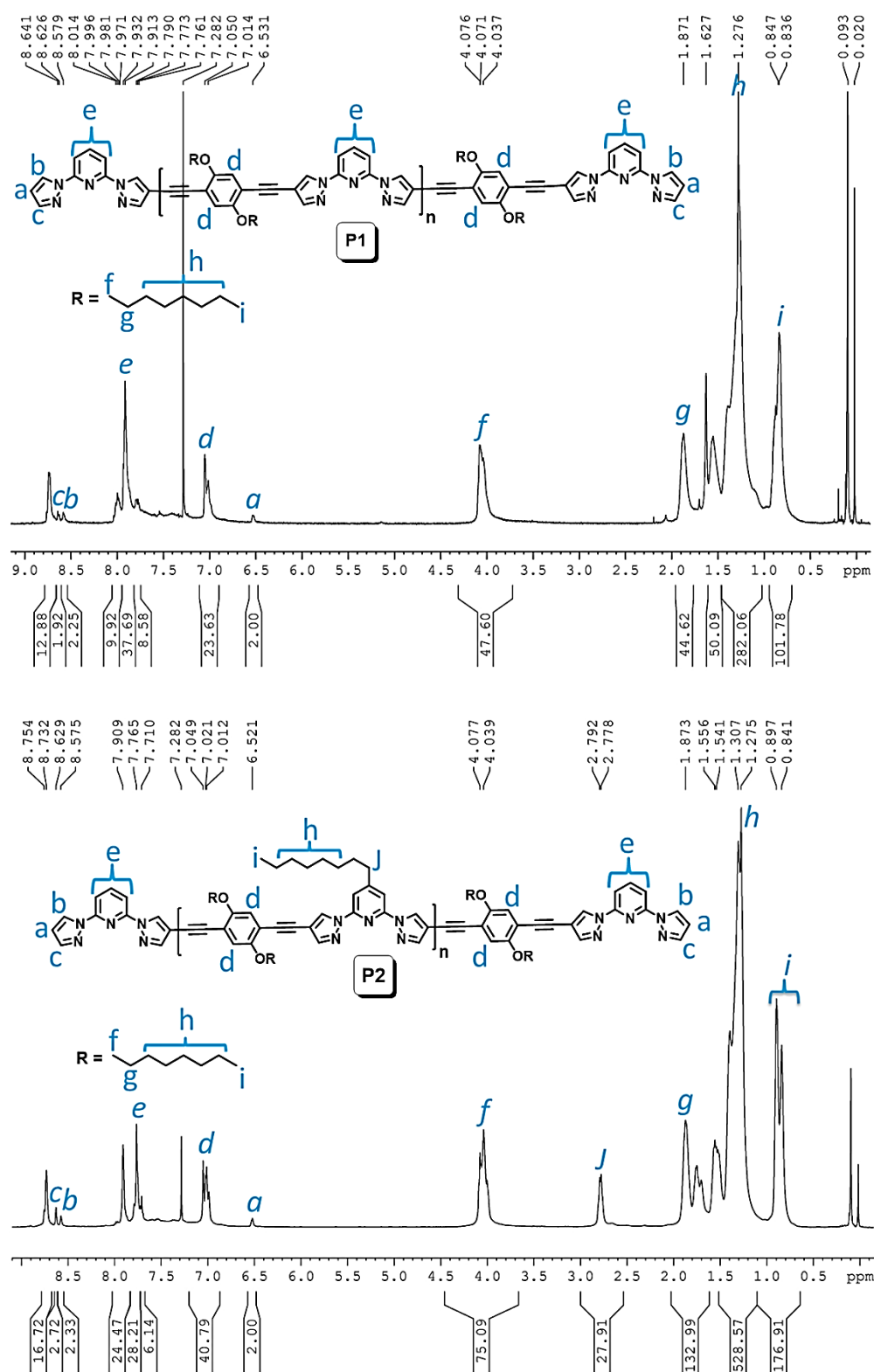
Figure 2.2 ^{1}H-NMR spectra of copolymers **P1** and **P2** in CDCl$_3$.

2.3.2 *Thermal Properties of Polymers*

The thermal stability of all the polymers was investigated by thermo-gravimetric analysis (Fig. 2.3). The copolymers **P1** and **P2** exhibited good thermal stability. It was found that the polymer **P1** was stable up to a temperature of ca. 285 °C (92.7%), above which it degraded with a ~28% weight loss at ~350 °C and further a ~21.5% weight loss was observed at 533 °C. Polymer **P2** was stable up to 312 °C (93.2%) with a 20.4% weight loss at 392 °C and with a slight stability the weight loss continued to ~

Figure 2.3 TGA curve of copolymers **P1** and **P2**

30.7% at 529 °C. The sequence of weight loss is probably as a result of the decomposition of the alkyl chains on phenyl rings followed by phenyl units.

2.3.3 *Optical Properties of Copolymers in Solution State*

The photo physical properties of the model compounds **EBOB**, (**m1** and **m2**) and copolymers (**P1** and **P2**) were studied in CHCl$_3$ solution and also as spin-casted thin films. All the spectroscopic data are summarized in Tables 2.2 and 2.3. The optical properties of model compounds in solution and solid states are presented Figure 2.4. All the model compounds showed two absorption bands in their in solution and solid states absorption spectra.

Table 2.2 Spectroscopic data of model compounds **EBOB**, **m1** and **m2** in solution and solid states.

	Solution (CHCl$_3$)			Solid state		
Monomer	Absorption λ_{max} (nm)	Extinction Coefficient (ε) x10^5(M^{-1}cm^{-1})	Emission λ_{max} (nm)	Absorption λ_{max} (nm)	Extinction Coefficient (ε) x10^3(M^{-1}cm^{-1})	Emission λ_{max} (nm)
EBOB	280, 316 371& 400 (shoulders)	5.92	363	318	6.17	380
m1	280, 316	6.94	372	282, 336	8.75	408, 461, 538
m2	280, 316	9.12	372	282, 337, 375	9.50	380, 430
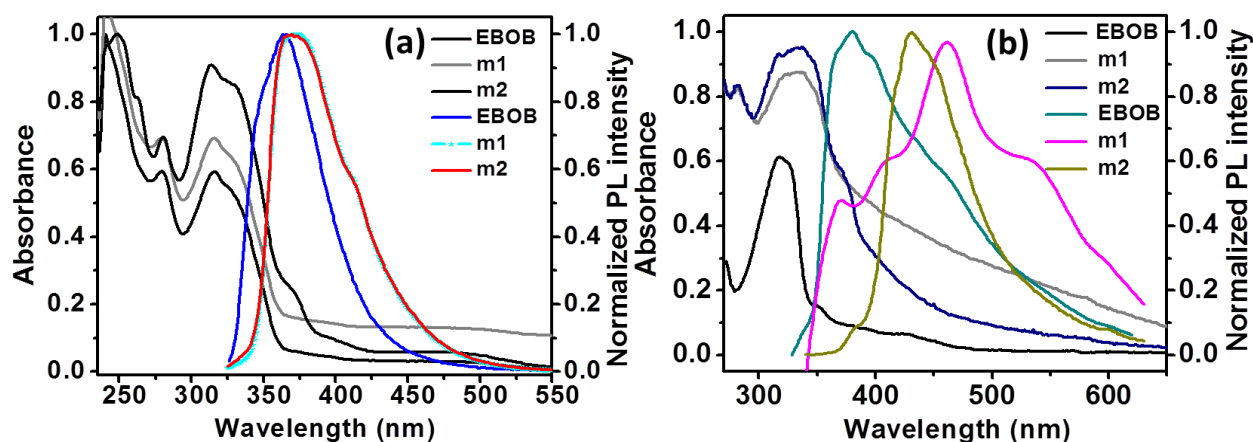
Figure 2.4 Absorption and emission spectra of **EBOB**, **m1** and **m2** in (a) solution (b) solid states.

The solution state absorption spectra of model compounds have two bands around at 280 and 316 nm. The lower wavelength 280 nm band corresponds to π-π* electronic transitions. The higher wavelength 316 nm is corresponds to n-π* electronic transitions. The solid state absorption spectra of model compounds showed two major bands around 282 and 336 nm. In comparison solution state absorption and emission, the solid state absorption and emission maxima were red shifted to higher wavelengths. This shift is probably due to the molecules aggregation in solid state. In comparison to model compounds, the absorption and emission spectra of copolymers (**P1** and **P2**) were also red shifted in solution and thin film states due to the extend conjugation (Fig. 2.5). The absorption spectra of copolymers showed mainly two bands 305 and 365 nm for **P1** and 324 and 373 nm for **P2** in solution state, here the higher wavelength band corresponds to n-π* transition, and lower wavelength band corresponds to π-π* transition. As shown in Table 2.3 and Fig. 2.5, the absorption and emission of thin films of polymers were red shifted and compared to their solution state, this a known phenomenon observed for many conjugated systems and is generally interpreted as formation of *J* -aggregates in the solid state.[12] In solution state **P1** and **P2** showed mostly bluish cyan color with emission peaks maxima centered at 401, 440, 460 nm and 399, 439, 466 nm, respectively for the excitation (λ_{ex}) performed at around 370 nm. The bpp unit of the polymer main chain is known to coordinate with red emitting Eu(tta)$_3$ (tta=3-thenoyltrifluoroacetonate) complex forming nine coordinated structures.[8g,h,i] Taking advantage of the metal coordinating ability of the bpp units available in the polymer main chain, the emission color of polymers were tuned by coordinating Eu^{+3} metal complex.

Table **2.3** Solution and solid state optical absorption and emission data of P1 and P2.

Polymer	Solution (CHCl₃)				Thin Film			
	Absorption λ_{max} (nm)	Excitation λ_{max} (nm)	Emission λ_{max} (nm)	$\Phi_f{}^a$	Absorption λ_{max} (nm)	Excitation λ_{max} (nm)	Emission λ_{max}(nm)	Optical band Gap^b/eV
P1	305,365, 420 (shoulder)	365	401, 440, 460	21%	320, 378, 431 (shoulder)	378	405, 470, 542	2.63
P2	324, 373, 423 (shoulder)	373	399, 439, 466	44%	322, 386, 437 (shoulder)	386	407, 446, 541	2.53

^{a}Quinine sulfate as reference ($Q_{ref} = 0.577$). ^{b}Estimated from the onset wavelength of optical absorption in the solid state film.
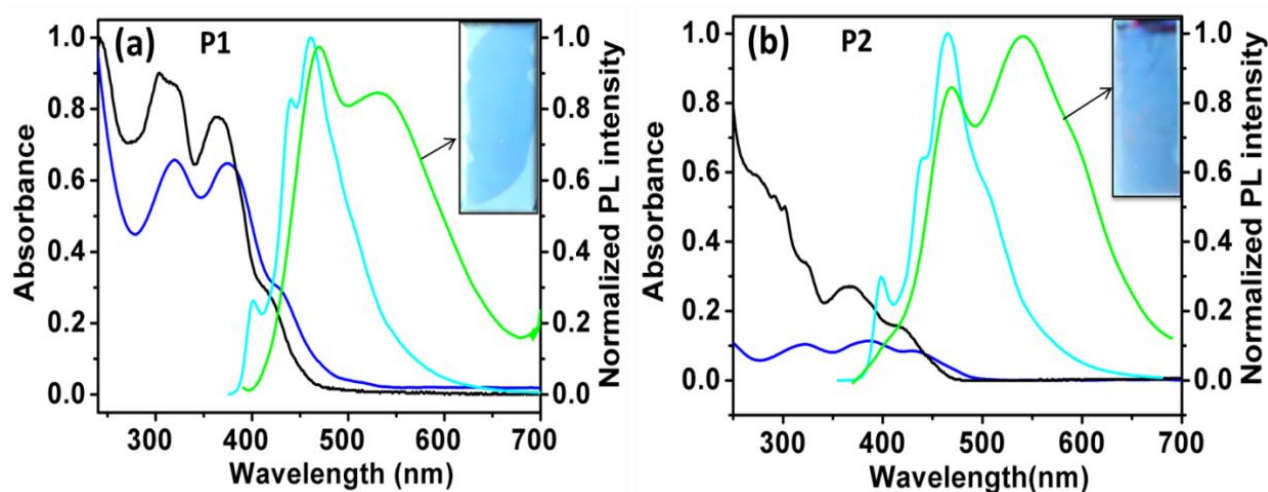
Figure 2.5 Optical absorption spectra of copolymers **P1** and **P2** in CHCl₃ (⎯) and spin casted film (⎯). PL spectra of copolymers in CHCl₃ solution (⎯), and spin-casted film (⎯). The insets show the emission colors of the copolymer films under UV light.

For example, a solution of **P1** (c ~1.0 × 10^{-1} mg/ 4 ml) showed cyan color emission and to this addition of THF solution of Eu(tta)₃ (c~1.58×10^{-2} mg/ 0.5 ml) displayed a white color light (Fig. 2.6a). The emission spectra of Eu^{3+} ion displays peaks at 581, 594, 612, 653, 705 nm due to $^5D_0 \rightarrow {}^7F_J$ (J = 0-4) f-f transitions.[13a-b] Amongst the peaks corresponding to that of Eu^{3+} ion, the

strongest emission was at 612 nm arises from the $^5D_0 \rightarrow {}^7F_2$ induced electronic dipole transition, this clearly indicates that the chemical environment around Eu^{3+} ions does not have an inversion center.[13c]
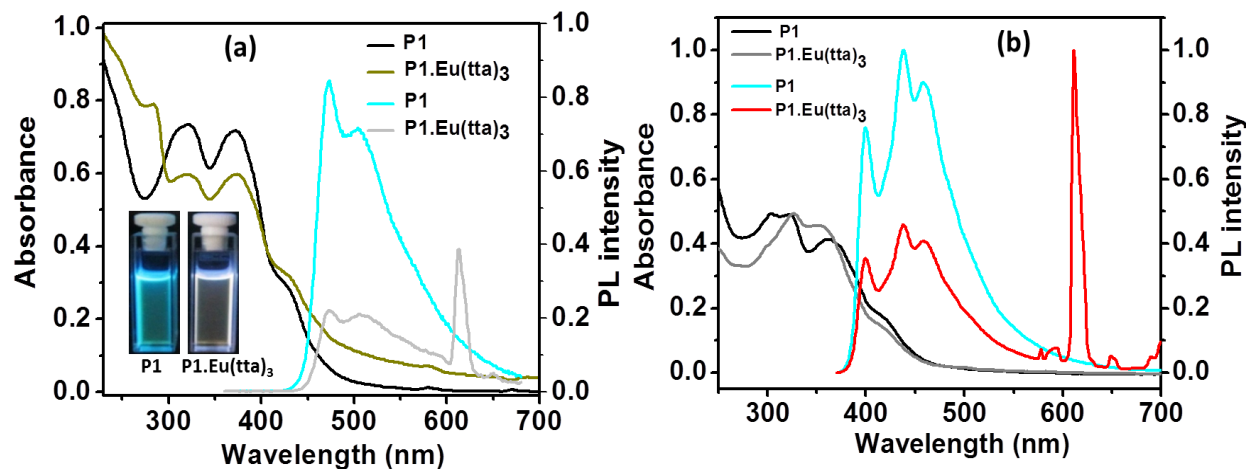
Figure 2.6 a) Absorption and emission spectra of copolymer **P1** and **P1**.Eu(tta)₃ in chloroform. The insets show the solutions under UV light irradiation. b) Absorption and emission spectra of pure copolymer **P1** and bulk complex (**P1**.Eu(tta)₃) in chloroform.

Further, bulk complex of **P1** with Eu(tta)₃ was also synthesized to confirm the **P1** complex formation with Eu(tta)₃. The solution state optical properties of **P1** and **P1**.Eu(tta)₃ is presented in Figure 2.6b. Excitation (λ_{ex} =360 nm) of bulk **P1**.Eu(tta)₃ complex in the showed slightly different optical band compared to simple mixed solution of **P1** and Eu(tta)₃ (Fig. 2.6a, b). This is probably because of the number of complexes formed along the polymer chain prepared by bulk reaction is different from the ones present in simple mixed solution of **P1** and Eu(tta)₃, which ultimately affect the electronic structures. The decrease of cyan PL intensity of polymer **P1** can be attributed to the energy transfer from polymer backbone to Eu^{3+} metal centre.

2.3.4 *Optical Properties of Pristine Films and Eu(III) Coordinated Thin Films*

All the polymers were readily processed into homogeneous films of good optical quality by spin-coating from CHCl₃ (for **P1** and **P2**) solution (c ~3 ×10^{-3} M for **P1**, c ~ 2× 10^{-3} M for **P2**) at 6000/1000 rpm on clean quartz substrates. The spin coated (from CHCl₃) dry thin films of **P1** and **P2** showed green emission (400–650 nm range) due to aggregation induced excimer like behavior.[14] A solid solution of **P1** prepared with a non-emissive polymer matrix (poly((tetrahydrofuran)-tetrathane-2900) supported this aggregation phenomenon (Fig.2.7).

Upon increase of terathane/**P1** ratio the solid film showed decrease of green emission due to the segregation of polymer chains. At 1:1 ratio (terathane/**P1**) the solid film almost behaved like solution. The polymer film emission intensity of I_{blue}/I_{green} was adjusted by tuning the polymer film thickness[5f,15] in such a way that a cyan color light can be obtained. Here the thickness of the film was varied by changing the concentration of the solution and keeping the injection amount (200 µL), spin coating time (10 sec) and rpm (6K/1K) rate same for each cases. The film obtained by spin coating of a $CHCl_3$ solution of concentration of 12.37 mg/mL of **P1** emitted a good cyan color with I_{blue}/I_{green}~1 (Fig. 2.8). Furthermore by using the metal coordination ability of main chain BPP tridentate ligand units of copolymers **P1** and **P2**, incorporation of red emitting $Eu^{(III)}(tta)_3$ (tta = thenoyltrifluoroacetonate) was envisioned to achieve a final white color light.[16]
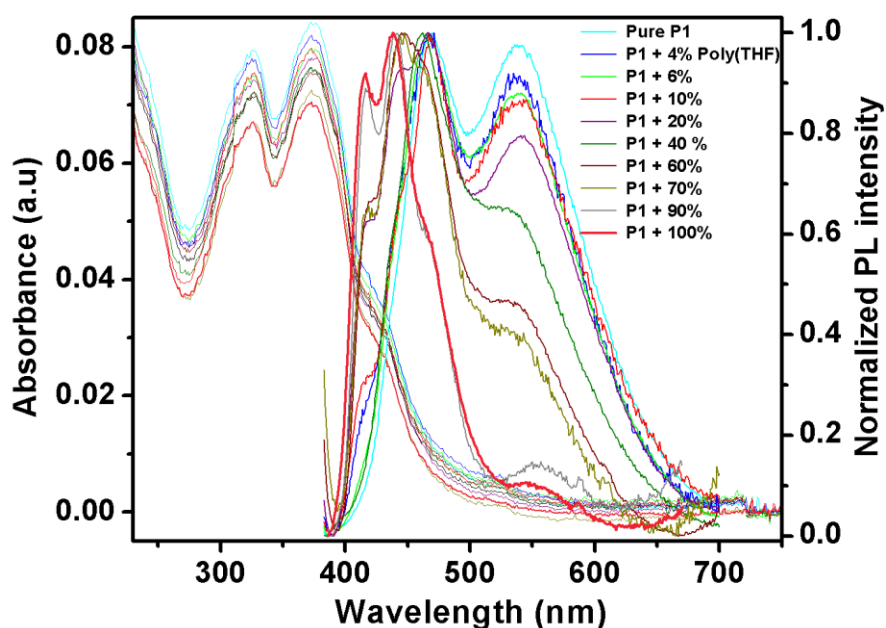
Figure 2.7 Spin cast films of copolymer **P1** in poly (tetrahydrofuran) from $CHCl_3$ solution. Films were excited at 373 nm.

For this the **P1** film was dipped in a 20 mL methanol solution containing 0.5 mg $Eu(tta)_3$ complex for half an hour. Here the amount of $Eu(tta)_3$ complex formation was adjusted to control the intensity of the $Eu^{(III)}$ centered red phosphorescence [$^5D_0{\rightarrow}^7F_J$ (J=0–4) transitions] according to the intensity of I_{blue}/I_{green} emissions to attain good quality white color. UV light exposure of **P1** film reacted with $Eu(tta)_3$ complex showed a white color light due to the mixing of 474/541/613 nm emissions (Fig. 2.9a). Similarly for **P2** white light (Fig. 2.9b) was obtained by controlling the
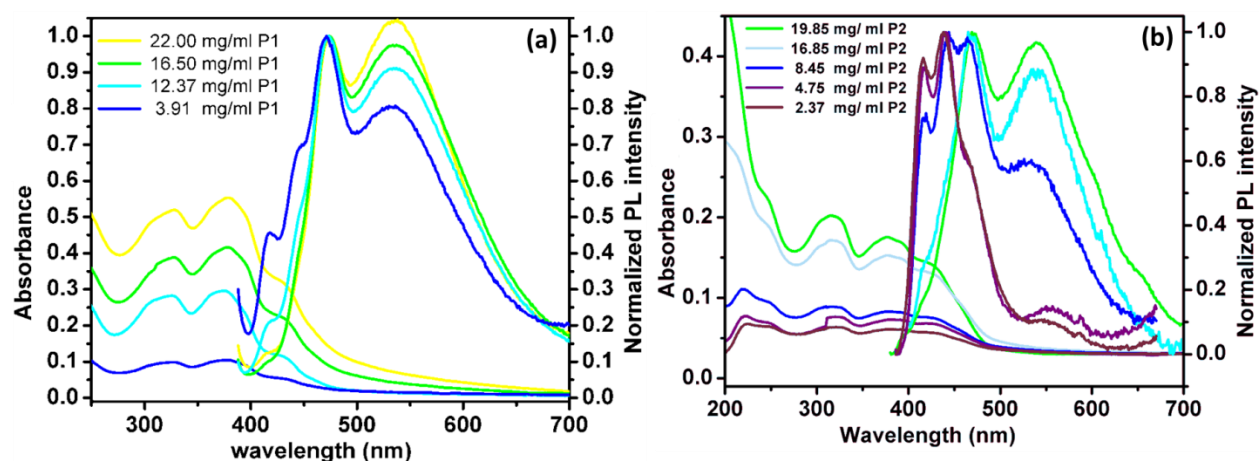
Figure 2.8 Absorption and emission spectra of **P1** (left) and **P2** (right) polymer films prepared by spin coating from a CHCl$_3$ solution at different concentration.
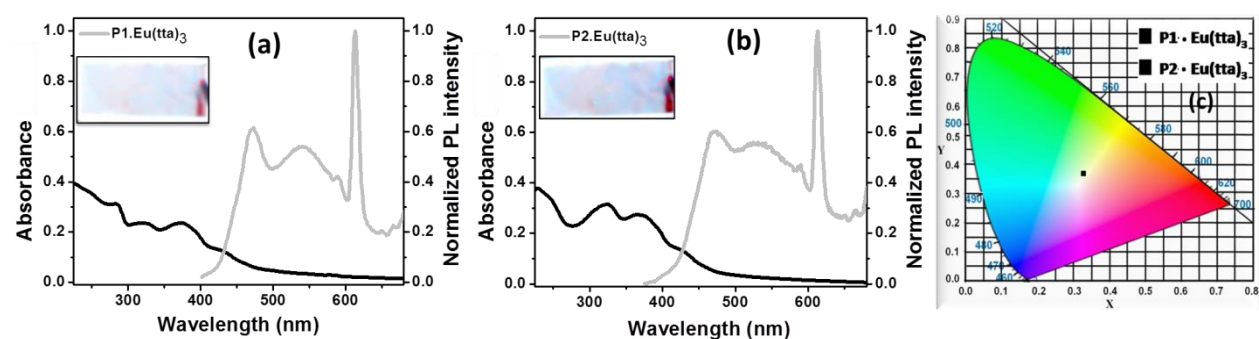
Figure 2.9 a) and b) Optical absorption and emission spectra of white emitting Eu(tta)$_3$ coordinated **P1** and **P2** films, respectively. c) Emission color of Eu(tta)$_3$ coated **P1** and **P2** film in a CIE 1931 2° Standard observer chromaticity diagram. The insets in (a) and (b) show the white emitting thin films under UV excitation.

polymer film thickness ($c \sim 16.87$ mg/ml of CHCl$_3$) and Eu(tta)$_3$ concentration. The purity of the emitted white-light was analyzed by chromaticity diagram (Fig. 2.9c), for which the CIE coordinates[17] were found to be ($x = 0.33$; $y = 0.37$) and ($x = 0.33$; $y = 0.37$) for films made from **P1** and **P2**, respectively, which are nearly close to the designed coordinates for perfect white-light ($x = 0.33$; $y = 0.33$).

Moreover, the involvement of energy transfer process between the polymer backbone and Eu^{III} coordinated centre in the white emitting polymer **P1** was investigated (Fig. 2.10). Excitation of white light emitting Eu(tta)$_3$ coordinated **P1** polymer at 373 nm (corresponding to the absorption maximum of **P1**), showed luminescence bands correspond to pure polymer and Eu^{III}(tta)$_3$ (Fig. 2.10c). While direct excitation of the same polymer at 413 nm (corresponding to the absorption of

Eu(tta)$_3$) exhibited no emission from Eu^{III}(tta)$_3$ (Fig. 2.10c), but at this wavelength pure Eu(tta)$_3$·3H$_2$O showed red emission (Fig. 2.10d). Similar behavior was observed for the **m$_2$**·Eu(tta)$_3$ model complex (Fig. 2.11). This observation established the reaction of six coordinated Eu(tta)$_3$ molecules with BPP unit of the copolymer and the formation of nine coordinated [PE-(BPP(Eu(tta)$_3$))]$_n$ complexes[8i] on the polymer surface. Moreover, the excitation spectrum of white light emitting Eu(tta)$_3$ coordinated **P1** polymer film monitored at λ_{em} of 613 nm (corresponds to $J = 2$ transition of Eu^{3+}) showed two maxima at 373 and 431 nm, matching with the absorption of pure **P1** film and Eu(tta)$_3$ (Fig. 2.10e), thus suggesting the operating energy transfer process from the polymer **P1** backbone to the Eu(III) center.[18]
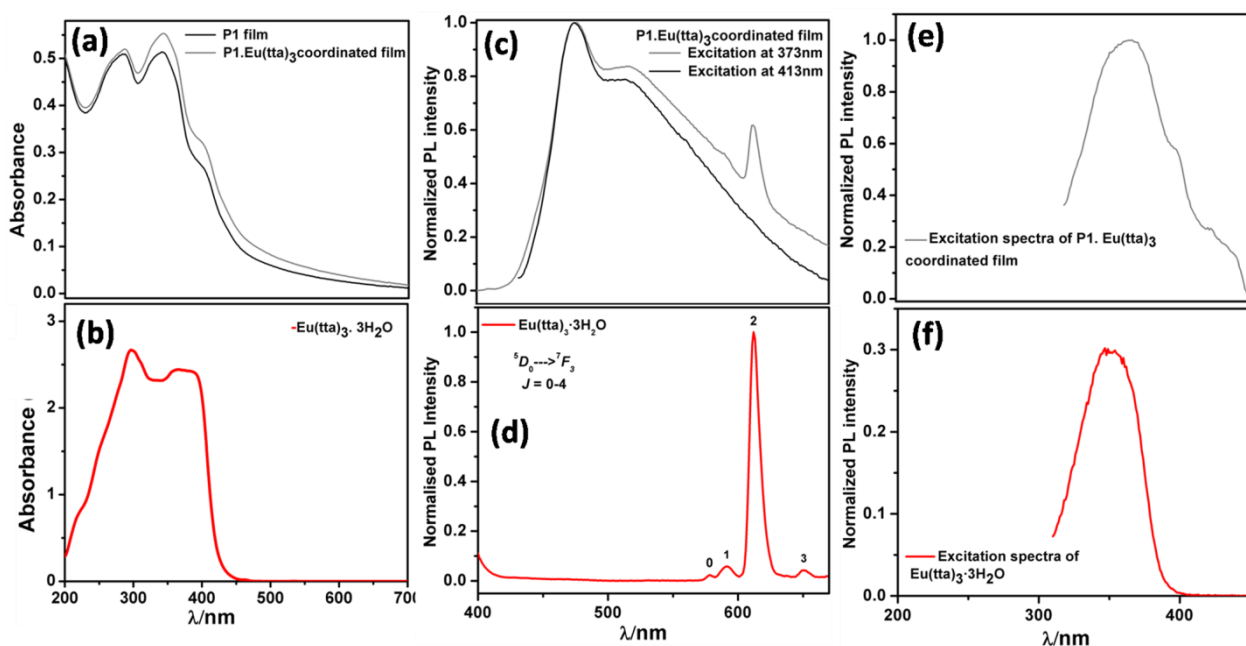
Figure 2.10 (a) Absorption: **P1** (——) and Eu(tta)$_3$ coordinated film(——). (c) Emission: Eu(tta)$_3$ coordinated film, λ_{exc} = 373 nm (——); λ_{exc} = 413 nm (——) (e) Excitation: Eu(tta)$_3$ coordinated film, λ_{em} = 613 nm (——). (b) Absorption, (d) emission (λ_{exc} = 413 nm), and (f) excitation (λ_{em} = 613 nm) spectra of Eu(tta)$_3$·3H$_2$O
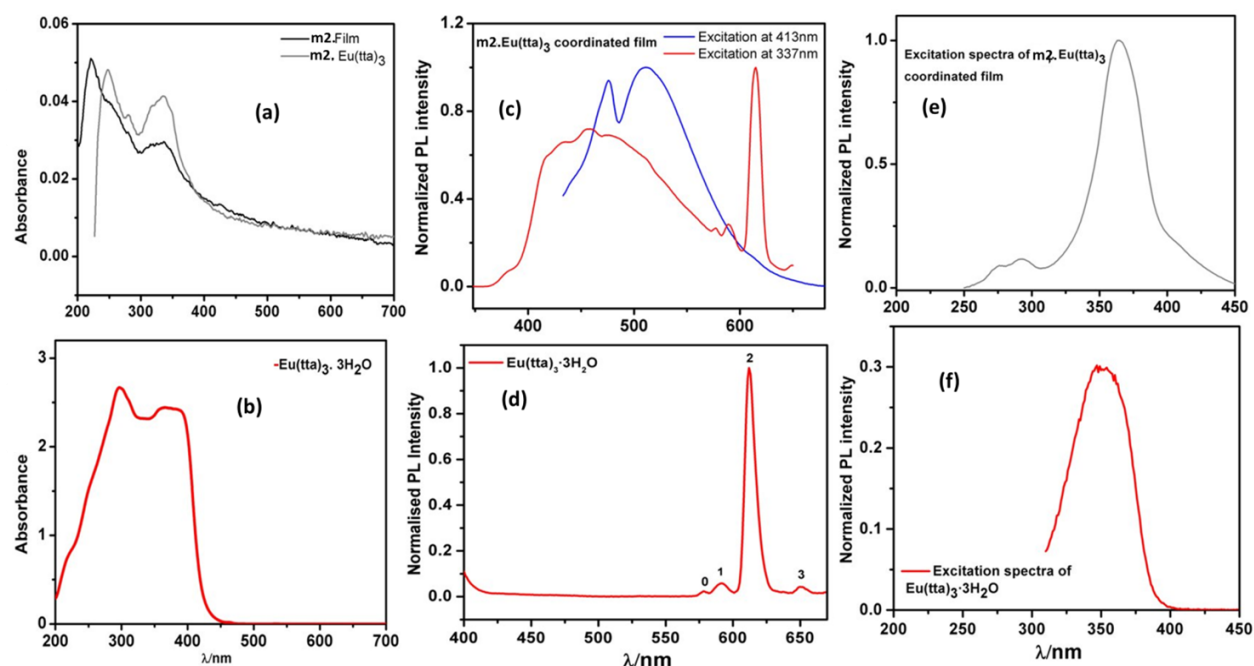
Figure 2.11 (a) Absorption: **m2** (▬) and Eu(tta)$_3$ coordinated film(▬). (c) Emission: Eu(tta)$_3$ coordinated film, λ_{exc} = 337 nm (▬); λ_{exc} = 413 nm (▬) (e) Excitation: Eu(tta)$_3$ coordinated film, λ_{em} = 613 nm (▬). (b) Absorption, (d) emission (λ_{exc} = 413 nm) and (f) excitation (λ_{em} = 613 nm) spectra of Eu(tta)$_3$·3H$_2$O.

2.3.5 *White Emitting Nano/Micro Scale Polymer Spheres*

The reaction of Eu(tta)$_3$ on the cyan colour films (**P1** and **P2**) was inhomogeneous, because of that the resultant white colour intensity varied along the film surface (Fig. 2.9). Hence, a bottom-up self-assembly route was adopted to prepare CP/MCCP based hybrid spheres. In a representative procedure, 1 mg of **P1** was dissolved in 1 mL of THF and the solution was kept for 15 min undisturbed to stabilize growth of spheres (Fig. 2.12). Illumination of the THF solution containing spheres with laser light displayed a fine Tyndall effect indicating the formation of solution-stable nanostructures (Fig. 2.13b (inset)).
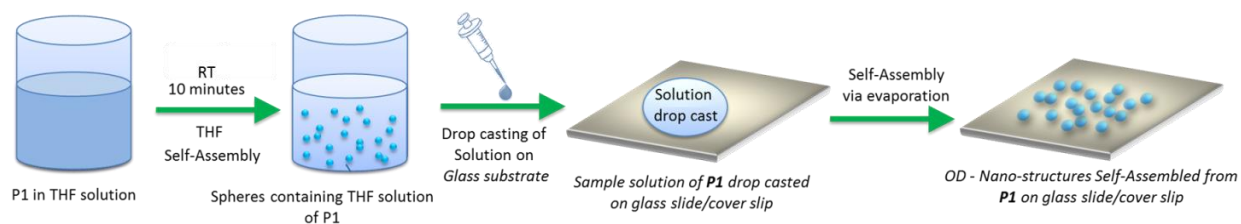
Figure 2.12 Bottom-up self-assembly route towards copolymer **P1** spheres.
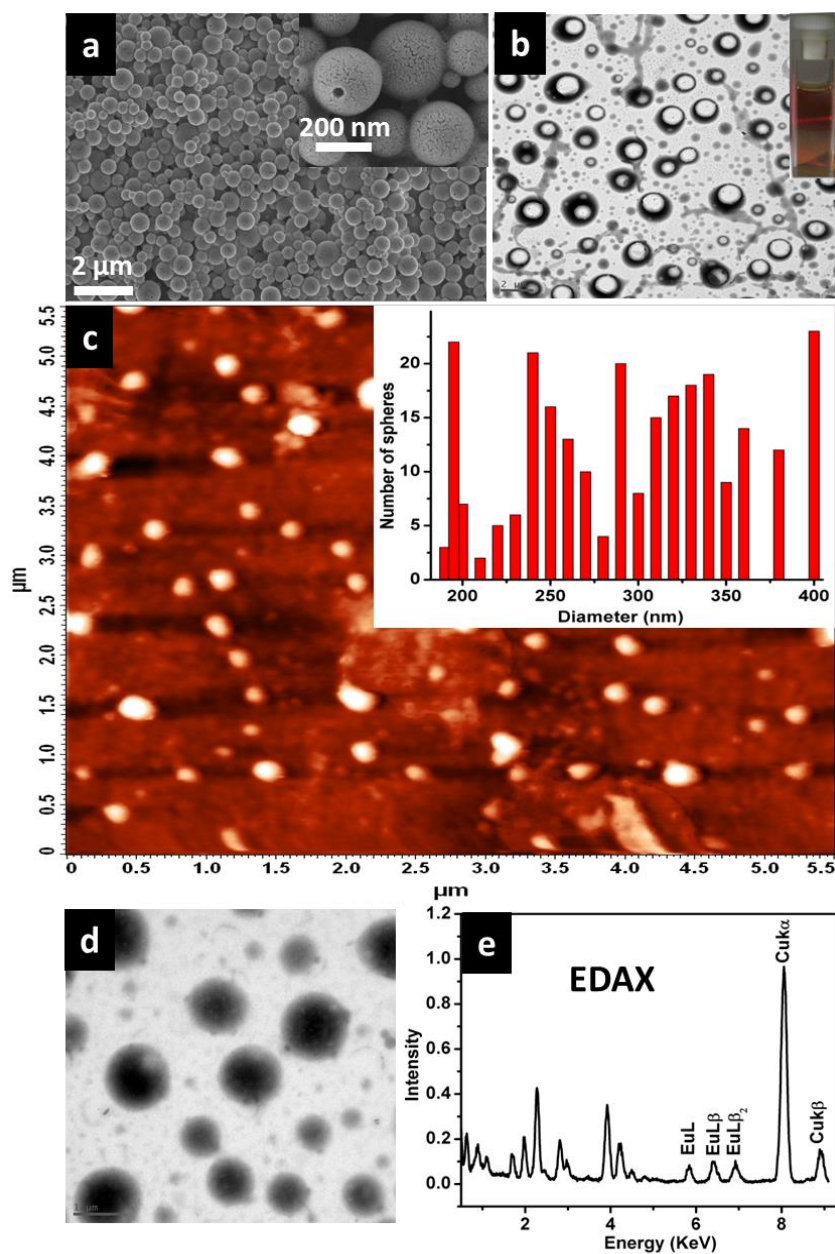
Figure 2.13 a) FESEM micrographs of CP spheres obtained from **P1** (scale bar is 2 μm), (inset shows a closer view of the spheres; b) bright field TEM image of spheres scale bar is 2 μm (inset- Illumation of laser through a THF containing **P1** nano/micro-spheres); c) AFM image of nanoscale spheres; (inset plot estimates the diameter/number of spheres in an area shown in c; d) TEM image of Eu(III) coordinated CP spheres (hybrid CP/MCCP) (scale bar is 1 μm). e) EDAX spectrum exhibiting Eu(III) ions peaks.

Further more dynamic light scattering (DLS) experiment (**P1** in THF) confirmed the presence of nano-spheres in the solution with the hydrodynamic radius in the range of $r_{\mathrm{H}} = 118$–143 nm. Two drops of this polymer solution were drop casted on a clean glass substrate at room temperature for FE-SEM, AFM and confocal fluorescence microscope studies or on a carbon

coated grid for TEM analysis. The FE-SEM and AFM examination of the sample revealed the formation of nano and micro spheres with rough surface and nano scale holes (Fig. 2.13a, c). TEM micrographs of CP spheres displayed a relatively weak contrast as usually observed for soft organic structures (Fig. 2.13b). AFM cross-section analysis of several spheres showed that the diameter is in the range of ca.190 nm - 400 nm (Fig. 2.13c). The self-assembly of cyan emitting CP spheres is possibly formed by the π-π stacking interactions of the polymer aromatic units thereby increasing the close packing of the hydrophobic octyl-chains forming a sphere like structures (Scheme 2.1). In order to obtain white colour from cyan emitting spheres our earlier original approach (i.e., coordination chemistry on the surface of self-assembled solids) was followed.[8h,i] Firstly, the CP spheres templates were grown in THF solution of **P1**, as mentioned before. Secondly, by injecting a THF solution of $Eu(tta)_3 \cdot (H_2O)_3$ (0.869 mg/0.02 mL) to the solution containing the CP spheres, followed by gentle shaking, a layer of [(Eu(tta)$_3$)(**P1**)] coordination complex[8h,i] was formed on the surface of the spheres.

The possible mechanisms of [(Eu(tta)$_3$)(**P1**)] complex formation on the spheres are: (i) by the coordination of Eu(tta)$_3$ with the surface exposed BPP units and (ii) diffusion of Eu(tta)$_3$ into the pores or defective sites of the spheres, and then coordinating with BPP units thereby blocking the pores and defects. Examination of the TEM-bright field images obtained from the CP/MCCP spheres exhibited an apparent dark contrast for the areas coated with Eu(III) complex compared to light contrast displayed by the unreacted CP spheres (Fig. 2.13b, d). In addition, the energy dispersive X-ray spectroscopy analysis (EDAX) performed on the surface of a sphere clearly confirmed the presence of Eu ions (Fig. 2.13e). In order to confirm the appearance of cyan and white colours from both CP and CP/MCCP spheres, respectively, scanning confocal fluorescence microscopy measurement was performed (Fig. 2.14a-f). The topographic structural data were directly coupled with the spectroscopic properties of the specimen. For excitation Ar$^+$ (UV-365) laser was used. As expected the **P1** based CP spheres displayed a cyan color due to the mixing of blue and green emissions. Whereas CP coated with Eu(III) complex (CP/MCCP spheres) showed emission spectrum covering the whole visible region (400 nm-700 nm) exhibiting a remarkable white-light. By using confocal data, the obtained CIE (x, y) purity of the emitted white-light of six various sized spheres provided the same x value = 0.30 and slightly varied y values = 0.35; 0.36; 0.37; 0.38; 0.39; 0.40, which are nearly close to the designated coordinates for ideal white-light (x=0.33; y=0.33) (Fig. 2.14f).
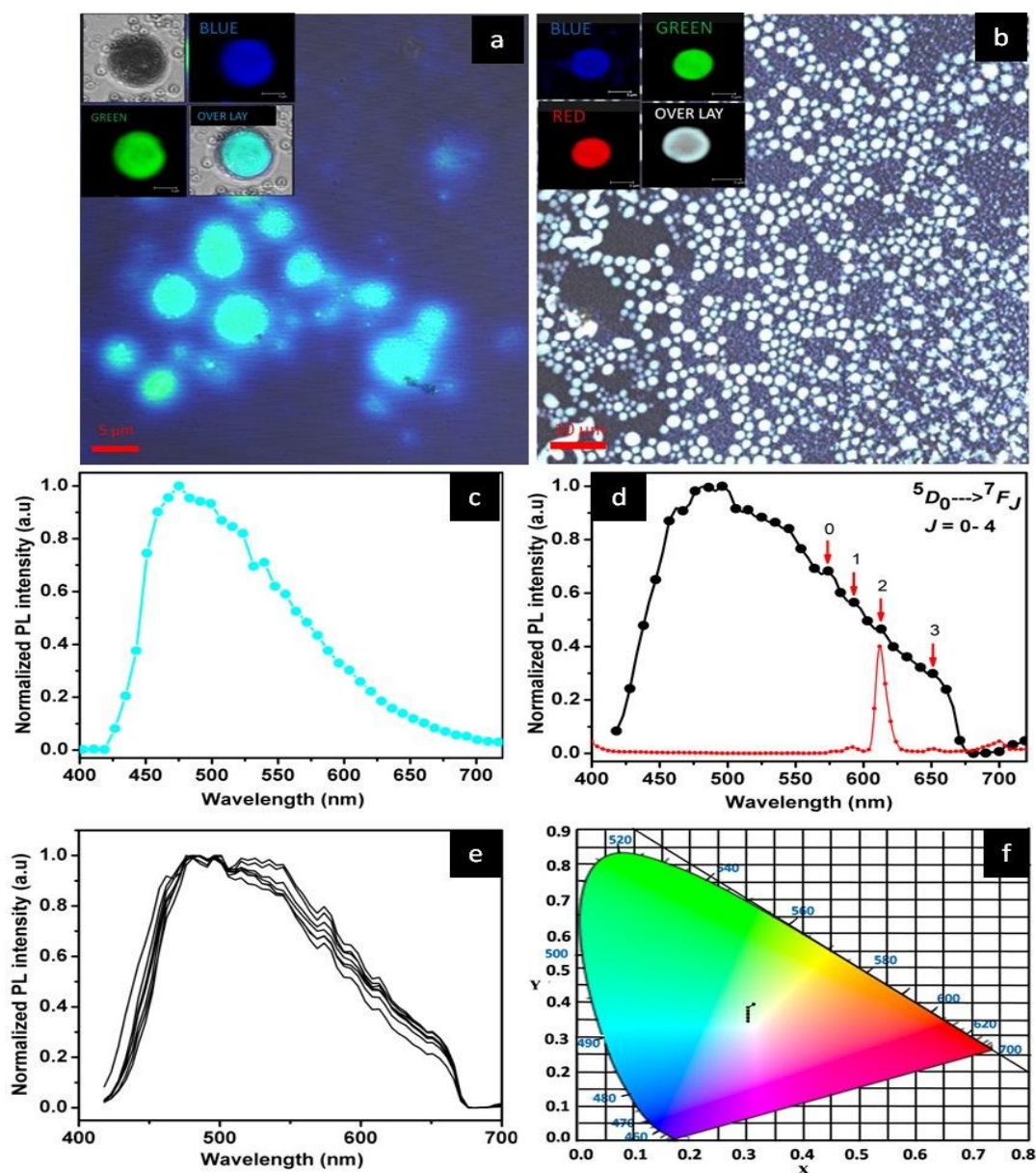
Figure 2.14 Confocal fluorescence micrographs of CP and hybrid CP/MCCP spheres. a) Cyan emitting CP spheres (insets show the bright field image of a single sphere obtained from **P1**, displaying mixed cyan emission due to blue and green dual emissions. (scale bar is 5 μm). b) White emission of hybrid CP/MCCP spheres (insets show blue, green and red emissions from CP/MCCP spheres, and the resultant white color)(scale bar is 10 μm). c, d, e) Confocal microscopy fluorescence spectra of cyan emitting CP sphere obtained from **P1**, white emitting hybrid CP/MCCP sphere, and six CP/MCCP spheres of varying sizes, respectively. f) CIE 1931 2° Standard Observer chromaticity diagram of white emission color displayed by six MCCP spheres (x=0.30 for 6 spheres and y=0.35; 0.36; 0.37; 0.38; 0.39; 0.40), corresponding to their spectra shown in e (λ_{ex} = 365 nm).

2.4 Conclusions and Future Aspects

This chapter demonstrated an innovative technique for the preparation of white emitting CP/MCCP based hybrid films and their nano/micro scale spheres by employing self-assembly techniques *i.e.*, formation of film/spheres template from a novel cyan color emitting copolymer **P1** in THF and subsequent reaction of Eu(tta)$_3$ with **P1** selectively, on the surface of the film/spheres. A crucial aspect of this work is controlling the aggregation behavior of polymers by varying their concentration to tune the colour emissions, for example in this case cyan colour. Further coordination of red emitting Eu(tta)$_3$ to generate a core-shell type particle displaying a mixed cyan (core) and red (shell) colour is an original strategy and this simple technique can eliminate tedious polymer synthesis route targeted towards pure white emission. It has been demonstrated in this chapter the self-assembled hybrid structures displayed brilliant white-light under UV light. This simple and efficient fabrication method to generate white colour displaying films and nano/micro spheres is an important method in the bottom-up nanotechnology of conjugated polymer based hybrid solid state assemblies.

Further this general principle can be applied to get wide variety of luminescent structures displaying diverse colors by varying the polymer aggregation and luminescent metal ions. One of the importance aspects of these spheres is studying the light trapping tendency (photonic behavior) via whispering gallery effect as discussed in the introduction (section 1.6). An important criterion for a light trapping polymer sphere is possessing high quality smooth surface, and unfortunately **P1** and **P2** failed to meet this requirement. As one can see in the SEM image of microsphere the surface is quite rough with nano scale holes (Fig. 2.13a). Nevertheless a successful alternative attempt in this direction to generate photonic microspheres is presented in Chapter 5.

References

1. a) A. Kraft, A. C. Grimsdale, A. B. Holmes, *Angew. Chem. Int. Ed.* **1998**, *37*, 402–428; b) R. Abbel, R. Weegen, W. Pisula, M. Surin, P. Leclre, R. Lazzaroni, E. W. Meijer, A. P. H. J. Schenning, *J. Am. Chem. Soc.* **2009**, *131*, 833–843; c) T. Adachi, L. Tong, J. Kuwabara, T. Kanbara, A. Saeki, S. Seki, Y. Yamamoto, *J. Am. Chem. Soc*. **2013**, *135*, 870−876; d) P. Samori, F. Cacialli, *Functional Supramolecular Architectures*; Wiley-VCH: Weinheim,

2011; e) J. Pecher, S. Mecking, *Chem. Rev.* **2010**, *110*, 6260–6279; f) E. Hittinger, A. Kokil, C. Weder, *Angew. Chem. Int. Ed.* **2004**, *43*, 1808 –1811; g) M. C. Baier, J. Huber, S. Mecking, *J. Am. Chem. Soc.* **2009***, 131,* 14267–14273.

2.   a) Y. Gao, H. L. Yip, K. S. Chen, K. M. O'Malley, O. Acton, Y. Sun, G. Ting, H. Chen, A. K Y. Jen. *Adv. Mater.* **2011**, *23*, 1903–1908; b) J. H. Burroughes, D. D. C. Bradley, A. R. Brown, R. N. M. K. Mackay, R. H. Friend, P. L. Burns, A. B. Holmes, *Nature* **1990**, *347*, 539-541; c) Q. Pei, G. Yu, C. Zhang, Y. Yang, A. J. Heeger, *Science* **1995**, *269*, 1086-1088; d) N. S. Sariciftci, L. Smilowitz, A. J. Heeger, F. Wudl, *Science* **1992**, *258*, 1474-1476; e) M. Deutsch, Y. A. Vlasov, D. J. Norris, *Adv. Mater.* **2000***, 12*, 1176–1180; f) A. J. C. Kuehne, D. A. Weitz, *Chem. Commun.* **2011**, *47*, 12379–12381; g) F. Garnier, R. Hajlaoui, A. Yassar, P. Srivastava, *Science* **1994**, *265*, 1684-1686; h) B. W. D'Andrade, S. R. Forrest, *Adv. Mater.* **2004**, *16*, 1585-1595; i) S. Satoh, H. Kajii, Y. Kawagishi, A. Fujii, M. Ozaki, K. Yoshino, *Jpn. J. Appl. Phys.* **1999**, *38*, L1475−L1477; j) R. C. Polson, A. Chipouline, Z. V. Vardeny, *Adv. Mater.* **2001**, *13*, 760−764; k) H. Yabu, A. Tajima, T. Higuchi, M. Shimomura, *Chem. Commun.* **2008**, *38*, 4588−4589; l) C. Vijayakumar, V. K. Praveen, A. Ajayaghosh, *Adv. Mater.* **2009**, *21*, 2059–2063; m) T. L. Andrew, T. M. Swager, *J. Polym. Sci. Part B: Polym. Phy.* **2011**, *49*, 476–498; n) G. Tu, C. Mei, Q. Zhou, Y. Cheng, Y. Geng, L. Wang, D. Ma, X. Jing, F. Wang, *Adv. Funct. Mater.* **2006**, *16*, 101–106.

3.   a) J. Liu, J. W. Y. Lam, B. Z. Tang, *Chem. Rev.* **2009**, *109,* 5799–5867; b) Y. Chen, J. Du, M. Xiong, H. Guo *Macromolecules,* **2007***, 40,* 4989-4992*;* c) J. Du, S. P. Armes, *J. Am. Chem. Soc.* **2005**, *127*, 12800-12801; d) R. Dong, W. Liu, J. Hao, *Acc. Chem. Res.* **2012**, *45,* 504–513; e) E. Elmalem, F. Biedermann, K. Johnson, R. H. Friend, W. T. S. Huck, *J. Am. Chem. Soc.* **2012**, *134*, 17769−17777.

4.   a) Y. Yan, J. Huang, *Coord. Chem. Rev.* **2010**, *254*, 1072–1080; b) S. S. Zhu and T. M. Swager, *J. Am. Chem. Soc.* **1997**, *119*, 12568-12577; c) R. Dobrawa, M. Lysetska, P. Ballester, M. Gru1ne, F. Wurthner *Macromolecules* **2005**, *38*, 1315-1325; e) G. R. Whittell, I. Manners, *Adv. Mater.* **2007**, *19*, 3439–3468; f) R. R. Pal, M. Higuchi, D. G. Kurth, *Org. Let.* **2009**, *11*, 3562-3565; g) J. D. Fox, S. J. Rowan, *Macromolecules* **2009**, *14*, 6823-6835; h) E. K. Pefkianakis, N. P. Tzanetos, J. K. Kallitsis *Chem. Mater.* **2008**, *20*, 6254– 6262; i) F. Schlutter, A. Wild, A. Winter, M. D. Hager, A. Baumgaertel, C. Friebe ,

U. S. Schubert, *Macromolecules* **2010**, *43*, 2759–2771; j) M. O. Wolf, *Adv. Mater.* **2001**, *13*, 545-553; k) T. Qin, J. Ding, M. Baumgarten, L. Wang, K. Müllen, *Macromol. Rapid Commun.* **2012**, *33*, 1036−1041.

5. a) K. L. Metera, H. Sleiman, *Macromolecules* **2007**, *40*, 3733-3738; b) K. A. Walters, L. Trouillet, S. Guillerez, K. S. Schanze, *Inorg. Chem.* **2000**, *39,* 5496-5509; c) T. Pautzsch, E. Klemm *Macromolecules* **2002**, *35,* 1569-1575; e) A. C. Benniston, A. Harriman, P. Li, and C. A. Sams *J. Am. Chem. Soc.* **2005**, *127*, 2553-2564; d) T. Qin, J. Ding, M. Baumgarten, L. Wang, K. Müllen, *Macromol. Rapid Commun.* **2012** *,33,* 1036−1041; e) A. C. Grimsdale, K. L. Chan, R. E. Martin, P. G. Jokisz, A. B. Holmes, *Chem. Rev.* **2009**, *109,* 897−1091; f) S. Basak, Y. S. L. V. Narayana, M. Baumgarten, K. Müllen, R. Chandrasekar, *Macromolecules* **2013**, *46*, 362−369.

6. a) H. Xu, R. Zhu, P. Zhao, Wei Huang, *J. Phys. Chem. C* **2011**, *115*, 15627–15638; b) A. Balamurugan, M. L. P. Reddy, M. Jayakannan, *J. Phys. Chem. B* **2009**, *113,* 14128–14138; c) H. K. Kim, J. B. Oh, N. S. Baek, S.G. Roh, M. K. Nah, Y. H. Kim, *Bull. Korean Chem. Soc.* **2005**, *26*, 1256-1260; d) R. Shunmugam, G. N. Tew *J. Am. Chem. Soc.* **2005**, *127*, 13567-13572; e) K. Binnemans, *Chem. Rev.* **2009**, *109,* 4283–4374.

7. a) U. S. Schubert, H. Hofmeier, G. R. Newkome, *Modern Terpyridine Chemistry*, Wiley-VCH: Weinheim, **2006**, 69; b) J. R. Kumpfer, J. J. Wie, J. P. Swanson, F. L. Beyer, M. E. Mackay, S. J. Rowan, *Macromolecules* **2012**, *45*, 473–480; c) M. Burnworth, L. Tang, J. R. Kumpfer, A. J. Duncan , F. L. Beyer, G. L. Fiore, S. J. Rowan, C. Weder, *Nature* **2011**, *472*, 334-337.

8. a) R. Dobrawa, M. Lysetska, P. Ballester, M. Grüne, F. Würthner, *Macromolecules* **2005**, *38,* 1315-1325; b) A. C. Benniston, A. Harriman, P. Li, C. A. Sams, *J. Am. Chem. Soc.* **2005**, *127*, 2553−2564; c) N. Chandrasekhar, R. Chandrasekar, *J. Org. Chem.* **2010**, *75*, 4852−4855; d) S. Basak, P. Hui, S. N. Boodida, R. Chandrasekar, *J. Org. Chem.* **2012**, *77*, 3620−3626; e) N. Chandrasekhar, R. Chandrasekar, *Angew. Chem. Int. Ed.* **2012**, *51*, 3556-3561; f) N. Chandrasekhar, M. A. Mohiddon, R. Chandrasekar, *Adv. Opt. Mater.* **2013**, *1*, 305-311; g) S. Basak, R. Chandrasekar, *Adv. Funct. Mater.* **2011**, *21*, 667–673; h) Y. S. L. V. Narayana, R. Chandrasekar, *Chem. Phys. Chem,* **2011**, *12*, 2391−2396; i) J. M. Stanley, X. Zhu, X. Yang, B. J. Holliday, *Inorg. Chem.* **2010***, 49*, 2035–2037;

9. X. J. Zhu, B. J. Holliday, *Macromol. Rapid Commun.* **2010**, *31*, 904−909.

10. a) R. Gao, M. Chen, W. Li, S. Zhou, L. Wu, *J. Mater. Chem. A*, **2013**, *1*, 2183–2191; b) H. Yang, S. H. Kim, L. Yang, S. Y. Yang, C. E. Park, *Adv. Mater.* **2007**, *19,* 2868–2872; c) S. Kwon, M. Shim, J. I. Lee, T. W. Lee, K. Chob, J. K. Kim. *J. Mater. Chem.* **2011**, *21*, 12449–12453.

11. a) J. Gupta, V. Sajini, V. Suresh, *Polymer* **2010**, *51*, 5078-5086; (b) C. Weder, M. S. Wrighton, *Macromolecules* **1996**, *29*, 5157-5165; c) G. Zoppellaro, M. Baumgarten, *Eur. J. Org. Chem.* **2005**, *14*, 2888–2892; d) Z. Szab, V. Vallet, I. Grenthe, *Dalton Trans.* **2010**, *39*, 10944–10952.

12. a) M. Seri, M. Bolognesi, Z. Chen, S. Lu, W. Koopman, A. Facchetti, M. Muccini, *Macromolecules* **2013**, *46*, 6419−6430; b) F. Würthner, C. Thalacker, S. Diele, C. Tschierske, *Chem. Eur. J.* **2001**, *7*, 2245-2253; c) S. Ghosh, X. Q. Li, V. Stepanenko, F. Wurthner, *Chem. Eur. J.* **2008**, *14*, 11343 – 11357.

13. a) W. T. Carnall, In *Handbook on the Physics and Chemistry of Rare Earths*; K. A. Gschneidner, L. Eyring, Eds.; Elsevier: Amsterdam, the Netherlands, **1987**; Vol. *3*, Chapter 24, 171-208; b) G. H. Dieke, *Spectra and Energy levels of Rare Earth Ions in Crystals*; Inter science: New York, **1968**; c) J. A. Fernandes, R. A. S. Ferreira, M. Pillinger, L. D. Carlos, I. S. Goncalves, P. J. A. Ribeiro-Claro, *Eur. J. Inorg. Chem.* **2004**, 3913-3919.

14. a) Y. Kim, J. Bouffard, S. E. Kooi, T. M. Swager, *J. Am. Chem. Soc.* **2005**, *127*, 13726 - 13731; b) A. Satrijo, S. E. Kooi, T. M. Swager, *Macromolecules* **2007**, *40,* 8833-8841.

15. E. Tekin, H. Wijlaars, E. Holder, D. A. M. Egbe, U. S. Schubert, *J. Mater. Chem.* **2006**, *16*, 4294–4298.

16. a) C. Giansante, G. Raffy, C. Schafer, H. Rahma, M.T. Kao, A. G. L. Olive, A. D. Guerzo *J. Am. Chem. Soc.* **2011***, 133,* 316–325; b) M. J. Park, J. Kwak, J. Lee, I. H Jung, H. Kong, C. Lee, D. H. Hwang, H. K. Shim, *Macromolecules* **2010**, *43*, 1379–1386.

17. Colorimetry: Commission Internationale de Lclairage (CIE), Paris, **1986**.

18. a) X. Y. Chen, X. Yang, B. J. Holliday, *J. Am. Chem. Soc.* **2008**, *130*, 1546-1547; b) K. Binnemans, P. Lenaerts, K. Driesen, C. Görller-Walrand, *J. Mater. Chem.* **2004**, *14*, 191–195; c) J. Li, F. Song, L. Wang, J. Jiao, Y. Cheng, C. Zhu, *Macromol. Rapid Commun.* **2012**, *33*, 1268−1272.

3

Tuning the Solid State Emission of Thin Films/Micro-Spheres Obtained From Alternating Oligo(3-octylthiophenes)and 2,6-Bis(pyrazolyl)pyridine Copolymers by Varying Conjugation Length and Eu^{+3}/Tb^{+3} Metal Coordination

3.1 Abstract

A series of dialkynyl functionalized oligo(3-octyl thiophene)$_m$ (m3-m10) were polymerized together with 2,6-bis(pyrazole)pyridine (bpp) to get alternating copolymers (P3-P10) with the number average molecular weights ($\overline{M}_n$) in the range of 5.3-11 KDa. These copolymers were further self-assembled into solid microspheres. The optical
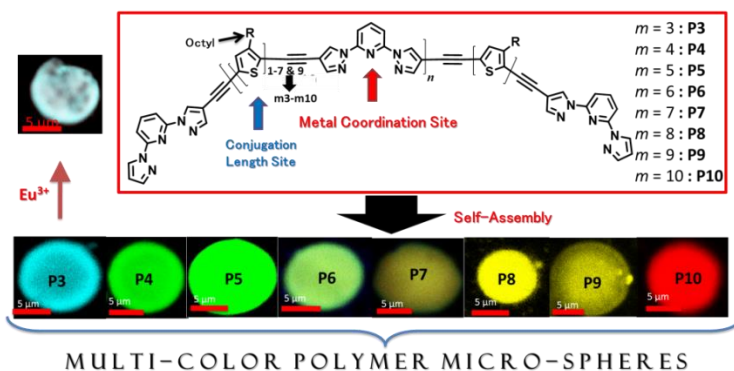
emission range of these copolymers were fine-tuned from blue to red and white by changing the conjugation length of thiophene oligomers (band gap ~ from 2.1 to 1.67 eV) and coordinating of metals like Eu^{+3} and Tb^{+3} both in the solution and solid states. A white color was obtained in solution, thin film and microsphere states upon UV excitation with CIE (Commission Internationale de l'Eclairage) coordinates close to the values of standard white color.

3.2 Introduction

Conjugated oligomeric and polymeric materials displaying various color emissions are extensively used in optoelectronic devices, including organic light-emitting diodes (OLEDs),[1] organic field-effect transistors (OFETs),[2] and solar cells.[3] For example, the oligomers of thiophene, widely known for their semiconductor properties in organic electronics, are also fluorescent compounds characterized by chemical inertness, good photo-stability, high optical absorbance and FL quantum yield. The FL emission can be easily modulated by varying the number of thiophene rings.[4] Polythiophene derivatives are the most widely investigated conjugated polymers, because of their strong visible range absorption, high charge carrier mobility, easy synthetic accessibility, strange electro-optical properties, structural flexibility, and environmental stability.[4a,5] Thiophene-containing polymers are now ubiquitous in a range of organic electronic materials such as organic solar cells, field effect transistors (FETs), light absorbing photoactive layers, and hole conducting layers in plastic electronics.[5] The emission properties of the conjugated polymers can be tuned by methods like altering the main chain molecular structure or the side chain molecular structure,[7] blending a luminescent polymer with another active polymer,[8] or with organic or inorganic molecules,[9] doping,[10a] and also by using multiple layer devices.[11] These tuning methodologies were used to synthesize a range of copolymers by combining oligo(thiophenes) and various light emitting monomers to alter the optical emission properties, solubility, and processability. Several research groups have been working on creating diverse collections of luminescent thiophene conjugated copolymer structures by incorporating transition metals into the polymer main chain.[12]

For example, Swager et al have prepared the first conducting polymetallorotaxanes by electrochemically polymerizing metallorotaxanes, which are tetrahedral complexes containing bithiophene-bipyridine, macrocyclic phenanthroline and Cu^{2+} or Zn^{2+} metal ions.[12a,b] The same group has reported another conducting redox active polymers based on polythiophene-$[Ru(bipyrdine)_3]^{n+}$.[12c] Reynolds et al have investigated the synthesis, metal binding (zinc, copper, nickel, and cobalt ions), and electrochemical properties of a ligand which is a condensation product of salicylaldehyde and 3,4-diaminothiophene derivatives, and further polymerized the α-positions of the thiophenes metal complexes to achieve polythiophenes with electro-chromic properties.[12d] Further to fine tune the electronic properties, both the metal center and diamine

backbone of the salen ligand were varied in a series of transition metal-polythiophene polymers based on metal salen and 3,4-ethylenedioxythiophene (EDOT).[12e] Pickup and coworkers have reported bithiophene-bipyridine copolymers prepared by electrochemical polymerization and explored an electron rich metal (Ru^{+2} and Os^{+2}) containing poly(bithiophene-co-bithiazole) backbone to lower the energy of the polymer HOMO to increase the electronic communication with the metal center.[12f-g] Guillerez et al have reported π-conjugated polymers based on regioregular 3-(octylthiophene) tetramers alternated with either 2,2′-bipyridine or its Ru(II) complex $[Ru(bipy)_3]^{2+}$.[12h] A conducting 5,5'-(2-thienyl)-2,2'-bithiazole based polymer coordinated to Rhenium showed stable metal coordination during oxidizing and conducting states.[12i] Holiday et al have electropolymerized Eu^{3+} containing 3,4-ethylenedioxythenyl (EDOT) monomer to get a red emitting conducting metallo-polymer.[12j]

In most of the reported literatures the copolymers of oligo(thiophenes) with metal coordinating ligand units were prepared by electrochemical polymerization and till now copolymerization of a well-known tridentate 2,6-bis(pyrazole)pyridine (bpp) ligand with various oligo(thiophenes) has not been attempted. bpp units are known to coordinate with diverse d and f block functional metal ions to form diverse coordination geometries. For example, bpp with Fe^{2+} or Zn^{2+} ions form octahedral complexes exhibiting magnetic spin cross-over effects and luminescence, resepectively.[13] Further bpp type ligands form 9-coordinated tricapped trigonal prismatic complexes with Eu^{3+} and Tb^{3+} ions displaying sensitized intense red and green emissions, respectively.[9a-d] Therefore copolymerization of oligo(thiophenes) with metal chelating bpp is another strategy to fine-tune the visible emission spectrum by coordinating luminescent f-block metal ions into the conjugated copolymer chains. Furthermore incorporation of red emitting Eu^{+3}, and green emitting Tb^{+3} ions into metal ion binding conjugated polymers alter the optical and electronic properties of these materials,[9,10a] improving the performance of the devices at the application level. Additionally, bottom up self-assembly[14] of conjugated polymers into various nano and micro scale structures is another important emerging research area directed towards opto-electronics, solar cells[10a] and recently photonic devices.[10b,c]

This chapter presents the syntheses, characterization and bottom-up self-assembly studies of a series of copolymers (**P3**-**P10**) with diverse optical band gaps (Scheme 3.1). The copolymers were prepared by reacting oligo(3-octyl thiophenes)$_m$ carrying dialkynyl groups (m =3-10) with
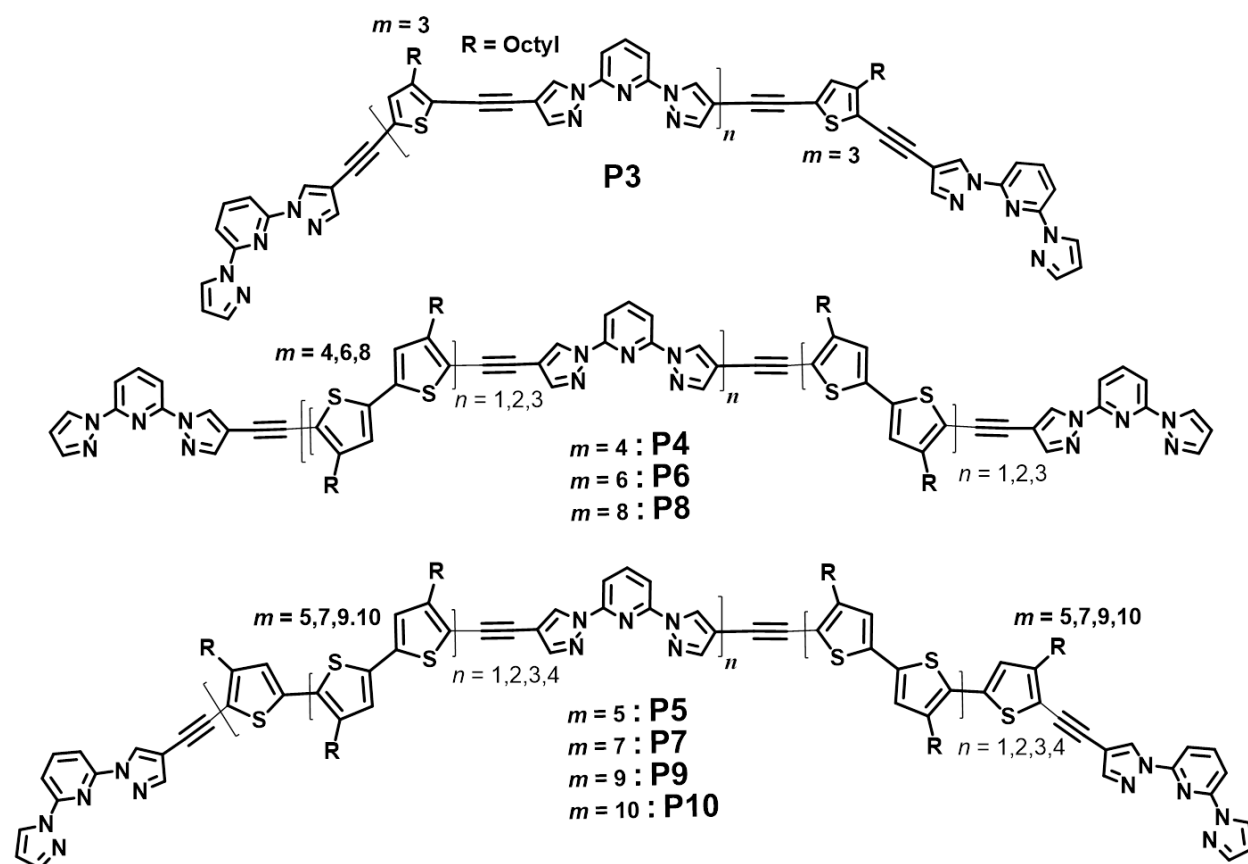
Scheme 3.1: Chemical structures of alternating oligo(3-octylthiophenes) and 2,6-Bis(pyrazole)pyridine (bpp) copolymers (**P3-P10**) with bpp end groups.

metal binding bpp units. This chapter also discusses the absorption and emission properties of these copolymers and also a method to achieve white emission by coordinating Eu^{3+} and Tb^{3+} ions to the polymers in solution, thin film, and microsphere states. The self-assembled microspheres were thoroughly investigated by electron-, atomic force- and laser confocal fluorescence microscopy techniques.

3.3 Results and Discussion

3.3.1 *Syntheses of Monomers, Copolymers and Metal-Complexes of Model Compounds and Copolymers*

3-Octylated thiophene and their dibromo derivatives of $m3$ and $m4$ (**8** and **9**) were prepared by following the reported procedure (Scheme 3.2).[15] Compound **6** was prepared by treatment of
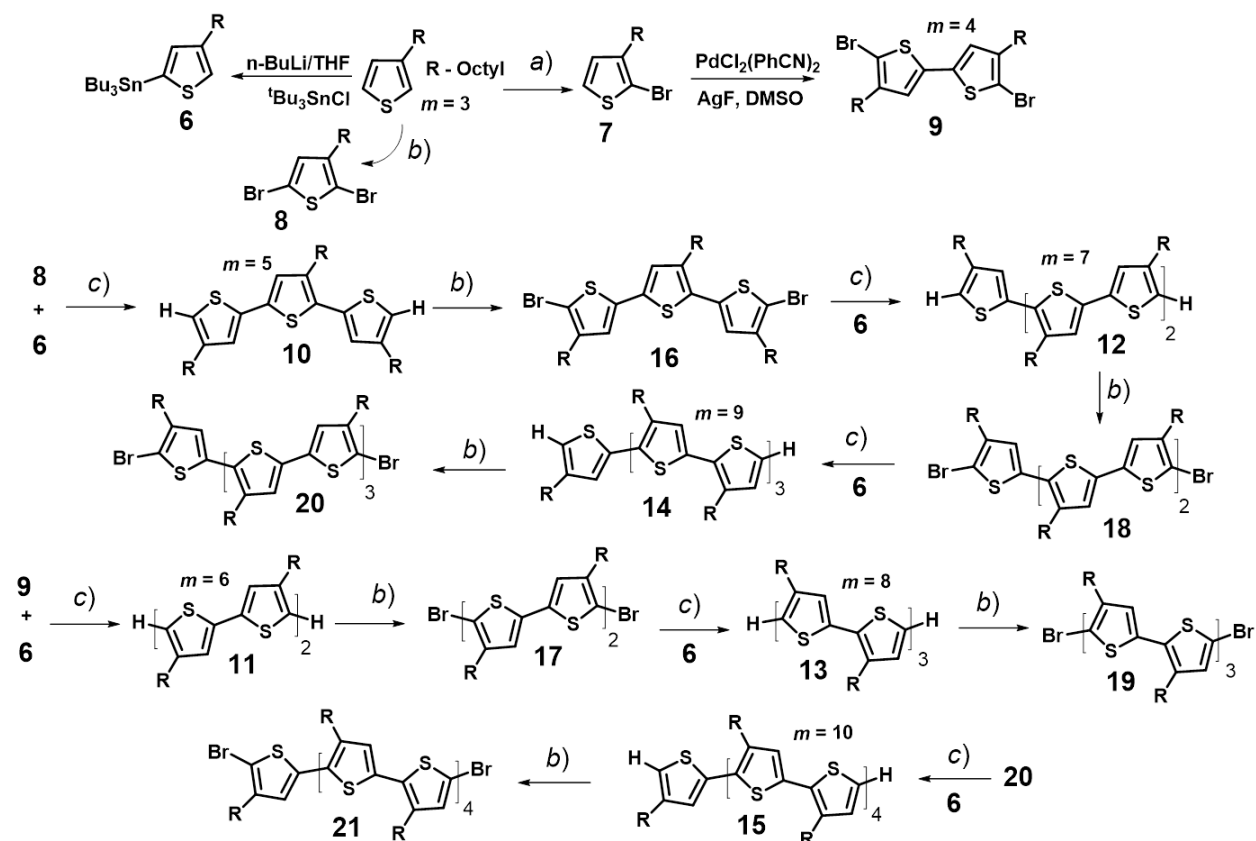
General Protocol for Polymers:
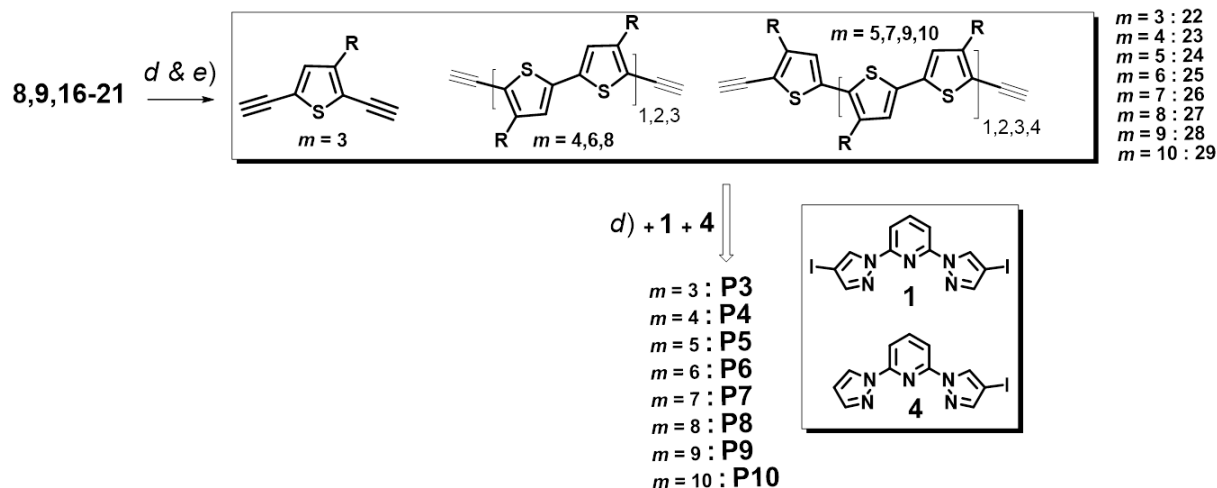
Scheme 3.2: Syntheses of diethynylated oligo(thiophenes) (*m*3-*m*10: **22**-**29**, respectively) and their corresponding copolymers with bpp unit (**P3**-**P10**). Reagents and conditions: a) 1 eq. N-bromo succinimide (NBS)/CHCl₃/AcOH.   b)   2   eq.   NBS/CHCl₃/AcOH.   c)   Pd(PPh₃)₂Cl₂/THF.   d)   Pd(PPh₃)₂Cl₂/CuI/ trimethylsilylacetylene/diisopropylamine/THF. e) KOH/THF/methanol.

octylthiophene with *n*-BuLi and tributyltinchloride and used without further purification. Dibromo-*m4* (**9**) was prepared from compound **7**. Further, 3-octylatedthiophene oligomers *m5*–*m10* (**10-15**), respectively were synthesized in ~60% yields by Stille coupling reactions of **6** with corresponding dibromo monomers (**13-18**) in the presence of catalytic amount of [PdCl$_2$(PPh$_3$)$_2$] in THF. Compounds (**10-15**) were converted into their analogous dibromo derivatives (**13-18**) in oil state using 2 eq. NBS/CHCl$_3$/AcOH in ~90% yields. Further dibromo derivatives of **8**, **9** and **13-18** were converted into their corresponding diethynyl products under Sonagashira cross coupling conditions followed by deprotection of TMS group to get the key intermediates (**22-29**) in >99% yields.

Metal chelating units 2,6-bis(4-iodo-1*H*-pyrazol-1-yl)pyridine (**1**), and 2-(4-iodo-1*H*-pyrazol-1-yl)-6-(1*H*-pyrazol-1-yl)pyridine (**4**) were also synthesized from 2,6-dibromopyridine in good yields (>80%) as per our reported procedure.[9b-e,16] Alternating copolymers (**P3**-**P10**) were prepared by polymerizing ethynyl derivative of *m3*–*m10* (**22-29**) with **1** under Sonagashira cross coupling reactions in presence of diisopropylamine/THF. All the copolymers were end capped with compound **4** under Sonogashira reaction condition. The molecular structures of the monomers and the polymers were confirmed by using nuclear magnetic resonance (NMR) measurements, mass spectrometry, and elemental analysis. All the synthesized polymers were soluble in organic solvents such as chloroform (CHCl$_3$), tetrahydrofuran (THF) and toluene.^{1}H NMR spectra of copolymers showed aromatic peaks of the thiophenes around 6.9–7.0 ppm. The peaks between 7.3–7.9 ppm were from pyrazole and pyridine protons of main chain bpp unit of the polymers. The peaks around 6.6–6.4 ppm and 8.5–8.6 ppm were from the pyrazole proton of end capped bpp (Fig 3.1). ^{1}H NMR end group analyses of polymers **P3**−**P10**, showed $\overline{M}_n$ values in the range of 4.5– 11.0 KDa. The obtained copolymers were further subjected to Soxhlet extraction to remove the low molecular weight oligomers from the polymers. The gel permeation chromatography (GPC) analyses of polymers after Soxhlet purification showed $\overline{M}_n$ in the range of 5.3 – 11.0 KDa (Table 3.1).

ppm
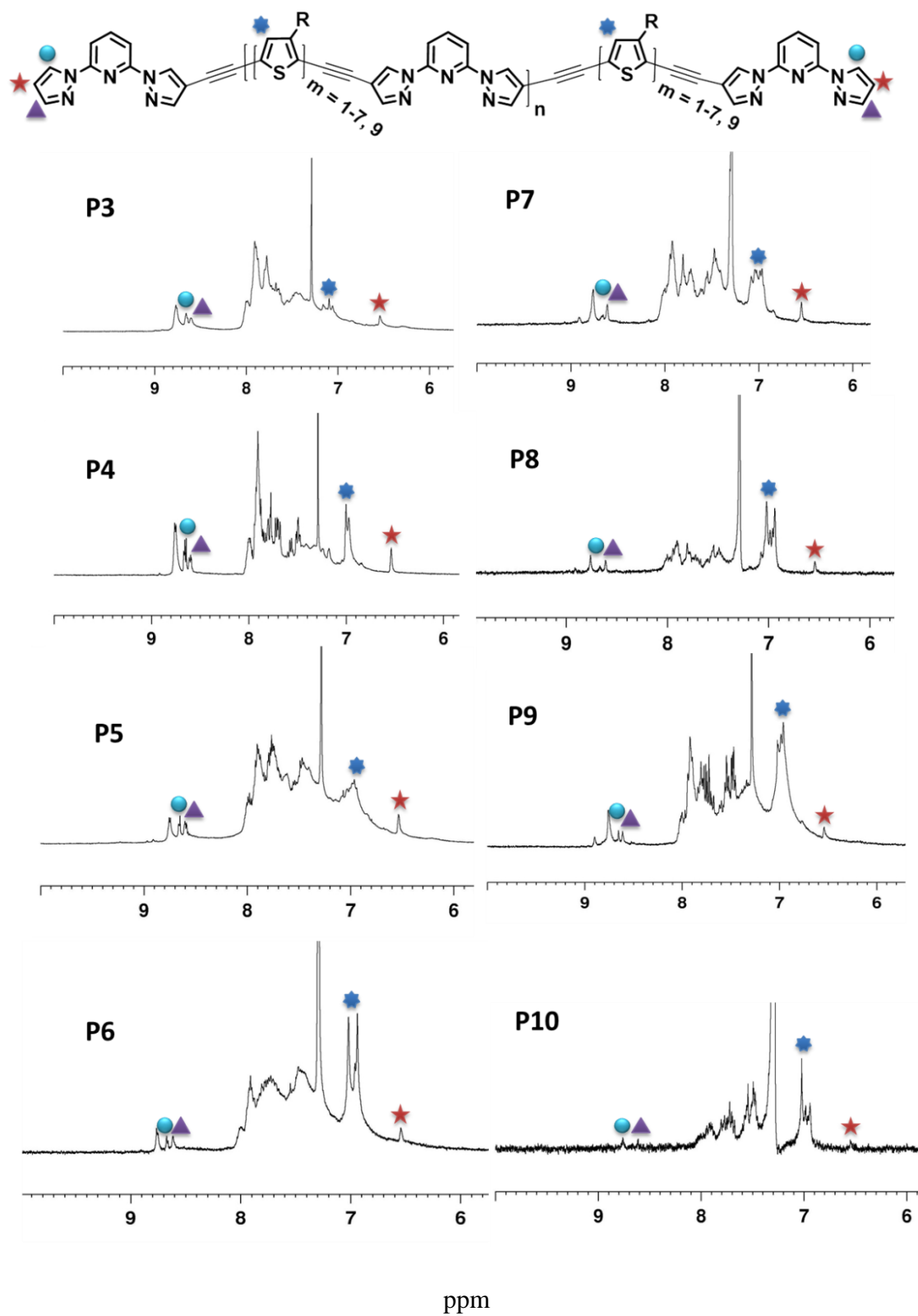
Figure 3.1 ^{1}H-NMR spectra of copolymers **P3**-**P10**. (Aromatic regions are shown).

Synthesis of tributyl(4-octylthiophen-2-yl)stannane (6): This compound was prepared as per the reported procedure.[15d]

A Schlenk tube containing 3-octylthiophene (3.0 g, 15.27 mol), anhydrous THF (50 mL), TMEDA (3.5 mL, 23.06 mmol) was degassed by a repeated sequence of freeze-pump-thaw cycles. The flask was cooled to -78 °C and then butyl-lithium in hexane (14.4 mL, 1.6 M hexanes, 23.06 mmol) was added drop wise. After, the reaction mixture stirred under nitrogen for 2.0 h at RT, the mixture was again cooled down to -78 °C and tributylchlorostannane (5.0 mL, 7.5 mmol) was added in a drop wise manner. The mixture was further stirred at -78 °C for 2 h, followed by quenching with H_2O (100 mL). After that, THF was removed under reduced pressure and the organic part was extracted with hexane (3 × 100 mL) and dried over Na_2SO_4. After removing the solvents, the residue was purified on a column chromatography (neutral alumina packing/hexane as eluent) to get compound (**6**) as colorless oil (6.00 g, 80.2%). R_f value ~ 0.45. ^{1}H-NMR (400 MHz, $CDCl_3$, 298 K) δ/ppm: 7.19 (s, 1H), 6.97 (s, 1H), 2.65 (t, J = 3.2 Hz 2H, Thiophene-CH_2), 1.60- 1.24 (m, 12H), 0.89 (t, J = 2.8 Hz, 3H, CH_3).

Synthesis of 2-bromo-3-octylthiophene (7): This compound was prepared as per the reported procedure.[15c]

To a solution of 3-octylthiophene (2.0 g, 10.18 mmol) in 10 mL glacial acetic acid was maintained at 10 °C, NBS (1.8 g, 10.18 mmol) was added, and the reaction mixture was stirred for 3 h. The reaction was quenched by adding H_2O (100 mL). The resultant solution was extracted with hexanes (2 × 100 mL) and dried over Na_2SO_4. The solvent was removed under reduced pressure to isolate 2.5 g of **7** as colorless oil (88 % yield). ^{1}H-NMR (400 MHz, $CDCl_3$, 298 K) δ/ppm: 7.19 (d, J = 5.2 Hz, 1H), 6.87 (d, J = 6.2 Hz, 1H), 2.63 (t, J = 3.2 Hz, 2H, Thiophene-CH_2), 1.60 (t, J = 2.8 Hz, 2H), 1.2–1.3 (br, 10H), 0.89 (t, J = 3.2 Hz, 3H, CH_3).

Synthesis of 2, 5-dibromo-3-octylthiophene (8): This compound was prepared as per the reported procedure.[15a]

3-Octyl thiophene (1.0 g, 5.09 mmol) and NBS (1.90 g, 10.69 mmol) were dissolved in a mixture of chloroform/glacial acetic acid (1/1, v/v) (40 mL) and the resulting solution was heated to reflux for 5 h under nitrogen atmosphere. The reaction mixture was cooled to RT, and then washed with water. The solution was extracted with hexane and the organic phase was dried over

anhydrous sodium sulfate. The product was further purified using column (SiO_2) chromatography with hexane as an eluent. To get compound (**8**) as colorless oil (1.60 g, 90% yield). R_f value ~ 0.40. ^{1}H-NMR (400 MHz, $CDCl_3$, 298 K) δ/ppm: 6.52 (s, 1H), 2.57 (t, $J = 3.2$ Hz, 2H, Thiophene-CH_2), 1.59-1.56 (m, 2H), 1.29-1.26 (m, 6H), and 0.96 (t, $J = 2.8$ Hz, 3H, CH_3).

Synthesis of 5, 5'-dibromo-4, 4'-dioctyl-2, 2'-bithiophene (9): This compound was prepared as per the reported procedure.[15b]

A two-neck round bottom flask covered with aluminum foil (for protection from light) was charged with AgF (0.598 g, 8.72 mmol), 2-bromo-3-octylthiophene (1.2 g, 4.36 mmol), $Pd(PhCN)_2Cl_2$ (50 mg, 0.175 mmol), and DMSO (10 mL). The reaction mixture was stirred and was allowed to proceed for 18 h at RT. The crude reaction mixture was filtered over celite and extracted with ethylacetate (150 mL). The filtrate was washed with water (2×100 mL) and brine (100 mL), dried over Na_2SO_4, filtered, and concentrated. The crude product was purified by silica gel column chromatography using hexane as an eluent to get the desired compound **9** as pale yellow oil (1.7 g, 50%). ^{1}H-NMR (400 MHz, $CDCl_3$, 298 K) δ/ppm: 6.75 (s, 2H), 2.50 (t, $J = 3.2$ Hz, 4H, Thiophene-CH_2), 1.57-1.29 (m, 24H), 0.89 (t, $J = 2.8$ Hz, 6H, CH_3).

Synthesis of 3-octyl thiophene oligomer (m5)–10: To a solution of 2, 5-dibromo-3-octylthiophene **8** (1.5 g, 4.2 mmol) and tributyl(4-octylthiophen-2-yl)stannane **6** (4.318 g, 8.8 mmol) in THF (25 mL), $PdCl_2(PPh_3)_2$ (59 mg, 2 mol %) was added under nitrogen atmosphere and the mixture was heated to reflux for 4 h. Then the solvent from the mixture was evaporated under reduced pressure to get pale green color oil. The residue was purified by column chromatography on silica gel using hexane eluent to obtain colorless oil. (1.49 g, 60%). R_f value ~ 0.50. ^{1}H-NMR (400 MHz, $CDCl_3$, 298 K) δ/ppm: 6.80-7.00 (m, 4H), 6.77 (s, 1H, Thiophene), 2.70 (t, $J = 3.2$ Hz, 2H), 2.59 (t, $J = 3.0$ Hz, 4H), 1.63-1.61 (m, 6H), 1.27-1.25 (m, 30H), 0.89 (t, $J = 2.8$ Hz, 9H, CH_3). ^{13}C-NMR (100 MHz, $CDCl_3$, 298 K) δ/ppm: 144.1, 143.9, 143.6, 139.9, 137.4, 136.9, 135.6, 135.2,129.8, 127.0,126.2, 124.8, 119.89, 118.9, 118.7,33.2, 31.9, 30.5, 30.4, 29.5, 29.4, 29.3, 28.91, 28.3, 26.8, 22.71, 14.1, 13.6. FT-IR (KBr) ν in cm^{-1}: 2964, 2920, 2860 (sp^3- CH_3, CH_2 and CH, str), 1463, 1375, 1260, 1219, 1084, 1019, 827, 717. HRMS (ESI) (*m/z*): $(M+H)^+$calcd for $C_{36}H_{57}S_3$ 585.3622; found 585.3620. Anal. Calcd for $C_{36}H_{56}S_3$: C, 73.91; H, 9.65. Found: C, 73.85; H, 9.76.

The above mentioned procedure was followed for the syntheses of oligomers *m4*-*m7*, and *m9*. Yields ~ 60% (Scheme 3.2). The characterization data of *m4*-*m7*, and *m9* are given below.

3-octyl thiophene oligomer (m6) –11: ^{1}H-NMR (400 MHz, CDCl$_3$, 298 K) δ/ppm: 6.80-7.00 (m, 6H), 6.77 (s, 2H), 2.74 (t, *J* = 3.2 Hz, 4H), 2.64-2.62 (m, 4H), 1.66-1.63 (m, 8H), 1.31-1.28 (m, 40H), 0.91 (t, *J* = 2.8 Hz, 12H, CH$_3$). ^{13}C-NMR (100 MHz, CDCl$_3$, 298K) δ: 143.9, 143.6, 140.0, 137.4, 135.6, 134.6, 130.0,128.3, 127.3, 127.0, 126.3, 125.0, 124.8, 119.9, 119.7, 118.9, 118.7, 31.9, 30.7, 30.5, 30.4, 29.6, 29.4, 29.39, 29.3, 22.7, 14.1. FT-IR (KBr) ν in cm^{-1}: 2926, 2854, 1745, 1620, 1572, 1498, 1466, 1394, 1273, 1219, 1114, 1082, 1039, 968, 866, 792, 758, 723, 652, 611. HRMS (ESI) (*m/z*): (M+H)$^+$calcd for C$_{48}$H$_{75}$S$_4$ 779.4752; found 779.4611. Anal. Calcd for C$_{48}$H$_{74}$S$_4$: C, 73.97; H, 9.57. Found: C, 73.85; H, 9.48.

3-octyl thiophene oligomer (m7) – 12: ^{1}H-NMR (400 MHz, CDCl$_3$, 298 K) δ/ppm: 6.99-6.97 (m, 4H), 6.89 (s, 2H), 6.78 (s, 1H), 2.75 (t, *J* = 3.0 Hz, 4H), 2.63-2.61 (m, 6H), 1.65-1.63 (m, 10H), 1.29-1.28 (m, 50H), 0.94 (t, *J* = 2.8 Hz, 15H, CH$_3$). ^{13}C-NMR (100 MHz, CDCl$_3$, 298K) δ/ppm: 144.1, 143.9, 143.6, 140.0, 137.3, 135.6, 134.6, 129.9, 128.2, 127.1, 126.3, 125.0, 124.8, 119.9, 119.7, 118.7, 31.9, 30.5, 30.4, 29.5, 29.4, 29.3, 29.2, 22.7, 17.2, 14.1, 13.6. FT-IR (KBr) ν in cm^{-1}: 2958, 2931, 2849, 1638, 1523, 1468, 1375, 1194, 832,728. HRMS (ESI) (*m/z*): (M+H)$^+$calcd for C$_{60}$H$_{92}$S$_5$ Na 995.5700; found 995.5698. Anal. Calcd for C$_{60}$H$_{92}$S$_5$: C, 74.01; H, 9.52. Found: C, 74.15; H, 9.48.

3-octyl thiophene oligomer (m8) –13: ^{1}H-NMR (400 MHz, CDCl$_3$, 298 K) δ/ppm: 6.99-6.97- (m, 8H), 2.75 (t, *J* = 3.2 Hz, 4H), 2.63-2.62 (m, 8H), 1.66-1.64 (m, 12H), 1.29-1.27 (m, 60H), 0.88 (t, *J* = 2.4 Hz, 18H, CH$_3$).^{13}C-NMR (100 MHz, CDCl$_3$, 298K) δ/ppm: 149.5, 144.7, 142.5, 134.4, 132.3, 132.2, 132.1, 132.0, 131.9, 131.5, 129.0, 128.4, 31.7, 29.7, 29.26, 29.36, 29.31, 29.2, 29.1, 26.0, 25.9, 22.63,14.1, 14.0. FT-IR (KBr) ν in cm^{-1}: 2964, 2914, 2849, 1742, 1468, 1413, 1380, 1254, 1095, 1013, 871, 810, 663. HRMS (ESI) (*m/z*): (M+H)$^+$calcd for C$_{72}$H$_{111}$S$_6$ 1167.7010; found 1167.7130. Anal. Calcd for C$_{72}$H$_{110}$S$_6$: C, 74.04; H, 9.49. Found: C, 74.21; H, 9.41.

3-octyl thiophene oligomer (m9) – 14: ^{1}H-NMR (400 MHz, CDCl$_3$, 298 K) δ/ppm: 7.03-6.98 (m, 8H), 6.80 (s, 1H), 2.80-2.78 (m, 6H), 2.66-2.64 (m, 8H), 1.71-1.69 (m, 14H), 1.39-1.37 (m, 70H), 0.94 (t, *J* = 2.4 Hz, 21H, CH$_3$). ^{13}C-NMR (100 MHz, CDCl$_3$, 298K) δ/ppm: 143.9, 143.6, 143.2, 140.2, 139.5, 137.4, 135.6, 135.5, 134.6, 133.6, 131.0, 130.0, 128.4, 128.2, 127.1, 126.5, 126.3, 125.0, 124.8, 120.0, 119.9, 119.7, 118.7, 31.9, 30.6, 30.5, 30.4, 29.7, 29.6, 29.5, 29.4,

29.3, 28.3, 26.8, 22.7, 17.30, 14.1, 13.6. FT-IR (KBr) ν in cm^{-1}:2953, 2920, 2854, 1523, 1462, 1380, 827, 728. HRMS (ESI) (m/z): (M+H)$^{+}$calcd for $C_{84}H_{129}S_7$ 1361.8139; found 1361.8354. Anal. Calcd for $C_{84}H_{128}S_7$: C, 74.05; H, 9.47. Found: C, 74.12; H, 9.36.

3-octyl thiophene oligomer (m10) – 15: ^{1}H-NMR (400 MHz, CDCl$_3$, 298 K) δ/ppm: 6.99-6.97 (m, 8H), 6.91-6.89 (m, 2H), 6.78 (s, 1H), 2.77-2.75 (m, 8H), 2.62-2.61 (m, 10H), 1.67-1.65 (m, 18H), 1.30-1.27 (m, 108H), 0.90 (t, J = 2.8 Hz, 27H, CH$_3$).^{13}C-NMR (100 MHz, CDCl$_3$, 298K) δ/ppm: 143.9, 143.6, 143.2, 140.2, 139.5, 137.4, 135.6, 135.5, 134.6, 133.6, 131.0, 130.0, 128.4, 128.2, 127.1, 126.5, 126.3, 125.0, 124.8, 120.0, 31.9, 30.6, 30.5, 30.4, 29.7, 29.6, 29.5, 29.4, 29.3, 28.3, 26.8, 22.7, 17.30, 14.1, 13.6. FT-IR (KBr) ν in cm^{-1}: 2953, 2925, 2854, 1468, 1375, 1194, 827, 728. HRMS (ESI) (m/z): (M+H)$^{+}$calcd for $C_{108}H_{165}S_9$ 1750.0398; found 1750.0354. Anal. Calcd for $C_{108}H_{164}S_9$: C, 74.08; H, 9.44. Found: C, 74.16; H, 9.32.

Synthesis of 2, 5-dibromo-3-octylthiophene (m5) - 16: 3-octyl thiophene trimer **13** (1.75 g, 2.90 mmol) and NBS (1.135 g, 6.38 mmol) were dissolved in chloroform/glacial acetic acid (1/1, v/v (10ml)) and the resulting solution was vigorously stirred under reflux for 5 h under nitrogen. The crude mixture was cooled to room temperature; washed with saturated NaHCO$_3$ (aq), and distilled water, extracted with dichloromethane. The organic layer was dried over anhydrous sodium sulfate and the solvent from the mixture was evaporated under reduced pressure to afford a yellow color oil. The product was further purified by silica column chromatography (SiO$_2$) with hexane as eluent. The compound was obtained as pale yellowish oil (2.65 g, yield ~ 90%). R_f value ~ 0.39. ^{1}H-NMR (400 MHz, CDCl$_3$, 298 K) δ/ppm: 6.98-6.80 (m, 3H), 6.77 (s, 2H), 2.70 (t, J = 3.0 Hz, 2H), 2.55 (t, J = 2.8 Hz, 4H), 1.63-1.61 (m, 6H), 1.27-1.26 (m, 30H), 0.89 (t, J = 2.4 Hz, 9H, CH$_3$). ^{13}C-NMR (100 MHz, CDCl$_3$, 298K) δ/ppm: 144.1, 143.9, 143.6, 139.9, 137.4, 136.9, 135.6, 135.2, 129.8, 127.0, 126.2, 124.8, 119.8, 119.9, 118.7, 33.19, 31.93, 30.55, 30.45, 29.5, 29.4, 29.3, 28.9, 28.3, 26.8, 22.7, 17.30, 14.1, 13.6. FT-IR (KBr) ν in cm^{-1}: 2947, 2920, 2849, 1780, 1747, 1534, 1457, 1375, 1227, 1183, 1013, 821, 717. HRMS (ESI) (m/z): (M+H)$^{+}$calcd for $C_{36}H_{55}Br_2S_3$ 741.1833; found 741.1854. Anal. Calcd for $C_{36}H_{54}Br_2S_3$: C, 58.21; H, 7.33. Found: C, 58.32; H, 7.26

The above mentioned procedure was adopted for the syntheses of oligomers *m6-m10*. Yields ~ 90% (Scheme 3.2). The characterization data of *m*6-*m*10 are given below.

2, 5-dibromo 3-octyl thiophene (m6) - 17: ^{1}H-NMR (400 MHz, CDCl$_3$, 298 K) δ/ppm: 6.99-6.95 (m, 6H), 6.77 (s, 2H), 2.76 (t, *J* = 3.2 Hz, 2H), 2.64-2.63 (m, 6H), 1.66-1.64 (m, 8H), 1.31-1.28 (m, 40H), 0.91 (t, *J* = 2.8 Hz, 12H, CH$_3$). ^{13}C-NMR (100 MHz, CDCl$_3$, 298K) δ/ppm: 149.5, 140.9, 136.2, 134.9, 129.3, 126.6, 126.3, 84.3, 31.9, 30.4, 30.10, 29.5, 29.3, 29.2, 22.6, 14.0. FT-IR (KBr) ν in cm^{-1}: 2958, 2920, 2860, 1726, 1457, 1380, 1273, 1219, 1114, 1082, 1039, 968, 866, 792, 758, 723, 652, 611. HRMS (ESI) (*m/z*): (M+H)$^+$calcd for C$_{48}$H$_{73}$Br$_2$S$_4$ 935.2962; found 935.2977. Anal. Calcd for C$_{48}$H$_{72}$Br$_2$S$_4$: C, 61.52; H, 7.74. Found: C, 61.48; H, 7.65.

2, 5-dibromo 3-octyl thiophene (m7) - 18: ^{1}H-NMR (400 MHz, CDCl$_3$, 298 K) δ/ppm: 7.0-6.93 (m, 3H), 6.84-6.80 (m, 2H), 2.68-2.65 (m, 4H), 2.60-2.58 (m, 6H), 1.57-1.54 (m, 10H), 1.28-1.25 (m, 50H), 0.89 (t, *J* = 2.4 Hz, 15H, CH$_3$). ^{13}C-NMR (100 MHz, CDCl$_3$, 298K) δ/ppm: 142.9, 142.4, 140.5, 136.1, 135.3, 134.9, 129.1, 128.2, 126.6, 126.4, 125.0, 124.4, 119.7, 108.6, 107.8, 31.9, 30.5, 30.3, 29.6, 29.5, 29.4, 29.2, 22.7, 14.1. FT-IR (KBr) ν in cm^{-1}: 2953, 2926, 2854, 1742, 1523, 1468, 1375, 1260, 1101, 1019, 827, 805, 723. HRMS (ESI) (*m/z*): (M+H)$^+$calcd for C$_{60}$H$_{91}$Br$_2$S$_5$ 1129.4091; found 1129.4082. Anal. Calcd for C$_{60}$H$_{90}$Br$_2$S$_5$: C, 63.69; H, 8.02; N, 10.30. Found: C, 63.56; H, 8.15.

2, 5-dibromo 3-octyl thiophene (m8) - 19: ^{1}H-NMR (400 MHz, CDCl$_3$, 298 K) δ/ppm: 7.00-6.81 (m, 6H), 2.73 (t, *J* = 3.2 Hz, 4H), 2.58-2.56 (m, 8H), 1.66-1.64 (m, 12H), 1.29-1.27 (m, 60H), 0.88 (t, *J* = 2.8 Hz, 18H, CH$_3$). ^{13}C-NMR (100 MHz, CDCl$_3$, 298K) δ/ppm: 149.5, 144.7, 142.5, 134.4, 132.3, 132.2, 132.1, 132.0, 131.9, 131.5, 129.0, 128.4, 31.9, 30.4, 30.10, 29.5, 29.4, 29.3, 29.2, 22.7, 22.6, 14.1. FT-IR (KBr) ν in cm^{-1}:2958, 2920, 2849, 1468, 1375, 1260, 866. HRMS (ESI) (*m/z*): (M+H)$^+$calcd for C$_{72}$H$_{109}$Br$_2$S$_6$ 1323.5220; found 1323.5387. Anal. Calcd for C$_{72}$H$_{108}$Br$_2$S$_6$: C, 65.23; H, 8.21. Found: C, 65.36; H, 8.16.

2, 5-dibromo 3-octyl thiophene (m9) - 20: ^{1}H-NMR (400 MHz, CDCl$_3$, 298 K) δ/ppm: 7.00-6.78 (m, 7H), 2.77-2.75 (m, 6H), 2.59-2.57 (m, 8H), 1.65 (t, *J* = 2.8 Hz 14H), 1.32-1.30 (m, 70H), 0.92 (t, *J* = 2.4 Hz, 21H, CH$_3$). ^{13}C-NMR (100 MHz, CDCl$_3$, 298K) δ: 142.9, 142.4, 140.5, 140.3, 140.1, 136.2, 135.3, 128.3, 128.2, 126.5, 126.4, 125.0, 124.4, 119.7, 108.6, 107.9, 31.9, 30.6, 30.5, 30.3, 29.7, 29.5, 29.4, 29.3, 27.9, 27.4, 27.1, 22.7, 16.4, 14.1, 13.7. FT-IR (KBr) ν in cm^{-1}: 2958, 2925, 2849, 1643, 1462, 1380, 1298, 1189, 1019, 821, 717. HRMS (ESI) (*m/z*): (M+H)$^+$calcd for C$_{84}$H$_{127}$Br$_2$S$_7$ 1517.6349; found 1517.6236. Anal. Calcd for C$_{84}$H$_{126}$Br$_2$S$_7$: C, 66.37; H, 8.35. Found: C, 66.45; H, 8.25.

2, 5-dibromo 3-octyl thiophene (m10) - 21: ^{1}H-NMR (400 MHz, CDCl$_3$, 298 K) δ/ppm: 7.03 - 6.79 (m, 9H), 2.82-2.80 (m, 10H), 2.62-2.60 (m, 8H), 1.68-1.64 (m, 18H), 1.36-1.34 (m, 108H), 0.96 (t, J = 2.4 Hz 27H, CH$_3$). ^{13}C-NMR (100 MHz, CDCl$_3$, 298K) δ/ppm: 143.9, 142.4, 140.5, 140.3, 140.0, 135.4, 134.9, 134.1, 129.9, 129.2, 128.3, 126.5, 126.3, 125.0, 124.7, 119.1, 118.6, 108.7, 32.0, 30.6, 29.7, 29.6, 29.5, 29.4, 29.3, 22.8, 14.2. FT-IR (KBr) ν in cm^{-1}: 2964, 2925, 2860, 2723, 2487, 1736, 1649, 1462, 1375, 1260, 1084, 1024, 799, 723. HRMS (ESI) (*m/z*): (M+H)$^+$calcd for C$_{108}$H$_{163}$Br$_2$S$_9$ 1905.8608; found 1905.8654. Anal. Calcd for C$_{108}$H$_{162}$Br$_2$S$_9$: C, 67.96; H. Found: C, 67.86; H, 8.61.

Synthesis of 2, 5-dialkyne of 3-octyl thiophenes oligomer (m5) - 24: 2,5-dibromo-3-octylthiophene oligomer (*m3*) **16** (0.700 g, 1.05 mmol), Pd(PPh$_3$)$_2$Cl$_2$ (70 mg, 0.105 mmol), CuI (10 mg, 0.05 mmol) were taken in a clean and dry 100 mL three neck round bottom flask. The flask was put under freeze-pump-thaw cycle for 3 times. To this dry THF (50 mL) and diisopropylamine (60 mL) were added. Trimethylsilylacetylene (0.22 g, 2.32 mmol) was injected drop-by-drop into the reaction mixture under nitrogen, and the resulting solution was heated to reflux overnight. It was then cooled to room temperature and left stirring for an additional hour. The mixture was neutralized in an ice-bath with dilute HCl (20% in H$_2$O, v/v, added drop wise) and the product was extracted with portions of CH$_2$Cl$_2$ (3×20 mL). The organic phase was collected and dried over Na$_2$SO$_4$, and the CH$_2$Cl$_2$ was evaporated under reduced pressure. *Deprotection Step*: The obtained crude silyl compound was discharged in a 250 ml two-neck round bottom containing N$_2$ flushed solution mixture of THF and methanol (1/1, v/v) and to this solid KOH (2 eq) was added and put into N$_2$ atmosphere. The resultant solution was left at room temperature for 1 h stirring. Then the solution was concentrated under reduced pressure and the obtained crude compound was further purified by silica column chromatography (SiO$_2$) with hexane as an eluent. The compound was obtained as brown color jelly like solid (0.590 g, yield ~ 90%). R_f value ~ 0.49. ^{1}H-NMR (400 MHz, CDCl$_3$, 298 K) δ/ppm: 6.80-7.10 (m, 3 H), 3.56 (s, 2H), 2.70 (t, J = 3.2 Hz, 2H), 2.59 (t, J = 2.6 Hz, 4H), 1.63-1.61 (m, 6H), 1.27-1.25 (m, 30H), 0.89 (t, J = 2.8Hz, 9H, CH$_3$). ^{13}C-NMR (100 MHz, CDCl$_3$, 298K) δ/ppm: 144.5, 142.9, 141.4, 136.1, 127.3, 126.7, 125.4, 124.4, 107.8, 31.9, 31.8, 29.7, 29.6, 29.4, 29.3, 29.2, 22.6, 14.1. FT-IR (KBr) ν in cm^{-1}: 3315 (C≡C-H, str) 2953, 2926, 2854, 2136 (C≡C, str) 1742, 1523, 1468, 1375, 1260, 1101, 1019, 827, 805,723, 652. HRMS (ESI) (*m/z*): (M+H)$^+$calcd for C$_{40}$H$_{57}$S$_3$

633.3622; found 633.3715. Anal. Calcd for $C_{40}H_{56}S_3$: C, 75.89; H, 8.92. Found: C, 75.68; H, 8.87.

Similar procedure was adopted for syntheses of oligomers *m6-m10*. Yields >99% (Scheme 3.2). The characterization data of *m*6-*m*10 are given below.

2, 5-dialkyne of 3-octyl thiophene oligomer (m6) – 25: ^{1}H-NMR (400 MHz, CDCl$_3$, 298 K) δ/ppm: 6.98 (s, 2H), 6.88 (s, 2H), 3.53 (s, 2H) 2.74-2.69 (m, 8H), 1.64-1.62 (m, 8H), 1.28 (m, 40H), 0.90 (t, *J* = 2.6 Hz, 12H). ^{13}C-NMR (100 MHz, CDCl$_3$, 298K) δ/ppm: 149.5, 140.9, 136.2, 134.9, 129.3, 126.6, 126.3, 116.6, 84.3, 31.9, 30.4, 30.10, 29.5, 29.3, 29.2, 22.6, 14.1. FT-IR (KBr) ν in cm^{-1}: 2964, 2920, 2849, 2142 (C≡C, str), 1462, 1249, 854, 750. HRMS (ESI) (*m/z*): (M+H)$^{+}$calcd for $C_{52}H_{75}S_4$ 827.4752; found 827.4748. Anal. Calcd for $C_{52}H_{74}S_4$: C, 75.48; H, 9.01; Found: C, 75.36; H, 9.12.

2, 5-dialkyne of 3-octyl thiophene oligomer (m7) – 26: ^{1}H-NMR (400 MHz, CDCl$_3$, 298 K) δ/ppm: 6.94-6.90 (m, 5H), 3.55 (s, 2H), 2.72 (t, *J* = 3.2 Hz, 6H), 2.58 (t, *J* = 2.8 Hz, 4H), 1.65-1.63-1.61 (m, 10H), 1.30-1.28 (m, 50H), 0.90 (t, *J* = 2.4 Hz, 15H, CH$_3$). ^{13}C-NMR (100 MHz, CDCl$_3$, 298K) δ/ppm: 149.5, 147.9, 144.6, 131.0, 127.0, 125.5, 124.8, 118.3, 114.4, 84.9, 84.4, 31.9, 30.3, 30.2, 30.1, 29.7, 29.5, 29.3, 29.2, 27.4, 22.6, 14.1. FT-IR (KBr) ν in cm^{-1}:2958, 2920, 2854, 2150 (C≡C, str), 1463, 1221, 1114, 1082, 1039, 968,866, 792, 767. HRMS (ESI) (*m/z*): (M+H)$^{+}$calcd for $C_{64}H_{93}S_5$ 1021.5881; found 1021.5821. Anal. Calcd for$C_{64}H_{92}S_5$: C, 75.23; H, 9.08; N. Found: C, 75.32; H, 9.16.

2, 5-dialkyne of 3-octyl thiophene oligomer (m8) – 27: ^{1}H-NMR (400 MHz, CDCl$_3$, 298 K) δ/ppm: 6.98-6.95 (m, 6H), 3.52 (s, 2H) 2.71-2.73 (m, 12H), 1.62-1.66 (m, 12H), 1.29-1.27 (m, 60H), 0.99 (t, *J* = 2.8 Hz, 18H, CH$_3$). ^{13}C-NMR (100 MHz, CDCl$_3$, 298K) δ/ppm: 149.4, 140.9, 140.4, 136.2, 134.9, 129.3, 126.6, 126.3, 116.6, 84.3, 31.9, 30.4, 30.10, 29.5, 29.4, 29.3, 29.2, 22.7, 22.6, 14.1. FT-IR (KBr) ν in cm^{-1}**:** 3309 (sp – C-H, str), 2953, 2925, 2854, 2098 (C≡C, str), 1654 (C=C, aromatic) 1462, 1375, 827, 761. HRMS (ESI) (*m/z*): (M+H)$^{+}$calcd for $C_{76}H_{111}S_6$ 1215.7010; found 1215.7017. Anal. Calcd for $C_{76}H_{110}S_6$: C, 75.06; H, 9.12. Found: C, 75.21; H, 9.16.

2, 5-dialkyne of 3-octyl thiophene oligomer (m9) – 28: ^{1}H-NMR (400 MHz, CDCl$_3$, 298 K) δ/ppm: 6.99-6.96 (m, 7H), 3.53 (s, 2H) 2.73 (t, *J* = 3.2 Hz, 10H), 2.60 (t, *J* = 3.0 Hz, 4H), 1.66-

1.64-1.62 (m, 14H), 1.29-1.27 (m, 70H), 0.90 (t, J = 2.8 Hz, 21H, CH$_3$). ^{13}C-NMR (100 MHz, CDCl$_3$, 298K) δ/ppm: 149.4, 140.9, 140.5, 136.2, 129.3,128.6, 128.5, 126.6, 126.3, 124.8, 116.6, 84.3, 31.9, 30.4, 30.10, 29.7, 29.5, 29.4, 29.2, 22.7, 14.1 FT-IR (KBr) ν in cm^{-1}: 3309 (C≡C-H, str), 2947, 2920, 2849, 2098 (C≡C, str), 1632 (C=C, aromatic), 1725, 1457, 1375, 827, 717. HRMS (ESI) (*m/z*): (M+H)$^+$calcd for C$_{88}$H$_{129}$S$_7$ 1409.8139; found 1409.8114 Anal. Calcd for C$_{88}$H$_{128}$S$_7$: C, 74.94; H, 9.15. Found: C, 74.82; H, 9.23.

2, 5-dialkyne of 3-octyl thiophene oligomer (m10) – 29: ^{1}H-NMR (400 MHz, CDCl$_3$, 298 K) δ/ppm: 7.00-6.98 (m, 9H), 3.54 (s, 2H) 2.78-2.76 (m, 14H), 2.73 (t, J = 3.2 Hz, 4H), 1.69-1.67 (m, 18H), 1.29-1.26 (m, 90H), 0.91-0.89 (t, J = 2.8 Hz, 27H, CH$_3$). ^{13}C-NMR (100 MHz, CDCl$_3$, 298K) δ/ppm: 149.4, 140.5, 140.4, 140.0, 136.2, 134.8, 134.2, 130.0, 129.5, 128.5, 126.5, 126.3, 116.6, 84.3, 31.9, 30.4, 30.10, 29.7, 29.6, 29.5, 29.4, 29.2, 28.9, 22.6, 14.0. FT-IR (KBr) ν in cm^{-1}: 3314 (C≡C-H, str), 2947, 2925, 2849, 2098 (C≡C, str), 1638 (C=C, aromatic), 1462, 1375, 827, 728. HRMS (ESI) (*m/z*): (M+H)$^+$calcd for C$_{112}$H$_{165}$S$_9$ 1798.0398; found 1798.0239. Anal. Calcd for C$_{112}$H$_{164}$S$_9$: C, 74.77; H, 9.19. Found: C, 74.65; H, 9.08.

Synthesis of Copolymer (P3): 2,5-diethynyl-3-octylthiophene **22** (100 mg, 0.409 mmol) 2,6-bis(4-iodo-1*H*-pyrazol-1-yl)pyridine **1** (185 mg, 0.400 mmol), 2-(4-iodo-1*H*-pyrazol-1-yl)-6-(1*H*-pyrazol-1-yl)pyridine **4** (14 mg, 0.04 mmol), THF (10.0 mL), and diisopropylamine (20.0 mL) were added to a two-neck round-bottom flask, and the solution was purged with nitrogen for 20 min. Afterwards, the reaction was degassed by a repeated sequence of freeze-pump-thaw cycles. PdCl$_2$(PPh$_3$)$_2$ (28 mg, 0.0409 mmol) and CuI (4.0 mg, 0.02 mmol) were added to the reaction under nitrogen, and the mixture was stirred at 60 °C overnight. After 16 h, a small excess of 2-(4-iodo-1*H*-pyrazol-1-yl)-6-(1*H*-pyrazol-1-yl) pyridine **4** (14 mg, 0.04 mmol) was added, and the reaction mixture was stirred for another 6 h. The hot suspension was subsequently poured into a saturated aqueous EDTA solution (100 mL), and the mixture was stirred for 2 h. The organic layer was separated, and the aqueous layer was extracted with CHCl$_3$. The combined organic layers were washed with deionized water, and the volume of the solvent was reduced under reduced pressure. The concentrated organic layer was redissolved in CHCl$_3$ (10 ml) and MeOH (100 ml) was added drop wise to form an off-brown color precipitate. The precipitate was filtered and washed with boiling MeOH, EtOH, hexane and MeOH at room temperature followed by cold CHCl$_3$. ^{1}H-NMR (400 MHz, CDCl$_3$, 298 K) δ/ppm: 8.75 (s, 4H), 8.65 (s, 2H),

8.59 (s, 2H), 8.0-7.97 (m, 56H), 7.45-7.43 (m, 20H), 7.09- 7.07 (m, 10H), 6.51 (t, J = 2.4 Hz

2H, Pyrazole-end group), 2.73 (t, J = 3.0 Hz 12H), 1.65-1.63 (m, 16H), 1.40-1.38 (m, 96H),

0.88-0.86 (m, 38H, CH$_3$). FT-IR (KBr) ν in cm^{-1}: 2920, 2848, 1599, 1582, 1511, 1462, 1391,

1193, 996, 969, 941, 804, 771, 651. $\overline{M}_n$ = 4530 by ^{1}H NMR. From GPC data: $\overline{M}_n$ = 5.3 KDa, $\overline{M}_w$

= 27.6 KDa, PDI = 5.21.

Similar procedure was adopted for the syntheses of polymers **P4-P10** (Scheme 3.2). The

characterization data of **P4-P10** are given below.

P4: ^{1}H-NMR (400 MHz, CDCl$_3$, 298 K) δ/ppm: 8.74 (s, 6H), 8.65 (s, 3H), 8.58 (s, 2H), 8.0-7.92

(m, 54H), 7.50-7.47 (m, 10H), 7.0 - 6.97 (m, 16H), 6.51 (t, 2H, J = 2.4 Hz, Pyrazole-end group),

2.71 (t, J = 3.2 Hz, 24H), 2.50 (t, J = 2.8 Hz, 6H) 1.69-1.67 (m, 36H), 1.37-1.35 (m, 200H),

0.90-0.88 (m, 64H, CH$_3$). FT-IR (KBr) ν in cm^{-1}: 2953, 2914, 2848, 1604 (C=C, aromatic), 1582,

1517, 1462, 1188, 996, 963, 947, 860, 799, 656. $\overline{M}_n$ = 5600 by ^{1}H NMR. From GPC data: $\overline{M}_n$ =

6.5 KDa, $\overline{M}_w$ = 17.1 KDa, PDI = 2.62.

P5: ^{1}H-NMR (400 MHz, CDCl$_3$, 298 K) δ/ppm: 8.74 (s, 2H), 8.64 (s, 1H), 8.57 (s, 2H), 8.0 -

7.98 (m, 48H), 7.45-7.42 (m, 26H), 7.07- 6.94 (m, 25H), 6.57 (t, 2H, J = 2.4 Hz, Pyrazole-end

group), 2.75 (t, J = 3.2 Hz, 22H), 2.54 (t, J = 2.8 Hz, 12H) 1.68-1.66 (m, 48H), 1.43-1.39 (m,

268H), 0.90-0.98 (m, 104H, CH$_3$). FT-IR (KBr) ν in cm^{-1}: 2953, 2914, 2848, 1599, 1577, 1473,

1188, 1095, 1040, 963, 941, 793. $\overline{M}_n$ = 6367 by ^{1}H NMR. From GPC data: $\overline{M}_n$ = 6.6 KDa, $\overline{M}_w$ =

13.3 KDa, PDI = 2.01.

P6: ^{1}H-NMR (400 MHz, CDCl$_3$, 298 K) δ/ppm: 8.76 (s, 1 H), 8.67 (s, 1H), 8.61 (s, 2H), 8.0 -

7.98 (m, 54H), 7.47-7.44 (m, 26H), 7.01- 6.98 (m, 30H), 6.54 (t, 2H, J = 2.4 Hz, Pyrazole-end

group), 2.74 (t, J = 3.4 Hz, 25H), 2.56 (t, J = 3.0, 10H) 1.69-1.67 (m, 64H), 1.49-1.46 (m, 294H),

0.91-0.87 (m, 104H, CH$_3$). FT-IR (KBr) ν in cm^{-1}: 2920, 2854, 1604 (C=C, aromatic), 1582,

1517, 1467, 1380, 1188, 963, 947, 799. $\overline{M}_n$ = 5180 by ^{1}H NMR. From GPC data: $\overline{M}_n$ = 6.8 KDa,

$\overline{M}_w$ = 18.9 KDa, PDI = 2.77.

P7: ^{1}H-NMR (400 MHz, CDCl$_3$, 298 K) δ/ppm: 8.90(s, 1H), 8.76 (s, 4H), 8.61 (s, 3H), 8.0 -7.72

(m, 66H), 7.59-7.30 (m, 28H), 7.08-6.96 (m, 30H), 6.54 (t, J = 2.4 Hz, 2H, Pyrazole-end group),

2.80 (t, J = 3.0 Hz, 46H), 2.60 (t, J = 2.8 Hz, 14H) 1.64-1.62 (m, 116H), 1.46-1.42 (m, 425H),

0.90-0.88 (m, 140H, CH$_3$). FT-IR (KBr) ν in cm^{-1}: 2925, 2843, 1610 (C=C, aromatic), 1577,

1522, 1467, 1429, 1177, 1095, 1040, 793. $\overline{M}_n$ = 7.5 KDa by ^{1}H NMR. From GPC data: $\overline{M}_n$ = 7.6 KDa, $\overline{M}_w$ = 37.4 KDa, PDI = 4.9.

P8: ^{1}H-NMR (400 MHz, CDCl$_3$, 298 K) δ/ppm: 8.74 (s, 4H), 8.65(s, 2H), 8.60 (s, 2H), 8.0-7.98 (m, 50H), 7.59-7.54 (m, 33H),7.07-6.94 (m, 51H), 6.54 (s, 2H, Pyrazole-end group), 2.76 (t, 74H), 2.60 (t, J = 2.8 Hz 36H) 1.64-1.62 (m, 388H), 1.46-1.42 (m, 1270H), 0.90-0.97 (m, 333H, CH$_3$). FT-IR (KBr) ν in cm^{-1}: 2947, 2920, 2854, 1604 (C=C, aromatic), 1468, 1433, 1390, 1269, 1188, 1143, 1116, 1006, 960, 947, 800. $\overline{M}_n$ = 11.0 KDa by ^{1}H NMR. From GPC data: $\overline{M}_n$ = 11.0 KDa, $\overline{M}_w$ = 51.7 KDa, PDI = 4.7.

P9: ^{1}H-NMR (400 MHz, CDCl$_3$, 298 K) δ/ppm: 8.90 (s, 1H), 8.74 (s, 2H), 8.65 (s, 1H),8.59(s, 1H), 8.0-7.72 (m, 30H), 7.49-7.46 (m, 22H), 7.01-6.95 (m, 34H), 6.53 (s, 2H, Pyrazole-end group), 2.78-2.76 (m, 30H), 2.55-2.53 (m, 15H) 1.68-1.65 (m, 76H), 1.42-1. 38 (m, 338H), 0.90-0.87 (m, 120H, CH$_3$). FT-IR (KBr) ν in cm^{-1}: 2953, 2920, 2848, 1604 (C=C, aromatic), 1582, 1528, 1473, 1429, 1188, 958, 804, 695. $\overline{M}_n$ = 6500 by ^{1}H NMR. From GPC data: $\overline{M}_n$ = 7.2 KDa, $\overline{M}_w$ = 15.2 KDa, PDI = 2.11.

P10: ^{1}H-NMR (400 MHz, CDCl$_3$, 298 K) δ/ppm: 8.76 (s, 5H), 8.65 (s, 2H), 8.60 (s, 2H), 7.99-7.94 (m, 114H), 7.60-7.57 (m, 95H), 7.02-6.98 (m, 73H), 6.54 (s, 2H, Pyrazole-end group), 2.78-2.74 (m, 122H), 1.93 -1.89 (m, 229H), 1.28-1.26 (m, 511H), 0.92-0.89 (m, 1085H, CH$_3$). FT-IR (KBr) ν in cm^{-1}: 2922, 2851, 2216, 1604 (C=C, aromatic), 1581, 1496, 1469, 1433, 1390, 1269, 1188, 1143, 1116, 1006, 960, 947, 860, 798, 777, 719, 692, 653, 613, 540. From GPC data: $\overline{M}_n$ = 7.2 KDa, $\overline{M}_w$ = 15.7 KDa, PDI = 2.16.

Table 3.1 Molecular weight of copolymers (**P3-P10**).

Polymer	$\overline{M}_n$ by ^{1}H-NMR (KDa)	$\overline{M}_n$ by GPC (KDa)	$\overline{M}_w$by GPC (KDa)	PDI
P3	4.5	5.3	27.6	5.21
P4	5.6	6.5	17.1	2.62
P5	6.4	6.7	13.4	2.01
P6	4.5	6.84	18.9	2.75
P7	7.5	7.7	37.5	4.90
P8	11	11	51.7	4.70
P9	6.5	7.2	15.2	2.11
P10	-	7.3	15.7	2.16

3.3.2 *Thermal Properties of Copolymers*

The thermal stability of copolymers (**P3-P10**) was investigated by thermo-gravimetric analysis (Figure 3.2). The copolymers exhibited good thermal stability up to a temperature in the range of 270 ℃ – 300 ℃. All the polymers showed a two-step weight loss. In step 1, around 20% weight loss in the temperature range of 340 ℃ – 360 ℃ above which (step-2) it degraded with around 40% - 50% weight loss at temperature in the range of 480 ℃ – 530 ℃. The sequence of decrease in weight probably is a result of the decomposition of alkyl chains of the thiophene rings followed by thiophene rings (Fig 3.2).
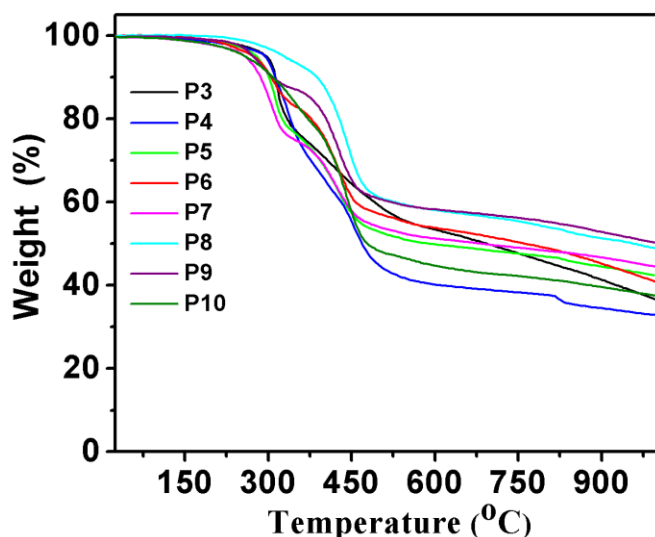
Figure 3.2 TGA data of polymers **P3**-**P10**.

3.3.3 *Optical Properties of Oligomers and Copolymers in Solution state*

The absorption and emission spectra of thiophene oligomers in solution state are presented in Figure 3.3. The spectral data of oligo(3-octyl thiophenes) (*m3-m*10) in chloroform solution are listed in Table 3.2.
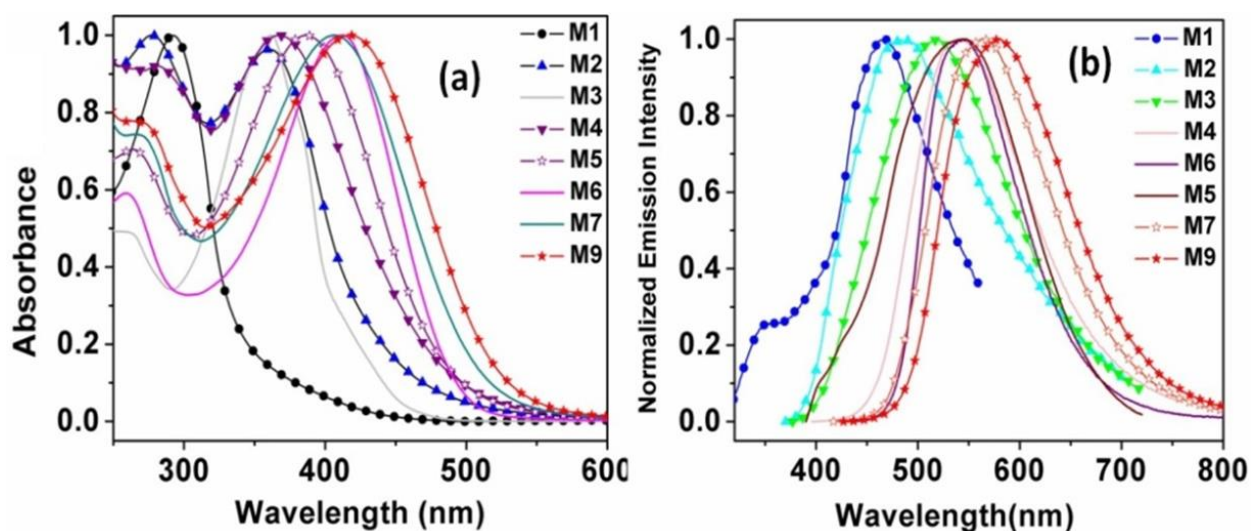
Figure 3.3 a) Absorption and b) emission spectra of thiophene oligomers (*m3-m10*) in CHCl$_3$.

Except oligomer *m3*, the other thiophene oligomers (*m4-m10*) mainly exhibited two absorption bands in solution state due to π-π*, and n-π* transitions; correspond to lower and higher wavelength bands, respectively. This dramatic change of the electronic states is as a result of two or more thiophene units which are in conjugation. For example, the low energy band had undergone a remarkable red shift from 466 to 579 nm, upon increasing the thiophene units from

Table 3.2 Optical spectroscopic data of thiophene oligomers and polymers

	Solution (CHCl$_3$)			Solution (CHCl$_3$)		$\Phi_f{}^a$	Thin Film		Optical band gap ^{b} (eV)
	Absorption λ_{max} (nm)	Emission λ_{max} (nm)		Absorption λ_{max} (nm)	Emission λ_{max} (nm)		Absorption λ_{max} (nm)	Emission λ_{max} (nm)	
m3	292	466	**P3**	318	390, 420, 480	31%	331	554	2.10
m4	277, 359	488	**P4**	315, 390	522	35%	309, 399	560	1.82
m5	265, 362	517	**P5**	309, 398	538	30%	309, 410	610	1.78
m6	280, 368	540	**P6**	309, 406	551	20%	309, 415	618	1.73
m7	262, 390	543	**P7**	317, 413	552	40%	317, 425	626	1.71
m8	260, 406	545	**P8**	309, 432	560	44%	309, 436	635	1.70
m9	270, 412	564	**P9**	309, 447	572	50%	309, 449	654	1.69
m10	269, 420	579	**P10**	308, 459	598	20%	308, 477	674	1.67

^{a}Quinine sulfate as reference (Q$_{ref}$ = 0.577). ^{b}Estimated from the onset wavelength of optical absorption in the solid state film.

two to nine, respectively. As expected the emission spectra of oligomers displayed red shifts from 466 to 545 nm due to increase of the π-conjugation length and subsequent decrease of the band-gap (Table 3.2). Compared to thiophene oligomers, the copolymers (**P3**-**P10**) showed red shift of the absorption and emission maxima (λ_{max}) in their optical spectra. This observation clearly showed the electronic coupling of the thiophene units with the ethynyl bpp units. The chloroform solution of copolymer **P3** showed blue emission in very diluted solution state (2.77×10^{-12} mol/mL) at 390 nm and 420 nm; upon increasing the concentration to 1.21×10^{-10} mol/mL, an additional aggregation induced emission appeared at ~480 nm, which was further red shifted to ~500 nm with the increase of intensity upon further increasing concentration to c ~ 4.77×10^{-8} mol/mL, giving cyan color emission (Fig. 3.4b). The absorption spectra did not show any noticeable shifts upon changing the concentrations (Fig. 3.4a).
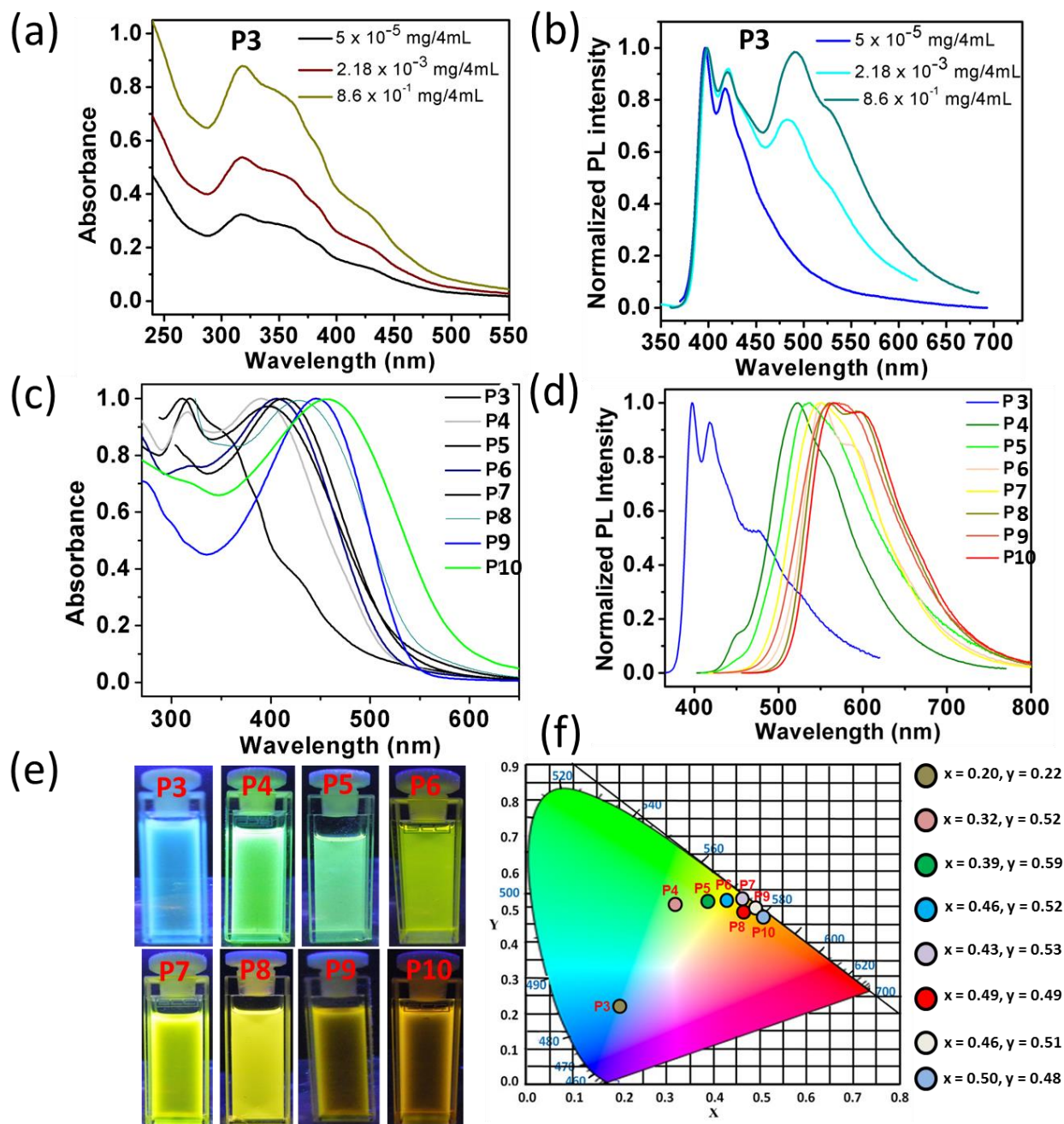
Figure 3.4 a) and b) Effect of concentration absorption and emission spectra of copolymer **P3** in CHCl$_3$, respectively. c) and d) Absorption and emission spectra of copolymers (**P3**-**P10**) in CHCl$_3$, respectively. e) Emission colors of polymers in solution state upon UV light-irradiation. f) Emission colors of copolymers in solution state (**P3**-**P10**) in a CIE 1931 2° standard observer chromaticity diagram.

This observed red shift is due to strong interchain interactions and excimer-like behavior which are prevalent in copolymers with large optical band gaps.[17] The optical data of copolymers are presented in Table 3.2. All the copolymers (**P3**-**P10**) showed red shift of the absorption and

emission maxima (λ_{max}) in their optical spectra because of the extension of π-conjugation lengths of the polymer upon increasing the thiophene units from one to nine (Fig. 3.4c,d), indicating a corresponding decrease of the optical band gap (Fig. 3.6).
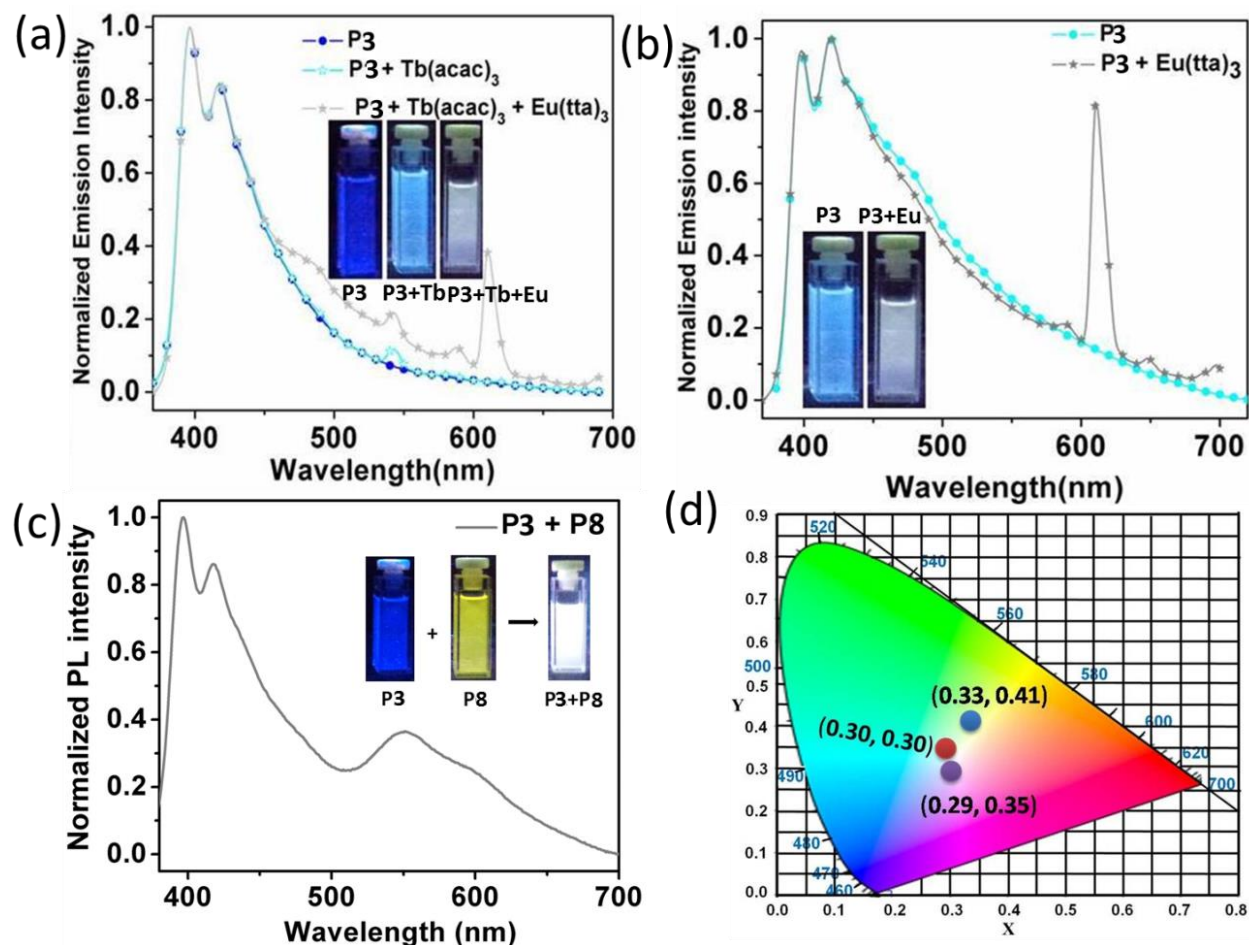
Figure 3.5 a) Emission spectra of **P3**, without and with metals (Tb^{+3}, Eu^{+3}) in CHCl$_3$. Insets show the photographs of emission colors from **P3**, **P3**+Tb^{+3}, **P3**+Tb^{+3}+Eu^{+3} upon UV light-irradiation. b) Emission spectra of copolymer **P3** with and without Eu^{+3} in CHCl$_3$, and the inset shows the emission colors of **P3** and **P3**+Eu^{+3} upon UV light-irradiation. c) Emission spectra of mixture of **P3** and **P8** in CHCl$_3$, the insert photographs are the emission colors of **P3**, **P8**, **P3**+**P8** upon UV light-irradiation. d) Emission color of polymers **P3**+Tb^{+3}+Eu^{+3}(0.29, 0.35), **P3**+Eu^{+3} (0.33, 0.41,) (**P3**+**P8**) (0.30, 0.30) in solution state CIE 1931 2° Standard Observer chromaticity diagram.

Correspondingly, under UV light copolymers displayed blue to orange emission in solution state for **P3** to **P10** respectively (Fig. 3.4e) and their emission colors in the CIE 1931 2° Standard Observer chromaticity diagrams showed *x*, *y* coordinate values of (0.20, 0.22) for 480 nm; (0.32,

0.52) for 522 nm; (0.39, 0.50) for 538 nm; (0.46, 0.52) for 551 nm; (0.43, 0.53) for 552 nm; (0.49, 0.49) for 560 nm; (0.46,0.51) for 572 nm; and (0.50,0.48) for 598 nm, respectively (Fig 3.4f).
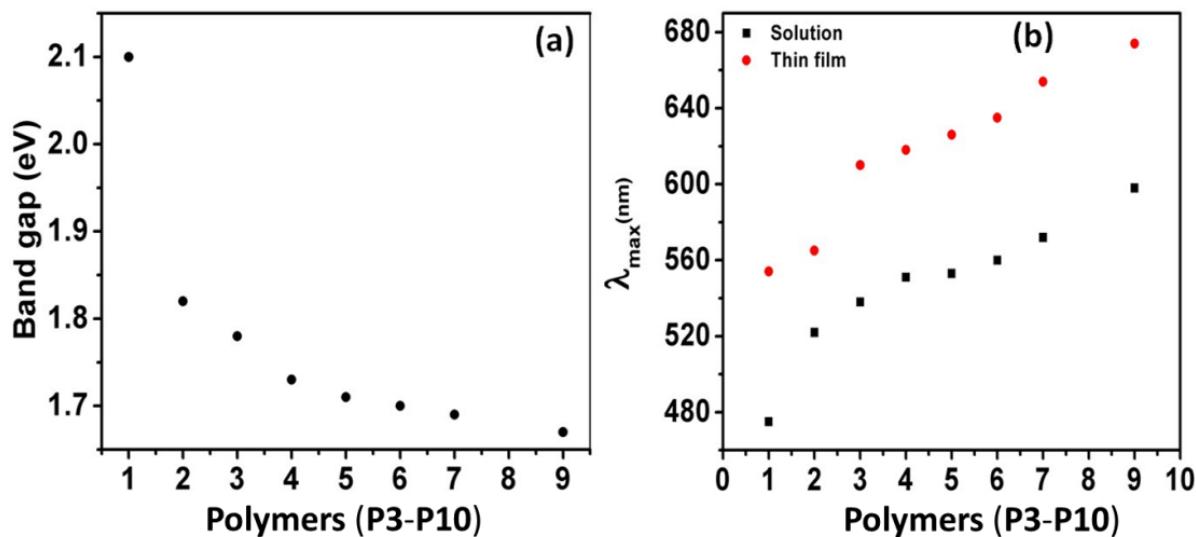
Figure 3.6 a) Optical band gap of copolymers **P3**-**P10**. b) Variation of emission maximum of copolymer in solution and thin film states.

The bpp unit of the copolymer main chain is known to coordinate with red emitting Eu(tta)$_3$ (tta = 3-thenoyltrifluoroacetonate) and green emitting Tb(acac)$_3$ (acac = acetylacetonate) complexes forming nine coordinated structures (see introduction Fig. 1.4).[9a-e] Taking advantage of the metal coordinating ability of the bpp units are available in the copolymer main chain, the emission color of polymers were tuned by coordinating metal complexes of Eu^{+3} and Tb^{+3} ions. For example, a very dilute solution of **P3** (4.4×10^{-12} mol/mL) showed blue color emission (Fig 3.4b and Fig 3.5a) and to this solution (4 mL) addition a 1:1 mixture of THF solution of Tb(acac)$_3$ and Eu(tta)$_3$ (0.2 mL; 4.0×10^{-15} mol/mL)   and (0.2 mL; 3.99×10^{-14} mol/mL,) respectively displayed a white color light (Figure 3.5a) with CIE (x, y) coordinates 0.29, 0.35 (Fig. 3.5d). The emission spectra of Tb^{3+} ion displayed sharp emissions λ_{max} at 490, 547, 585, and 620 nm due to $^5D_4 \rightarrow ^7F_J$ (J = 3-6) *f-f* transitions and Eu^{3+} ion exhibited peaks at 581, 594, 612, 653, 705 nm due to $^5D_0 \rightarrow ^7F_J$ (J= 0-4) *f-f* transitions[18] (Fig 3.7). Amongst the peaks corresponding to that of Eu^{3+}& Tb^{3+} ions, the strongest emission was observed at 612 nm and 547 nm, respectively.[19] White emission was also achieved by mixing highly concentrated solution of cyan emitting **P3** (4 mL; 1.38×10^{-11} mol/mL) (Fig 3.4b and Fig 3.5b) with THF

solution of Eu(tta)$_3$ (0.5 mL; 1.1×10^{-10} mol/mL). In an alternative route, white radiation was also obtained by simple mixing THF solutions of blue emitting copolymer (**P3**) (2 mL; 4.4×10^{-12} mol/mL) and yellow emitting copolymer (**P8**) (2 mL; (2.27×10^{-11} mol/mL) in 1:1 ratio (Fig 3.5c, d) to get CIE (*x*, *y*) coordinates of 0.30, 0.30.
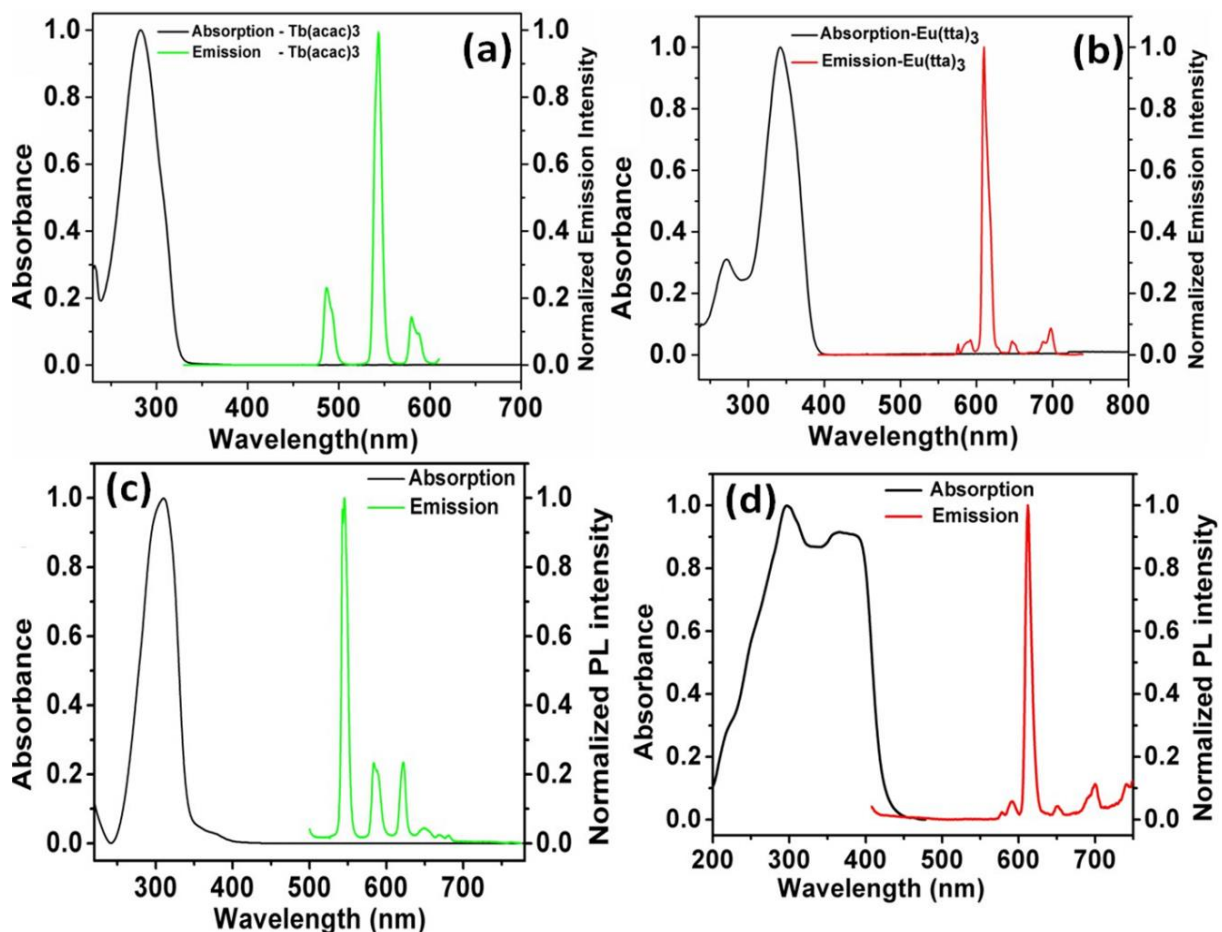
Figure 3.7 Absorption and emission spectra of Tb(acac)$_3$ and Eu(tta)$_3$ in solution and solid states: a) Tb(acac)$_3$ (solution) b) Eu(tta)$_3$ (solution) c) Tb (acac)$_3$ (solid state) d) Eu(tta)$_3$ (solid state).

3.3.4 *Optical Properties of Copolymers and Metal–Coordinated Copolymers in Thin Film State*

The emission spectra of spin coated (c ~7 mg/1 mL of CHCl$_3$) copolymers in thin film state displayed a strong red shift from green (554 nm) to orange red emission (674 nm) compared to their solutions, owing to molecular chain ordering (Fig 3.8a, c).[17a,20] This shift is generally

observed for many conjugated polymers and is generally inferred as the formation of *J*-aggregates.[19] Likewise, the optical band gap of the polymers were also decreased with increasing number of thiophene units in the main chain of copolymers **P3**-**P10** from 2.1 to 1.67 eV (Table 3.2 and Fig 3.6a). The CIE plot of emission colors of polymers in solid thin film state showed the following *x*, *y* coordinate values: **P3:** (0.42, 0.48) for 554 nm; **P4:** (0.51, 0.46) for 560 nm; **P5:** (0.47, 0.50) for 610 nm; **P6:** (0.55, 0.44) for 618 nm; **P7:** (0.51, 0.47) for 626 nm; **P8:** (0.57, 0.41) for 635 nm; **P9:** (0.55, 0.43) for 654 nm; **P10:** (0.54,0.45) for 674 nm (Fig 3.8d).
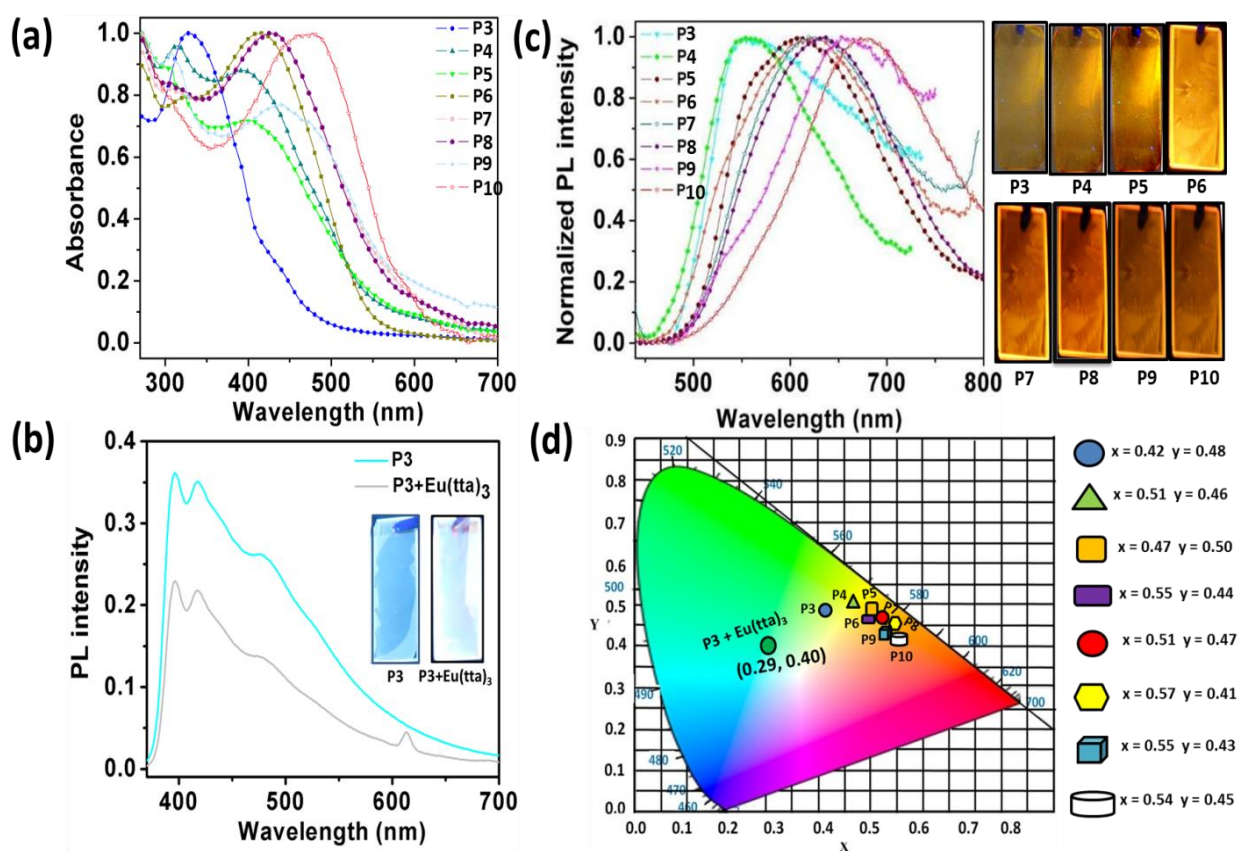
Figure 3.8 a) and c) Absorption and emission spectra of copolymer thin films, respectively. Right inset shows emission colors of copolymer thin films on quartz slide upon UV-irradiation. b) Emission spectra of thin films of **P3** and **P3**+Eu[+3].The insets show the emission colors of **P3**, and **P3**+Eu[+3]upon UV-irradiation d) Emission color of copolymer thin films(**P3**-**P10**) and **P3**+Eu[+3],in a CIE 1931 2° standard observer chromaticity diagram.

To generate white emission in the solid state, a quartz slide was spin coated with various concentration of CHCl$_3$ solution of **P3** from 2.0×10^{-7} mol/mL to 1.4×10^{-6} mol/mL (2.0 mg/mL to 6.5 mg/mL). It was found that upon increase of **P3** concentration the emission colour

dramatically changed from cyan to green with various transitional colours at the intermediate concentrations (Fig. 3.9). To create white colour emission by mixing with red emitting Eu(tta)$_3$ complex, a 300 μL of **P3** solution of concentration 6.6×10^{-7} mol/mL exhibiting cyan emission in the film was identified.
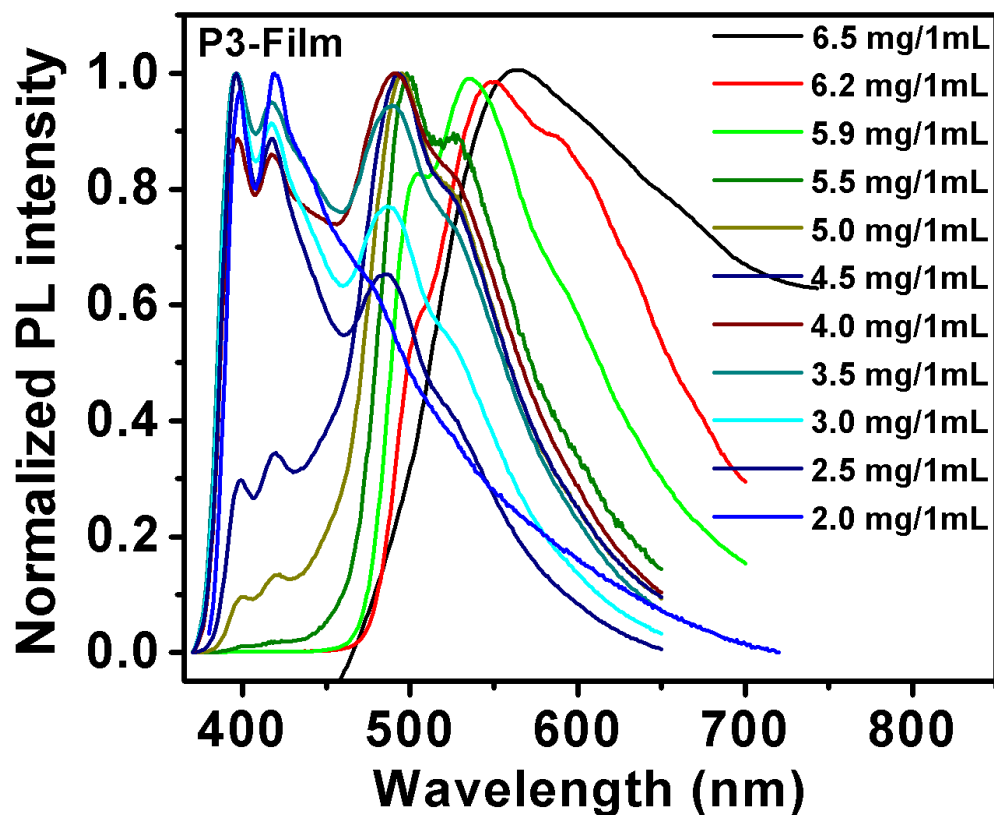
Figure 3.9 Concentration effect on copolymer **P3** – thin film. The thickness of the film was varied by changing the concentration of the solution and keeping the injection amount (300 μL), spin coating time (10 sec) and rpm (6K/1K) same for each cases. (Films were excited at 360 nm).
Note – (**P3** - 3.5 mg – 2.2 mg/ 1ml gives cyan emission).

This cyan emitting **P3** thin film was dipped in a methanol solution of Eu(tta)$_3$ ($c \sim 6.9 \times 10^{-8}$ mol/mL) for 20 min (Fig 3.8b, d). It was expected that the Eu(tta)$_3$ molecules diffused into the polymer thin film from the solution and coordinated with exposed bpp units of the polymer back bone. The intensity of the Eu^{3+} centered red phosphorescence [$^5D_0 \rightarrow {^7}F_J$ ($J = 0$–4) transitions] was controlled by the amount of **P3·**Eu(tta)$_3$ complex formation and adjusted according to the intensity of I$_{blue}$/I$_{green}$ emissions to attain good quality white color with CIE (x, y) coordinates

0.29, 0.40. It is interesting to observe that the purity of all these emitted white colors are close to standard coordinates for pure white color (x= 0.33, y=0.33).

3.3.5 *Self-assembly of Copolymers*

Copolymers (**P3-P10**) were self-assembled in a mixture of THF/H$_2$O (2:1) solution. In a typical self-assembly procedure, water (1mL) was drop-wise added to a THF solution of **P3** (1.1×10^{-7} mol/mL) and the solution was kept undisturbed for 15 min to stabilize the growth of particles (Fig. 3.10).
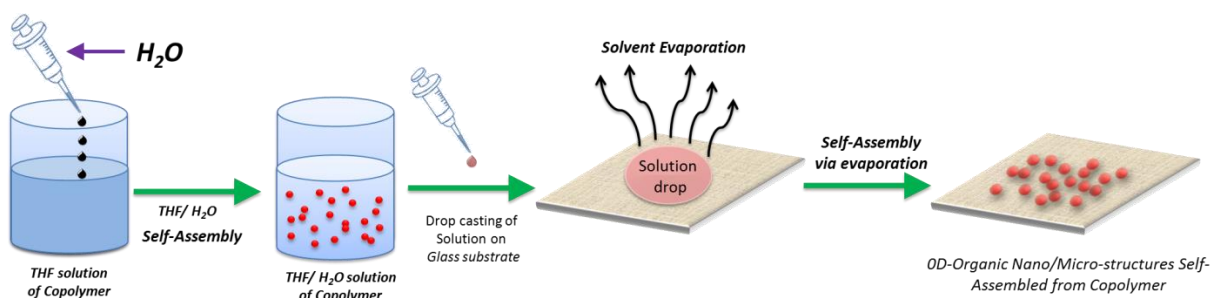
Figure 3.10 Bottom-up self-assembly route toward copolymer **P3-P10** spheres.

Similar procedure was followed to self-assemble **P4-P10**. FESEM images of all the polymer samples confirmed the formation of nano/micro spheres of various diameters via self-assembly (Fig. 3.12). Further illumination of the THF solution of **P3-P10** nano/micro spheres with laser light displayed a fine Tyndall effect due to light scattering, indicating the presence of solution-stable nano/micro structures (Fig. 3.12 insets). The detailed electron microscopy (FESEM and TEM) and AFM examination of **P3** assemblies clearly ascertain the formation of nano and micro spheres (Fig. 3.11a-d). FESEM micrographs displayed several aggregated nano/microspheres of various sizes (Fig. 3.11a). TEM micrographs exhibited the presence of nano/micro spheres displaying a relatively weak contrast as typically observed for soft organic structures (Fig. 3.11b). AFM cross-section analysis of spheres showed that the diameter is in the range of ca.700 nm – 1.2 μm (Fig 3.11c, d). The laser confocal fluorescence micrographs of the solid microspheres composed of **P3**-**P8** and the nano/microsphere containing solutions exhibited FL colors corresponding to their emission wave lengths (Fig 3.11e, f). The self-assembly of cyan to

red emitting conjugated copolymer spheres is possibly mediated by the π-π stacking interactions of the copolymer aromatic units; thereby increasing the close packing of the hydrophobic octyl-chains on the thiophene rings forming sphere like structures.
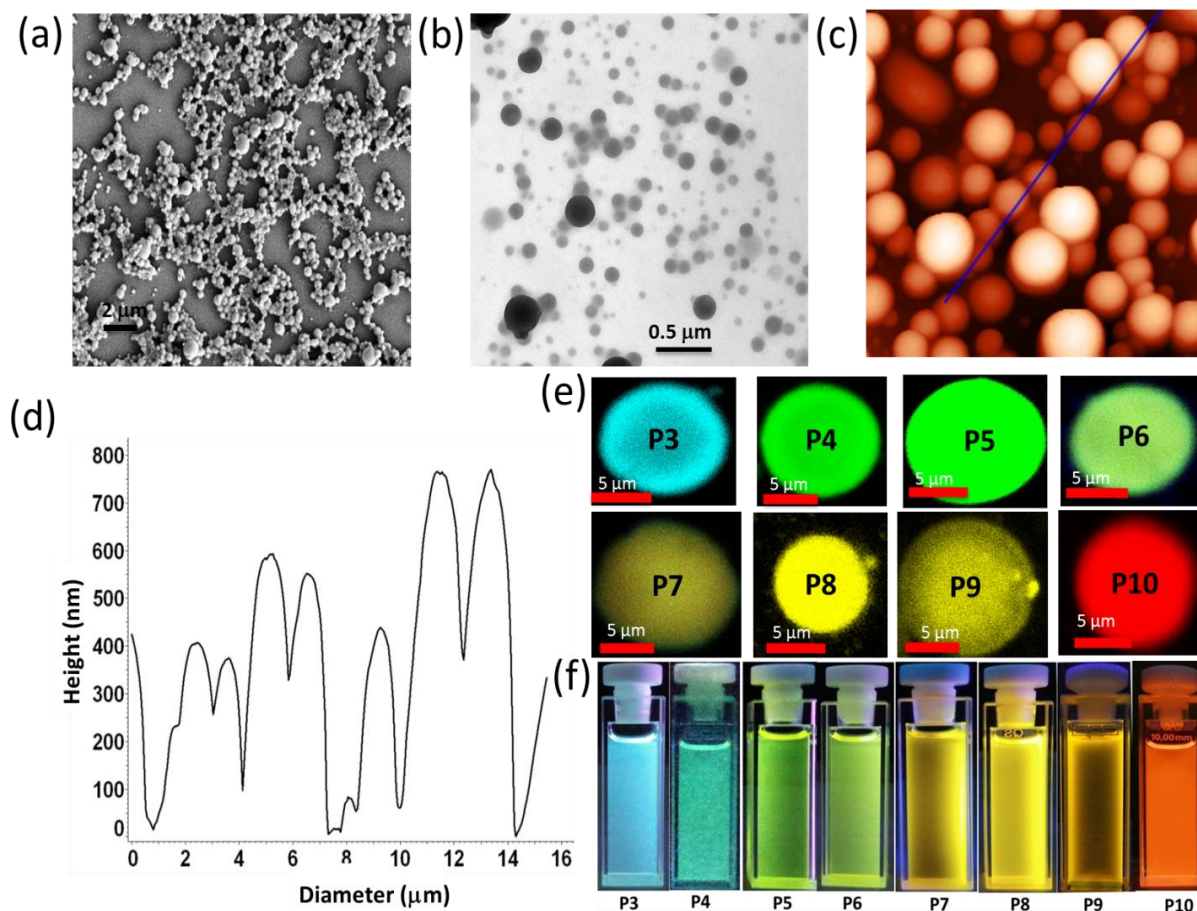
Figure 3.11 a) FESEM images of copolymer spheres obtained from **P3** (scale bar is 2 μm). b) TEM image of **P3** spheres (scale bar is 0.5 μm). c) and d) Non-contact mode AFM image of nano/microscale spheres and their height and diameter profiles. e) Confocal fluorescence images of copolymer spheres (**P3-P10**). f) Emission colors of nano/microspheres containing copolymers solutions (under UV-visible excitation).
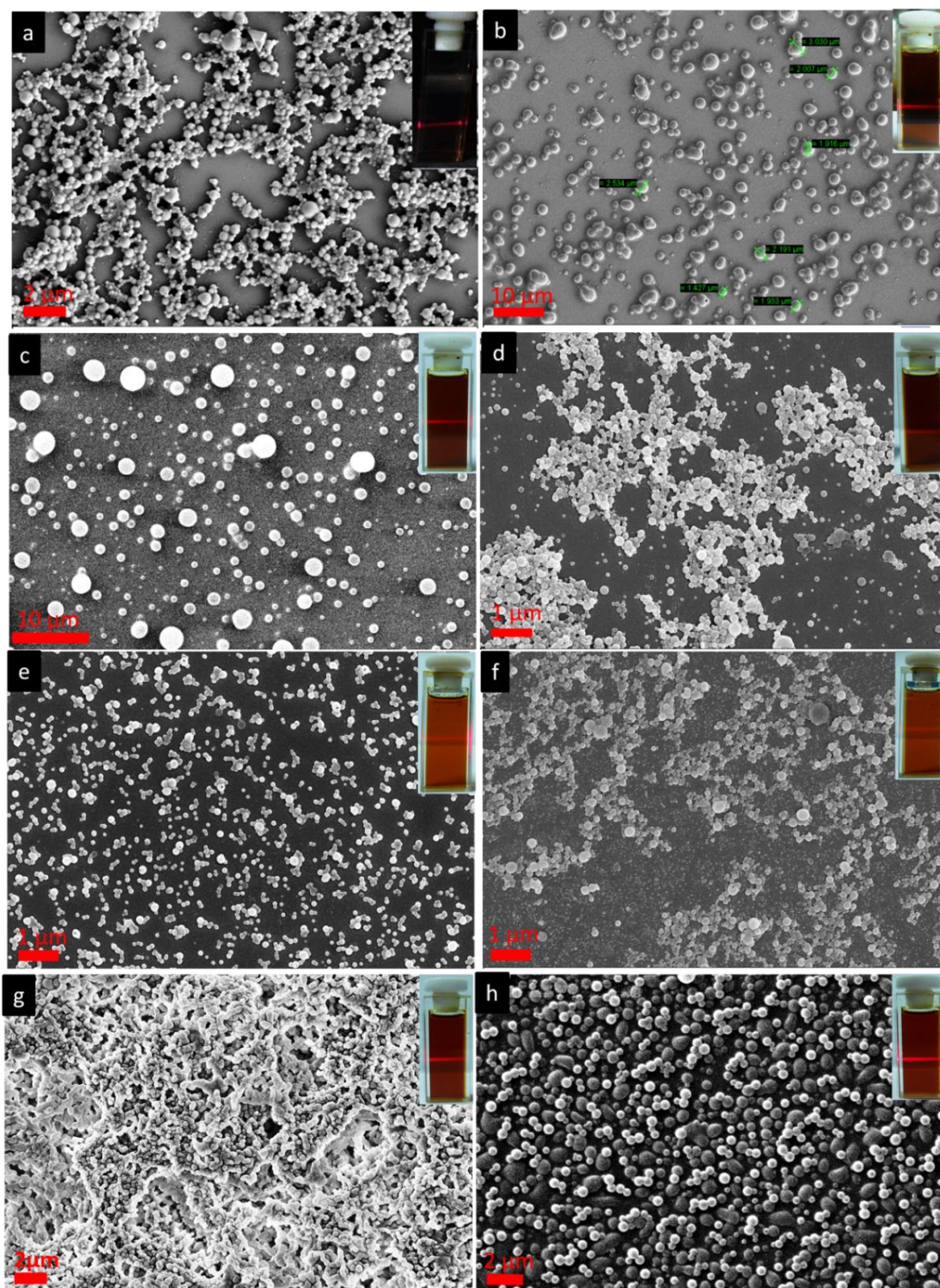
Figure 3.12 FESEM images of copolymer spheres **P3-P10**. a) **P3** (scale bar is 2 μm), b) **P4** (scale bar is 10 μm) c) **P5** (scale bar is 10 μm) d) **P6** (scale bar is 1 μm) e) **P7** (scale bar is 1 μm) f) **P8** (scale bar is 1 μm). g) **P9** (scale bar is 2 μm). h) **P10** (scale bar is 2 μm).
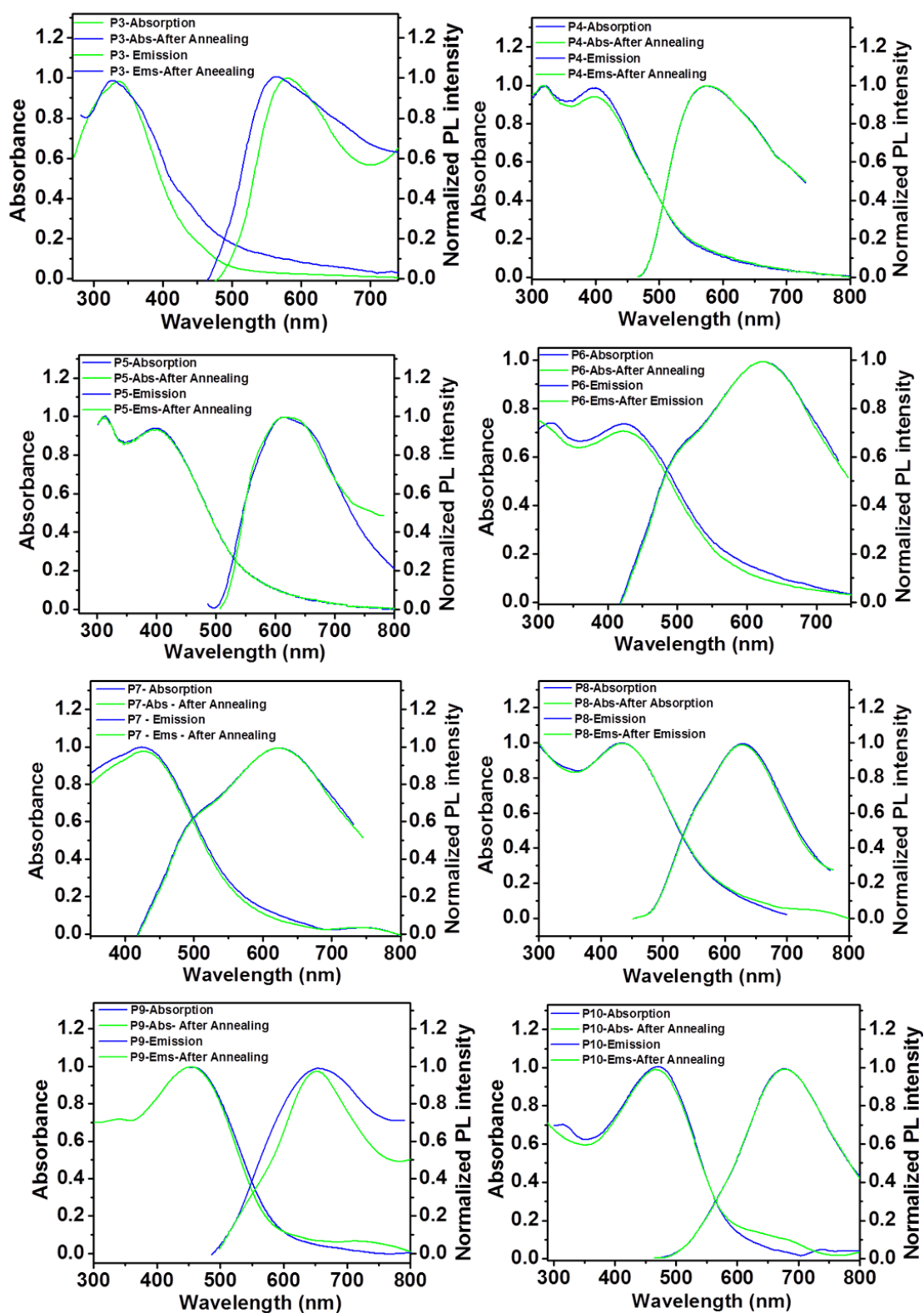
Figure 3.13 UV-Vis absorption spectra of copolymer thin films (**P3-P10**) annealed with solvent vapor.

To study the influence of solvent vapor annealing the copolymer thin films (see Fig 3.8a, c), were exposed to vapors of THF/H_2O (2:1) solution in a closed vessel for 10 h. The optical studies of the annealed copolymer films showed insensitivity of all the copolymer films to annealing (Fig. 3.13), except **P3**, which showed ~7 nm and 15 nm blue shifts in the absorption and emission spectra, respectively (Fig. 3.13a), indicating possible alteration of the copolymer chains. The observed blue shift of the annealed **P3** film is probably due to a slight ordering of copolymer film akin to polymer organization in microspheres via solvent diffusion, softening the polymer chains allowing their movement. Further the AFM investigation of the **P3** film without solvent exposure, exhibited a smooth surface of the film over majority of the area (Fig. 3.14a), whereas solvent vapor annealed **P3** film showed growth of nanospheres of diameter in the range of ~ 180 nm via *h*-aggregation (Fig. 3.14b), indicating the dramatic change of the film morphology due to solvent interactions. This result also supported the observed blue shifts of the absorption and emission bands compared to pure **P3** thin film.
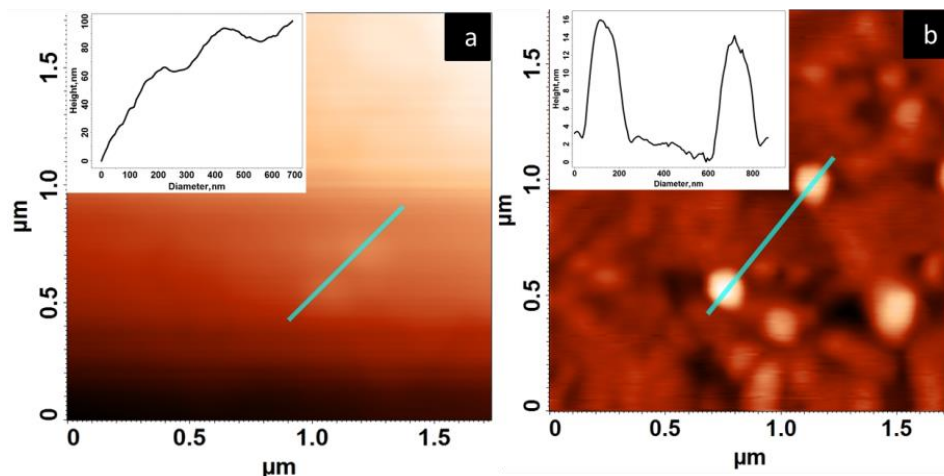
Figure 3.14 Spin cast film of **P3**, a) Before annealing and b) After solvent annealing.

The comparative optical data of polymers in solution, microsphere and thin film states were summarized in Table 3.3. The optical property of π-conjugated polymers in the aggregated state differs from those in the secluded chain state. The copolymer solution containing nano/micro spheres can be treated as an intermediate state between a solution state and solid film state. Compared to dilute non aggregated polymer solution state, the copolymer nano/micro spheres solution is a mixed state containing well dispersed copolymer particles and dilute non-

aggregated polymer solution, whereas the copolymer chains strongly aggregate with each other in solid films.

Table 3.3 Comparative optical data of copolymers in solutions, micro spheres containing solutions, microspheres, and spin coated thin films.

Polymer	Solution state		Microspheres solution		Microspheres	Spin coated thin film state	
	Absorption λ_{max} (nm)	Emission λ_{max} (nm)	Absorption λ_{max} (nm)	Emission λ_{max} (nm)	Emission λ_{max} (nm)	Absorption λ_{max} (nm)	Emission λ_{max} (nm)
P3	318	475	319	397, 417, 480	464, 497	331	554
P4	315, 390	522	318, 392	531	532	309, 399	560
P5	309, 398	538	309, 399	538	540	309, 410	610
P6	309, 406	551	310, 407	552	556	309, 415	618
P7	317, 413	552	314, 428	566	567	317, 425	626
P8	309, 432	560	309, 439	583	580	309, 436	635
P9	309, 447	572	309, 447	611	612	309, 449	654
P10	308, 459	598	305, 454	633	636	308, 477	674

The copolymer solution containing nano/micro spheres can be considered as a dispersed ordered copolymer particle system. As a result of aggregation, the quenching efficiency was well pronounced in cast films, and it decreased for nano/micro spheres solutions and the effect was not observed for polymer in dilute solution. The emission spectra for the copolymer solution containing micro/nano spheres (Fig. 3.15a) and several solid micro spheres (Fig. 3.15b) were found to be very much similar.
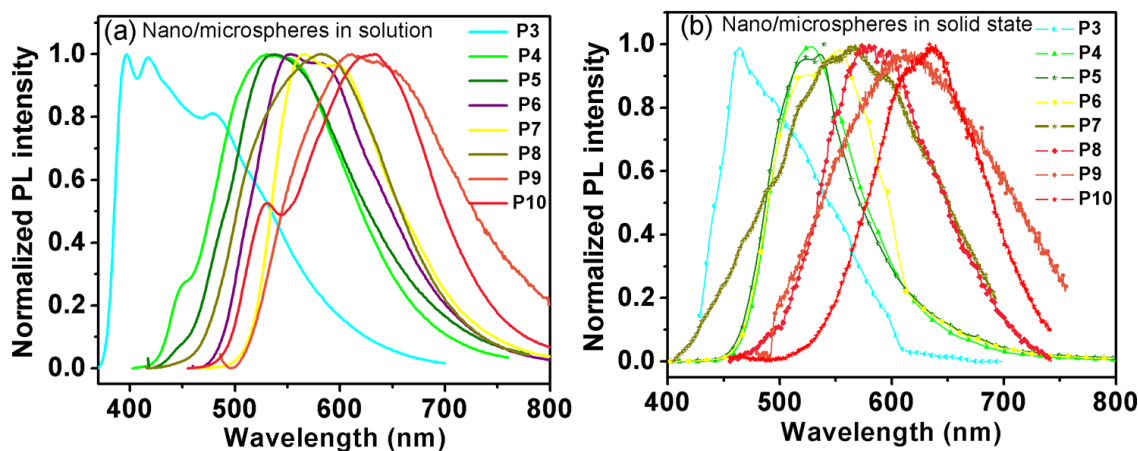
Figure 3.15 a) and b) emission spectra of micro/nano spheres containing copolymer solution and laser fluorescence confocal spectra of a bunch of microspheres.

3.3.6 *White Emitting Nano/Micro Scale Polymer/Inorganic Hybrid Spheres*

In order to obtain white color emitting core-shell spheres, coordination chemistry on the self-assembled solid surface approach was followed (see introduction, Fig. 1.5 for details).[9b-d] Firstly the cyan emitting copolymer spheres were grown in THF/H_2O solution of **P3**, as mentioned before. Secondly, by injecting a THF solution of $Eu(tta)_3 \cdot (H_2O)_3$ (0.02 ml; 1.0×10^{-6} mol/mL) to the solution containing the spheres, followed by gentle shaking, a layer of a nine coordinated complex[9a-e] was formed on the surface of the spheres. It is expected that the cyan emitting microsphere act as core and the red emitting $Eu(tta)_3$ molecules act as shell around the core. The possible mechanism of complex formation on the spheres is the coordination of $Eu(tta)_3$ with the surface exposed bpp units and diffusion through nano/micro pores and defects as well. Examination of the TEM-bright field images obtained from the metal coordinated
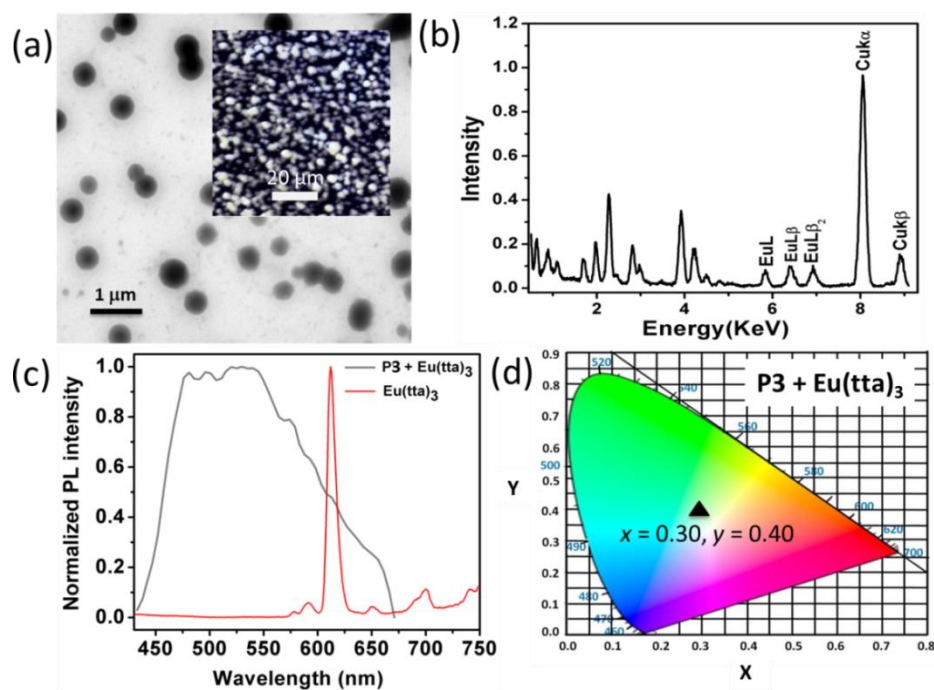
Figure 3.16 a) TEM image of $Eu(tta)_3$ coordinated **P3** spheres (scale bar is 1 μm), inset shows their corresponding confocal fluorescence microscopic image. b) EDS spectrum exhibiting Eu^{3+} peaks from the metal ion coordinated spheres. c) Spectra of Eu^{3+} coordinated **P3** spheres displaying white emission in comparison with pure $Eu(tta)_3$ (λ_{ex} = 365 nm). d) CIE 1931 2° standard observer chromaticity diagram of white mitting spheres (*x*=0.30, *y*=0.40).

copolymer/inorganic hybrid spheres exhibited an apparent dark contrast due to the presence of Eu(III) complexes compared to light contrast displayed by pure **P3** spheres (Fig. 3.16a). In addition, the energy dispersive X-ray spectroscopy analysis (EDS) performed on the surface of a sphere clearly confirmed the presence of Eu ions (Fig. 3.16b).

In order to verify the appearance of cyan and white color emissions from **P3** spheres and Eu(tta)$_3$ coordinated **P3** spheres, respectively, scanning laser confocal fluorescence microscopy measurements were performed (Fig. 3.11e; see **P3** and Fig. 3.16a inset). The topographic structural data were directly coupled with the spectroscopic properties of the specimen (Fig. 3.16c), and for excitation Ar$^+$ (UV-365nm) laser was used. As expected, the **P3** spheres displayed a cyan color due to the mixing of blue and green (aggregation induced) emissions (Fig. 3.11e; see **P3** and Fig. 3.4b), whereas **P3** spheres coated with Eu^{3+} ion showed FL emission spectrum covering the whole visible region (400 nm-700 nm) exhibiting a significant white-light (Fig. 3.16c). The CIE (*x*, *y*) data provided the *x*, *y* values of 0.30; 0.40 for the white emitting spheres which are in the range of designated coordinates for an ideal white-light (*x*=0.33; *y*=0.33) (Fig. 3.16d).

3.4 CONCLUSIONS

In summary, this chapter demonstrated design, synthesis and characterization a series of alternating copolymers based on dialkynyloligo(3-octylthiophene) oligomers and tridentate bis(pyrazol)pyridine (bpp) ligand to generate MCCPs (see Introductory section-1.2.2 for more details on MCCPs). The light emission of these conjugated copolymers was tuned primarily by changing the thiophene oligomer length. Thiophene oligomers showed dramatic change in the optical band gap upon increasing its length from one to nine. Further coupling of these thiophene oligomers with ethynyl-bpp further shifted the emission intensities towards red side, indicating an efficient electronic coupling between the thiophene oligomers and bpp fragments.

Further white colors in solution and solid states were generated by incorporating metals like Tb^{+3} and Eu^{+3} to the bpp unit of the copolymer back bone. These polymers were successfully self-assembled into nano/micro scale copolymer spheres emitting a range of colors from cyan to red. Subsequently by following surface assisted coordination chemistry, white emitting core-shell microspheres were obtained by reacting red emitting Eu(tta)$_3$ on the surface of the cyan

emitting spheres. This easy and efficient fabrication method to generate multicolor displaying self-assembled spheres is an important development in the bottom-up technology of conjugated polymers. Further, this general methodology can be applied to achieve soft polymer structures displaying dissimilar colors by coordinating with various luminescent metal ions. Future work can be directed towards utilizing these polymer microspheres for trapping the light and also to generate laser lines of various colors from these **P3-P10** microspheres.

REFERENCES

1. a) R. H. Friend, R. W. Gymer, A. B. Holmes, J. H. Burroughes, R. N. Marks, C. Taliani, D. D. C. Bradley, D. A. Dos Santos, J. L. Bredas, M. Logdlund, W. R. Salaneck *Nature* **1999**, *397*, 121-128; b) M. Muccini, *Nat. Mater.* **2006**, *5*, 605-613; c) S. Reineke, F. Lindner, G. Schwartz, N. Seidler, K. Walzer, B. Lueesem, K. Leo, *Nature* **2009**, *459*, 234-238; d) A. J. Heeger, *Solid State Commun.* **1998**, *107*, 673-679; e) L. Xiao, Z. Chen, B. Qu, J. Luo, S. Kong, Q. Gong, J. Kido, *Adv. Mater.* **2011**, *23*, 926-952; f) C. Zhou, Y. Liang, F. Liu, C. Sun, X. Huang, Z. Xie, F. Huang, J. Roncali, T. P. Russell, Y. Cao, *Adv. Funct. Mater.* **2014**, *24*, 7538-7547; g) Organic Light Emitting Devices: Synthesis, Properties and Applications; K. Müllen, U. Scherf, Eds.; Wiley VCH: Weinheim, Germany, **2006**. h) C. Li, M. Liu, N. G. Pschirer, M. Baumgarten, K. Müllen, *Chem. Rev*. **2010**, *110*, 6817−6855; i) B. J. Holliday, T. M. Swager, *Chem. Comm.* **2005**, 23–36; j) D. T. McQuade, A. E. Pullen, T. M. Swager, *Chem. Rev.* **2000**, *100*, 2537–2574; k) Conjugated Polymers: Processing and Applications; T. A. Skotheim, J. Reynolds, CRS Press: **2006**.

2. a) Z. Bao, J. Locklin, Eds.; CRC Press: Boca Raton, FL, **2007**; b) C. Wang, H. Dong, W. Hu, Y. Liu, D. Zhu, *Chem. Rev*. **2012**, *112*, 2208-2267; c) T. Lee, C. A. Landis, B. M. Dhar, B. J. Jung, J. Sun, A. Sarjeant, H. J. Lee, H. E. Katz, *J. Am. Chem. Soc*. **2009**, *131*, 1692-1705; d) T. V. Pho, J. D. Yuen, J. A. Kurzman, B. G. Smith, M. S. Miao, W. T. Walker, R. Seshadri, F. Wudl, *J. Am. Chem. Soc*. **2012**, *134*, 8185-8188; e) C. Mitsui, J. Soeda, K. Miwa, H. Tsuji, J. Takeya, E. Nakamura, *J. Am. Chem. Soc*. **2012**, *134*, 5448-5451; f) S. Shinamura, I. Osaka, E. Miyazaki, A. Nakao, M. Yamagishi, J. Takeya, K. Takimiya, *J. Am. Chem. Soc*. **2011**, *133*, 5024-5035; g) K. Niimi, S. Shinamura, I. Osaka, E. Miyazaki, K. Takimiya, *J. Am. Chem. Soc*. **2011**, *133*, 8732-8739; h) X. Guo, S. R. Puniredd, M. Baumgarten, W. Pisula, K. Müllen, *J. Am. Chem. Soc*. **2012**, *134*, 8404-8407; i) S. Wang, A. Kiersnowski, W. Pisula, K. Müllen, *J. Am. Chem. Soc.* **2012**, *134*, 4015-4018.

3. a) Y. J. Cheng, S. H. Yang, C. S. Hsu, *Chem. Rev.* **2009**, *109*, 5868-5923; b) S. Haid, A. Mishral, M. Weil, C. Uhrich, M. Pfeiffer, P. Bäuerle, *Adv. Funct. Mater*. **2012**, *22*, 4322-4333; c) J. Y. Zhou, X.J. Wan, Y. S. Liu, Y. Zuo, Z. Li, G. R. He, G. K. Long, W. Ni, C. X. Li, X. C. Su, Y. S. Chen, *J. Am. Chem. Soc.* **2012**, *134*, 16345-16351; d) Y. Li, *Acc. Chem. Res.* **2012**, *45*, 723-733; e) V. Kamm, G. Battagliarin, I. A. Howard, W. Pisula, A. Mavrinskiy, C. Li, K. Müllen, F. Laquai, *Adv. Energy Mater.* **2011**, *1*, 297-302.

4. a) D. Fichou, Ed. Handbook of Oligo- and Polythiophenes; Wiley-VCH:Weinheim, Germany, **1999**; b) A. Mishra, C.-Q. Ma, P. Bauerle, *Chem. Rev*. **2009**, *109*, 1141-1278; c) I. F. Perepichka, D. F. Perepichka, H. Meng, F. Wudl, *Adv. Mater*. **2005**, *17*, 2281-2305.

5. a) P. C. Ewbank, D. Laird, R. D. McCullough, Handbook of Thiophene-Based Materials: Applications in Organic Electronics and Photonics; Wiley: Chichester, **2009**; b) R. J. Kline, M. D. McGehee, M. F. Toney, *Nat. Mater*. **2006**, *5*, 222-228; c) X. Yu, K. Xiao, J. Chen, N. V. Lavrik, K. Hong, B. G. Sumpter, D. B. Geohegan, *ACS Nano* **2011**, *5*, 3559-3567; d) W. Ma, C. Yang, X. Gong, K. Lee, A. J. Heeger, *Adv. Funct. Mater*. **2005**, *15*, 1617-1622; e) P. M. Beaujuge, J. M. J. Frechet, *J. Am. Chem. Soc*. **2011**, *133*, 20009−20029; f) B. C. Thompson, J. M. J. Frechet, *Angew. Chem. Int. Ed.* **2007**, *47*, 58−77; g) R. D. McCullough, *Adv. Mater.* **1998**, *10*, 93−116; h) O. Bubnova, Z. U. Khan, H. Wang, S. Braun, D. R. Evans, M. Fabretto, P. Hojati-Talemi, D. Dagnelund, J. B. Arlin, Y. H. Geerts, S. Desbief, D. W. Breiby, J. W. Andreasen, R. Lazzaroni, W. M. M. Chen, I. Zozoulenko, M. Fahlman, P. J. Murphy, M. Berggren, X. Crispin, *Nat. Mater*. **2014**, *13*, 190−194; i) J. S. Qian, X. Y. Li, D. J. Lunn, J. Gwyther, Z. M. Hudson, E. Kynaston, P. A. Rupar, M. A. Winnik, I. Manners, *J. Am. Chem. Soc*. **2014**, *136*, 4121−4124; j) Electronic Materials: The Oligomer Approach; K. Müllen, G. Wenger, Eds.; Wiley -VCH: Weinheim, Germany, **1997**; k) W. D. Oosterbaan, J. C. Bolsee, L. J. Wang, V. Vrindts, L. J. Lutsen, V. Lemaur, D. Beljonne, C. R. McNeill, L. Thomsen, J. V. Manca, D. J. M. Vanderzande, *Adv. Funct. Mater*. **2014**, *24*, 1994−2004; l) X. Guo, M. Baumgarten, K. Müllen, *Prog. Polym. Sci.* **2013**, *38*, 1832–1908;. m) J. Roncali. *Chem. Rev*. **1992**, 92, 711-738; n) M. J. Marsella, P. J. Carroll, T. M. Swager, *J. Am. Chem. Soc*. **1995**, *117*, 9832-9841; o) M. J. Marsella, R. J. Newland, P. J. Carroll, T. M. Swager, *J. Am. Chem. Soc*. **1995**, *117*, 9842-9848.

6. a) W. Li, W. S. C. Roelofs, M. M. Wienk, R. A. J. Janssen, *J. Am. Chem. Soc*. **2012**, *134*, 13787−13795; b) Y. Huang, X. Guo, F. Liu, L. Huo, Y. Chen, T. P. Russell, C. C. Han, Y.

Li, J. Hou, *Adv. Mater.* **2012**, *24*, 3383–3389; c) J. Hou, M. Park, S. Zhang, Y. Yao, M. L. Chen, H. J. Li, Y. Yang, *Macromolecules* **2008**, *41*, 6012-6018.

7. a) M. Jianguo, B. Zhenan, *Chem. Mater.* **2014**, *26*, 604−615. b) I. Osaka, M. Saito, T. Koganezawa, K. Takimiya, *Adv. Mater*. **2014**, *26*, 331–338; c) J. H. Dou, Y.Q. Zheng, T. Lei, S. D, Zhang, Z. Wang, W. B. Zhang, J. Y. Wang, J. Pei, *Adv. Funct. Mater*. **2014**, *24*, 6270–6278; d) A. T. Yiu, P. M. Beaujuge, O. P. Lee, C. H. Woo, M. F. Toney, J. M. J. Frechet, *J. Am. Chem. Soc*. **2012**, *134*, 2180−2185.

8. R. Asahi, T. Morikawa, T. Ohwaki, K. Aoki, Y. Taga, *Science* **2001**, *293*, 269-271.

9. a) J. M. Stanley, X. Zhu, X. Yang, B. J. Holliday, *Inorg. Chem.* **2010**, *49*, 2035−2037; b) Y.S.L.V. Narayana, S. Basak, M. Baumgarten, K. Muellen, R. Chandrasekar, *Adv. Funct. Mater*. **2013**, *23*, 5875-5880; c) S. Basak, M. A. Mohiddon, M. Baumgarten, K. Muellen, R. Chandrasekar, *Sci. Rep*. **2015**, *5*, 8406; d) Y. S. L. V. Narayana, R. Chandrasekar, *Chem. Phys. Chem.* **2011**, *12*, 2391−2396; e) S. Basak, R. Chandrasekar, *Adv. Funct. Mater*. **2011**, *21*, 667−673; f) S. Welter, K. Brunner, J. W. Hofstraat, L. De Cola, *Nature* **2003**, *421*, 54-57; g) G. N. Panin, T. W. Kang, A. N. Aleshin, A. N. Baranov, Y. J. Oh, I. A. Khotina, *Appl. Phys. Lett.* **2005**, *86,* 113114.

10. a) M. Gross, D. C. MuÈller, H.G. Nothofer, U. Scherf, D. Neher, C. BraÈuchle, K. Meerholz, *Nature* **2000**, *405*, 661-665; b) V. D. Ta, R. Chen, H. D. Sun, *Sci. Rep.* **2013**, *3*, 1362; c) K. Tabata, D. Braam, S. Kushida, L. Tong, J. Kuwabara, T. Kanbara, A. Beckel, A. Lorke, Y. Yamamoto, *Sci. Rep.* **2014**, *4*, 5902.

11. a) A. Kraft, A. C. Grimsdale, A. B. Holmes, *Angew. Chem. Int. Ed.* **1998**, *37*, 402 – 428; b) M. Sessolo, D. Tordera, H. J. Bolink, *ACS Appl. Mater. Interfaces.* **2013**, *5*, 630−634; c) Y. Z. Wang, R. G. Sun, F. Meghdadi, G. Leising, T. M. Swager, A. J. Epstein, *Synth. Met*. **1999**, *102*, 889-892.

12. a) S. S. Zhu, P. J. Carroll, T. M. Swager, *J. Am. Chem. Soc.* **1996**, *118*, 8713-8714; b) S. S. Zhu, T. M. Swager, *J. Am. Chem. Soc.* **1997**, *119*, 12568−12577; c) S. S. Zhu, T. M. Swager, *Adv. Mater.* **1996**, *8*, 497-500. d) J. L. Reddinger, J. R. Reynolds, *Chem. Mater*. **1998**, *10*, 3–5; e) R. P. Kingsborough, T. M. Swager, *J. Am. Chem. Soc*. **1999**, *121*, 8825-8834; f) I. H. Jenkins, N. G. Rees, P. G. Pickup, *Chem. Mater*. **1997**, *9*, 1213-1216; g) B. J. MacLean, P. G. Pickup, *J. Phys. Chem. B* **2002**, *106*, 4658–4662; h) L. Trouillet, A. De Nicola, S. Guillerez, *Chem. Mater*. **2000**, *12*, 1611-1621; i) M. O. Wolf, M. S. Wrighton,

Chem. Mater. **1994**, *6*, 1526-1533; j) X. Y. Chen, X. Yang, B. J. Holliday, *J. Am. Chem. Soc*. **2008**, *130*, 1546-1547.

13. a) R. Chandrasekar, O. Fuhr, R. Kruk, M. Ghafari, H. Hahn, M. Ruben, *Chem. Commun*. **2007**, 2636-2638; b) B. Ajay Kumar, S. Basak, R. Chandrasekar, *RSC Adv*. **2014**, *4*, 34760-34763; c) S. Basak, P. Hui, S. Boodida, R. Chandrasekar, *J. Org. Chem.* **2012**, *77*, 3620-3626.

14. G. M. Whitesides, B. Grzybowski, *Science* **2002**, *295*, 2418-2421.

15. a) M. R. Callstrom, T. X. Neenan, G. M. Whitesides, *Macromolecules* **1988**, *21*, 3528-3530; b) S. Zrig, G. Koeckelberghs, T. Verbiest, B. Andrioletti, E. Rose, A. Persoons, I. Asselberghs, K. Clays, *J. Org. Chem.* **2007**, *72*, 5855-5858; c) J. A. Letizia, S. Cronin, R. P. Ortiz, A. Facchetti, M. A. Ratner, T. J. Marks, *Chem. Eur. J.* **2010**, *16*, 1911–1928; d) T. Cai, Y. Zhou, E. Wang, S. Hellstrom, F. Zhang, S. Xu, O. Inganas, M. R. Andersson, *Sol. Energy Mater. Sol. Cells.* **2010**, *94*, 1275–1281.

16. G. Zoppellaro, M. Baumgarten, *Eur. J. Org. Chem.* **2005**, 2888–2892.

17. a) Y. Kim, J. Bouffard, S. E. Kooi, T. M. Swager, *J. Am. Chem. Soc*. **2005**, *127*, 13726-13731; b) E. Tekin, H. Wijlaars, E. Holder, D. A. M. Egbe, U. S. Schubert, *J. Mater. Chem*. **2006**, *16*, 4294−4298.

18. a) W. T. Carnall, In *Handbook on the Physics and Chemistry of Rare Earths*; K. A. Gschneidner, L. Eyring, Eds.; Elsevier: Amsterdam, the Netherlands, **1987**; Vol. 3, Chapter 24, 171-208; b) G. H. Dieke, *Spectra and Energy levels of Rare Earth Ions in Crystals*; Inter science: New York, **1968**; c) S. Biju, M. L. P. Reddy, A. H. Cowley, K. V. Vasudevan, *J. Mater. Chem.* **2009**, *19*, 5179-5187.

19. a) L. D. Carlos, Y. Messaddeq, H. F. Brito, R. A. Sa Ferreria, V. de Zea Bermudez, S. J. L. Ribeiro, *Adv. Mater*. **2000**, *12*, 594-598; b) J. A. Fernandes, R. A. S. Ferreira, M. Pillinger, L. D. Carlos, I. S. Goncalves, P. J. A. Ribeiro-Claro, *Eur. J. Inorg. Chem*. **2004**, 3909-3913.

20. a) M. Seri, M. Bolognesi, Z. Chen, S. Lu, W. Koopman, A. Facchetti, M. Muccini, *Macromolecules* **2013**, *46*, 6419−6430; b) F. Würthner, C. Thalacker, S. Diele, C. Tschierske, *Chem. Eur. J.* **2001**, *7*, 2245-2253; c) S. Ghosh, X. Q. Li, V. Stepanenko, F. Wurthner, *Chem. Eur. J.* **2008**, *14*, 11343–11357.

4

Triple Emission from Organic/Inorganic Hybrid Nano/Micro-Spheres

4.1 Abstract

Triple color (blue, green and red) emitting organic/inorganic hybrid nano/micro-spheres were successfully prepared in a single-pot via step-wise self-assembly approach. Further these microspheres were used as optical resonator to confine emission light inside their cavities. This innovative "bottom-up" methodology can be used to fabricate multi-luminescent organic/inorganic hybrid nanostructures displaying diverse colors and corresponding micro lasers.
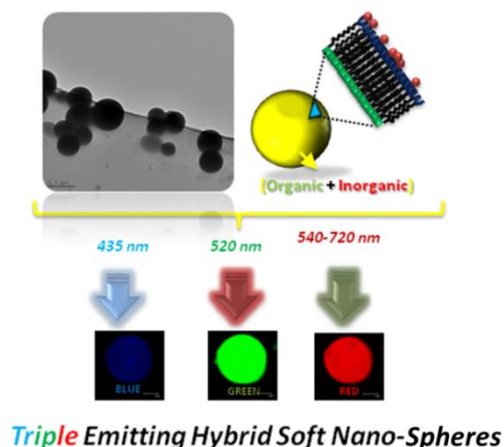
4.2 Introduction

The fabrication of shape-defined luminescent nano/micro scale objects from small molecules has attracted increasing attention among scientist owing to their unique optical and electronic properties.[1,2] Particularly, the generation of multicolor emissions from single organic and organic/inorganic hybrid nano-object in a single wavelength excitation is of great interest due to their potential use in solid state lighting and color barcode applications. In order to achieve this goal, post-metal functionalization has to be performed on the surface of the self-assembled organic architecture. Surprisingly, although several self-assembled organic particles are reported in the literature,[4] none of them are based on ligand molecules, and hence no further metal functionalization can be performed. Consequently, till 2010, there were no preparative strategy available to on a molecularly engineer single organic or organic/inorganic nano/micro particle displaying multi colour emissions. In 2011, Chandrasekar et al have reported[2] the preparation of nanostructure templates self-assembled from ligand molecules and subsequently demonstrated their use by performing "coordination chemistry on the surface of the organic ligand templates" to generate dual emitting (blue and red) organic/inorganic hybrid nanotubes.

Adopting a similar strategy,[2] this chapter presents a single-pot fabrication method to generate tricolor (blue, green and red) emitting organic/inorganic nano/micro particles by single wavelength excitation. The goal indeed required a step-by-step approach (Scheme 4.1): i) careful design and synthesis of a novel dual (blue and green) emitting amphiphilic type ligand molecule (**L1**), ii) selection of appropriate solvent(s) for the growth of self-assembled nanostructure templates and iii) subsequent sub-stochiometric incorporation of red luminescent Eu(III) metal ions on the surface of the ligand nanostructures. Firstly, a dual emitting (blue and green) amphiphilic ligand molecule **L1** was synthesized by connecting two units of blue emitting 4-triazolyl-2,6-bis(pyrazolyl)pyridine derivative with a green emitting 4,7-triazolyl-benzo-1,2,5-thiadiazole derivative using two octyl chain linkers via Click chemistry. Ligand **L1** was self-assembled in THF/water to create dual (blue/green) emitting soft spheres. A triple color emitting organic/inorganic hybrid spheres were produced by performing coordination chemistry using red-emitting Eu(III) ions on the surface of the dual emitting spheres in the same pot. The resultant molecularly engineered organic/inorganic hybrid spheres displaying tricolor emissions in a single wavelength excitation is unusual and first of its kind in luminescent nano/micro materials (Scheme 4.1).
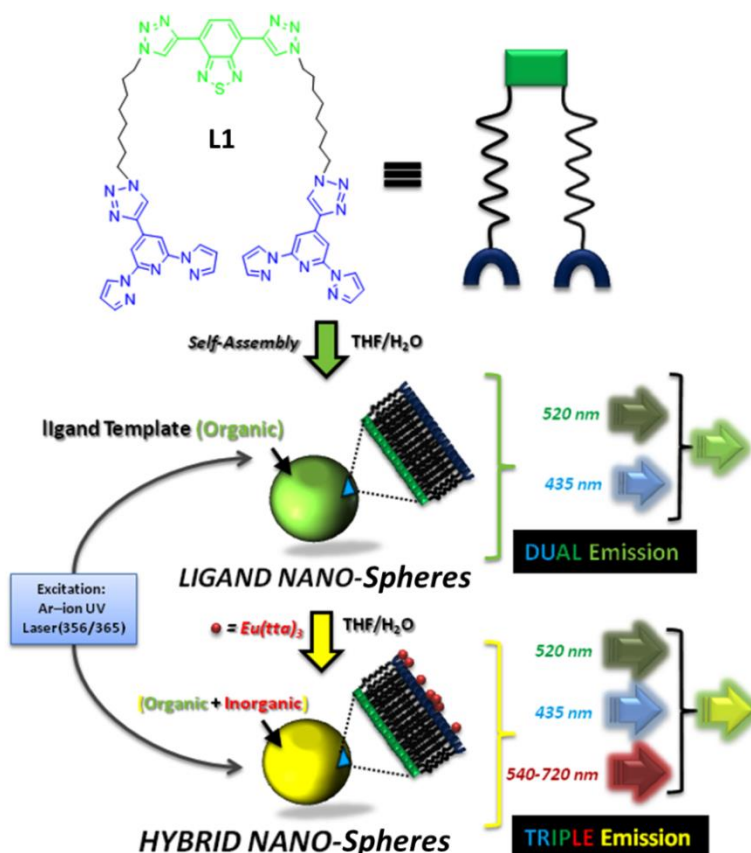
Scheme 4.1 Schematic representation of the formation of dual (Blue and Green) emitting organic nano/micro spheres obtained from ligand **L1** and an innovative route towards triple (Blue, Green and Red) color emitting hybrid organic/inorganic nano/micro-spheres via coordination of Eu(III) ions on the surface of the ligand spheres in THF/water. The colour coded arrows indicate the emission colours.

4.3 Results and Discussion

4.3.1 *Syntheses*

For the synthesis of dual emitting compound **L1** (Scheme 4.2), a click precursor 4,7-bis(ethynyl)-2,1,3-benzothiadiazole **33** was prepared from 4,7-dibromo-2,1,3-benzothiadiazole **32** under Sonogashira cross-coupling conditions.[5] For Click reaction, the saturated linker molecule 1,8-diazidooctane **34** was synthesized in 95% yield from 1,8-dibromooctane using sodium azide in DMSO at room temperature. Formation of five-member triazole units on **33** was effected under selective Click reaction conditions with compound **34** in presence of CuSO$_4$/sodium ascorbate to synthesize a green emitting diazide functionalized compound **35** in 50% yield. Latter two molecules of blue emitting 4-ethynyl-2,6-bis(pyrazole)pyridine[6] **36** units

were Clicked with **35** to obtain a novel blue and green dual-color emitting ditopic ligand molecule **L1** in 73% yield. Here both green and blue emitting units are not in conjugation due to
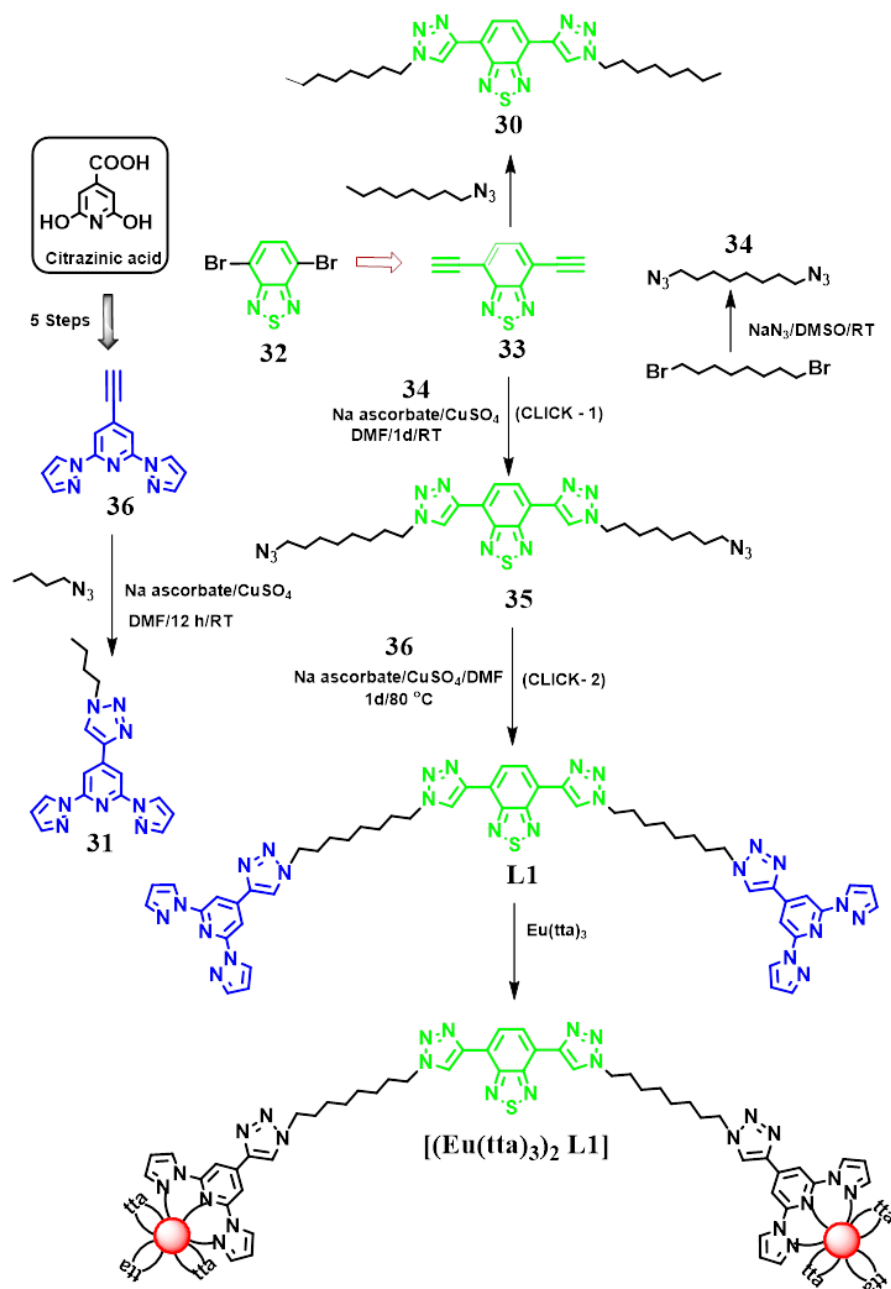
Scheme 4.2 Syntheses of dual emitting ligand **L1** and its triple emitting Eu(III) complex [(Eu^{III}(tta)$_3$)$_2$(**L1**)]. Model compounds **30** and **31** are also presented. (tta: thenoyltrifluoroacetonate). The color codes indicate the emission color of different units before and after Eu(III) complexation in the bulk state.

the presence of saturated octane chain linkers between them. To compare the optical properties both green and blue emitting model compounds **30** and **31**, respectively were also synthesized. From the ditopic ligand **L1**, by reacting Eu(tta)$_3$·3H$_2$O in THF/water a dual color (red and green) emitting nine coordinated dinuclear inorganic complex [(Eu^{III}(tta)$_3$)$_2$(**L1**)] (tta: thenoyltrifluoroacetonate) was prepared in good yield (80%).

Synthesis of 4,7-dibromobenzo[c][1,2,5]thiadiazole (32):

The compound was prepared as per the reported procedure.[5a]

To a 100 mL two-necked round bottom flask were added benzothiadiazole (1.0 g, 7.34 mmol) and 15 mL of HBr (48%). A solution containing Br$_2$ (3.5 g, 22.0 mmol) in 10 mL of HBr was added drop wise slowly. After complete addition of the bromine, the solution was heated to reflux for 12 h to obtain an orange color precipitate. The reaction mixture was cooled to room temperature and saturated solution of NaHSO$_3$ was added to quench any excess Br$_2$. The mixture was filtered under vacuum and washed with water. The solid was further washed once with cold hexane and put under vacuum, to get the desired dibrominated product **32** in 90% yield (1.94 g, 6.6 mmol). ^{1}H-NMR (400 MHz, CDCl$_3$, 25 °C) δ/ppm: 7.72 (s, 2H).

Synthesis of 4,7-diethynylbenzo[c][1,2,5]thiadiazole (33):

The compound was prepared as per the reported procedure.[5b]

In a 250 mL flask, a mixture of **32** (2.0 g, 6.8 mmol), trimethylsilylacetylene (1.74 g, 17.68 mmol), Pd(PPh$_3$)$_2$Cl$_2$ (25 mg), CuI (25 mg), and PPh$_3$ (90 mg) was suspended in triethylamine (30mL), and the resulting suspension was stirred and heated at 90 °C for 6 h. The solvent was evaporated and the crude product chromatographed directly with hexane, affording a yellow solid. The isolated product was dissolved in methanol (30 mL), and reacted with KF (1.577 g, 27.2 mmol) by stirring at room temperature for 4 h. The solvent was evaporated and the crude product was further purified using silica chromatography with eluent 10% ethyl acetate/hexane, to isolate a yellow color solid in 90% yield. ^{1}H-NMR (400 MHz, CDCl$_3$, 25 °C) δ/ppm: 7.75 (s, 2H), 3.66 (s, 2H, -C≡C-H). R_f value ~ 0.45.

Synthesis of 4-ethynyl-2,6-di(1H-pyrazol-1-yl)pyridine (36):

The compound was prepared as per the reported procedure.[6a]

A mixture of 4-iodo-2,6-di(pyrazol-1-yl)pyridine (0.93 g, 2.76 mmol), $Pd(PPh_3)_2Cl_2$ (80 mg), CuI (20 mg), and PPh_3 (60 mg) was suspended in a 100 mL capacity three neck round bottom flask. Afterwards the flask was subjected to a repeated sequence of freeze-pump-thaw cycles. Then, freshly distilled dry diisopropylamine (50 mL) was added. Trimethylsilylacetylene (0.4 g, 4.10 mmol) was added to this mixture using a syringe drop-by-drop through a rubber septum attached to the flask. Finally, the reaction mixture was stirred at 70-80 °C for overnight. The solvent was removed by rotary evaporation under vacuum, and the obtained black crude solid (TMSA-bpp) was purified by column chromatography on silica using a mixture of ethyl acetate/hexane (1:50) as eluents. For the deprotection of the TMS group, the obtained compound (2 g, 6.5 mmol) was dissolved in chloroform (80 mL) followed by the addition of methanol (80 mL). Potassium carbonate (7 g, 50 mmol) was added to this mixture, and it was stirred at room temperature overnight (18 h). The solvents were evaporated from the yellowish solution in vacuo by rotary evaporation, and the crude solid was purified by column chromatography on silica using ethyl acetate/hexane (1:20) to get compound **36** in 79% yield. ^{1}H-NMR (400 MHz, CDCl$_3$, 25 °C) δ/ppm: 8.54 (dd, ^3J = 2. 6 Hz, ^4J = 0.7 Hz, 2H, Pyrazole), 7.90 (s, 2H), 7.77 (dd, ^3J = 1. 6 Hz, ^4J = 0.8 Hz, 2H), 6.50 (t, J = 2.5 Hz, 2H, Pyrazole), 3.36 (s, 1H, -C≡C-H), R_f value ~ 0.32.

Synthesis of diazido octane (34):

1,8-dibromooctane (5.0 mL, 27.5 mmol, 1 eq) was added to a 100 mL round bottom flask containing 30 mL DMSO, to this solution sodium azide (7.714 g, 110.3 mmol, 4 eq) was added and stirred at ambient temperature. After 30 min a white solid was formed and the reaction was continued further for 2 h, latter 50 mL of water was added to the reaction mixture for quenching the excess of sodium azide (*CAUTION: quenching process is an exothermic reaction*). The reaction mixture was extracted with 250 mL of water in a separating funnel; the upper layer of the solution was collected and used for further reaction without any purification. The compound **34** was obtained as colorless oil (6.0 mL) in 95% yield. ^{1}H-NMR (400 MHz, CDCl$_3$, 25 °C) δ/ppm: 3.23 (t, J = 6 Hz, 4H, Azide-CH$_2$), 1.55-1.51 (m, 4H), 1.33-1.29 (m, 8H). ^{13}C NMR (100 MHz, CDCl$_3$, 25 °C) δ/ppm: 26.6, 28.8, 29.0, 51.4. FT-IR (KBr) ν in cm^{-1}: 3315, 2924, 2860,

2092 (azide, str), 2513, 1726, 1610, 1464, 1350, 1259, 1111, 1010, 898, 725, 636. LCMS analysis m/z: experimental value: 196.15, calculated value: 196.25. Elemental analysis: (%) $C_8H_{16}N_6$: Anal. Calcd. C 48.96, H 8.22, N 42.82; Found. C 48.85, H 8.26, N 42.75.

Synthesis of [4,7-bis(1-(8-azidooctyl)-1H-1,2,3-triazol-4-yl)benzothiadiazole] (35):

Compound **33** (0.100 g, 0.54 mmol), octyldiazide **34** (0.13 mL, 0.59 mmol), and sodium ascorbate (0.011 g, 0.054 mmol, 10 mol %) were taken in 5 ml of dry DMF and stirred at room temperature. To this solution $CuSO_4$ (0.007 g, 0.027 mmol) was added, immediately a sharp color change from a pale yellow to intense wine red color was observed. During the course of the reaction the color changed to deep green color. The progress of the reaction was monitored by TLC (8:2 ratio of Hexane: EtOAc), and further concentrated by rotary evaporator. The residue was dissolved in chloroform and passed through a celite plug. The collected solution was concentrated in vacuo, and it was further purified by washing with hexane to get pure yellow color solid of **35**. Yield 0.155 g (50%). ^{1}H-NMR (400 MHz, CDCl$_3$, 25 °C) δ/ppm: 8.67 (d, 2H, $^3J_{H,H}$ = 4.0 Hz), 8.73 (d, 2H, $^3J_{H,H}$ = 3.8 Hz), 4.45 (t, 4H, $^3J_{H,H}$ = 2.4 Hz, Triazole-CH$_2$), 3.26 (t, 4H, $^3J_{H,H}$ = 4.0 Hz, Azide-CH$_2$) 2.03-1.98 (m, 4H), 1.59-1.52 (m, 4H), 1.34-1.29 (m, 16H). ^{13}C NMR (100 MHz, CDCl$_3$, 25 °C) δ/ppm: 152.5, 142.6, 138.7, 128.2, 126.9, 125.7, 125.5, 125.0, 119.2, 51.4, 50.3, 30.3, 28.9, 28.9, 28.8, 26.6, 26.4. FT-IR (KBr) ν in cm^{-1}: 3150, 2926, 2852, 2097 (azide, str), 1584, 1464, 1231, 1049, 880, 849, 721, 619. LCMS analysis m/z: experimental value: 577.20, calculated value: 576.70. Elemental analysis: (%) $C_{26}H_{36}N_{14}$: Anal. Calcd. C 54.15, H 6.29, N 34.00; Found. C 54.31, H 6.22, N 33.85.

Synthesis of [4, 7-bis(1-octyl-1H-1,2,3-triazol-4-yl)benzothiadiazole] (30):

Compound **33** (0.100 g, 0.54 mmol), octylazide (0.23 mL, 1.08 mmol) and sodium ascorbate (0.011 g, 0.054 mmol, 10 mol %) were taken in 5 mL of dry DMF and stirred at room temperature. To this solution $CuSO_4$ (0.007 g, 0.027 mmol) was added, immediately a sharp color change from a pale yellow to intense wine red color was observed. During the course of the reaction the color changed to deep green color. The progress of the reaction was monitored by TLC (8:2 ratio of Hexane: EtOAc) and further concentrated by rotary evaporator. The residue was dissolved in chloroform and passed through a celite plug. The collected solution was concentrated by using rotary evaporator and the solid was further washed with hexane to get pure

yellow color solid of **30**. Yield 0.140 g (54%). ^{1}H-NMR (400 MHz, CDCl$_3$, 25 °C) δ/ppm: 8.72 (d, J = 4.0 Hz, 2H, Triazole), 8.67 (d, J = 6.0 Hz, 2H, Benzothiadiazole), 4.51 (t, J = 4.2 Hz, 4H, Triazole-CH$_2$), 2.04-2.01 (m, 4H), 1.34-1.33 (m, 4H), 1.29-1.27 (m, 16H). ^{13}C NMR (100 MHz, CDCl$_3$, 25 °C) δ/ppm: 152.3, 143.1, 126.1, 123.7, 122.7, 50.6, 31.7, 30.4, 29.1, 29.0, 26.5, 22.6. FT-IR (KBr) ν in cm^{-1}: 3238.7, 3150, 2920, 2852, 1699, 1585, 1467, 1373, 1311, 1226, 1049, 889, 850, 810, 734, 686, 623, 507. LCMS analysis m/z: experimental value: 494.7, calculated value: 494.7. Elemental analysis: (%) C$_{26}$H$_{38}$N$_8$: Anal. Calcd. C 63.12, H 7.74, N 22.65; Found. C 63.25, H 7.71, N 22.81.

Synthesis of [4-(1-butyl-1H-1,2,3-trizole-4-yl)-2,6-di (1H-pyrazole-1-yl)pyridine] (31):

Compound **36** (100 mg, 0.425 mmol), butylazide (0.1 mL, 0.425 mmol) and sodium ascorbate (8.5 mg, 0.0425 mmol) were taken in 5 ml of dry DMF and stirred at room temperature. To this solution CuSO$_4$ (5 mg, 0.0212 mmol) was added, immediately a sharp color change from a colorless to intense brown color was observed. The progress of reaction was monitored by TLC (8:2 ratio of Hexane: EtOAc) and the crude reaction mixture was further concentrated by rotary evaporator. The residue was dissolved in chloroform and passed through a celite plug. The collected solution was concentrated and the obtained residue was washed with hexane to get pure solid compound **31**. Yield 0.130 g (91%). ^{1}H-NMR (400 MHz, CDCl$_3$, 25 °C) δ/ppm: 8.73 (d, J = 4.4 Hz, 2H), 8.65 (d, J = 3.6 Hz, 2H), 8.59 (d, J = 5.6 Hz, 2H, Pyrazole), 8.30 (s, 4H), 8.05 (s, 2H, Triazole), 7.78 (d, J = 2.4 Hz, 4H), 6.51 (t, J = 2.2 Hz, 4H, Pyrazole), 4.49 (t, J = 3.2 Hz, 8H, Triazole-CH$_2$), 2.02 (t, J = 2.8 Hz, 8H), 1.39-1.35 (m, 16H). ^{13}C NMR (100 MHz, CDCl$_3$, 25 °C) δ/ppm: 152.3, 150.7, 145.0, 143.7, 143.1, 142.4, 127.2, 126.1, 123.8, 122.6, 121.7, 108.0, 105.7, 50.6, 50.4, 30.3, 30.1, 29.8, 29.4, 26.3, 26.3. FT-IR (KBr) ν in cm^{-1}: 3121, 2928, 1761, 1620, 1572, 1554, 1523, 1466, 1396, 1259, 1232, 1205, 1122, 1037, 997, 952, 937, 872, 781, 748, 613, 468. LCMS analysis m/z: experimental value: 334.30 calculated value: 334.45. Elemental analysis: (%) C$_{17}$H$_{18}$N$_8$: Anal. Calcd. C 61.06, H 5.43, N 33.51; Found. C 60.85, H 5.41, N 33.

Ligand L1: In a 250 mL round bottom flask 4,7-bis(1-(8-azidooctyl)-1*H*-1,2,3-triazol-4-yl)benzo[c][1,2,5]thiadiazole **35** (50 mg, 0.086 mmol), 4-ethynyl-2,6-di(1*H*-pyrazol-1-yl)pyridine **36** (32 mg, 0.172 mmol), sodium ascorbate (17 mg, 0.0086 mmol) were taken together with 5 ml of dry DMF and stirred at 80 °C. To this solution CuSO$_4$ (1.1 mg, 0.0043

mmol) was added, immediately a sharp color change from a green to intense brown color was observed. During the course of the reaction the color changed to deep green color. The progress of reaction was monitored by TLC (80:20 ratio of Hexane: EtOAc). After the reaction the solvent from the mixture was rotary evaporated. The residue was dissolved in chloroform and passed through a celite plug. The collected solution was concentrated and the obtained yellow color residue was washed with hexane to get pure yellow color solid of **L1** in 73% yield (66 mg). mp: 178 °C-180 °C; ^{1}H-NMR (400 MHz, CDCl$_3$) δ/ppm: 8.73 (d, J = 4.4 Hz, 2H), 8.65 (d, J = 3.6 Hz, 2H, Benzothiadiazole), 8.59 (d, J = 5.6 Hz, 2H, Pyrazole), 8.30 (s, 4H), 8.05 (s, 2H, Trizole), 7.78 (d, J = 2.8 Hz, 4H), 6.51 (t, J = 2.4 Hz, 4H, Pyrazole), 4.49 (t, J = 3.2 Hz, 8H, Trizole-CH$_2$), 2.02 (t, J = 2.8 Hz, 8H), 1.39-1.34 (m, 16H); ^{13}C NMR (100 MHz, CDCl$_3$) δ/ppm: 152.3, 150.7, 145.0, 143.7, 143.1, 142.4, 127.2, 126.1, 123.8, 122.6, 121.7, 108.0, 105.7, 50.6, 50.4, 30.3, 30.1, 29.8, 29.4, 26.3, 26.3; FT-IR (KBr) ν in cm^{-1}: 2926, 2853, 1697, 1622, 1521, 1466, 1396, 1040, 760, 613; LCMS (m/z): calcd for C$_{52}$H$_{54}$N$_{24}$S, 1047.45; found,1047.0; Anal. calcd for C$_{52}$H$_{54}$N$_{24}$S: C 59.64, H 5.20, N 32.10; found: C 59.45, H 5.28, N 32.31.

Complex [(Eu^{III}(tta)$_3$)$_2$ **L1**]: In a 100 mL flask ligand **L1** (10 mg, 0.0095 mmol) and Eu^{III}(tta)$_3$ (0.019 mmol) were dissolved in toluene (20 mL). The reaction mixture was stirred for 12 h at 110 °C. The solvent was removed under vacuum to get a yellow solid in 78 % yield (20 mg). mp: 186 °C-188 °C. FT-IR (KBr) ν in cm^{-1}: 3117, 2924, 2854, 1608, 1537, 1464, 1412, 1356, 1304, 1228, 1184, 138, 1059, 972, 933, 858, 785, 719,679, 640, 578. Anal. calcd for C$_{100}$H$_{78}$Eu$_2$F$_{18}$N$_{24}$O$_{12}$S$_7$: C 44.85, H 2.94, N 12.55; found: C 44.81, H 2.89, N 12.45.

^{1}H NMR and ^{13}C NMR Spectra of Compounds L1, 30, 31, 34, and 35:
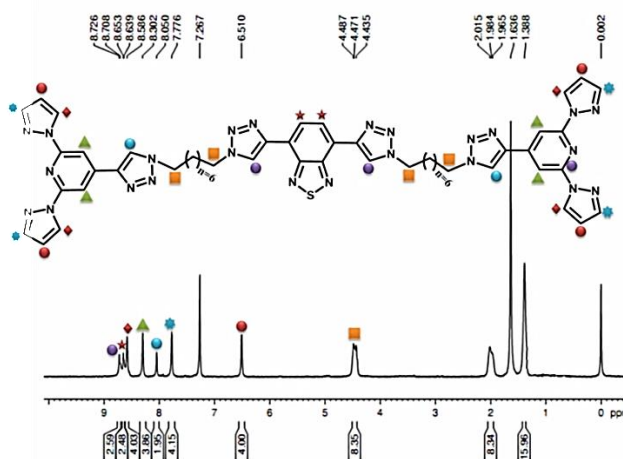
Figure 4.1 ^{1}H NMR spectrum of ligand **L1**.

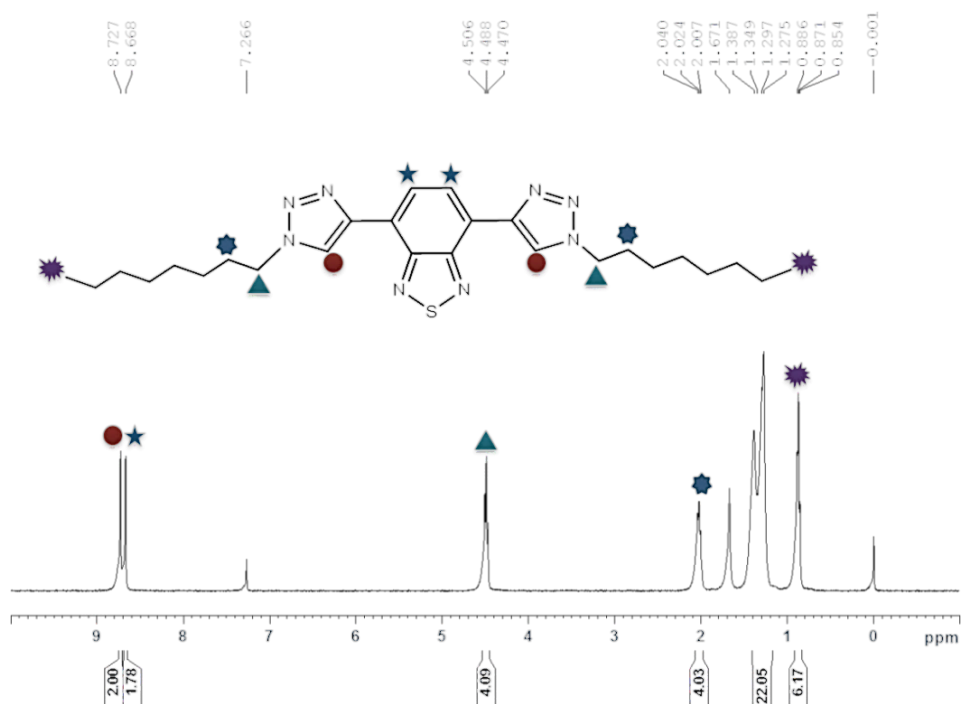**Figure 4.2** ^{1}H NMR spectrum of 4,7-bis(1-octyl-1*H*-1,2,3-triazol-4-yl)benzothiadiazole (**30**).
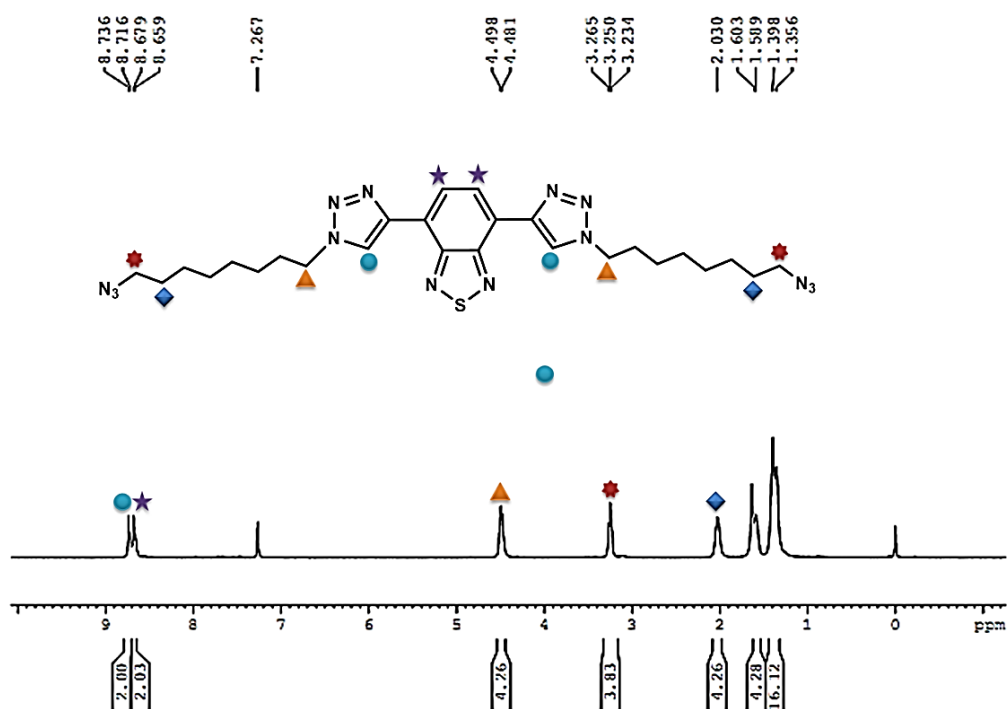

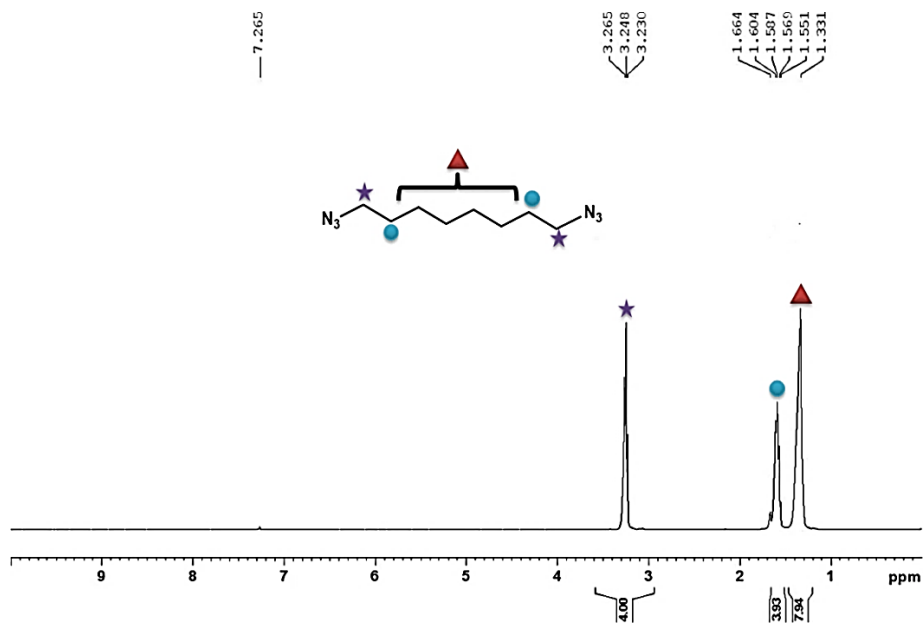**Figure 4.3** ^{1}H NMR spectrum of 4,7-bis(1-(8-azidooctyl)-1*H*-1,2,3-triazol-4 yl)benzothiadiazole (**35**).
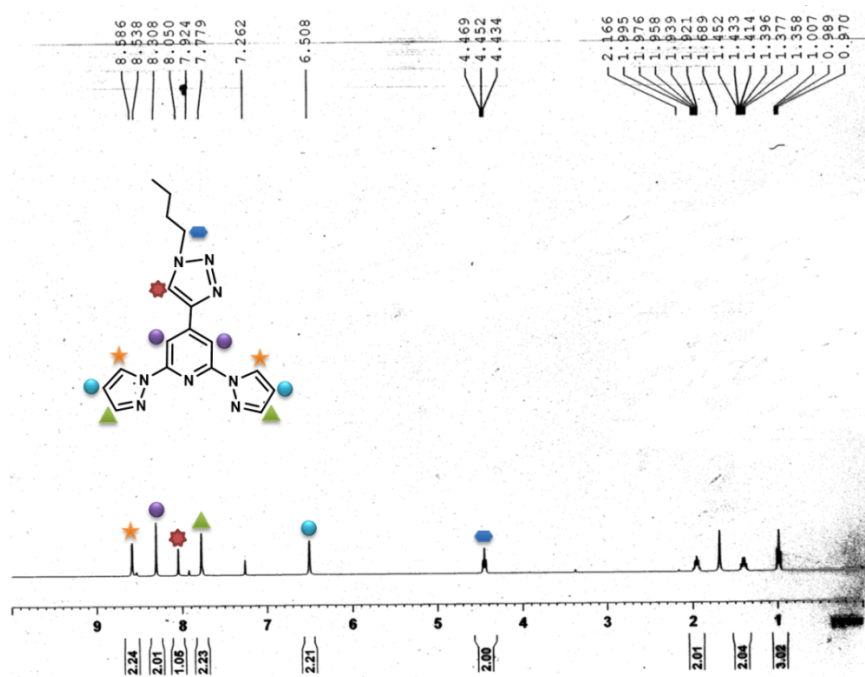
Figure 4.4 ^{1}H NMR spectrum of diazido octane (**34**).

Figure 4.5 ^{1}H NMR spectrum of 4-(1-butyl-1*H*-1,2,3-trizole-4-yl)-2,6-di (1*H*-pyrazole-1-yl)pyridine (**31**).

4.3.2 *Optical Properties*

The solution state absorption and emission spectra of **L1**, [(Eu^{III}(tta)$_3$)$_2$(**L1**)], **30**, and **31** are presented in Figure 4.6. The absorption spectrum of **L1** exhibited three major bands centered at 404 nm, 323 nm and 269 nm which correspond to the individual absorption of model compounds **30** and **31** (Fig. 4.6a). Further the absorbance spectra of **30** and **31** also overlap very well with that of **L1**. As per the design principle ligand molecule **L1** displayed a dual color emission in the blue region at 350 nm ($\Phi_f = 0.09$) and also in the green region at 524 nm ($\Phi_f = 0.99$) for the single excitation (λ_{ex}) performed at 327 nm (Fig. 4.6b), which again correspond to the model compound emissions. The blue and green emission maxima of the **L1** super impose well with the emission spectra of model compounds **30** and **31**, indicating the absence of through bond conjugation between the blue and green emitting units in **L1** due to the octane chain linkers. Here the blue part of the emission is 40 nm lower than its conjugated back-to-back coupled bpp ligand analogue, namely 4,4'-bis(2,6-di(1*H*-pyrazol-1-yl)pyridin-4-yl)biphenyl (390 nm: $\Phi_f = 0.16$; THF), due to reduction in the conjugation length.[2,6c,d] The solution state quantum yield of the green emitting unit is almost ten times higher than that of the blue emitting unit giving a final light green color due to the mixing of blue and green colors in 1:10 ratio.

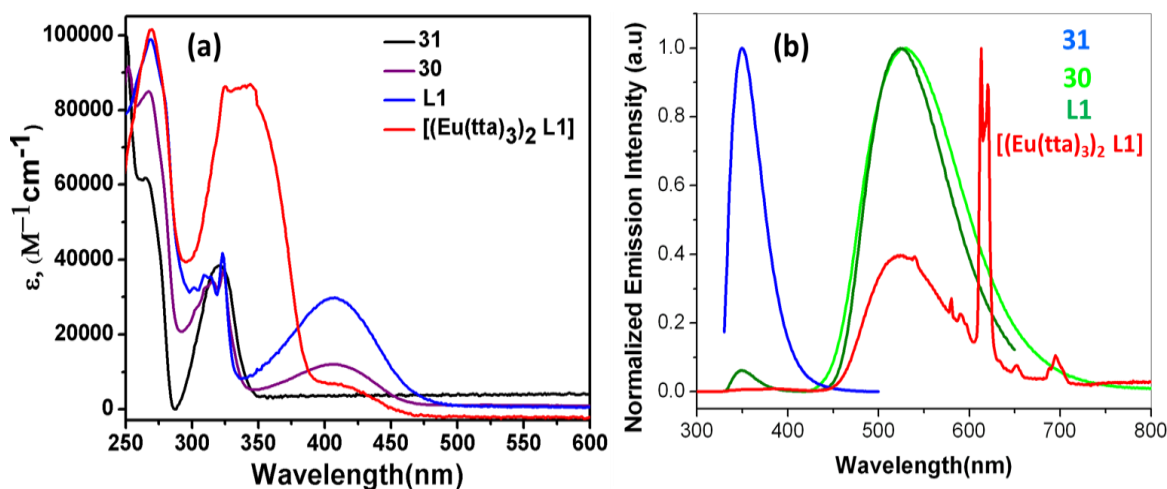**Figure 4.6** Absorption (a) and emission (b) spectra of molecules **L1**, [(Eu^{III}(tta)$_3$)$_2$(**L1**)], **30**, and **31** in DCM ($c \sim 1\times10^{-6}$ M).

Dinuclear complex [(Eu^{III}(tta)$_3$)$_2$(**L1**)] also displayed a Eu(III) centered red [$^5D_0 \rightarrow {}^7F_J$; (J =0-4)] and organic centered green (4,7-bis(triazolyl)-2,1,3-benzothiadiazole part) color

emissions. Further due to the coordination of red emitting Eu(III) ions with two blue emitting bpp units the emission of the bpp ligand was quenched completely giving finally a red and green color emitting complex [(Eu^{III}(tta)$_3$)$_2$(**L1**)] (Fig. 4.6b). The absorption and emission spectra and solution state emission colors of model compounds **30** and **31** under UV-irradiation were presented in Figure 4.7 for comparison, together with the solution state emission colours.
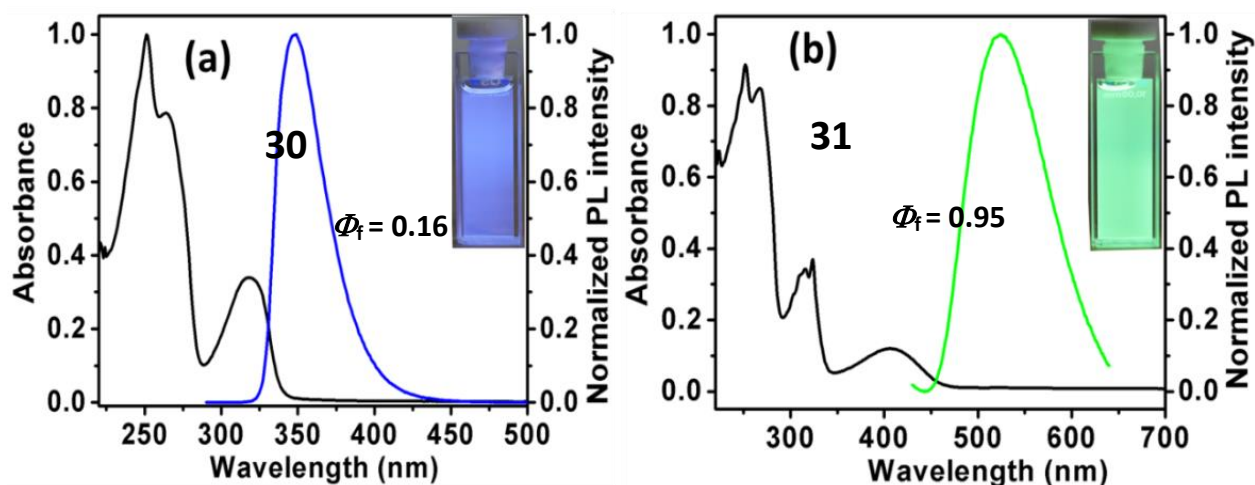
Figure 4.7 Absorption (black lines) and emission spectra of model compounds **30** and **31** in solution states. Insets show their corresponding emission colours under UV exposure.

4.3.3 *Self-Assembly of Ligand Molecule L1*
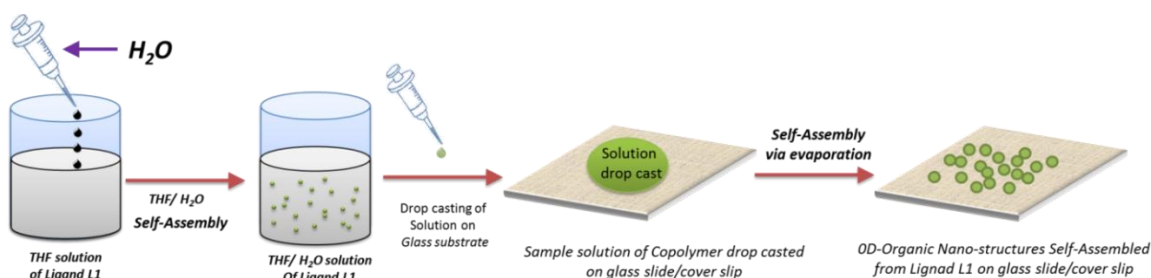
Figure 4.8 Bottom-up self-assembly route towards micro spheres composed of Ligand **L1**.

Typically for the in-situ preparation of triple color emitting spheres, 1 mL of water was slowly injected into a solution containing 1 mg of **L1** dissolved in 2 mL of THF. The solution was kept for 5 min undisturbed to stabilize growth of particles (Fig. 4.8). Two drops of this solution was slowly evaporated on a clean glass substrate at room temperature for SEM and AFM studies or directly deposited on a carbon coated grid for TEM analysis. The electron microscopy (SEM and TEM) investigation of the sample revealed the formation of spheres in the

range of nano and micro scale. (Fig. 4.9 a,d and e). In contrast to hard spheres, the electron contrast is relatively weak as typically observed for soft spheres in TEM studies.
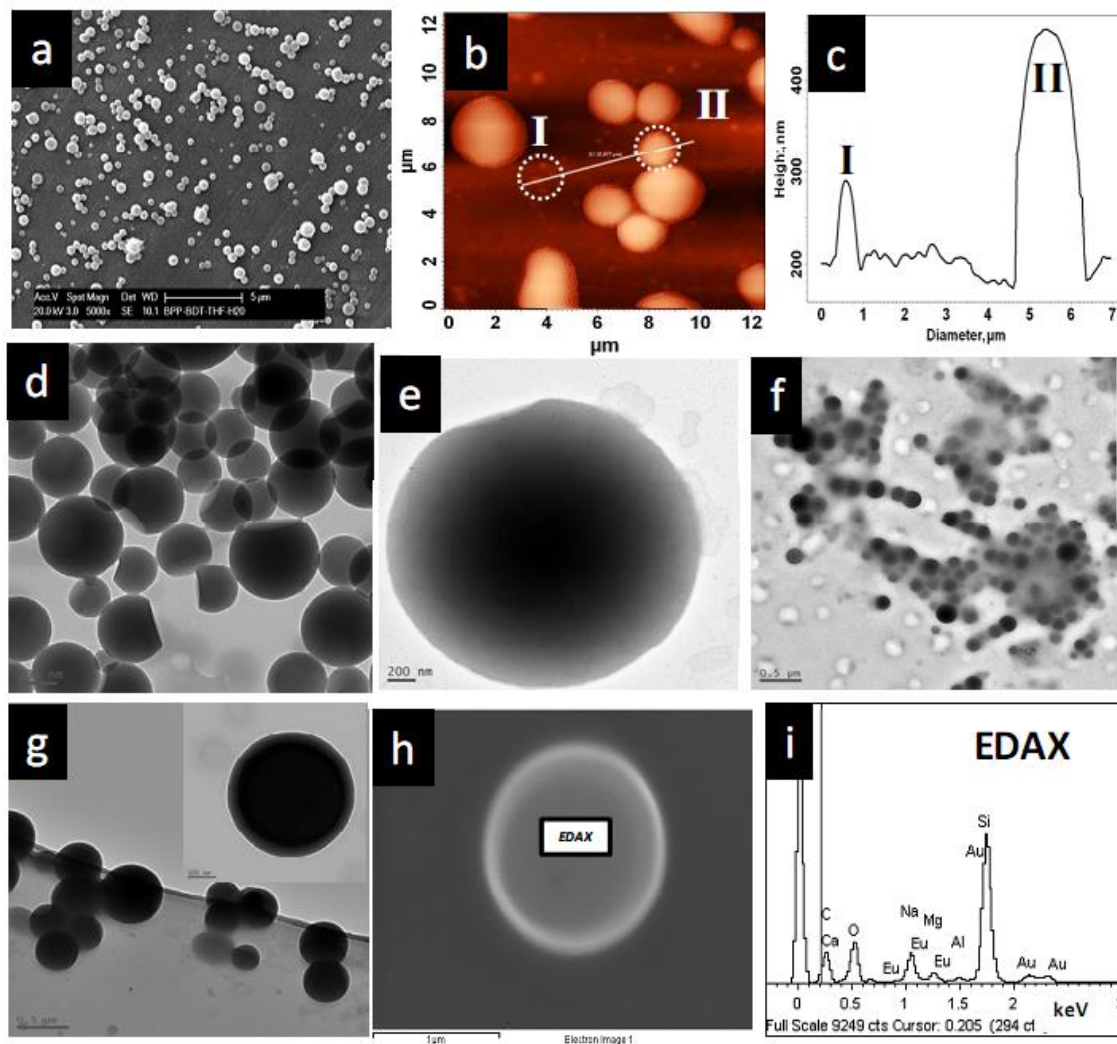
Figure 4.9 a) SEM micrographs of organic dual (Blue and Green) emitting ligand sphere templates obtained from **L1** (scale bar is 5 μm); b) Non-contact mode AFM image of organic nano- and micro-spheres, c) height and diameter profiles of an organic nano- and micro-spheres I and II, respectively shown in Figure b; Bright-field TEM micrographs: d) a collection of dual emitting organic nano-spheres (scale bar is 200 nm); e) close-up view of a single organic sphere (scale bar is 200 nm); f) triple emitting (Blue, Green and Red) organic nano-spheres coated with Eu(III) displaying dark contrast (scale bar is 500 nm); g) view of organic/inorganic hybrid spheres exhibiting dark contrast; inset shows a close-up view of a hybrid spheres; FESEM micrographs: h) a Eu(III) coated organic/inorganic hybrid nano-sphere; i) EDAX spectrum of obtained from the rectangular area shown in Figure h confirms the presence of Eu(III) ions on the organic/inorganic nano-sphere. (Scale bars are 500 nm and 1 μm for g and h, respectively).

Further some of the spheres were hemispherical in shape indicating their complex formation or deformation mechanism (Fig. 4.9d, e). AFM cross-section analysis of a nano-sphere showed that the diameter (ca. 500 nm) of the sphere is larger than its height profile (ca. 90 nm) due to the flattening of the spheres on the substrate due to its soft nature (Fig. 4.9b, c). Further more dynamic light scattering (DLS) experiment [**L1** in THF/water] confirmed the presence of nano-spheres in the solution with the hydrodynamic radius of ca. r_H = 10-125 nm. The formation of spheres from molecule **L1** containing two different polar organic units connected by hydrophobic octyl-chain linkers is unique due to their dual emitting nature. The spheres are self-assembled possibly due to the folding of the ligand **L1** and stacking of the aromatic units via π-π interactions thereby increasing the close packing of the hydrophobic octyl chains (Scheme 4.1).

4.3.4 *Yellow Emitting Organic/Inorganic Hybrid Spheres*

In order to prepare triple emitting (Blue, Green, and Red) core-shell type spheres structure from dual emitting (Blue and Green) spheres the following procedure was followed. Firstly, the ligand spheres were grown in a mixture of THF/water solvents as mentioned before (see Section 4.3.3). Secondly, by injecting a THF solution of $Eu(tta)_3 \cdot (H_2O)_3$ (tta: thenoyltrifluoroacetonate) (0.016 mg/0.02 mL ; 1 mol%) to the solution containing the spheres obtained from ligand **L1**, followed by gentle shaking, a layer of $[(Eu(tta)_3)_2(L1)]$ coordination complex was formed on the surface of the spheres.
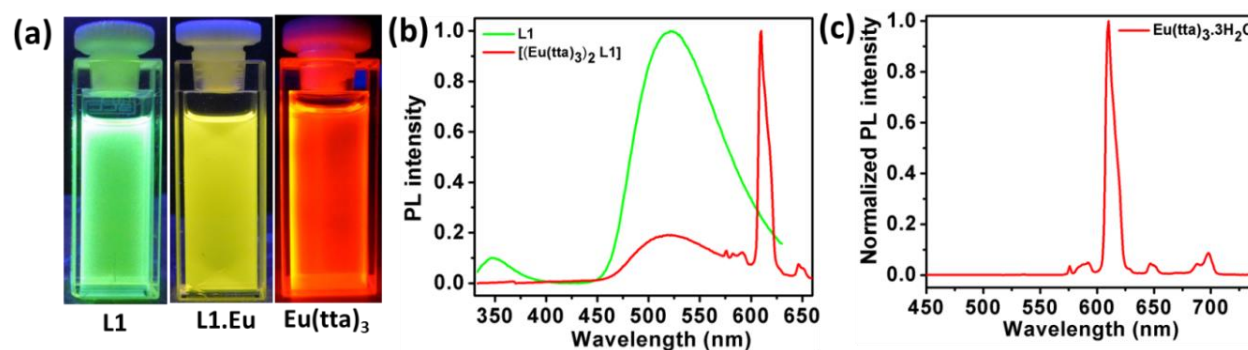
Figure 4.10 (a) (left) THF-H_2O solution of nano/microspheres obtained from ligand (**L1**); (middle) [Eu(tta)$_3$]$_2$(**L1**) coated tube (0.1 mL mother solution of Eu(tta)$_3$·3H$_2$O added); (right) Eu(tta)$_3$·3H$_2$O solution. (b) Solution state emission spectra of ligand (**L1**) and complex [Eu(tta)$_3$]$_2$(*L1*) in THF (excited at 323 nm) [(Eu(tta)$_3$)$_2$(**L1**)] complex displaying Eu(III) centred red emission and complete quenching of the ligand **L1** blue emission (bpp) and partial quenching of green emission (BDT). (c) Solid state confocal emission spectra of the powder sample of Eu(tta)$_3$.

Here, the bpp moieties present in ligand **L1** acts as a tridentate ligand and expels the water molecules out of the first coordination sphere of the $Eu(tta)_3 \cdot (H_2O)_3$ complex forming a Eu(III)complex $[(Eu(tta)_3)_2(\mathbf{L1})]$ with a distorted tricapped trigonal prismatic geometry around the Eu^{III} ion.[2b,7] Due to the use of sub-stochiometric quantity (1 mol%) of Eu(III), not all the exposed blue emitting ligand molecules available on the surface of sphere were reacted. This technique incorporates red emitting inorganic complex $[(Eu(tta)_3)_2(\mathbf{L1})]$ centers on the surface. Investigation of the TEM-bright field images obtained from the resultant organic/inorganic core-shell structures showed a clear dark contrast (Fig. 4.9f, g) for the areas coated with complex $[(Eu(tta)_3)_2(\mathbf{L1})]$ and compared to light contrast shown by unreacted spheres (Fig. 4.9d). This observation clearly supported the growth of complex $[(Eu(tta)_3)_2(\mathbf{L1})]$ on the nano/micro-spheres. Furthermore, the energy dispersive X-ray spectroscopy analysis (EDAX) performed on core-shell type spheres clearly confirmed the presence of Eu ions (Fig. 4.9i).

In order to determine dual color emission from the organic sphere self-assembled from **L1** and triple emission from the complex $[(Eu(tta)_3)_2(\mathbf{L1})]$ coated sphere, scanning confocal fluorescence microscopy measurement was performed (Fig. 4.11a-h). The topography of the spheres (XYT- mode) and the corresponding emission (XYλ-mode; the λ step width is 10 nm) properties were recorded. The topographic structural data were directly coupled with the spectroscopic properties of the specimen. For the excitation Ar-ion (UV 356/365) laser light was used. As expected the organic spheres displayed a dual color emissions in the blue (435 nm) and green (516 nm) regions. To compare the dual emission intensities of the spheres, the emissions were detected in the blue and red channels of the photo multiplier tube (PMT) with the same power gain. The solid state blue emissions intensity of the sphere was about seven times lower than the green emissions (Fig. 4.11i), thereby a final light green emission was obtained due to the mixing of these two colors of different intensities (Fig. 4.11d). As expected, the organic spheres coated with complex $[(Eu(tta)_3)_2(\mathbf{L1})]$ (hybrid core-shell type spheres) displayed a remarkable triple emission (blue, green and red) i.e., a blue (435 nm)/green (516 nm) emissions from the organic part (**L1**) of the spheres and green (516)/red (~540-720 nm region) emissions from the complex $[(Eu(tta)_3)_2(\mathbf{L1})]$ part of the sphere. Due to the unequal mixing intensities the resultant organic/inorganic hybrid sphere exhibited yellow color (Fig. 4.11h).
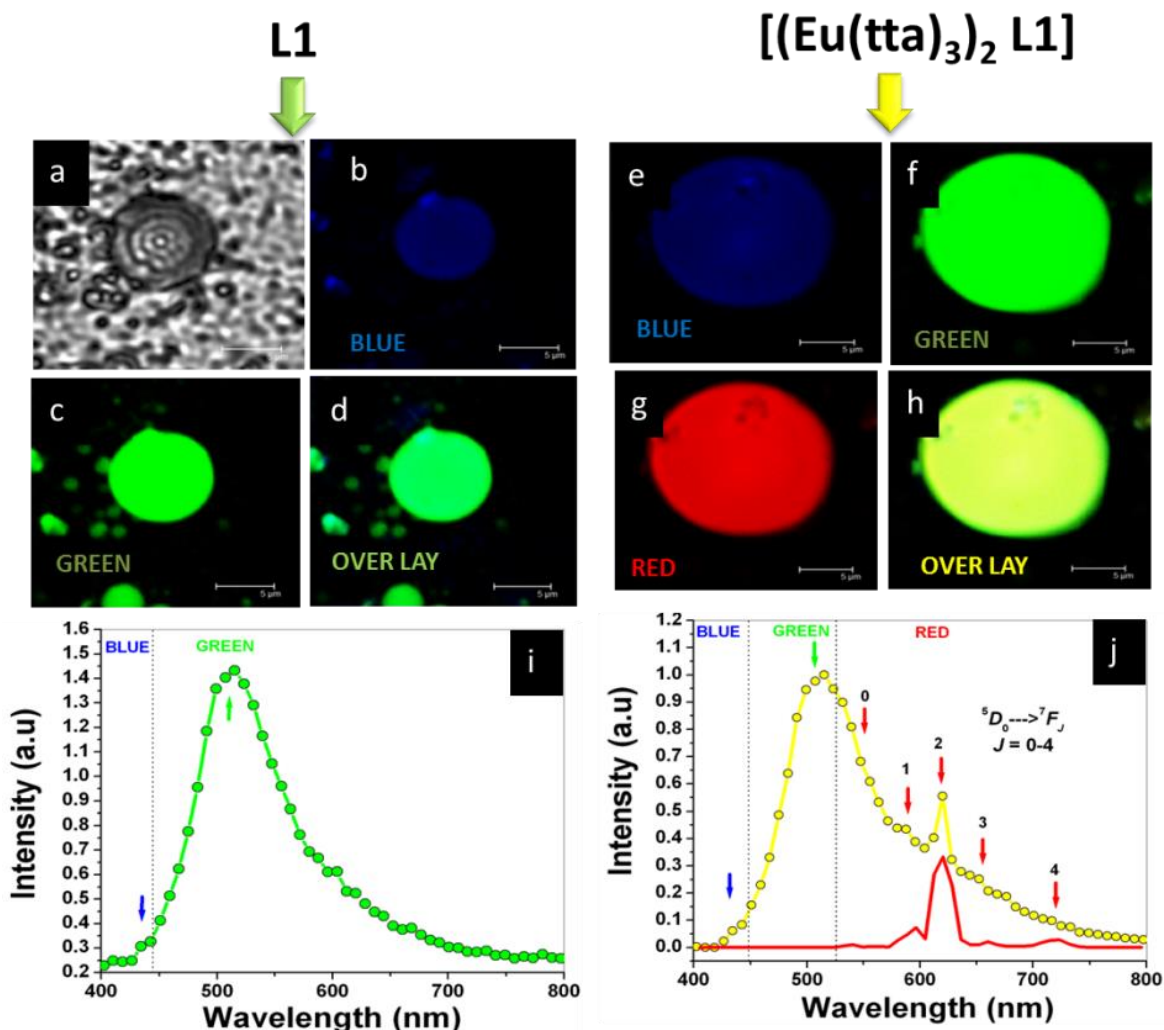
Figure 4.11 a) Bright field image of a **L1** sphere. b and c) blue and green dual emissions of the organic ligand sphere. d) The resultant light green emission of the sphere due to the unequal intensity ratios of the blue and green colors. (scale bar is 5 μm). i) The confocal fluorescence microscopic spectrum of organic sphere displaying blue and green dual emissions. e and f) blue and green emissions from the organic part of the organic/inorganic hybrid vesicle. g) Eu(III) centered red emissions from the inorganic part [(Eu(tta)$_3$)$_2$(**L1**)] of the hybrid sphere. h) The resultant yellow color due to the unequal intensity ratios of blue, green and red emissions. j) Confocal fluorescence microscopic spectrum of hybrid spheres displaying blue, green and red emissions with varying intensities. For comparison the spectrum of Eu(tta)$_3$·H$_2$O displaying the hyper sensitive transitions [^{5}D$_0$→^{7}F$_J$;(J = 0-4)] also given in red color in Fig. j. Excitation wavelength λ_{ex} = 356/365 nm (Ar ion UV laser).

4.3.5 *Energy Transfer Studies of Complex [(Eu(tta)₃)₂(L1)]*

The contribution of any energy transfer process between ligand **L1** and the coordinated Eu(III) center in the [(Eu(tta)$_3$)$_2$(**L1**)] complex was studied. There is a significant amount of overlap between the ligand emission spectra and the complex absorption spectra (Fig. 4.12). Excitation of the complex at 323 nm (corresponding to the absorption maximum of the complex) showed a collective luminescence bands of pristine ligand together with features corresponding to Eu(tta)$_3$ emission [$^5D_0 \rightarrow {}^7F_J$; see visible $J = 2$ transition at 611 nm] (Fig. 4.13b, d). Remarkably the ligand **L1** centered blue emission and green emission completely and partially quenched, respectively due to possible energy transfer from the ligand to Eu(III) centre. This result confirmed the coordination of Eu(tta)$_3$ with **L1** and the formation of [(Eu(tta)$_3$)$_2$(**L1**)] complex in the solution state. Furthermore, the excitation spectrum of [(Eu(tta)$_3$)$_2$(**L1**)] complex monitored at λ_{em} of 611 nm ($J = 2$ transition) resulted in a profile with four maxima at 273, 325, 349, and 411 nm, assignable to the absorption of **L1** complex (Fig. 4.13c). This results signified the operating energy transfer from the ligand backbone to Eu(III) center.
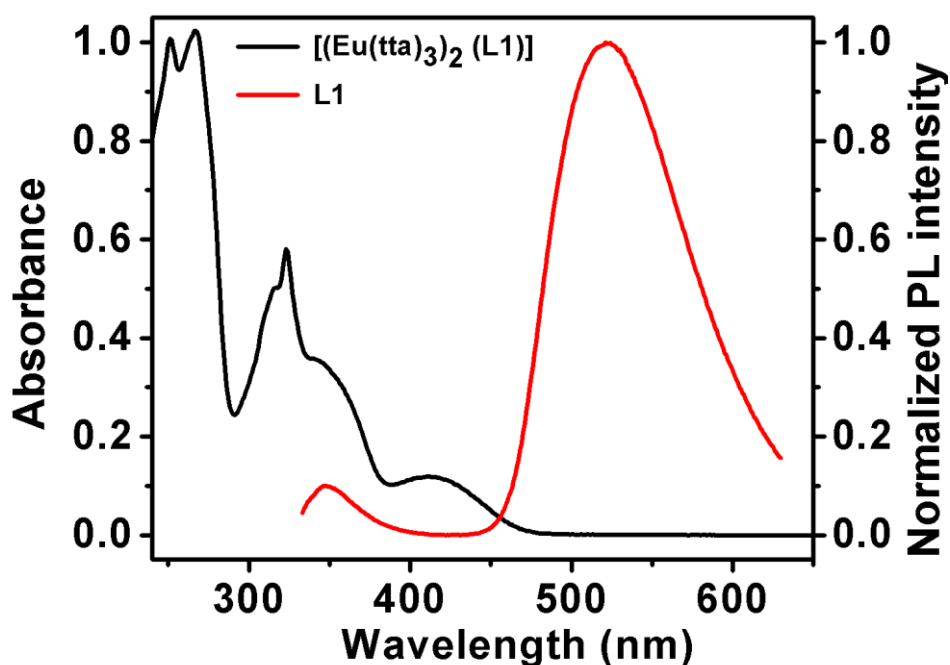
Figure 4.12 Absorption spectra of complex [(Eu(tta)₃)₂(**L1**)] (——); Emission spectra of **L1** (——).
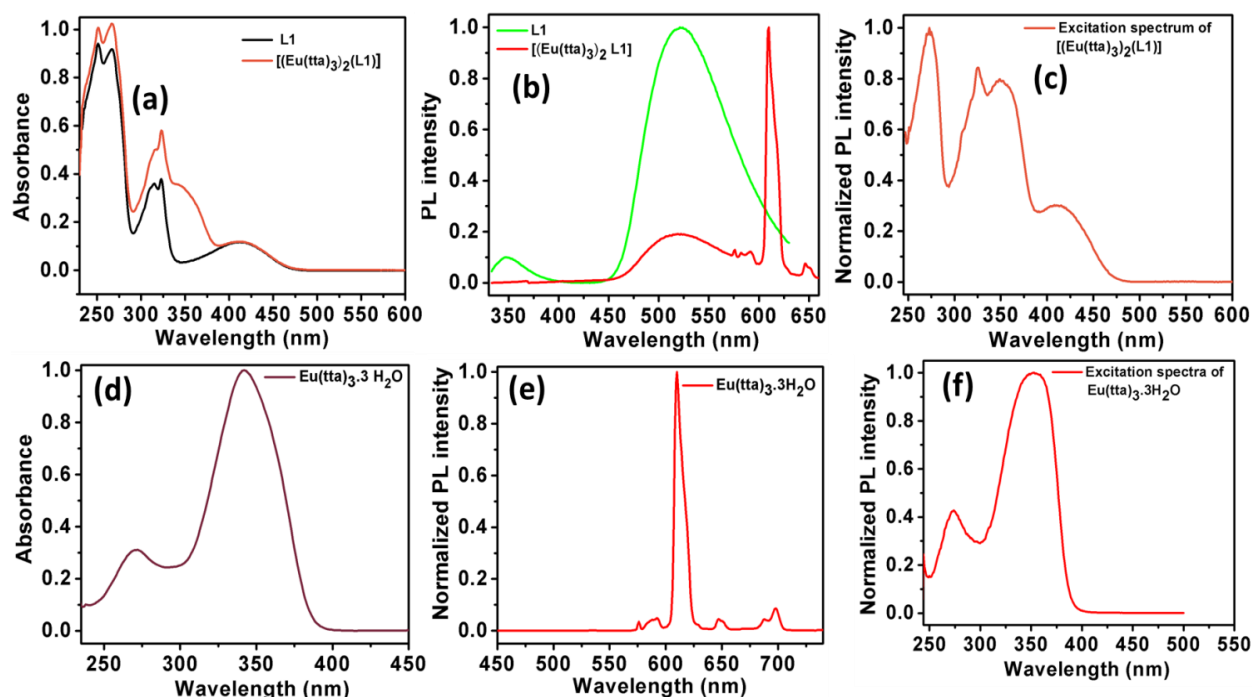
Figure 4.13 a) absorption: *L1* (——) and [(Eu(tta)$_3$)$_2$(**L1**)] (——). b) Emission: [(Eu(tta)$_3$)$_2$(**L1**)], λ_{exc} = 323 nm (——); **L1** (——), λ_{exc} = 323 nm; c) Excitation: [(Eu(tta)$_3$)$_2$(**L1**)], λ_{em} = 613 nm (——). d) Absorption (——) e) Emission (λ_{exc} = 353 nm) and f) Excitation (λ_{em} = 613 nm) spectra of Eu(tta)$_3$·3H$_2$O (——).

4.3.6 *Applications of Microspheres in Photonics*

As mentioned earlier the spherical organic particles are promising candidates for applications in nanophotonics area. For example, interaction of laser beam with a single particle (in this case a sphere) might reveal the resonating tendency of the particle by displaying whispering gallery modes (WGMs) in the PL spectrum. For this a single particle μ-PL measurements using confocal laser measurements was performed using 355 UV laser. The ligand spheres samples were prepared by drop casting **L1** solution (THF/H$_2$O (2:1) / 1mg/2ml / c ~ 4.7×10^{-1}) on Si/SiO$_2$ substrate of refractive index ~ 1.5. Excitation of a single microsphere with (355 nm) laser beam exhibited a periodic modulation of intensity in the fluorescence spectrum. The spectrum consisted of narrow lines of due to WGM resonance in the range of 400-750 nm at room temperature (Fig. 4.14b). This observed resonance lines are due to multiple total internal reflections of the trapped light at the spherical boundary. From the resonance peak a Q-factor of around 100 was estimated. The low Q factor is due broadened resonance lines (within our spectrometer resolution), which further indicated the weak light confinement tendency of the

microspheres. A free spectral range (FSR) value of ~14 μm was calculated from two resonance lines appeared at the center of the spectrum.
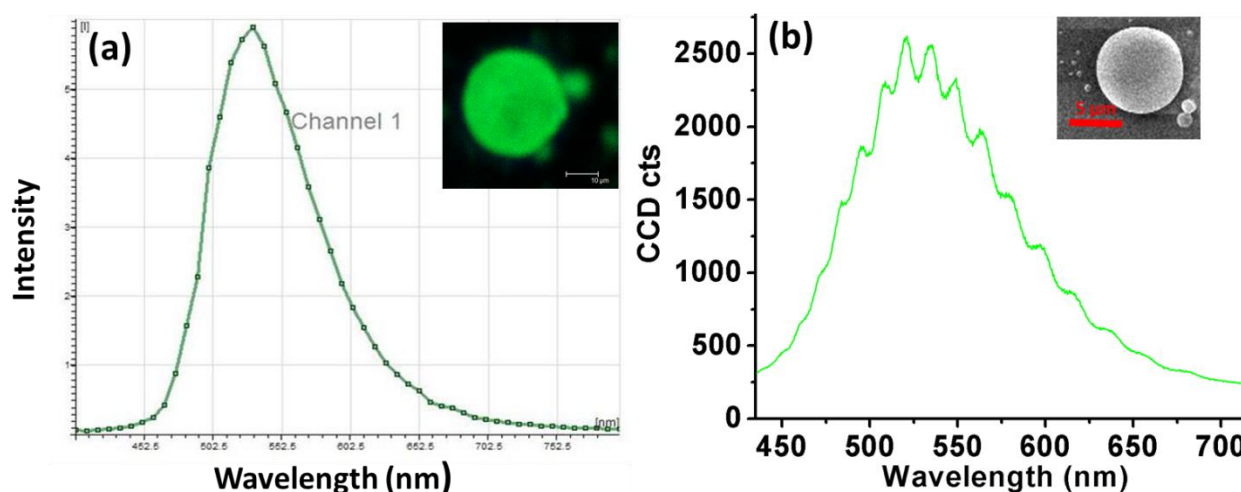
Figure 4.14 a) Confocal fluorescence micrograph of a microsphere (Inset-fluorescence image of **L1** microsphere). b) The whispering gallery modes (WGMs) observed from a microsphere upon pumping 355 nm laser.

4.4 Conclusions

In summary, in this chapter an efficient one-pot technique for the fabrication of tricolor emissive organic/inorganic hybrid spheres by employing a step-wise self-assembly technique was demonstrated. The formation of organic spheres from a novel dual emitting ligand molecule **L1** in THF/water and subsequent reaction of Eu(tta)$_3$ with ligand molecules **L1** available on the surface of the spheres is an insitu process. The self-assembled hybrid spheres displayed blue-green-red triple emissions. This simple and efficient technique of fabrication of tri-color emissive shape-defined nano/micro spheres signifies an innovative and important method in the bottom-up nanotechnology of multi-luminescent organic/inorganic hybrid nanostructures. This general principle can be applied to get wide variety of luminescent nanostructures displaying diverse colors.

Further the organic microspheres were used to confine the FL light inside the sphere by performing light-matter interaction studies down to single-particle level. Interestingly, WGM

resonances were observed in self-assembled organic microspheres upon single particle excitation with 355 nm continuous laser, indicating the defect free nature of the microspheres. On the other hand the low Q-factor suggested that the tightness of the molecular packing and the smoothness of the resonator surface need to be improved, which are not trivial tasks from a flexible molecule such as **L1**. Nevertheless the lessons learnt from this experiment were applied to modify the resonator composition with a blend of high molecular weight polymer and conjugated polymer, which will be discussed in Chapter 5.

References

1. a) Y. S. Zhao, H. Fu, A. Peng, Y. Ma, Q. Liao, J. Yao, *Acc. Chem. Res*. **2010**, *43*, 409-418; b) Y. S. Zhao, J. Xu, A. Peng, H. Fu, Y. Ma, L. Jiang, J. Yao, *Angew. Chem. Int. Ed.* **2008**, *47*, 7301-7305; c) Q. Liao, H. Fu, J. Yao, *Adv. Mater.* **2009**, *21*, 4153-4157; d) Y. S. Zhao, A. Peng, H. Fu, Y. Ma, J. Yao, *Adv. Mater.* **2008**, *20*, 1661-1665; e) L. Zhao, W. Yang, Y. Ma, J. Yao, Y. Li, H. Liu, *Chem. Commun.* **2003**, 2442-2443; g) A. Ajayaghosh, V. K. Praveen, *Acc. Chem. Res.* **2007**, *40*, 644-656; h) A. Ajayaghosh, R. Varghese, V. K. Praveen, S. Mahesh. *Angew. Chem. Int. Ed.* **2006**, *45*, 3261-3264; i) A. Ajayaghosh, V. K. Praveen, C. Vijayakumar, S. J. George. *Angew. Chem. Int. Ed.* **2007**, *46*, 6260-6265; j) Y. S. Zhao, H. Fu, A. Peng, Y. Ma, D. Xiao, J. Yao, *Adv. Mater.* **2008**, *20*, 2859-2876; k) A. Peng, D. Xiao, Y. Ma, W. Yang, J. Yao, *Adv. Mater.* **2005**, *17*, 2070-2073; l) B. –K. An, S. –K. Kwon, S. Y. Park, *Angew. Chem. Int. Ed.* **2007**, *46*, 1978-1982; m) Y. S. Zhao, H. Fu, F. Hu, A. Peng, J. Yao, *Adv. Mater.* **2000**, *19*, 3554-3558; n) K. Takazawa, Y. Kitahama, Y. Kimura, G. Kido, *Nano Lett.* **2005**, *5*, 1293-1296; o) J. Hu, T. W. Odom, C. M. Lieber, *Acc. Chem. Res.* **1999**, *32*, 435-445; p) P. Jonkheijm, P. van der Schoot, A. P. H. J. Schenning, E.W. Meijier, *Science,* **2006**, *313*, 80-83.

2. a) N. Chandrasekhar, R. Chandrasekar, *Chem. Commun.* **2010**, *46*, 2915-2917; b) S. Basak, R. Chandrasekar, *Adv. Funct. Mater.* **2011**, *21*, 667-673.

3. a) G. D. Desiraju, *Angew. Chem. Int. Ed.* **1995**, *34*, 2311-2327; b) C. J. Medforth, Z. Wang, K. E. Martin, Y. Song, J. L. Jacobsen, J. A. Shelnutt, *Chem. Commun.* **2009**, 7261-7277; c) J. M. Schnur, *Science* **1993**, *262*, 1669-1676; d) A. Harada, J. Li, M. Kamachi, *Nature*, **1993**, *364*, 516-518; e) T. Shimizu, *J. Polym. Sci. Part A: Polym. Chem.* **2008***, 46*, 2601-2611; f) T. Nakanishi, *Chem. Commum.* **2010**, *46*, 3425-3436; g) N. Kimizuka, T. Kawasaki,

K. Hirata, T. Kunitake, *J. Am. Chem. Soc.* **1995**, *117*, 6360-6361; h) S. Mann, *Nat. Mater.* **2009**, *8*, 781-792; i) E. R. Zubarev, E. D. Sone, S. I. Stupp, *Chem. Eur. J.* **2006**, *12*, 7313-7327; j) R. Iwamura, F. J. M. Hoeben, M. Masuda, A. P. H. J. Scenning, E. W. Meijer, T. Shimizu, *J. Am. Chem. Soc.* **2006**, *128*, 13298-13304; k) G. M. Whitesides, B. Grzybowski, *Science*, **2002**, *295*, 2418-2421.

4.   a) Y. Li, X. Li, Y. Li, H. Liu, S. Wang, H. Gan, J. Li, N.Wang, X. He, D. Zhu, D. *Angew. Chem. Int. Ed*. **2006**, *45*, 3639-3643; b) C. Huang, L. Wen, H. Liu, Y. Li, X. Liu, M. Yuan, J. Zhai, L. Jiang, D. Zhu, *Adv. Mater.* **2009**, *21*, 1721-1725; c) C. Huang, Y. Li, Y. Song, Y. Li, H. Liu, D. Zhu, D. *Adv. Mater.* **2010**, *22*, 3532-3536; d) K. Wang, D.-S. Guo, Y. Liu, *Chem. Eur. J.* **2010**, *16*, 8006-8011.

5.   a) K. Pilgran, M. Zupan, R. J. Skiles, *Heterocycl. Chem.* **1970**, *7,* 629-633; b) B. A. D. Neto, A. S. A. Lopes, G. Ebeling, R. S. Goncalves, V. E. U. Costa, F. H. Quina J. Dupont *Tetrahedron* **2005**, *61*, 10975–10982.

6.   a) R. Chandrasekar, F. Schramm, O. Fuhr, M. Ruben, *Eur. J. Inorg. Chem.* **2008**, *17*, 2649-2653; b) C. Rajadurai, F. Schramm, S. Brink, O. Fuhr, R. Kruk, M. Ghafari, M. Ruben, *Inorg. Chem.* **2006**, *45*, 10019-10021; c) C. Rajadurai, O. Fuhr, R. Kruk, M. Ghafari, H. Hahn, M. Ruben, *Chem. Commun.* **2007**, 2636-2638; d) F. Schramm, R. Chandrasekar, T. A. Zevaco, M. Rudolph, H. Görls, W. Poppitz, M. Ruben, *Eur. J. Inorg. Chem.* **2009**, *17*, 53-63; e) S. Basak, P. Hui, R. Chandrasekar, *Synthesis* **2009**, *23*, 4042-4048.

7.   a) J. -C. G. Bunzli, C. Piguet, *Chem. Soc. Rev*. **2005**, *34*, 1048-1077; b) J. M. Stanley, X. Zhu, X. Yang, B. J. Holliday, *Inorg. Chem*. **2010**, *49*, 2035-2037; c) P. Kadjane, M. Starck, F. Camerel, D. Hill, N. Hildebrandt, R. Ziessel, L. J. Charbonnière, *Inorg. Chem.* **2009**, *48*, 4601-4603; d) N. Chandrasekhar, R. Chandrasekar, *J. Org. Chem.* **2010**, *75*, 4852-4855.

8.   a) J. Li, F. Song, L. Wang, J. Jiao, Y. Cheng, C. Zhu, *Macromol. Rapid Commun.* **2012**, *33*, 1268-1272; b) M. D. McGehee, T. Bergstedt, C. Zhang, A. P. Saab, M. B. O'Regan, G. C. Bazan, V. I. Srdanov, A. J. Heeger, *Adv. Mater.* **1999**, *11*, 1349-1354; c) K. Binnemans, P. Lenaerts, K. Driesen, C. Gorller-Walrand, *J. Mater. Chem.* **2004**, *14*, 191-195.

5

Visible-Near Infrared Range Whispering-Gallery Resonance from Photonic μ-Sphere Cavities Self-Assembled from a Blend of Polystyrene and Poly[4,7-bis(3-octylthiophene-2-Yl)benzothiadiazole-*co*-2,6-bis(pyrazolyl)pyridine] Coordinated to Tb(acac)$_3$

5.1 Abstract

Two novel red emitting copolymers (*P11 and P12)* were prepared by regioselective *copolymerizing of tridentate ligand, namely 2,6-bis(pyrazolyl)pyridine (bpp) with 4,7-bis(2-ethynyl-5-thienyl)-2,1,3-benzothiadiazole ($\overline{M}_n$ value of ~10.7 and 8.3 KDa, respectively). These polymers readily form an orange yellow emitting metal containing conjugated polymers (P11.Tb and P12.Tb) upon coordination with Tb(acac)$_3$. Further, a* judicial *blend of P11.Tb with polystyrene and its subsequent self-assembly in THF/water produced microspheres with smooth surface area. Interestingly, CW laser excitation of a single microsphere displayed a broad whispering-gallery-mode (WGM) resonance in the visible and near infrared (NIR) regions, with a Q factor of up to 700. Further, compared to pure MCCP, the MCCP blended micro-resonators showed about 7 fold increases of the optical emission intensity.*
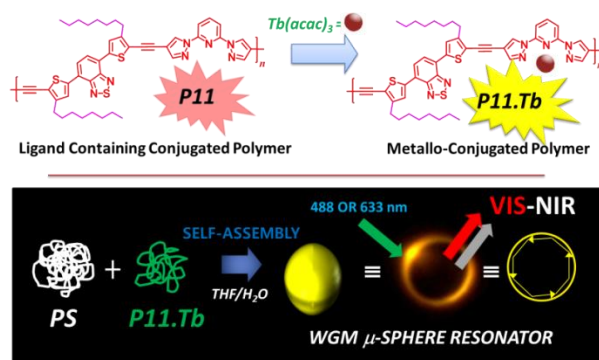
5.2 Introduction

One of the great challenges in the polymer photonic device structure is improving the emission intensity. Enhanced emission can be achieved in a feed-back system, if the light field is by some means confined in an optical cavity.[1] One way of achieving this enhancement is by fabricating microcavity structures, for example by sandwiching a film of organic light emitting material of thickness close to its emission wave length in between two planar reflecting mirrors.[2,3] As a result of repeated total internal reflection of the emitted photons, the device normally produce standing waves and displays sharp and periodic strong signals in the emission spectrum. For example, a microcavity device constructed by using ladder-type poly(*para*-phenylene) (PPV) films displayed an enhanced emission with tunable colours.[4] Alternatively, nano/micro scale fluorescent polymer structures obtained through self-assembly process can also be used for emission signal enhancement via WGM like resonator action. Particularly WGM microcavities are very important for essential studies of light-mater interaction and applications such as optical mode filters,[1,5] micro coherent lasers,[1] optical switches[6] and biosensors.[7] To date, WGM photoemission has been observed mostly in the visible electromagnetic region from microstructures of varying shapes (such as hemispheres, rings, spheres, fibers and disks), which are built from inorganic[8] and organic compounds,[9-11] dye doped polymers,[12] and conjugated polymer.[13] and mostly the resonances were observed in the visible region.

Recently, there has been growing interest to use NIR emissive organic materials in microscale WGM resonators to create miniaturized NIR lasers. Hence we envisioned using metal containing conjugated polymer (MCCP) as a novel emissive material to self-assemble polymer WGM resonators operating in the visible and NIR range. Further, MCCPs containing lanthanide (Ln^{3+}) ions are also known to display tunable emissions from visible to NIR regions.[14-24] However one of the major challenges in the area of MCCPs is, synthesizing novel ligand containing polymers to achieve good processability, compatibility, mechanical strength, wide emission properties, and to bring about new nano/micro scale photonic functions. In this context, till now, in our knowledge, no example has been reported on WGM photonic microcavity, which is using MCCP as an active luminescent material. Therefore in this chapter report a simple and inexpensive self-assembly route to craft Vis-NIR range WGM resonators from a judicial blend of polystyrene and novel orange yellow emitting MCCP, namely, poly[4,7-bis(3-octylthiophene-2-

yl)benzothiadiazole-*co*-2,6-bis(pyrazolyl)pyridine] coordinated to Tb(acac)$_3$ (**P11.Tb**), where acac stands for acetyl acetonate. The polymers and the microspheres were comprehensively analysed by using NMR, gel permeation chromatography (GPC), UV-Vis, electron microscopy (FESEM/SEM/TEM), and atomic force microscopy (AFM) techniques. Single particle microscopy and μ-PL spectroscopy studies were carried out on a laser confocal μ-spectroscopy set-up.

5.3 Results and Discussion

5.3.1 *Synthesis of Monomers, Copolymers and Metal-Complex of Copolymer*
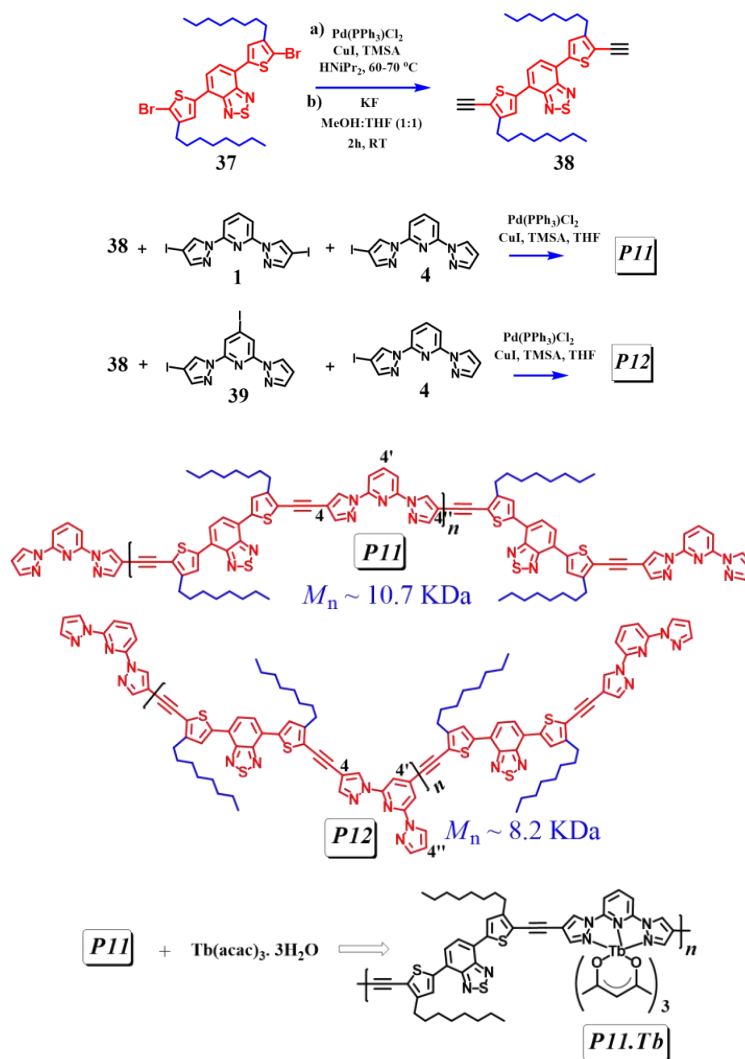
Scheme 5.1 Synthesis of ligand containing conjugated copolymers (**P11** and **P12**) and MCCP of **P11**.

At first, two ligand containing conjugated polymers were prepared by copolymerizing 4,7-Bis(2-ethynyl-5-thienyl)-2,1,3-benzothiadiazole (BDT) with 2,6-bis(pyrazolyl)pyridine (bpp) regioselectively (4,4' and 4,4'') to prepare dark red color emitting (upon exposure to UV light) conjugated copolymers **P11** and **P12**, respectively (Scheme 5.1). Precursor compounds **37**-**39**, **1**, and **4** were synthesized as per our reported procedures.[20-22] To synthesizes trimethylsilyl precursor of **37** (yield 85%), Sonogashira cross-coupling reaction was carried out using 4,7-bis(5-bromo-4-octylthiophen-2-yl)benzo[c][1,2,5]thiadiazole **37** and TMSA in presence of diisopropyl amine/THF. The diethynyl-BDT monomer **38** was prepared in 99% yield from trimethylsilyl precursor by deprotection of the TMS group using KF in THF/MeOH (1:1). The absence of methyl groups of TMS and appearance of a new peak at 3.58 ppm ($\equiv$C-H) in the ^{1}H NMR spectrum and a sharp stretching band at 2959 cm^{-1} (Stretch, $\equiv$C-H) in the infrared spectrum confirmed the structure of compound **38**.

Synthesis of linear red emitting ligand containing copolymer **P11** end-capped with bpp was carried out under Sonogashira cross-coupling reaction conditions using **38** and **1** in presence of diisopropyl amine/THF, and compound **4** as an end capping agent. After over night reaction, the polymer **P11** was obtained as red solid. To determine the molecular weight ($\overline{M}_n$) of **P11** from the ^{1}H-NMR spectrum (see Fig. 5.1), the pyrazole proton chemical shift ($\delta \sim$ 6.53 ppm) of the end-capping unit (**4**) was used. The ratio of the first CH_2 protons (of alkyl chain) attached to thiophene rings (marked by "i") to bpp (marked as "a") was 48:2, but for a corresponding monomer (i.e. having two thiophene units) the ratio is 2:1. This ratio showed that there are 12 repeating BDT units in the polymer; from this result the estimated $\overline{M}_n$ value was in the range of 10.6 KDa (by ^{1}H-NMR end-group analysis). For the synthesis of a bent copolymer (**P12**), a similar polymerization procedure was undertaken with **38** and **39**, using **4** as an end capping agent. Here a clear-cut estimation of $\overline{M}_n$ value by ^{1}H-NMR end-group analysis is not possible due the presence of bpp end group protons ($\delta \sim$6.54 ppm) in the main chain as well. GPC analysis of polymer **P11** and **P12** showed high molecular weights ($\overline{M}_n$) in the range of 10.7 KDa and 8.2 KDa, respectively. To fine tune the emission colour **P11** Tb(III) containing metallo-copolymer (**P1.Tb**) was prepared by heating the THF solutions of **P1** and excess of Tb(acac)$_3$ hydrate at 60 °C for 6 h. It is expected that each of the BPP unit present in the polymer act as tridentate ligand and react with Tb(acac)$_3$ forming MCCP of **P1.Tb** with a distorted tricapped trigonal prismatic geometry around the Tb(III) ion.
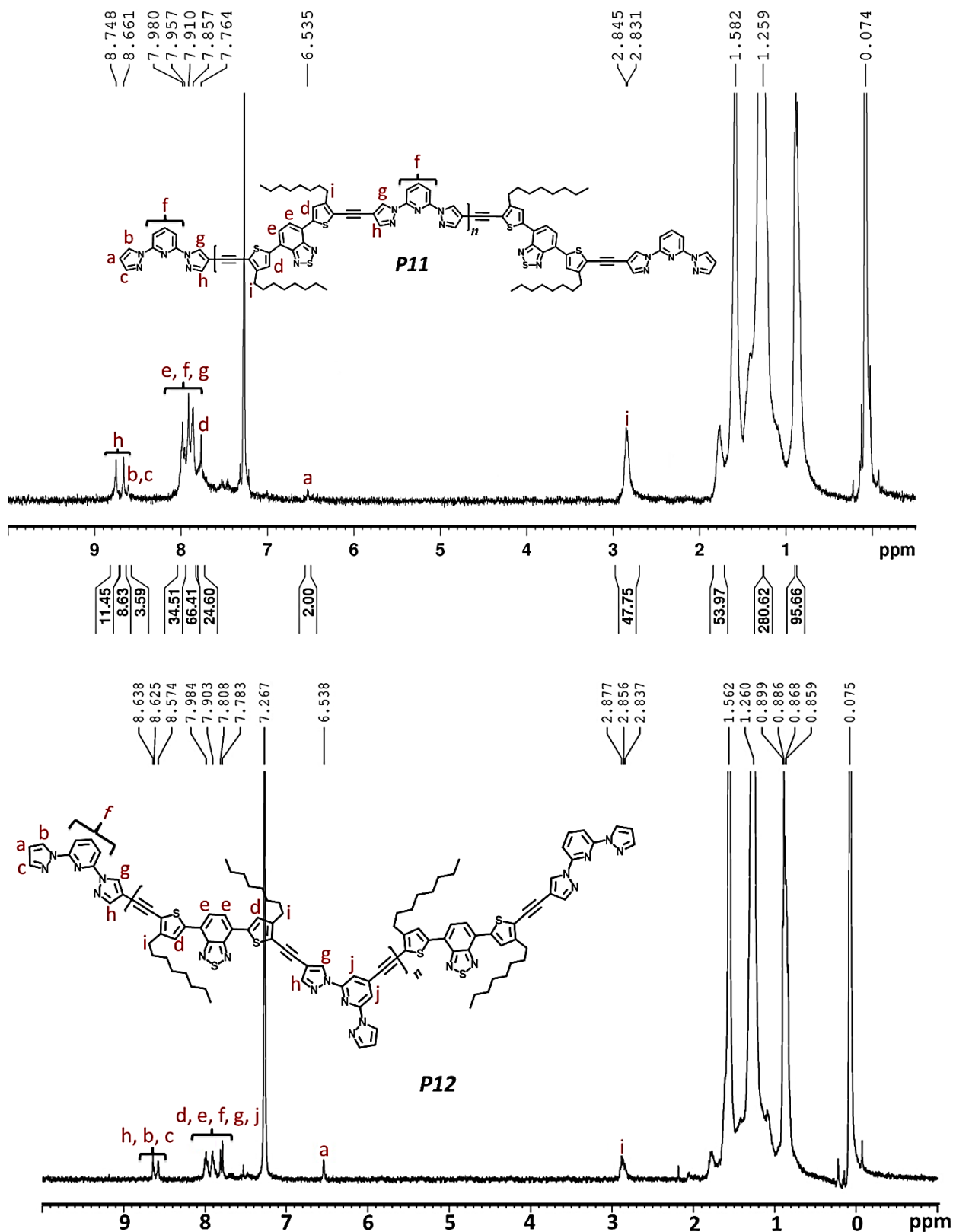
Figure 5.1 ^{1}H-NMR spectra ofcopolymers **P11** and **P12** in CDCl$_3$.

Table 5.1 $\overline{M_n}$, and $\overline{M_w}$ of Copolymers (**P11** and **P12**).

Polymer	$\overline{M_n}$ by ^{1}H- NMR (KDa)	$\overline{M_n}$ by GPC (KDa)	$\overline{M_w}$ by GPC (KDa)	PDI
P11	10.6	10.7	15.4	1.43
P12	-	8.2	22.5	2.72

^{1}H NMR spectra of complex **P11.Tb** showed broadening of the polymer peaks and appearance of Tb(acac)$_3$ peaks due to complex formation (Fig. 5.3). Raman spectroscopy (He-Ne: 785 nm laser) investigation of **P11.Tb** clearly showed peaks (812, 828, 854, and 872 nm) correspond to Tb(acac)$_3$ under the FL background of **P11**. Here, the relative intensity of 812 nm peak has diminished considerably after complex formation with **P11** (Fig. 5.2b). In the FTIR spectrum the absence of a broad hydrate peak (~3000-3500 cm^{-1}) from **P11.Tb** further supported the exclusion of hydrates from Tb(acac)$_3$•xH$_2$O due to complex formation (Fig. 5.2a). Further the intensity of sharp peaks observed at 1463 and 1391 cm^{-1} in **P11** has diminished drastically in **P11.Tb**. Upon exposure of UV light, solid **P11.Tb** displayed an orange yellow emission (Fig. 5.2a).
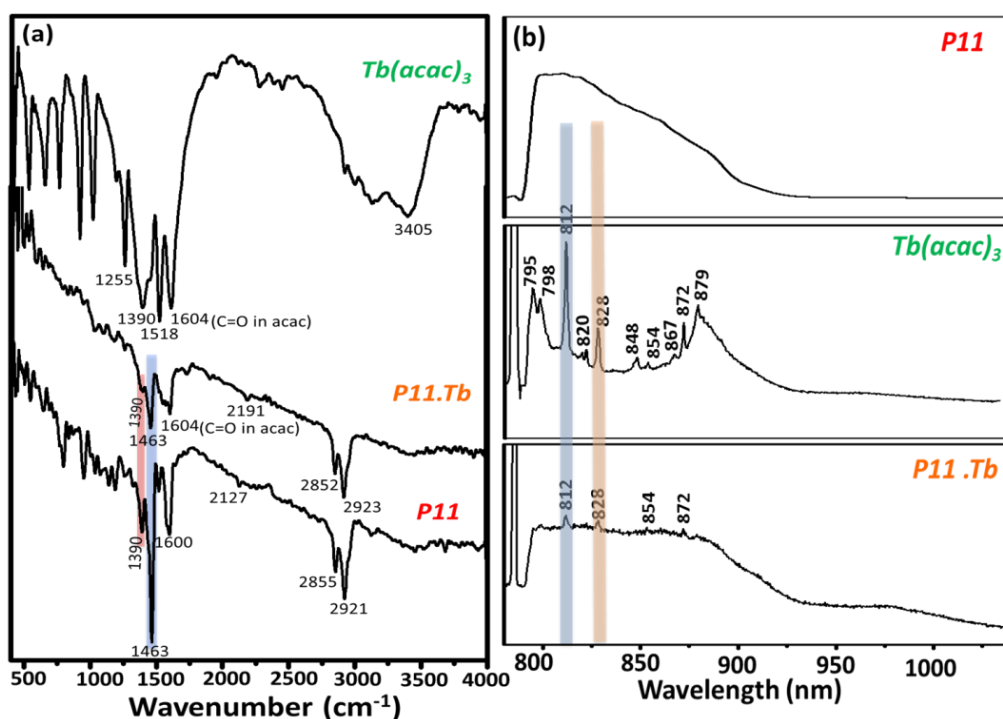
Figure 5.2 Comparative FT-IR and Raman spectra of **P11** and **P11.Tb**.

4, *7-bis(5-bromo-4-octylthiophen-2-yl)benzo[c][1,2,5]thiadiazole* (*37*)**:**

This compound was prepared as per the reported procedure.[21b]

A mixture of 4,7-bis(4-octylthiophen-2-yl)benzo[c][1,2,5]thiadiazole (2 g, 3.782 mmol) and N-bromosuccinimide (NBS) (1.414 g, 7.94 mmol in THF (20 mL) was stirred at room temperature for 2 h. The reaction was quenched with water (100 mL) and then extracted with chloroform for 2 times. The combined $CHCl_3$ solution was washed with water and dried over anhydrous sodium sulfate. The concentrated solution was then purified by a silica gel column using hexanes as eluent to isolate the desired product **37** as a scarlet red solid (2.2 g, 85%). R_f value ~ 0.45. ^{1}H NMR (400 MHz, $CDCl_3$, 298 K) δ/ppm: 7.78 (s, 2H, Phenyl), 7.76 (s, 2H, Thiophene), 2.64 (t, J = 2.8 Hz, 4H, CH_2), 1.67 (t, J = 3.2 Hz, 4H), 1.35-1.32 (m, 20H), 0.93-0.89 (m, 6H, CH_3). ^{13}C NMR (100 MHz, $CDCl_3$) δ/ppm: 151.5, 151.3, 142.7, 138.3, 138.1, 127.6, 124.4, 123.9, 111.5, 32.0, 29.5, 22.8, 14.3. FT-IR (NEAT; ν in cm^{-1}): 2964, 2854, 1737, 1496, 1468, 1255, 1101, 1019, 805.

4, *7-bis(5-ethynyl-4-octylthiophen-2-yl)benzo[c][1,2,5]thiadiazole* (*38*)**:**

A mixture of $Pd(PPh_3)_2Cl_2$ (25 mg, 0.035 mmol) and CuI (4 mg, 0.02 mmol) were added to a two-neck round-bottom flask, and was purged with nitrogen for 10 min. Afterwards the reaction was degassed by a repeated sequence of freeze-pump-thaw cycles. Then, **37** (1.34 g, 1.97 mmol), tri-methlysilyl acetylene (TMSA) (0.53 ml, 4.14 mmol), THF (30.0 mL), and diisopropylamine (30.0 mL) were added to the reaction under nitrogen, and the mixture was stirred at 60 °C overnight. The suspension was subsequently poured hot into a saturated aqueous EDTA solution (100 mL), and the mixture was stirred for 2 h. The aqueous layer was separated, and the organic layer was extracted with $CHCl_3$. The concentrated solution was then purified by a silica gel column using hexanes as the eluent to get the desired product (1.145 g, 81%). ^{1}H NMR (400 MHz, $CDCl_3$, 298 K) δ/ppm: 7.88 (s, 2H, Phenyl), 7.78 (s, 2H, Thiphene), 2.76 (t, J = 3.2 Hz 4H), 1.72-1.69 (m, 4H), 1.29-1.26 (m, 20H), 0.89-0.86 (m, 6H, CH_3), 0.29 (s, 18H, Me-TMSA). ^{13}C NMR (100 MHz, $CDCl_3$) δ/ppm: 151.8, 149.5, 138.6, 128.2, 124.9, 119.8, 102.9 (C≡C), 97.8 (C≡C), 32.0, 30.2, 29.8, 22.8, 14.3 (CH_3). FT-IR (NEAT; ν in cm^{-1}): 2914, 2915, 2849, 2137 (C≡C, Stretch), 1490, 1249, 1129, 1112, 844, 751. R_f value ~ 0.50. *Deprotection Step*: A mixture of silyl compound (0.411 g, 0.574 mmol) and KF (0.1 g, 1.721 mmol) were added to a two-neck round-bottom flask, and was purged with nitrogen for 10 min. Then, CH_3OH (20.0 ml) and THF

(20.0 ml) were added to the reaction mixture under nitrogen, and the mixture was stirred at room temperature for 2 h. The aqueous layer was separated, and the organic layer was extracted with $CHCl_3$. The organic layer was dried over anhydrous sodium sulfate and evaporated to give the desired product **38** (0.32 g, 98%). ^{1}H NMR (400 MHz, $CDCl_3$, 298 K) δ/ppm: 7.84 (s, 2H, Phenyl), 7.69 (s, 2H, Thiophene), 3.58 (s, 2H, ≡C-H), 2.75 (t, J = 2.8 Hz, 4H, Thiophene-CH_2-), 1.70-1.67 (m, 4H), 1.29-1.26 (m, 20H), 0.89-0.85 (m, 6H, CH_3). FT-IR (NEAT; ν in cm^{-1}): 2959 (≡C-H, stretch), 2920, 2849, 2137 (C≡C, stretch), 1266, 1096, 1019, 795, 740. R_f value ~ 0.40.

4-iodo-2-(4-iodo-1H-pyrazol-1-yl)-6-(1H-pyrazol-1-yl)pyridine (39):

This compound was prepared as per the reported procedure.[21a]

In two neck 100 ml round bottom flask, 4-iodo-2,6-di(1*H*-pyrazol-1-yl)pyridine (0.200 g, 0.60 mmol) in AcOH (10 mL), and aq H_2SO_4 (25%, 1.5 mL) was taken. An aqueous deep-violet solution (20 mL) containing HIO_3 (0.02 g, 0.11 mmol), I_2 (0.06 g, 0.24 mmol) and two drops of concd H_2SO_4 was added into the flask drop wise. The reaction mixture was stirred for 4 h under nitrogen at 60 °C, and then compound **39** was purified by silica column chromatography eluent as (CH_2Cl_2–hexane, 2:3). 0.140 g (Yield 50%).

Synthesis of copolymer (P11):

A mixture of **38** (0.08 g, 0.139 mmol), **1** (0.06 g, 0.13 mmol), **4** (0.005 g, 0.014 mmol), $PdCl_2(PPh_3)_2$ (15 mg, 0.021 mmol) and CuI (5 mg, 0.026 mmol) were added to a two-neck round-bottom flask, and was purged with nitrogen for 10 min. Afterwards the reaction was degassed by a repeated sequence of freeze-pump-thaw cycles. Then, THF (30.0 mL), and diisopropylamine (30.0 mL) were added to the reaction under nitrogen, and the mixture was stirred at 60 °C overnight. The suspension was subsequently poured hot into a saturated aqueous EDTA solution (100 mL), and the mixture was stirred for 2 h. The aqueous layer was separated, and the organic layer was extracted with $CHCl_3$. The organic layer was dried and methanol was added to dissolve monomeric species and the mixture was kept undisturbed for 20 min to precipitate the polymer. The solution was decanted and methanol was added again and the process repeated till no more of the monomeric impurities remained, as exhibited by a colorless methanol layer. The mixture was then evaporated to dryness and washed with hexane to further get rid of any other impurities. The residue was put under high vacuum and latter **P11** was collected as red color powder (0.049 g). ^{1}H NMR (400 MHz, $CDCl_3$, 298 K) δ/ppm: 8.75-8.73

(m, 11H), 8.66-8.63 (m, 8H), 7.9-7.88 (m, 35H), 7.85-7.81 (m, 66H), 7.76-7.74 (m, 34H), 6.54 (t, J = 2.8 Hz, 2H), 2.85 (s, 48H), 1.85 (t, J = 3.2 Hz, 53H), 1.25-1.21 (m, 280H), 0.88-0.86 (m, 95H). By ^{1}H NMR end-cap analysis, $\overline{M_n}$ = 10616. From GPC data $\overline{M_n}$ = 10745 and $\overline{M_w}$ = 15450, PDI = 1.43. FT-IR (KBr) ν in cm^{-1}: 2980, 2944, 2868, 1615 (C=C, aromatic), 1592, 1527, 1482, 1198, 896, 860, 799, 763, 686.

Synthesis of copolymer (P12):

Similar procedure was followed as in **P11** synthesis. Here 2,6-bis(4-iodo-1*H*-pyrazol-1-yl)pyridine was replaced by 4-iodo-2-(4-iodo-1*H*-pyrazol-1-yl)-6-(1*H*-pyrazol-1-yl)pyridine **39** (0.06 mg, 0.13 mmol). For purification the brown color polymer precipitate was filtered and washed with boiling MeOH, EtOH, CH₃CN, and at room temperature hexanes and MeOH followed by cold CHCl₃. The solution was decanted and methanol was added again and the process repeated till no more of the monomeric impurities remained, as exhibited by a colorless methanol layer. The mixture was then evaporated to dryness and washed with hexane to further get rid of any other impurities. The residue was put under high vacuum and to obtain **P12** as red color powder (0.052 g). ^{1}H NMR (400 MHz, CDCl₃, 298 K) δ/ppm: 8.64-8.62 (m), 8.57-8.55 (m), 7.99-7.98 (m), 7.9-7.87 (m), 7.78-7.76 (m), 6.54-6.52 (m), 2.86-2.82 (m), 1.56-1.52 (m), 1.26-1.22 (m), 0.88-0.85 (m). FT-IR (KBr) ν in cm^{-1}: 2920, 2854, 1610 (C=C, aromatic), 1582, 1551, 1476, 1390, 1198, 974, 799. From GPC data $\overline{M_n}$ = 8236 and $\overline{M_w}$ = 22483, PDI = 2.72.

P11.Tb complex preparation:

 In a 100 mL flask polymer **P11** (10 mg, 0.00095 mmol) and terbium acetylacetonate (III) hydrate (5.1 mg, 0.0114 mmol) were dissolved in 20 mL THF. The reaction mixture was stirred for 5 h at 60 °C. The solvent was removed under vacuum to get an orange-red color solid. The excess and unreacted metal was removed by washing with MeOH. Yield 13.0 mg. FT-IR (KBr) ν cm^{-1}: 2922, 2855, 2190 (C≡C, stretch), 1909, 1605 (-C=O, stretch), 1460, 1263, 1103, 1035, 951, 875, 834, 799, 687. Raman (785 nm) ν cm^{-1}: 812, 828, 854, 872.

^{1}H-NMR (400 MHz, CDCl₃, 298 K) δ/ppm: 8.89-8.50 (br), 8.1-7.65 (br), 5.6 (s), 3.7 (s), 6.54 (br), 2.85 (s), 2.2 (s), 2.0 (s), 1.85 (t, J = 3.2 Hz), 1.25-1.22 (m), 0.88-0.86 (m, 95H).
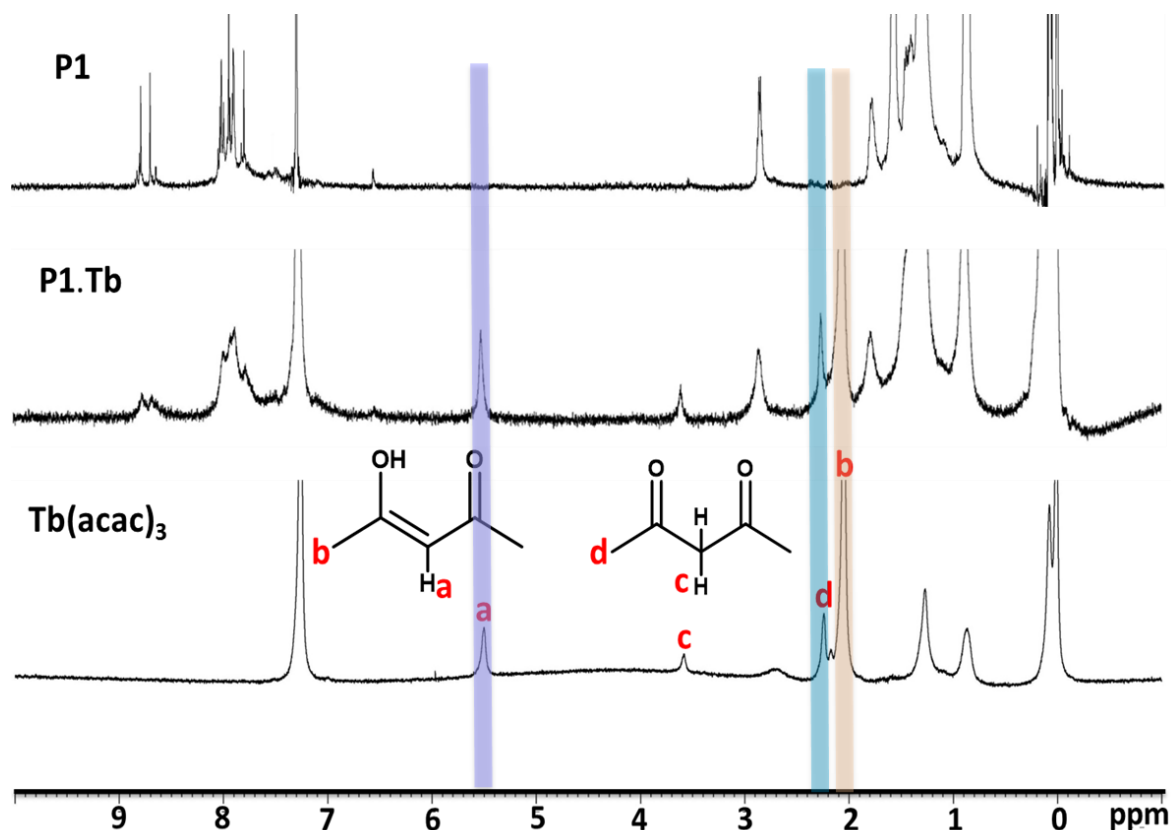
Figure 5.3 ^{1}H-NMR spectra of copolymer **P11, P11**.Tb(acac)$_3$ and Tb(acac)$_3$.

5.3.2 *Thermal Properties of Polymers*

The thermal stability of two polymers was investigated by thermo-gravimetric analysis. The copolymers **P11** and **P12** exhibited good thermal stability (Fig 5.4). It was found that the polymer **P11** was stable up to a temperature of ca. 350 °C (94%), above which it degraded with a ~33% weight loss at ~554 °C. Polymer **P12** exhibited almost similar behaviour like **P11** and showed thermal stability up to 315 °C
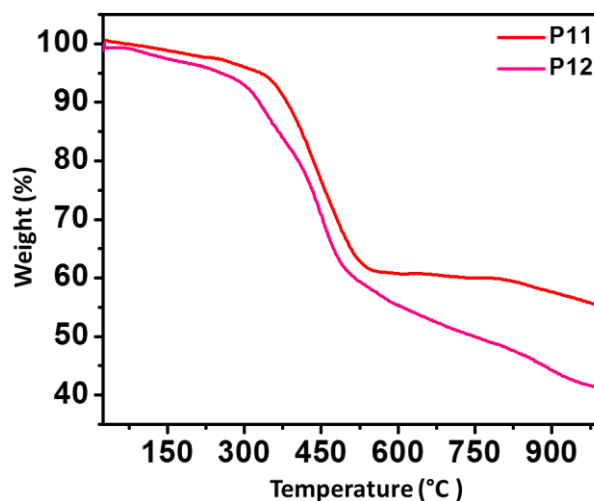
Figure 5.4 TGA curve of copolymers **P11** and **P12**.

(92%) and with a slight stability the weight loss continued to ~ 32% at 515 °C. The sequence of

weight loss is probably as a result of the decomposition of the alkyl chains attached to thiophene rings in BDT-T followed by BPP units. The observed difference in the thermal behavior of **P11** and **P12** indicated the consequence of linear and bent structures. Here **P11** is expected to have more inter-chain interaction in the solid state due to linear chain structure compared to **P12**.

5.3.3 *Optical Properties of Copolymers and Metal-Coordinated Copolymers in Solution and Thin Film States*

The photo physical properties of the copolymers (**P11** and **P12**) and metal coordinated polymers were studied in $CHCl_3$ solution and also as spin-casted thin films. All the spectroscopic data were presented in Table 5.2.

Table 5.2 Optical data of copolymers (**P11** and **P12**).

| Polymer	Solution ($CHCl_3$)		Φ_f [a]	Thin Film		Optical band gap [b] (eV)
	Absorption λ_{max} (nm)	Emission λ_{max} (nm)		Absorption λ_{max} (nm)	Emission λ_{max} (nm)	
P11	315, 355, 509	637	25%	325, 371, 538	708	1.76
P12	355, 509	636	30%	381, 538	709	1.76

[a]Quinine sulfate as reference (Q_{ref} = 0.577). [b]Estimated from the onset wavelength of optical absorption in the solid state film.

In solution ($CHCl_3$) state, **P11** and **P12** showed multiple absorption bands at 315/355/509 nm and 355/509 nm, respectively. Upon excitation (λ_{ex}) at 509 nm, **P11** and **P12** showed red emission with a peak maxima (λ_{max}) centered at 637 nm and 636 nm, respectively (Fig 5.5 A and B). The solution state absorption spectra of terbium coordinated polymers (**P11** and **P12**) exhibited mixture both polymer and Tb features. Optical excitation of **P11.Tb** or **P12.Tb** at 485 nm clearly showed an yellow emission with a characteristic high intensity Tb(III) centered emission band at 545 nm ($^5D_4 \rightarrow {}^7F_5$ transition) together with broad polymer emissions. At this excitation wavelength pure Tb(acac)$_3$ did not show any *f-f* transitions (Fig. 5.5 A,C). This result

clearly confirmed the coordination of Tb(acac)$_3$ with polymers in the solution state. In comparison to solution state absorption spectra, thin polymer films exhibited *red shift* due to possible *J* type molecular aggregations and inter-chain interactions.[11] The absorption spectra of spin coated terbium coordinated polymer (**P11** and **P12**) thin films (from CHCl$_3$) showed a mixture both polymer and Tb peaks. Upon optical excitation at 500 nm, the film clearly show characteristic polymer emission together with a high intensity Tb(III) centred emission band centered at 545 nm ($^5D_4\rightarrow^7F_5$ transition) with its emission tail extended beyond 800 nm (Fig 5.5 B,D).

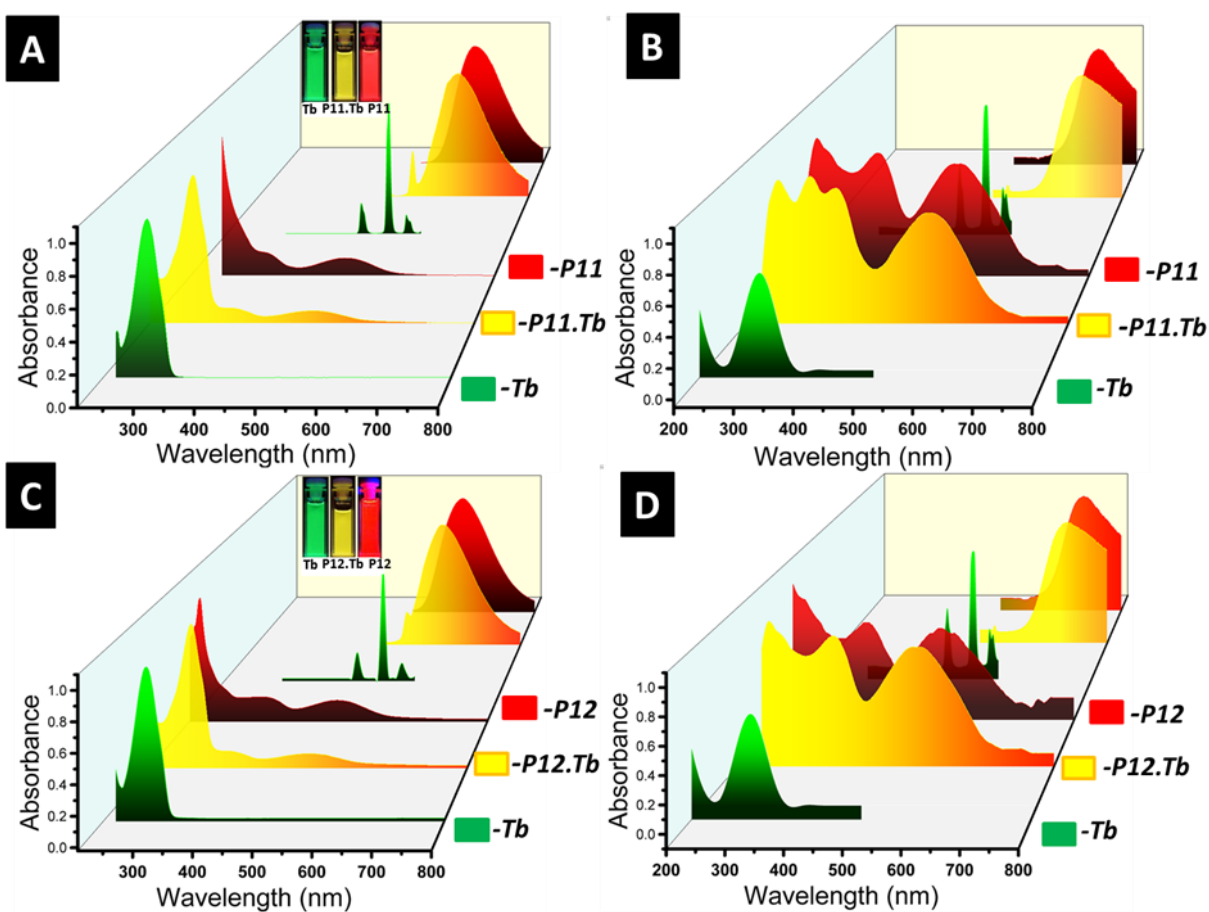**Figure 5.5** Optical absorption and emission spectra of **P11**, **P12**, **Tb**, **P11.Tb**, and **P12.Tb**, where Tb = Tb(acac)$_3$. A and C) solution state, B and D) solid state. The insets in A and C show the corresponding solution state emissions.

5.3.4 Self-assembly of Polymers

These copolymers (**P11** and **P12**) self-assemble into polydispersed "soft" microspheres in THF solution (1 mg/1 mL) as depicted by the SEM images (Fig 5.6A). Further the TEM images exhibited nano/micro spheres in grey contrast indicating their soft nature which is normally observed for organic molecular assemblies (Fig 5.6B). The self-assembly of red-emitting
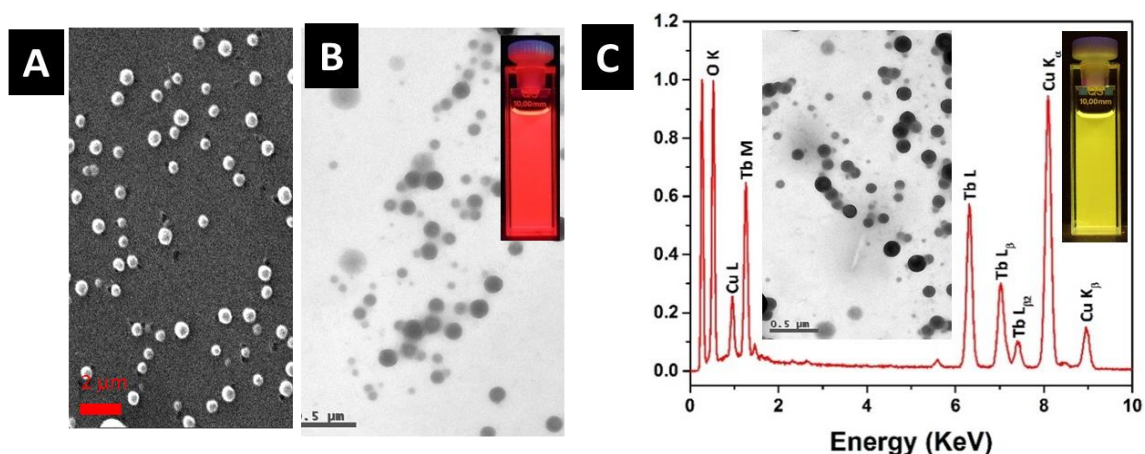
Figure 5.6 A and B) SEM and TEM images of **P11** microspheres. The inset shows the red emission from the **P11** solution. C) EDAX spectra of **P11** microsphere surface coordinated with Tb(acac)$_3$. The inset shows the corresponding TEM image and yellow emission of the solution.

copolymers into spheres is possibly mediated by the π-π stacking interactions (*J*-aggregates) of the polymer aromatic units, thereby increasing the close packing of the hydrophobic octyl-chains forming a sphere like structures. In order to obtain orange yellow color emitting spheres, we have performed the *coordination chemistry on self-assembled solid surface*.[23-26] Firstly, to the THF solution of **P11** microspheres, a THF solution of Tb(acac)$_3$.(H$_2$O)$_3$ (0.5 mg/0.02 mL) was injected, followed by gentle shaking; a layer of a nine coordinated complex[19] was formed on the surface of the spheres. The possible mechanism of complex formation on the spheres is the coordination of Tb(acac)$_3$ with the surface exposed bpp units followed by diffusion to the interior part of the sphere. Examination of the TEM-bright field images obtained from the metal coordinated polymer/inorganic hybrid spheres exhibited an apparent dark contrast due to the presence of Eu(III) complexes compared to light contrast displayed by pure **P11** spheres (Fig 5.6 C, inset). In addition, the energy dispersive X-ray analysis confirmed the presence of Tb in **P11**.**Tb** microspheres (Fig 5.6C). The origin of strong Cu peaks is due to Cu-TEM grids.

5.3.5 Single Particle μ-FL Studies of Self-assembled Microspheres Obtained from a Blend of Bulk P1.Tb and Polystyrene

MCCP of **P11.Tb** was self-assembled into polydispersed microspheres in THF/H$_2$O solution (1 mg/1 mL) (Fig. 5.7). Single particle confocal micro-fluorescence (μ-FL) spectroscopy (Reflection mode; Ar$^+$ 488 nm; objective: 150x) studies showed a normal Gaussian type orange yellow emission (525-800 nm) profile without any features of WGM resonance. This is probably due to the presence of nano/micro scale defect sites inherited during their microspheres natural growth process. Therefore, to exploit the Vis-NIR emitting MCCP for WGM emission, we blended bulk **P11.Tb** with high molecular weight polystyrene (PS) to create defect free high quality microspheres which can act as optical gain medium. For this, a THF solution of **P11.Tb** (100 μl; c~ 4.70 x 10^{-8} M) was mixed with a polystyrene solution (20 mg/4 ml THF). To this resultant PS:**P11.Tb** solution, water (1mL) was drop-wise added and the solution was kept undisturbed for 30 min to stabilize the growth of microspheres composed of **P11.Tb**:PS. Two drops of this solution were drop-casted on a clean glass substrate at room temperature and the solvent was allowed to evaporate to prepare samples for confocal microscopy and FESEM investigations.
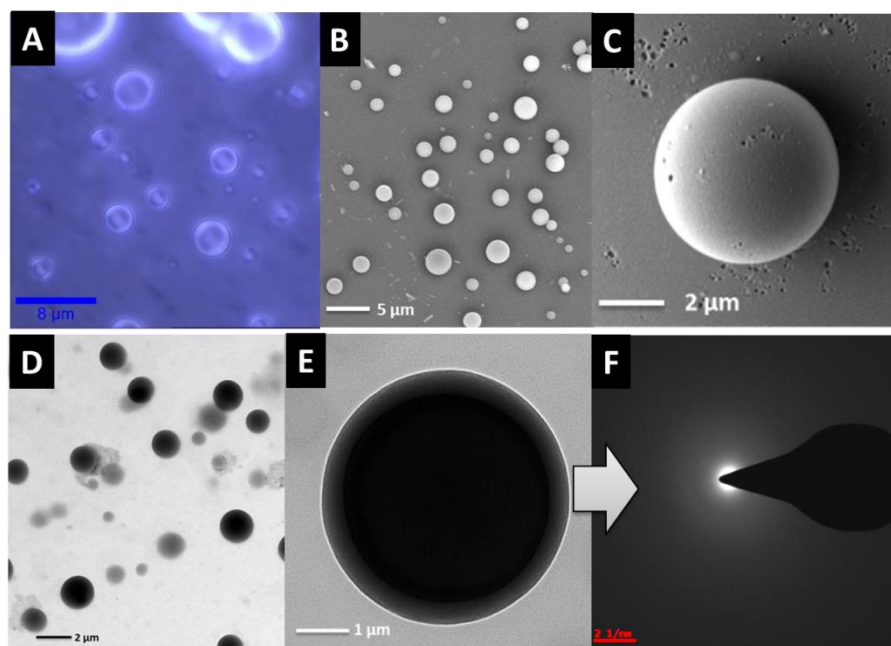

Figure 5.7 A) Confocal optical micrograph of PS microspheres obtained blended with **P11.Tb.** B) Its FESEM images. C) FESEM image of a single particle. D) Bright field TEM image of PS microspheres coated with **P11.Tb**. E) TEM image of a single particle. F) SAED displaying amorphous nature single particle.

The Confocal microscopy image of the sample showed the formation of spherical particles of varying sizes (Fig. 5.7 A). FESEM images of the same sample clearly exhibited the presence of polydispersed microspheres of good quality (Fig 5.7B). Further the tilted view of the particle confirmed its spherical nature and its smooth surface (Fig 5.7C). TEM micrographs showed relatively dark contrast of the microspheres due to the presence of MCCP in PS (Fig 5.7D, E). Selected area electron diffraction of a single microsphere indicated its amorphous nature (Fig 5.7F).

Additionally AFM cross-sectional analysis of selected polymer sphere showed diameters in the range of 400 nm - 4μm (Fig 5.8A). To confirm the chemical composition of the MCCP coated PS microsphere, FESEM and energy-dispersive X-ray spectroscopy (EDS), studies were performed in a single microsphere level. The resultant EDS elemental mapping of a single MCCP blended PS microsphere clearly indicated the presence of N, S and Tb elements confirming **P11.Tb** incorporation into PS microsphere (Fig 5.8B-F).
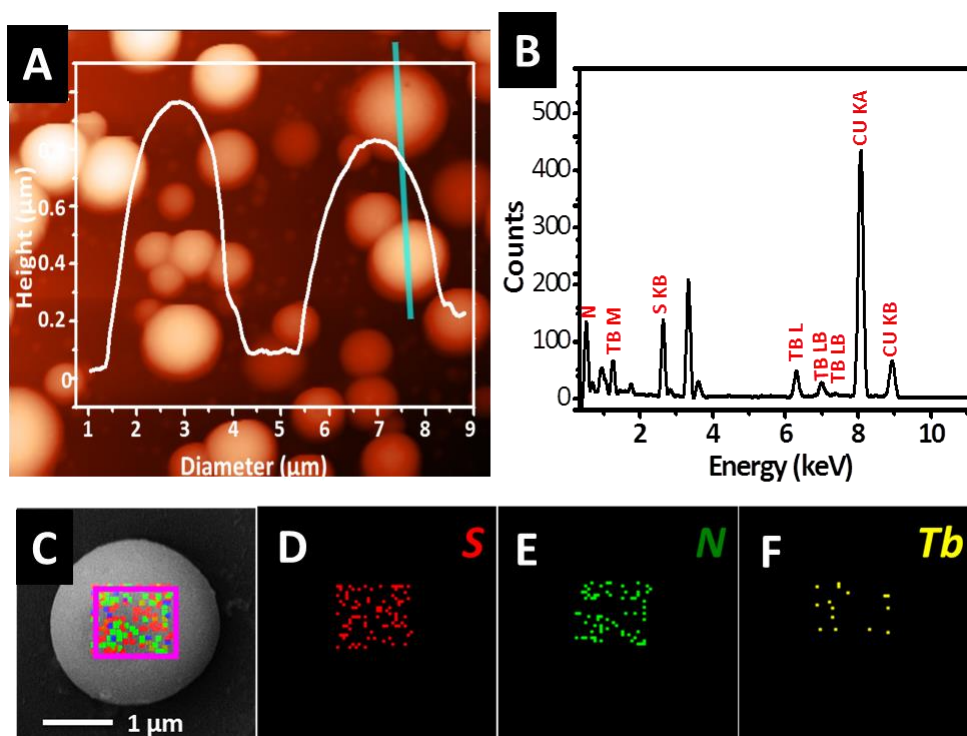

Figure 5.8. A) AFM image of spheres. The inset shows the diameter-profile of the spheres corresponds to the straight line shown in the figure. B) EDAX spectrum of a sphere exhibiting Tb(III) ions peaks. C-F) EDAX elemental mapping of **P11.Tb** doped PS microsphere displaying the distribution of S, N and Tb, respectively.
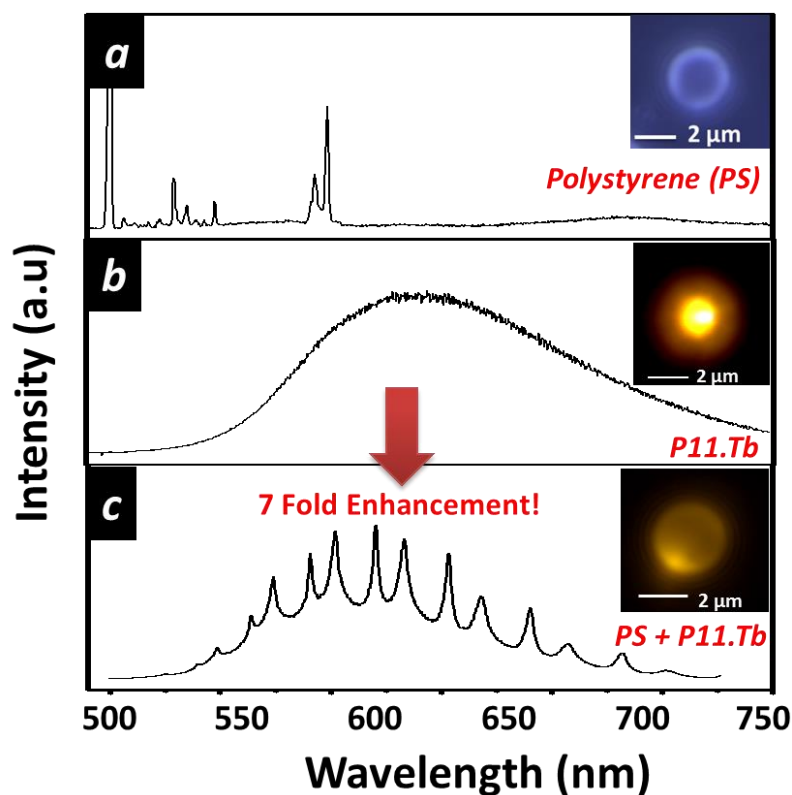
Figure 5.9. Single particle spectroscopy studies (λ_{ex} = 488 nm). A) Raman spectrum of a single PS microsphere. B) FL spectrum of a **P11.Tb** microsphere not supporting WGM resonance. C) PL spectra of **P11.Tb** blended polystyrene microspheres displaying WGM like resonance. The insets show the corresponding images. Power: 20 µW, Integration time: 0.5 sec.

As expected the single particle µ-FL spectrum (Objective: 150x; NA: 0.98; power: 20 µW; 0.5 integration time) of pure PS microsphere alone did not show any emissions except Raman peaks of PS (Fig 5.9a). While the **P11.Tb** microsphere exhibited a broad and weak FL emission centered at ~ 650 nm (see Fig 5.9b). In contrast to pure **P11.Tb** and PS microspheres similar localized electronic excitation of **P11**.**Tb**:PS blend microsphere of comparable size (D ~ 2 µm) displayed about seven fold increase in the emission intensity, with its tail reaching the NIR region (Fig 5.9c). Additionally, the broad spectrum comprised of a pair of multiple sharp lines indicating the occurrence of WGM type resonance within the single microsphere. These pair of peaks corresponds to transverse electric (TE) and transverse magnetic (TM) modes, which are normally observed due to breakdown of degeneracy.[27] The optical resonance in these cavity structures is a function of cavity geometry and refractive index. Further the spacing between modes or free spectral range (FSR) and the number of observed modes are very much sensitive to the cavity diameter, in other words the microsphere diameter (D).
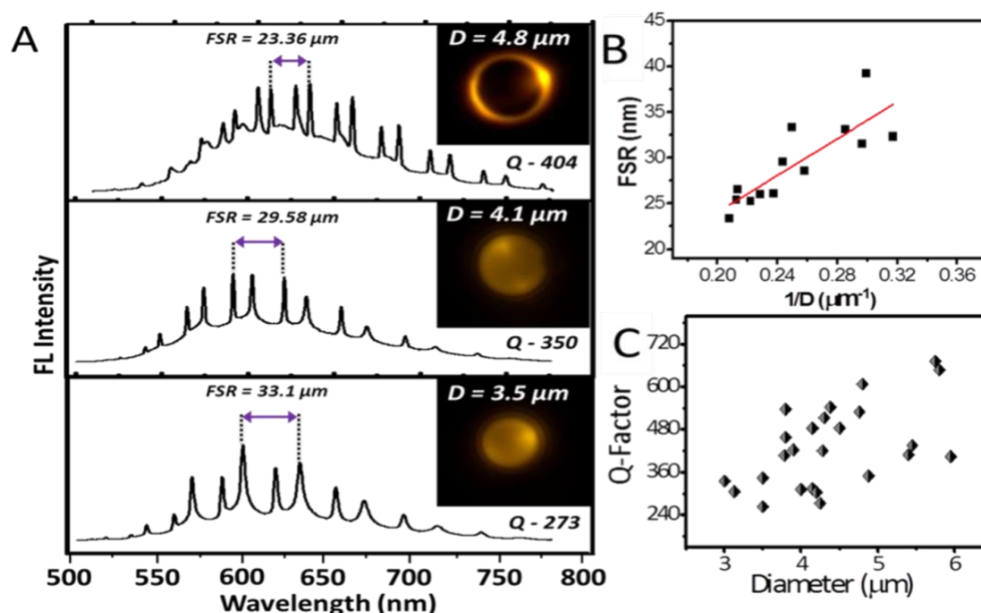
Figure 5.10 A) Single particle FL spectra of **P11.Tb** doped polystyrene microspheres with three different diameters displaying size dependent cavity action through WGM resonance. The insets show the corresponding images. B and C) Plots of FSR and *Q* factor as a function of microspheres diameter, respectively. The red line in plot B shows the linear fit (FSR~ 1/D).

To study these effects three representative microspheres of varying diameter was identified. A larger microsphere with cavity diameter of D = 4.8 µm showed FSR of 23.36 nm. As expected, upon decreasing the sizes to D = 4.1 µm, and 3.5 µm, the FSR value correspondingly increased to 29.58 nm and 33.1 nm, respectively (Fig. 5.10A). Additionally, the FSR values increased linearly with the decreasing D values (FSR~1/D) (Fig. 5.10B; the linear fit is shown as red line). The observed narrow resonance lines is inversely related to the Quality factor (Q = $\lambda/\Delta\lambda$; where λ is the wavelength at which a resonance occurs and $\Delta\lambda$ the resonant wavelength line width at FWHM). The Q-factor of the microspheres improved with increasing the diameter with a value up to ~700 (Fig 5.10C) with in the spectrometer resolution. Further to probe the resonance modes appearing in the NIR region, similar single particle experiments were performed using 633 nm (He-Ne ion) laser. The resultant emission spectrum evidently showed sharp modes at about 808.8, 832.5, 850.3, and 877.3 nm ranges confirming the confinement of NIR waves within the optical cavity (Fig. 5.11).
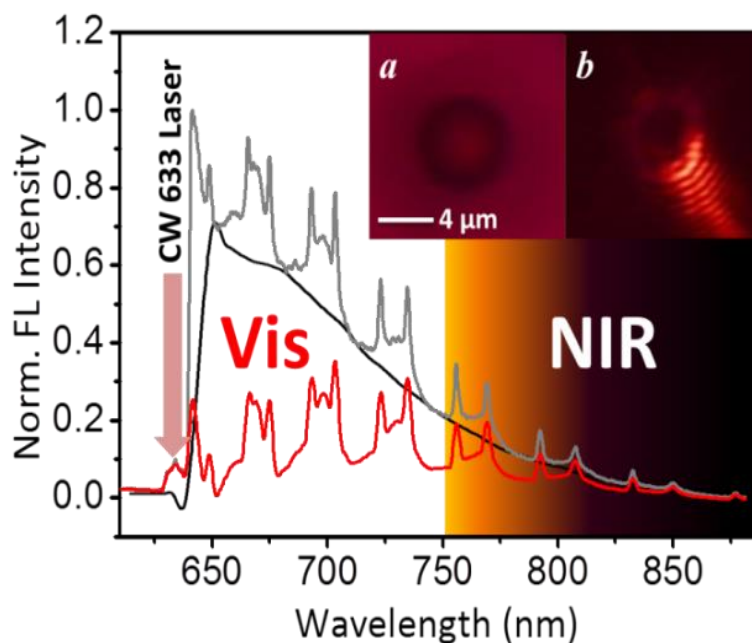
Figure 5.11 Single particle FL spectra of **P11.Tb**:PS microspheres displaying WGM resonance in the NIR range (Nd-YAG; λ_{ex} = 633 nm). The insets images show: a) before excitation, b) after excitation. Spectra with and without WGM resonance is shown in black lines. The back ground subtracted spectrum is given in red line.

5.4 Conclusions

In summary, this chapter represented a successful strategy to generate polymer blend micro-resonators by judicially blending MCCP (Tb.**P11**) with PS. Optical excitation of these polymer blend micro-resonators showed WGM resonance in the visible and NIR range. Compared to pure microsphere of **Tb**.**P11**, the PS:Tb:**P11** micro resonators displayed an enhanced emission (almost seven times) upon localized optical excitation. Similar principle can also be used to achieve various frequency resonances by changing the emissive property of the metal and polymers. This chapter again stressed the importance of high molecular weight polymers to achieve high quality polymer microspheres for photonic studies. The obtained Q factor is quite high and thus demonstrating its superior light trapping capabilities.

Future possibilities are also there to generate NIR emitting photonic solids by blending NIR emitting polymers. In future, a particular resonance mode can be excited by pumping a single particle with femto-second laser to generate single mode organic lasers. This will ultimately lead to coherent lasing action at room temperature operating at low threshold laser power.

References

1.   K. J. Vahala, *Nature* **2003**, *424*, 839-846.

2.   G. Wegner, D. Neher, M. Remmers, V. Cimrova, M. Schulze, *Mater. Res. Soc. Symp. Proc*. **1996**, *413*, 23–34.

3.   H. F. Wittmann, J. Gruner, R. H. Friend, G. W. C. Spencer, S. C. Moratti, A. B. Holmes, *Adv. Mater*. **1995**, *7*, 541–544.

4.   V. Cimrova, U. Scherf, D. Neher, *Appl. Phys. Lett*. **1996**, *69*, 608– 610.

5.   O. *J.* Schwelb, *Lightwave Technol.* **2004**, *22*, 1380–1394.

6.   M. Pöllinger, A. Rauschenbeutel, *Opt. Exp*. **2010**, *18*, 17764-17775.

7.   F. Vollmer, S. Arnold, *Nat. Methods* **2008***, 5*, 591–596.

8.   D. K. Armani, T. J. Kippenberg, S. M. Spillane, K. J. Vahala, *Nature* **2003**, *421*, 925-928.

9.   K. Takazawa, J. Inoue, K. Mitsuishi, T. Kuroda, *Adv. Funct. Mater*. **2013**, *23*, 839–845.

10.   X. Wang, Q. Liao, X. Lu, H. Li, Z. Xu, H. Fu, *Sci. Rep.* **2014**, *4*, 7011.

11.   C. Wei, S. –Y. Liu, C.-L. Zou, Y. Liu, J. Yao, Y. S. Zhao, *J. Am. Chem. Soc*. **2014**, *137*, 62–65.

12.   K. Tabata, D. Braam, S. Kushida, L. Tong, J. Kuwabara, T. Kanbara, A. Beckel, A. Lorke, Y. Yamamoto, *Sci. Rep*. **2014**, *4*, 5902.

13.   D. Venkatakrishnarao, R. Chandrasekar, *Adv. Opt. Mater.* **2015**, DOI: 10.1002/adom.201500362.

14.   A. C. Grimsdale, K. L. Chan, R. E. Martin, P. G. Jokisz, A. B. Holmes, *Chem. Rev.* **2009**, *109,* 897–1091.

15.   D. T. McQuade, A. E. Pullen, T. M. Swager, *Chem. Rev.* **2000**, *100*, 2537–2574.

16.   T. A. Skotheim, J. Reynolds, *Conjugated Polymers: Processing and Applications* CRS Press: **2006**.

17.   K. Müllen, U. Scherf, *Organic Light Emitting Devices: Synthesis, Properties and Applications,* Wiley-VCH: Weinheim, Germany, **2006**.

18.   L. Trouillet, A. De Nicola, S. Guillerez, *Chem. Mater*. **2000**, *12*, 1611-1621.

19.   X. Y. Chen, X. Yang, B. J. Holliday, *J. Am. Chem. Soc*. **2008**, *130*, 1546-1547.

20.   Q. Hou, Q. Zhou, Y. Zhang, W. Yang, R. Q. Yang, Y. Cao, *Macromolecules* **2004**, *37*, 6299-6305.

21. a) S. Basak, P. Hui, R. Chandrasekar, *Synthesis* **2009**, *23*, 4042-4048; b) N. Berton, C. Ottone, V. Labet, R. Bettignies, S. Bailly, A. Grand, C.Morell, S. Sadki, F. Chandezon, *Macromol. Chem. Phys*. **2011**, *212*, 2127–2141.

22. G. Zoppellaro, M. Baumgarten, *Eur. J. Org. Chem*. **2005**, 2888-2892.

23. S. Basak, Y. S. L. V. Narayana, M. Baumgarten, K. Müllen, R. Chandrasekar, *Macromolecules* **2013**, *46*, 362−369.

24. Y. S. L. V. Narayana, M. Baumgarten, K. Müllen, R. Chandrasekar, *Macromolecules* **2015**, *48*, 4801-4812.

25. Y. S. L. V. Narayana, S. Basak, M. Baumgarten, K. Müllen, R. Chandrasekar, *Adv. Funct. Mater.* **2013**, *23*, 5875-5880.

26. S. Basak, R. Chandrasekar, *Adv. Funct. Mater*. **2011**, *21*, 667−673.

27. V. D. Ta, R. Chen, H. D. Sun, *Sci. Rep.* **2013**, *3*, 1362.

6

Conclusions

This thesis entitled "Nano/Micro Scale Macromolecular Materials: Design, Synthesis, Self-Assembly, Lighting and Photonic Applications" covered the material chemistry features of fluorescent macromolecules and its luminescent *f*-block metal complexes. The introduction part (Chapter 1) mainly focused on the history of bis(pyrazolyl)pyridine (bpp), overview of metallo-supramolecular polymers, metal containing conjugated polymers, white light emitting materials, self–assembly of macromolecules (bottom-up approach), polymer/inorganic hybrid materials, basic principle of whispering gallery modes and finally highlighted the potential use of self-assembled conjugated polymer micro spheres as photonic μ-resonators.

Chapter 2 presented a novel one-pot approach to accomplish white color emission from conjugated polymers (CP), metal containing conjugated polymer (MCCP) and their corresponding hybrid films and nano/micro scale spheres. The beginning of this chapter presented the syntheses of phenylethynyl and bpp containing model compounds (m1 and m2) and two cyan colour (blue and green emission) displaying high molecular weight 2,6-bis(pyrazolyl)pyridine-*co*-octylated phenylethynyl conjugated polymers (CPs) **P1** and **P2**. A detailed study of optical properties of polymers in solution and solid states were presented. The fabrication strategy for cyan emitting copolymer film and spheres from **P1** was demonstrated. A novel preparation method to fabricate white color emitting films and spheres via coordination with $Eu(tta)_3$ was also discussed. The nano/micro scale polymer spheres and hybrid films exhibited Commission Internationale de l'Eclairage (CIE) coordinates of $x = 0.33$; $y = 0.37$ and $x = 0.30$; $y = 0.35$, respectively. Additionally, this chapter focused also on a comparative photophysical and energy transfer studies of model complex ($m2 \cdot Eu(tta)_3$) with **P1** polymer coordinated with $Eu(tta)_3$.

The syntheses of a series of dialkynyl functionalized oligo(3-octyl thiophenes) and their alternating copolymers with bpp (**P3-P10**) were presented in chapter 3. This chapter also discussed the absorption and emission properties of these copolymers and also a method to achieve white emission by coordinating Eu^{3+} and Tb^{3+} ions to the polymers in solution, thin film, and microsphere states. The self-assembled microspheres were thoroughly investigated by electron-, atomic force- and laser confocal fluorescence microscopy techniques. A white color was obtained in solution, thin film and microsphere states upon UV excitation with CIE coordinates close to the values of standard white color. In this chapter main attention was paid to tune optical emission of copolymers by changing the conjugation length of thiophene oligomers and coordination of luminescent metals like Eu^{+3} and Tb^{+3} to achieve colour tunability. The emission color was tuned from blue to red and white in the solution and solid states.

In chapter 4, an original approach was developed to generate dual emission from organic molecule and tricolor emitting organic/inorganic nano/micro particles. Initially, this chapter presented the synthesis of a dual emitting (blue and green) amphiphilic ligand molecule **L1** by connecting two units of blue emitting 4-triazolyl-2,6-bis(pyrazolyl)pyridine derivative with a green emitting 4,7-triazolyl-benzo-1,2,5-thiadiazole derivative using two octyl chain linkers via a Click chemistry reaction. Afterwards, the discussion was also extended to single-pot self-assembly of ligand **L1** in THF/water to create dual (blue/green) emitting soft spheres and subsequently production of triple color emitting organic/inorganic hybrid core-shell spheres by performing coordination chemistry with red-emitting Eu(III) ions on the surface of the dual emitting spheres. Finally a preliminary single particle examination to confine FL light inside the microsphere cavities was also presented.

At last chapter 5 showed a successful route to generate novel polymer blend micro-resonators from polystyrene (PS) and novel orange yellow emitting MCCP namely, terbium coordinated poly[4,7-bis(3-octylthiophene-2-yl)benzothiadiazole-*co*-2,6-bis(pyrazolyl)pyridine] (Tb.**P11**). Firstly, this chapter presented the syntheses of two novel red emitting copolymers (**P11** and **P12)** by regio-selective copolymerization of tridentate ligand, namely bpp with 4,7-bis(2-ethynyl-5-thienyl)-2,1,3-benzothiadiazole (M_n ~ 10.7 and 8.3 KDa, respectively). These polymers readily form orange yellow emitting MCCP with Tb(acac)₃. Further this chapter also demonstrated a solution based technology by judicially blending Tb.**P11** MCCP with PS and

subsequent self-assembly of the blend in THF/water to fabricate photonic microspheres capable of trapping yellow FL light. Single particle microscopy and μ-PL spectroscopy studies were carried out on a laser confocal μ-spectroscopy set-up to investigate the photonic properties of microspheres. Further discussion also showed a seven fold increased optical emission intensity of MCCP blended micro-resonators compared to pure MCCP. The conclusion parts of the chapter showcased the wide spectral operating capability of the micro-resonators from visible to NIR range.

Appendix A

MATERIALS

Citrazinic acid	Aldrich, 98%
[Pd(PPh$_3$)$_4$]	Aldrich, 99%
Pd(PPh$_3$)$_2$Cl$_2$	Aldrich, 99%
Pd(PhCN)$_2$Cl$_2$	Aldrich, 99%
Ni(dPPP)Cl$_2$	Aldrich, 99%
TMEDA	Aldrich, 97%
TMSA	Aldrich, 99%
AgF	Aldrich, 98%
Mg	Avra Synthesis Pvt.Ltd. 98%
CuI	Avra Synthesis Pvt. Ltd. 98%
Tetramethyl ammonium chloride	Avra Synthesis Pvt. Ltd. 98%
Eu(tta)$_3$·3H$_2$O	Acros, 98%
Tb(acac)$_3$.H$_2$O	Aldrich, 99%
HIO$_3$	Aldrich, 99.5%
KIO$_3$	Aldrich, 99%
Diglyme/diethylene glycol dimethylether	Aldrich, 99.5%
K-metal	Aldrich, 98%
I$_2$	Finar Reagents, 99.5%
KI	Merck Chemicals Pvt. Ltd. 99%
LiOH	Avra Synthesis Pvt. Ltd.98%
KOH	Avra Synthesis Pvt.Ltd. 98%
K$_2$CO$_3$	Avra Synthesis Pvt.Ltd. 97%
NaN$_3$	Avra Synthesis Pvt. Ltd. 98%
NaNO$_2$	Merck Chemicals Pvt. Ltd. 99%
POCl$_3$	Avra Synthesis Pvt. Ltd. 98%
PPh$_3$	Avra Synthesis Pvt. Ltd. 98%
Br$_2$	Aldrich, 99%
HBr	Aldrich, 99%
Pyrazole	Aldrich, 98%
Trifloro acetic acid	Aldrich, 99%
(COCl)$_2$	Avra Synthesis Pvt. Ltd. 98%
Hydroquinone	Avra Synthesis Pvt.Ltd. 95%
Thiophene	Aldrich, 99%
3-Bromothiophene	Aldrich, 98%
2,1,3-Benzothiadiazole	Aldrich, 95%
1-bromooctane	Aldrich, 99%
1,8-Dibromooctane	Aldrich, 99%
Sodium ascorbate	Aldrich, 98%
Cu(II)SO$_4$•5H$_2$O	Aldrich, 98%
KF	Aldrich, 99%

Appendix B

INSTRUMENTATION

Nuclear Magnetic Resonance Spectroscopy

^{1}H and ^{13}C NMR spectra were recorded on a Bruker 400 MHz NMR spectrometer. Spectra were recorded using the solvent peaks as the internal standard.

Mass Spectroscopy

Shimadzu LC-MS 2010A equipment was used to record the mass spectra of the isolated compounds following atmospheric pressure chemical ionization (APCI) technique.

Elemental Analysis

Elemental analysis was carried out on a Thermo Finnigan Flash EA-1112 series) CHNS analyzer.

UV-Vis Absorption Spectroscopy

Absorption spectra were recorded on a Shimadzu UV-3600 UV-Vis-NIR Spectrophotometer or Cary 100 Bio UV-Visible spectrophotometer.

Solid State Absorbance Studies

The solid state absorbance spectra were collected from a Shimadzu UV-3600 spectrometer in a diffuse reflectance UV-visible (DR-UV-Vis) mode. The reflectance spectra were converted to a absorbance spectra using Kubelka-Munk function.

Fluorescence Spectroscopy

Steady state fluorescence emission and excitation spectra were recorded on a JobinYvon Horiba model Fluoromax-3 spectrofluorimeter.

Ultra-Sonification Studies

Bandelin SONOREX® SUPER with built-in heating Ultrasonic baths, model Z659584 -RK 100 H, capacity 3 L. HF-Frequency 35 kHz and H-types with built-in heating, 30 - 80 °C (86 to 176 °F) thermostatically adjustable.

Transmission Electron Microscopy (TEM)

TEM images were obtained on a TECNAI G^2 FEI F12 TEM at an accelerating voltage of 120 kV. Samples were prepared by placing a drop of the samples on a polymer (polyvinyl formvar) − coated copper grid (200 mesh).

Scanning Electron Microscopy (SEM)

SEM and FESEM images were recorded on a Philips XL30 ESEM and a Carl Zeiss (Model Ultra55) FESEM respectively using beam voltages of 20 kV and 5 kV. The samples were fixed on aluminum platforms using carbon tapes; a conducting connection was made between samples and aluminum platform by palladium or silver paint and then subjected to gold sputtering with suitable time intervals.

Atomic Force Microscopy (AFM)

Atomic Force Microscopy (AFM) imaging was carried out on NT-MDT Model Solver Pro M microscope using a class 2R laser of 650 nm wavelength having maximum output of 1 mW. All calculations and image processing was carried out by a software NOVA 1.0.26.1443 provided by the manufacturer. The images were recorded in a semi-contact mode using a noncontact super sharp silicon cantilever (NSG 10_DLC) diamond like carbon (DLC) tip purchased from NT-MDT, Moscow. The dimension of the tip is as follows: Cantilever length = 100 (±5) μm, Cantilever width 35 (±5) μm, and Cantilever thickness = 1.7-2.3 μm, Resonate frequency = 190-325 kHz, Force constant = 5.5-22.5 N/m, Chip size = 3.6×1.6×0.4 mm, Reflective side = Au, Tip height = 10-20 μm, DLC Tip curvature radius = 1-3 nm.

Laser Confocal FluorescenceMicroscopy (LCFM)

The luminescence behavior of the samples was observed with a Leica Laser scanning confocal microscope, Germany [model No - TCS − SP2 (spectral confocal microscope)] equipped with an Acousto-Optical Beam Splitter (AOBS) emission filter. The wavelength and amplitude of the ultrasound can be changed (programmed) to deflect certain band of wavelength and its amount passing through the field to collect emissions in high efficiency. The topographic structural data were directly coupled with the spectroscopic properties of the specimen. The emission spectral curves were recorded in XYλ (spectral scan mode) scan mode, and the images were recorded in XYT mode (time scan mode). Argon-ion Laser (Power- 280 mW) was used as UV excitation source. Scanning was done by a 20.0× optical lens, later it was further magnified by a factor 3.45 using digital magnification by the Leica confocal software (LCS). The data were recorded with a (Continuous scan) scanning speed of 400 Hz (image lines per second) with a scan format of 512 pixel × 512 pixel resolution. The active emission

colors were detected using the different color detection channels of the photomultiplier tube (PMT)

The pinhole size was 36 μm and six frames were taken to make an average of the final frame.

The confocal fluorescence images illustrated in *chapter-3* were recorded on a Carl-Zeiss laser confocal microscopy (Model number NL0710). The emission spectra were recorded in XYλ scan mode, and the fluorescence images collected in XYT mode. Argon-ion laser (power- 280 mW) was used as an excitation source (λ = 365 nm).
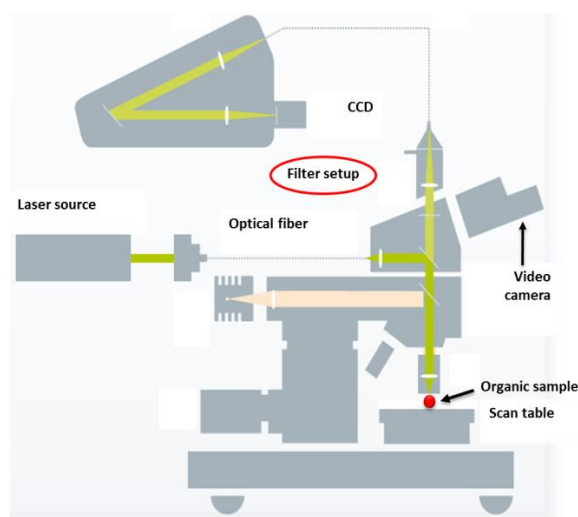
Confocal Micro Raman Spectroscopy Studies

Raman spectra of the samples were recorded on a WI-Tec alpha 300 confocal Raman spectrometer equipped with a Peltier-cooled CCD detector. Using a 600 grooves/mm grating BLZ = 500 nm, the accumulation time was typically 10 s and integration time was typically 0.5000 s. Ten accumulations were performed for acquiring a single spectrum. Argon laser operating at 488 nm, He-Ne laser 633 nm, and diode laser 785 nm were used as an excitation source for the Raman scattering. All measurements were collected in airand images were processed by using WI-TEC 2.08 software.

Whispering Gallery Modes (WGM) (or) Light Confinement Studies in a Back-Scattering Mode (BLCOM)

Photonic studies were performed on a WI-Tec alpha 300 confocal microscope coupled with 488 nm Argon ion laser (Maximum output 500 mW) and 633 nm He-Ne laser (maximum output power is 40 mW). The images of nano/micro structured materials were captured by color eyepiece video camera in bright-field and dark field mode respectively by using either 150× or 20× objective lens. The corresponding long edge pass filter (LPEF) adopted for the experiment in order to remove the unwanted Rayleigh scattered light coming from the sample.

In the case of chapter-4, the whispering gallery modes studies of microspheres were performed on a WI-Tec Alpha 200 SNOM instrument coupled with a 355 nm Nd:YAG laser. A 100× objective lens was used to for the local excitation and for the collection of FL photons. The collected FL signal was sent to a CCD detector through a 25/120 μm (core/cladding) diameter multimode optical fiber. The FL spectrum was recorded using a

General experimental set up for WGM studies.

355 nm long pass edge filter (LPEF) and a 600 grooves/mm grating BLZ = 500 nm, with a 5s integration time. Four accumulations were performed to acquire a single spectrum and the spectral resolution maximum was 0.1 nm. All measurements were carried out under ambient conditions. Where as in case of chapter-5 the optical spectra of single spherical particles were recorded on a WI-Tec alpha 300 AR confocal Raman spectrometer equipped with a Peltier-cooled CCD detector. 488 nm Argon ion laser (Maximum output 500 mW) and 633 nm He-Ne laser were used in presence of corresponding filters. All measurements were performed in air. The power used for to collect signals from microsphere was 20 μW. And with this power, 100 sec scan with 10 accumulations, 0.022 s intergration time and with 1024 pixels a spectrum was recorded. The points per line is 50 and lines per image is 90. Here with 150x objective – 300g/mm = 750 nm grating was used to get pl image of microsphere.

RESEARCH PUBLICATIONS

1. **Y. S. L. V. Narayana**, S. Basak, M. Baumgarten, K. Müllen, R. Chandrasekar, "*White-Emitting Polymer/Inorganic Hybrid Spheres: Phenylethynyl and 2,6-Bis(pyrazolyl)pyridine Copolymer Coordinated to Eu(tta)₃*".

   Adv. Funct. Mater. (**2013**), *23,* 5875–5880.   **(Chapter 2)**

2. **Y. S. L. V. Narayana**, M. Baumgarten, K. Müllen, R. Chandrasekar, "*Tuning the Solid State Emission of Thin Films/Micro-Spheres Obtained From Alternating Oligo(3-octylthiophenes) and 2,6-Bis(pyrazole)pyridine Copolymers by Varying Conjugation Length and Eu^{+3}/Tb^{+3} Metal Coordination*"
   Macromolecules. (**2015**), *48*, 4801–4812.   (**Chapter 3**)

3. **Y. S. L. V. Narayana**, R. Chandrasekar, "*Triple Emission from Organic/Inorganic Hybrid Nanovesicles in a Single Excitation*"
   Chem.Phys.Chem. (**2011***), *12,* 2391–2396.   (**Chapter 4**)

4. **Y. S. L. V. Narayana**, D.Venkatakrishnarao, A. Biswas, A. M. Mohaiddon, R. Chandrasekar, "*Visible-Near Infrared Range Whispering-Gallery Resonance from μ-Sphere Photonic Cavities Self-Assembled from a Blend of Polystyrene and Poly[4,7-Bis(3-Octylthiophene-2-Yl)benzothiadiazole-co-2,6-Bis(pyrazolyl)pyridine] Coordinated to Tb(acac)₃*"
   ACS Appl. Mater. & Interfaces (**2016),** *8*, 952-958. **(Chapter 5)**

5. S. Basak, **Y. S. L. V. Narayana**, M. Baumgarten, K. Müllen, R.Chandrasekar, "*White Light Emitting Films from Eu(III) Complexed Copolymers of Alternating Fluorene and Bis(pyrazolyl)pyridine Derivatives*".

   Macromolecules (**2013**), *46*, 362–369.

PRESENTATIONS IN CONFERENCES AND SYMPOSIUMS

1. **Y S L V Narayana**, R. Chandrasekar.

   "Triple Emission from Organic/Inorganic Hybrid Nano vesicles in a Single Excitation".

   Poster presented at the International symposium on recent trends in spectroscopy and dynamics of chemical systems,

   University of Hyderabad, Hyderabad, India. December 7-8, **2011**.

2. **Y S L V Narayana**, R. Chandrasekar.

   "Ligand Nano Surface-Assisted Coordination Chemistry: Triple Emission from Organic/Inorganic Hybrid Nano vesicles in a Single Excitation".

   *Poster presented at the Conference on Modern Trends in Inorganic Chemistr*y (MTIC-XIV), University of Hyderabad, Hyderabad, India, December 10–13, **2011**.

3. **Y S L V Narayana**, S. Basak, R. Chandrasekar.

   "White-Emitting conjugated polymer Organic/Inorganic Hybrid spheres: Phenylethynyl and 2,6-Bis(pyrazolyl)pyridine Copolymer Coordinated to Eu(tta)$_3$".

   Poster presented at 3th International Conference on Advanced Nanomaterials and Nanotechnology (ICANN-2013),

   Indian Institute of Guwahati (IIT-Guwahati), Guwahati, India, December 1-3, **2013**.

4. S. Basak, **Y. S. L. V. Narayana**, R. Chandrasekar.

   "White Light Emitting Films from Eu(III) Complexed Copolymers of Alternating Fluorene and Bis(pyrazolyl)pyridine Derivatives".

   *Oral presentation as well as a poster presentation in Chemfest-***2013** held in University of Hyderabad.

5. **Y S L V Narayana**, A. Biswas, R. Chandrasekar.

   "Light-Emitting Conjugated Polymers: Syntheses and Characterization".

   *Oral presentation as well as a poster presentation in Chemfest-***2014** held in *School of Chemistry, University of Hyderabad*

6. **Y S L V Narayana**, S. Basak, R. Chandrasekar.

   "White-Emitting Conjugated Polymer Organic/Inorganic Hybrid Spheres: Phenylethynyl and 2,6-Bis(pyrazolyl)pyridine Copolymer Coordinated to $Eu(tta)_3$". *Oral presentation in Chemfest-***2014**, *11th Annual In-House Symposium in School of Chemistry, University of Hyderabad, Hyderabad, India.*

7. **Y S L V Narayana**, R. Chandrasekar.

   "Tuning the Light Emission of Conjugated Bis(pyrazoyl) pyrdine (BPP), Thiophene and 4,7-di(thiophen-2-yl)benzo[c][1,2,5]thiadiazole (DTBT) Based Co-Polymers".
   Short invited talk and poster presentation at Third International Conference on Polymer Processing and Characterization *(*ICPPC-2014),
   Mahatma Gandhi University, Kottayam, Kerala, India, October 11-13, **2014**.

8. **Y S L V Narayana**, R. Chandrasekar.

   "Light Emitting Conjugated Polymers: Synthesis, Characterization and Self-assembly studies".
   Poster presentation at the Indo-Taiwan Symposium on Recent Trends in Chemical Sciences (RTCS). University of Hyderabad, Hyderabad, India, November 17-18, **2014**.

9. **Y S L V Narayana**, R. Chandrasekar.

   "Light Emitting Conjugated Polymers: Synthesis and Characterization".
   Poster presentation at RSC India Road Show, University of Hyderabd, Hyderabad, India, November 7, **2014**.

10. **Y S L V Narayana**, R. Chandrasekar.

    "Tuning the light emission of conjugated bis(pyrazoyl)pyridine and thiophene copolymers"
    Poster presentation at 13th Eurasia conference on chemical sciences, Indian Institute of Science, Bangalore, India, December 14-18, **2014**.

Y S L V Narayana

slvnarayanay@gmail.com/ch09ph54@uohyd.ernet.in

Personal Details:

Date of Birth: 09/07/1986

Nationality: Indian

Sex: Male

Marital status: Married

Education:

2010-2015:   Ph.D in Polymer Materials Chemistry, School of Chemistry, University of Hyderabad, Hyderabad, India.

2006-2008:   M.Sc (Chemistry), School of Chemistry, Andhra University, Andhra Pradesh, India.

2003-2006:   B.Sc (M.P.C), S.V.R.M College, (Acharya Nagrjuna University), Nagaram, Andhra Pradesh, India.

2001-2003:   12th (Inter M.P.C), S.V.R.M College, Nagaram, Andhra Pradesh, India.

Awards and Recognitions:

- Visiting student at Max-Planck institute for polymer research in June 2014, Germany.
- Awarded as senior research fellow (SRF) during the period 2012-2015 from CSIR. New Delhi, India.
- Awarded as junior research fellow (JRF) during the period 2010-2012 from CSIR.
- Qualified Graduate Aptitude Test for Engineering (GATE 2009).
- Qualified CSIR-Junior research fellowship conducted by joint council of scientific and industrial research (CSIR) – University grants commission (UGC) national eligibility test (NET) in June 2008, 2010 and December-2010.
- College first and merit scholarship holder in B.Sc. Program during the period 2003-2006.